Development of Biomaterial Scaffolds for Cultured Meat and Engineered Muscle

Callue, Travis

Award date:
2020

Awarding institution:
University of Bath

Development of Biomaterial Scaffolds for Cultured Meat and Engineered Muscle

Travis Jeff Callue

A thesis submitted for the degree of Doctor of Philosophy

University of Bath
Department of Pharmacy and Pharmacology

March 2020

Signed on behalf of the Faculty of Science: _____

Acknowledgements

First and foremost, I would like to thank my lead supervisor Dr Paul De Bank, who's guidance, patience, and kindness have been invaluable to me over the last 5 years, and who has my undying gratitude and respect. I only hope that I have made a worthy student.

I also thank my second supervisor, Dr Marianne Ellis, as well as Dr Lorenzo Caggiano, for giving me their insights, advice, and sage counsel whenever I've needed it.

I also extend my gratitude to the friends I have made during my time at Bath (within and beyond the scientific community), who have brought that extra bit of light into the last 5 years: Scott Allan, Dr Christina Keating, Jonathan Rowney and Savannah Britton (who have also provided essential, much-appreciated support as members of technical staff), Jessica Schulz, Suet Lee, Nikki Sykes, and Somsee of Salathai: the best restaurant in Bath!

My former personal tutor, Patricia Proctor, and senior laboratory demonstrator, Dr Jenny Moran, who were kind enough to provide the reference letters which allowed me to begin my PhD, and have offered words of encouragement since. I hope I have managed to do justice to the sentiments contained in those letters.

The members of the medical and mental health facilities of the university, as well as wider Bath and Bristol, who's services I have frequently prevailed upon.

And of course my family. Especially my parents, little sister, and grandparents, without whom my life would be empty.

Abstract

The sustainability of conventional meat production has long been in question [1]. An alternative may be found in *in vitro* production of meat from myogenic progenitor cells. A crucial component in this model is a highly renewable, easily processed, edible, and non-animal-derived bioscaffold [2, 3]. This thesis explores the compatibility of a small number of natural biomaterials, mainly plant-based to satisfy the aforementioned criteria, and their development into a bioscaffold on which myogenic cells may be cultured into muscle tissue.

Hydrogel scaffolds were produced from κ-carrageenan by crosslinking aqueous carrageenan solutions using potassium chloride (KCl). The resultant hydrogels were highly susceptible to degradation, and results provide evidence that this is due to displacement of the crosslinking potassium ions by ambient sodium ions. Results showed that the surface coating of these hydrogels imparted stability, particularly when chitosan was used as the coating material. However, coated hydrogels still appeared to lack the ability to support C2C12 cell growth. Another coating material, *Bombyx mori* silk fibroin (SF), was briefly analysed independently for its biocompatibility with myogenic cells. Films of this silk fibroin were able to support C2C12 proliferation and differentiation. Microfluidic flow focusing was used to produce SF microcarriers. When a mixture of methanol, oleic acid, and span 80 was used as the continuous / outer phase, SF particles with mean diameters as high as 318.87 μm ± 17.89 μm were produced.

Zein was analysed for its ability to support the growth (measured by resazurin metabolic assay), spreading (via image analysis), and differentiation (image analysis after immunostaining for myosin heavy chain) of myogenic cells on zein films alongside tissue culture plastic (TCP) controls. Zein displayed an ability to facilitate these cell functions to a degree comparable to that of TCP Various methods were employed in order to produce scaffolds from zein which would be well-suited for implementation in commonly used bioreactor designs: microfluidic flow focusing and emulsification precipitation for microcarrier scaffolds, as well as wet-spinning into a non-solvent (water) for macrofibre membranes, and electrospinning for nanofibres. The attempts to produce microcarriers and wet-spun fibres were unsuccessful, with the majority of particles exhibiting mean diameters consistently below 50 μm, and fibres failing to precipitate into solid constructs. Electrospun nanofibers were successfully produced, but showed instability in water. Carbodiimide-crosslinking appeared to stabilise the fibres, but reduced their cytocompatibility. Crosslinking via treatment with citric acid also imparted stability, but considerably increased the time taken for production. Allowing the fibres to remain adsorbed to a substrate stabilised the fibres without these drawbacks, and so electrospun zein fibres show great potential as a bioscaffold for cultured meat and wider tissue engineering applications.

List of abbreviations

ACTA1 – Actin alpha 1

ANOVA – Analysis of variance

BMP4 - Bone morphogenetic protein 4

cDNA - Complementary DNA

CMFDA - 5-chloromethylfluorescein diacetate

DDA – Degree of deacetylation

DNA – Deoxyribonucleic acid

dH_2O – Distilled water

DMEM - Dulbecco's Modified Eagle's Medium

DMSO - Dimethylsulphoxide

ECM – Extracellular matrix

EDC – 1-Ethyl-3-(3-dimethylaminopropyl) carbodiimide

EDTA - Ethylenediaminetetraacetic acid

ERK - Extracellular signal-regulated kinases

FABP4 - Fatty-acid-binding protein 4

FAK – Focal adhesion kinase

FBS – Fetal bovine serum

FN1 - Fibronectin domain 1

GASGER – Glycine, alanine, serine, glycine, glutamic acid, and arginine

GDA – Glutaraldehyde

GFOGER – Glycine, phenylalanine, pyrrolysine, glycine, glutamic acid, and arginine

GHR – Growth hormone receptor

GLOGER - Glycine leucine, phenylalanine, glycine, glutamic acid, and arginine

HARV – High aspect ratio vessel

HMDS – Hexamethyldisilazane

HPLSCs - Human periodontal ligament stem cells

HSV-2 - Herpes simplex virus 2

MES - 2-ethanesulfonic acid

mH_2O – MilliQ water

MRF4 - myogenic regulatory factor 4

MTT - 3-(4,5-dimethylthiazol-2-yl)-2,5-diphenyltetrazolium bromide

MYf5 - Myogenic factor 5

MYH – Myosin heavy chain

MyoD – Myoblast determination protein

NADH - Nicotinamide adenine dinucleotide

N-cadherin – Neural cadherin

NMR – Nuclear magnetic resonance

NHS – N-Hydroxysuccinimide

Pax7 – Paired box 7

PBS - Phosphate buffered saline

PCL - Polycaprolactone

pH – Potents of hydrogen

PGA – Polyglycolic acid

PLGA - Poly(lactic-*co*-glycolic acid

PLLA - Poly-L-lactic acid

PPARγ - Peroxisome proliferator-activated receptor gamma

PVA - Polyvinyl alcohol

P/S - Penicillin-Streptomycin

RGD - Arginylglycylaspartic acid

SEM – Scanning electron microscopy

SF – Silk fibroin

TCP – Tissue culture plastic

UV – Ultraviolet

VCAM-1 – Vascular cell adhesion protein 1

YAP – Yes-associated protein

Lists of Figures, tables, and equations

Equation number	Equation title	Page
1	DDA from the magnetic resonance of various hydrogen nuclei in chitosan.	96

Chapter 1 – Introduction

1.1 Thesis overview

This work attempts to determine whether a purely plant-based bioscaffold can be produced which can support the proliferation and differentiation of myogenic cells to a degree comparable to scaffolds produced from animal-derived or synthetic biomaterials, in order to further develop the field of cultured meat. This chapter contains a literature review of tissue engineering with particular emphasis on muscle-tissue culture. Topics of focus will include an overview of tissue engineering, an overview of cultured meat, sources of myogenic cells and their development into muscle tissue, choices of biomaterials for use in scaffolds, and considerations for scaffold design. The aims and objectives of this body of research will be stated at the end of the chapter. Chapter 2 details the experimental methodologies (and materials) used in this research. Chapters 3, 4, and 5 present and discuss the results of the research. Chapter 3 explores the use of carrageenan scaffolds for the culture of myogenic cells. Chapter 4 analyses the cytocompatibility of zein and silk fibroin (from *bombyx mori*) with regard to myogenic cells, and chapter 5 explores methods of developing these materials into more complex bioscaffolds whose morphologies are well-suited to bioreactor implementation. Chapter 6 summarises the work presented throughout this thesis, drawing conclusions and discussing potential avenues for further work.

1.2: Tissue Engineering

Any work in which engineering and biological sciences are applied to the production, maintenance, or restoration of biological tissue can be classed as part of the multidisciplinary field of tissue engineering [4]. Though tissue engineering is a highly interdisciplinary field, the general paradigm is usually geared toward regenerative medicine applications, as outlined in figure 1.01.

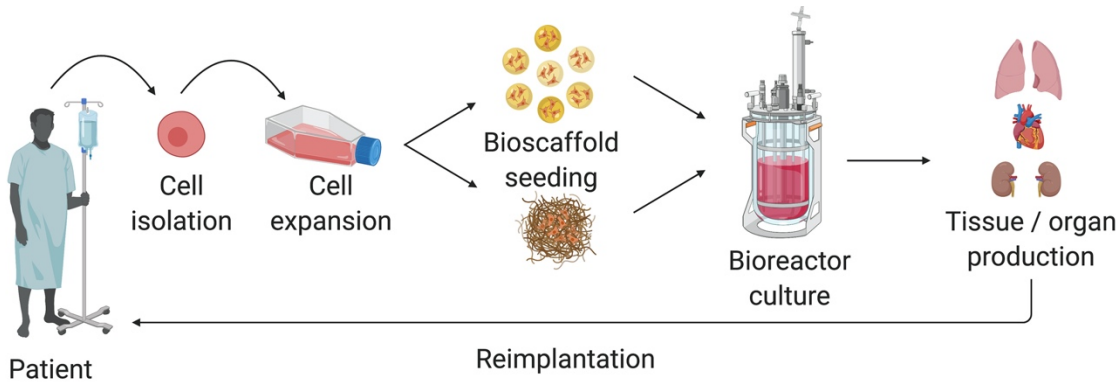

Figure 1.01: Overview of the tissue engineering process with emphasis on regenerative medicine: the usual application of the field. Created with Biorender.com.

As can be seen in figure 1.01, the typical process involves the isolation of stem cells from a patient, the expansion of their numbers (which can be greater than 10^{10} cells if transplanting fully differentiated cells which will no longer proliferate in vivo [5]), and their seeding onto scaffolds. These scaffolds (shown in figure 1.01 as particulate and fibrous scaffolds) are placed into a bioreactor to facilitate their development into complex 3-dimensional tissue, which can then be implanted into the patient in order to replace defective tissue or grafted to aid recovery of damaged tissue.

1.2.1 Scaffold design

1.2.1.1 Biomaterial sources

Biomaterials from which scaffolds are constructed are typically one of three general classes [6]. Natural polymers are perhaps the most effective choice, as these are commonly bioactive; containing molecular structures that bind cells and induce signalling pathways [6]. Synthetic biomaterials have the drawback of not typically being innately bioactive (for which reason areas of research such as bioprinting are key, wherein scaffolds can be effectively functionalised via 3-dimensional (3D) printing of bioactive features), though their structure and mechanical properties can be tuned more easily than natural polymers [7]. A third category, ceramics, are typically defined by their mechanical properties: in that they exhibit high levels of brittleness [6]. They are not typically applied to scaffold designs for soft tissues, being more suited for bone-tissue culture [6].

1.2.1.2 Fibrous scaffolds

Scaffolds for tissue engineering can be produced by a wide variety of methods [8]. Fibrous scaffolds can, for example, come in the form of nanofibers [9] or macro-sized hollow fibre membranes [10]. The former are particularly attractive as they mimic the structure of the fibrous extracellular matrix (ECM) [11, 12].

Electrospinning is a notable method by which nanofibrous scaffolds can be produced. In the electrospinning design, a polymer solution is extruded through a spinneret onto which an electrode is attached [13, 14]. When the electric charge administered to the spinneret is sufficient to overcome the surface tension of the polymer solution droplet at its tip, the polymer solution erupts as a jet [13, 14]. As the solution is drawn out into an ultrathin stream, the solvent evaporates, leaving the polymer as a solid fibre [13, 14]. The charged polymer fibre is drawn to an earthed collector, causing it to stretch [13, 14]. The surface charges of the fibre also give rise to repulsion forces, which causes a whipping effect as the fibre travels to the collector [13, 14]. This is similar to the practice of dry-spinning, wherein a polymer solution extruded from a spinneret is subjected to heat instead of electrostatic forces, which causes evaporation of the solvent and leaves behind a solid, ultrathin polymer fibre [14].

Wet-spinning is a process by which macroscopic fibres can be produced. In this model, the polymer solution is extruded directly into a coagulation bath, which contains a liquid which is miscible with the polymer solvent but is a non-solvent for the polymer itself [14]. Phase exchange takes place between the polymer solvent and the coagulation bath's non-solvent, leading to precipitation of solid polymer fibres [14]. This approach can also be used to produce hollow fibre membranes via the simple addition of a boring element at the centre of the polymer solution stream [10, 15].

These methods for producing fibrous scaffolds are illustrated in figure 1.02.

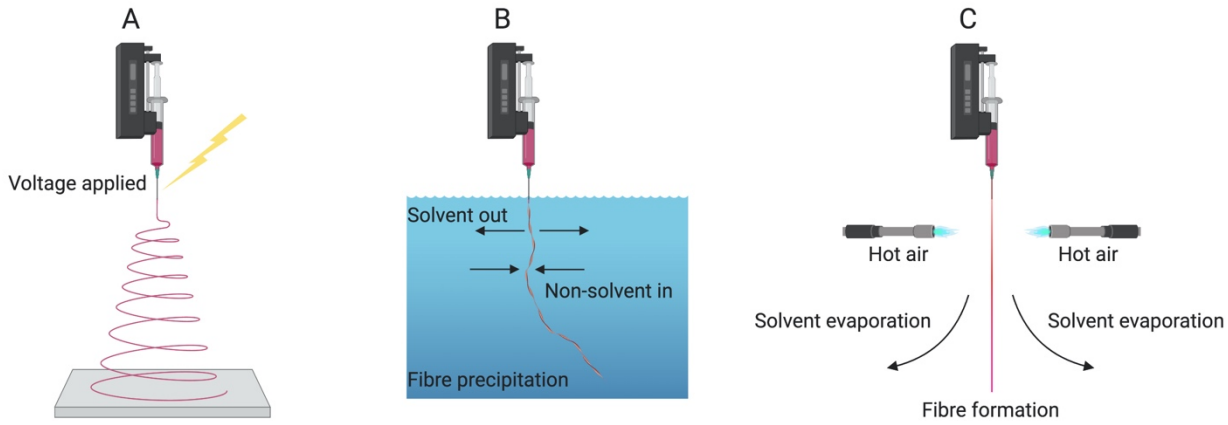

Figure 1.02: Overview of various methods of producing fibrous scaffolds. A: electrospinning, B: wet-spinning, C: dry-spinning. Created with Biorender.com

1.2.1.3 Particulate scaffolds

Particulate scaffolds may be used in two ways. Cells may be encapsulated within the particles, commonly by suspending them in the polymer solution before being formed into solid particles. Cells may also be seeded on the surface of the particles, and particles used for this purpose are termed microcarriers. Microcarriers have the advantage of a large (combined) surface area on which to seed cells, as well as being compatible with various designs of bioreactors (to be discussed in section 1.2.2). Another advantage of the use of particulate scaffolds, is that more microparticles can be added to the culture environment as cell proliferation occurs, as cells are able to migrate between beads [16].

There are various methods by which microparticles can be produced. Emulsification precipitation, illustrated in figure 1.03, is perhaps the most commonly employed method by which microparticles are generated [17]. This procedure involves mixing the polymer solution with a non-solvent, often hydrophobic in nature [17]. The solutions are agitated, which generates shear stress [17]. This in turn causes the polymer solution to form droplets which are suspended as an emulsion in the non-solvent, and can then be precipitated or crosslinked to generate solid particles [17].

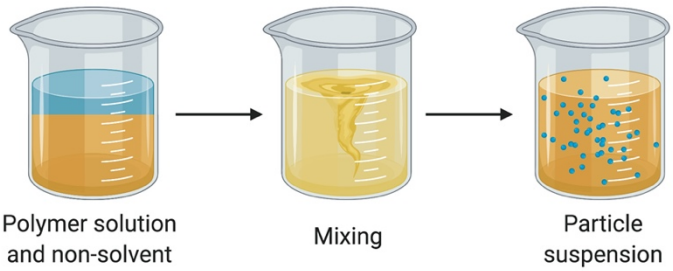

Figure 1.03: Overview of emulsification precipitation production of microparticles. Created with Biorender.com.

Another method by which microparticles can be produced, microfluidic flow focusing (illustrated in figure 1.04), also relies on generating shear forces between two immiscible solutions in order to generate microparticles: in this design, a solution of non-solvent (be it a hydrophobic phase such as oil [18], or a crosslinker solution [17], as appropriate for the polymer) is pumped through a the double-ended section of a T-shaped flow channel and allowed to flow out of the exit aperture. This non-solvent is referred to as the “continuous” or “outer” phase. The polymer solution, referred to as the “disperse” or “inner” phase, is then pumped in, at a slower flow rate, via the second flow channel. The mechanical sheer exerted upon the incoming, slower-flowing polymer solution (the disperse phase) by the faster-flowing non-solvent solution (the continuous phase) causes the disperse phase to enter the continuous phase as droplet suspensions [17]. Microfluidic flow focusing is noted to provide a higher degree of control over resultant particle size when compared to other particle producing techniques [17].

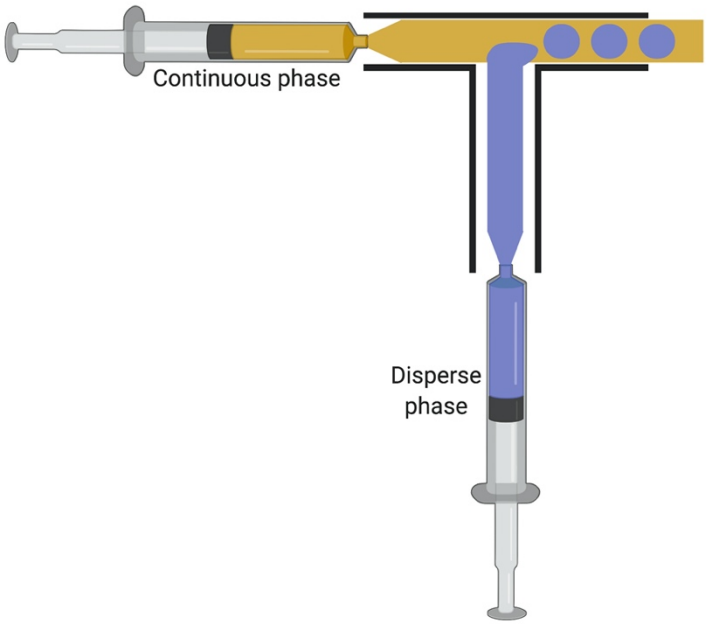

Figure 1.04: Overview of microfluidic flow focusing for production of microparticles. Created with Biorender.com.

To summarise, fibrous and particulate designs for scaffolds each have their own distinct merits that make them suitable for the work presented here: nanofibrous scaffolds have the distinct advantage of simulating the fibrous nature of the extracellular matrix (ECM) [11, 12]. Larger macrofibre membranes have the potential to be applied to innovative bioreactor designs (see section 1.4.4.1), wherein large amounts of cells can be cultured on their vast surface area, whilst requiring relatively little growth medium [10, 15]. Particulate scaffolds are highly versatile; being applicable to a wide-range of bioreactor designs [19, 20], and afford the ability to add more particles to a culture system as cell populations increase [16].

1.2.2 General function and design of bioreactors

A bioreactor is an umbrella term for a vessel in which cell culture can take place, and whose conditions (such as temperature, potents of hydrogen (pH), oxygen (O_2) and carbon dioxide (CO_2) concentration) can be precisely monitored and controlled [20-22]. Whilst the role of the bioscaffold is essentially, as mentioned, to provide a mechanical framework to which cells may adhere, and to provide molecular stimulation for their signalling pathways, the role of the bioreactor is essentially to provide for the cells' needs in terms of physiological environment.

Critically, with regard to tissue engineering applications, a bioreactor must aim to reproduce the physiological conditions the cultured cells would experience *in vivo* [20]. Other important aspects of an ideal bioreactor are the ability to carry out cell culture under antimicrobial conditions and a high degree of adaptability; since fully developed tissue is usually composed of more than one type of cell, and the physiological needs of the cells are likely to change over time [21] (for example, a reduction in serum triggering differentiation of densely populated myoblasts). Another is the capacity to produce dynamic conditions within the culture environment; static conditions in bioreactors are unfavourable, as they lead to the build-up of variances in factors such as pH, oxygen and CO_2 concentration, and presence of nutrients of cellular waste products throughout the culture environment [21]. Many types of cells also experience mechanical stimuli in vivo: a need which bioreactors must also accommodate [21]. Notably, the aforementioned dynamic environment of the bioreactor produced the first mechanical force exerted on the cells (in the form of sheer stress) [21, 23]. Of particular relevance to this work, muscle tissues experience stretching and self-generated contractile forces. Bioreactors can facilitate the former by exerting tensile stress on the cultured cells, and the latter by application of electrical current [23], to be discussed further in section 1.5.

Bioreactors come in many forms, usually (but not always) classified by their method of producing a dynamic internal environment. Notable examples include: Stirred tank bioreactors, in which a physical stirrer agitates the liquid environment of the vessel, are perhaps the most common form of bioreactor. The aforementioned stirred flask is of course an example of the stirred tank bioreactor [20, 24, 25]. Rotating wall bioreactors, which involve a horizontal, cylindrical vessel whose outer wall rotates, these bioreactors have the advantage of producing a dynamic environment for cultured cells whilst maintaining low shear stresses [20, 23, 26]. Stirred-tank and rotating wall vessels are particularly suited to particulate scaffolds. Hollow fibre bioreactors, which are specially designed to work with a particular type of scaffold, that being (as the name implies) hollow fibre membranes. Hollow fibres allow cells to adhere to the internal or external surface of the fibre, presenting a large amount of scaffold surface area on which cells may adhere, and their structure replicates blood capillaries which supply cells with essential factors in vivo, as culture medium can be transported along the hollow interior and diffuse through the porous walls [10, 20, 27]. Alternately, medium can be perfused across the outer surface of the fibres, and cells adhered to the interior surface are shielded from shear stress of the liquid flow, which may allow for higher flow rates and higher degrees of nutrient delivery [10, 20]. The hollow fibres of Ellis *et al.* were applied to a bioreactor by taking a bundle of 10 such fibres and encasing them in a glass tube, culture medium could then be applied coaxially [15]. Airlift bioreactors,

which inject gasses at the base of a vertical cylinder. As the gases rise through the culture medium, they create dynamicity in the liquid, before escaping through the top [28]. Fixed-bed bioreactors, which involve the immobilisation of cells onto a static matrix (usually affixed to the interior wall of a cylindrical vessel), with medium and oxygen delivered by radial flow through the centre [29]. These are perhaps well-suited for fibre matrices. Fluidised-bed bioreactors, which involve cells on or encapsulated within microparticles that are not fixed to a surface within the vessel. The culture medium flows through a vertical cylinder with filters to prevent the microparticles escaping the reactor with the outflow of medium, and the microparticles are thusly fluidised within the reactor [30]. These are also suited for particulate scaffolds. A summary of these bioreactor designs is illustrated overleaf in figure 1.05.

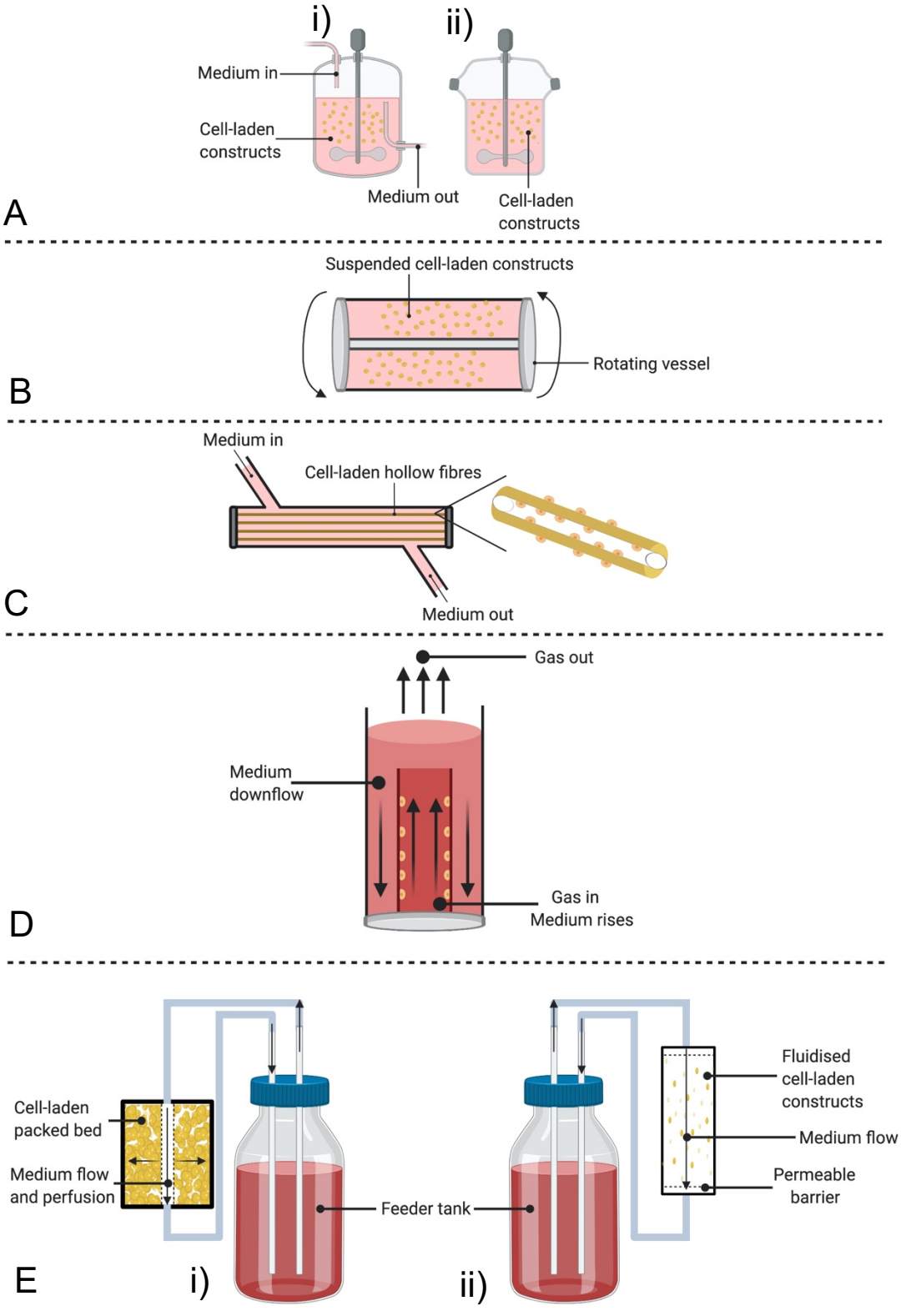

Figure 1.05: Summary of bioreactor designs discussed in section 1.2.2. A: Stirred-tank bioreactors as described by Martin *et al.* [20] i) continuous flow, ii) batch feed. B: Rotating wall bioreactor as described by Martin *et al*. [20] C: Hollow-fibre bioreactor as described by Wung *et al.* [10]. D: Airlift bioreactor as described by Ondrey [28] E: i) Fixed-bed bioreactor as described by Pörtner and

Barradas [29], ii) fluidised-bed bioreactor as described by Nikravesh *et al.* [30]. Created with Biorender.com

1.3 Myogenic cells and myogenesis

1.3.1 Features of muscle tissue

Muscle cells are characterised by their high degree of actin and myosin expression, giving rise to a contractile system far more developed than that of other types of cell [11]. It is well known that mammalian muscle tissue comes in four varieties: skeletal muscle, cardiac muscle, smooth muscle, and myoepithelial muscle [11]. The skeletal and cardiac varieties differ from the latter two in that their contractile proteins (actin and myosin) are arranged into aligned structures, allowing the cells to contract more efficiently along an axis [11]. Specifically, thick myosin bands are enclosed by thin actin bands in long chains whose repeating units are known as sarcomeres [31]. These two categories of striated muscle are distinct from one another in that skeletal muscle is the variety of muscle tissue responsible for voluntary movement, whereas cardiac muscle operates on an involuntary basis [11]. Smooth muscle cells are not striated, and so not specialised for contraction along any particular axis, and are involved in involuntary mechanical processes such as the movement of food along the gastrointestinal tract [11].

Skeletal muscle is the tissue of focus in this work, as it is the type of muscle most often consumed as meat. In addition to their actin / myosin striations, skeletal muscle cells are defined by their being composed of multiple nuclei from numerous progenitor cells which have fused together into a tubular shaped cell, termed a myotube [11]. These myotubes align together in bundles surrounded by connective tissue (termed the perimysium) to form superstructures known as muscle fibres, which in turn align to form a complete skeletal muscle (also surrounded by connective tissue, termed the epimysium) [11, 31].

The myotubes of skeletal muscle are further subcategorised by the nature of their contractile ability: “fast twitch” muscle fibres are specialised for quick contraction, operate via anaerobic respiration and contain fewer mitochondria than their “slow twitch” counterparts, which are specialised for slower but sustained contraction powered by aerobic respiration [11, 31, 32].

1.3.2 Origin of myogenic progenitor cells *in vivo*

The term “myogenesis” refers to the formation of muscle tissue, and of course myogenic cells are precursors of differentiated muscle cells. Skeletal muscle is the tissue of focus in this work, as it is the type of muscle tissue which is most often consumed as meat. The defining traits of fully developed skeletal muscle cells are their arrangements of actin and myosin to create striations, the presence of multiple nuclei, an overall tubular shape, and their involvement in voluntary movement (as opposed to cardiomyocytes, which have striations but are not under voluntary control of the larger organism) [11]. Skeletal muscle cells, also referred to as myotubes, are formed from multiple myogenic precursor cells termed myoblasts [11]. Myoblasts first appear during embryonic development; arising from cell-blocks called somites (which in term arise from the mesoderm (one of three germ layers in early embryos) [11, 33]. These cell blocks give rise to more specialised forms of cells, including myoblasts which, as stated, are precursors for skeletal muscle cells [11].

1.3.3 Formation of myotubes from myoblasts

While proliferating, myoblasts exhibit spreading (also referred to as migration or motility) where rearrangement of the actin cytoskeleton produces changes in the overall shape of the cell, which becomes elongated and jagged [34]. This spreading / migration is a precursor stage to myoblastic aggregation, wherein myoblasts interact by way of their cell surface receptors [35]. Knudsen *et al.* noted that neural cadherin (N-cadherin), a surface-expressed adhesion molecule which facilitates cell-cell adhesion via homophilic associations [11], is involved in myoblast aggregation: the introduction of anti-N-cadherin antibodies inhibited this aggregation [35]. This also had a deleterious effect on the subsequent stage of myotube development: fusion [35].

With removal of signal proteins such as fibroblast growth factor and hepatocyte growth factor, myoblastic proliferation becomes arrested, and the individual myoblasts merge to form multinucleated myotubes [11]. The number of cells fusing to form myotubes is commonly expressed as a percentage of the total cell population, and termed the fusion index. Myoblast fusion is facilitated by activation of various genes [11], which lead to increased expression of a variety of adhesion proteins, both cell-cell surface adhesion proteins as previously described, and cell-matrix adhesion proteins such as integrin α3, whose inhibition also leads to reduced myoblast fusion [36]. The ability of myoblasts to fuse into myotubes was not fully eliminated in the aforementioned study of Knudsen *et al.* owing

to the presence of adhesion glycoproteins that, unlike N-cadherin, operate independent of calcium [37]. The various adhesion proteins interact with each other to form complexes: for example, integrin α3 associates with CD9 and CD81, while integrin α4 associates with vascular cell adhesion protein 1 (VCAM-1) and then also with integrins β1 or β7, denoting the highly intricate nature of cell-cell binding in myoblast fusion [36]. Binding of myoblasts via cell-cell binding proteins is not sufficient to produce myotubes, however. Following this, the adhered cells begin to rearrange their actin cytoskeleton in order to bring their membranes as close as possible [38]. It is theorised by Kim *et al.* that the bilayer membranes of the cells are then rearranged in order to bring phosphatidylserine lipids (which typically reside on the interior surface of the membrane bilayer) of each into contact, which facilitates destabilisation and subsequent merging of the cell membranes [38, 39]. Phosphatidylserine expression on the outer membrane surface is noted to play a role in apoptosis by signalling for macrophage engulfment [39], which would also involve structural changes in the membrane of the macrophage. Indeed, Jeong *et al.* demonstrated that phosphatidylserine is presented on the cell surface during myoblastic fusion, and that the introduction of phosphatidylserine produced in vitro enhances the formation of myotubes [39]. Once myoblasts have been incorporated into the larger structure of the myotube, their nuclei permanently cease replication of DNA [11]. More myoblasts can be added to the myotube structure, but this process is eventually halted by the secretion of a signalling protein, myostatin, from the myotube itself, which prevents proliferation and differentiation of myoblasts [11].

1.3.4 Satellite cells

This cessation of deoxyribonucleic acid (DNA) replication and prevention of additional myoblasts to the myotube does not, however, mean that the myotube cannot grow further. Cells termed satellite cells are found in between the basal lamina of the myotube and the cell membrane [11, 40]. Even upon their first published identification by Mauro, satellite cells were correctly hypothesised to recommence myoblastic function in the event of damage to the myotube [41]. The degree of damage to the myotube(s) have a direct impact on the number of satellite cells activated, and the length of their period of proliferation before entering the differentiation stage [40]. The activation of satellite cells is likely induced by the release of inflammatory response molecules when damage to the myotubes occur [40]. In their dormant state, satellite cells have been noted to hold low densities of organelles within their cytoplasm (including Golgi apparatus, endoplasmic reticulum, and mitochondria) [42]. Upon stimulation however, satellite cells were observed to increase their volume of cytoplasm and increase organelle development [42]. Satellite cells can be found in larger

numbers in slow-twitch muscle fibres as opposed to fast-twitch fibres, and are generally found toward the ends of the muscle fibres [40]. It has been noted that the stage of satellite cell activity can be ascertained by analysis of the markers they express; satellite cells in a state of proliferation will express paired box 7 (Pax7) and myoblast determination protein (MyoD), whereas those in a state of differentiation will express only MyoD [40]. The capacity of satellite cells to form new muscle tissue is not unlimited: excessive and repeated stimulation will eventually exhaust their ability to proliferate [11].

1.3.5 The use of myoblasts versus satellite cells

Whether for production of muscle grafts for reimplantation into a patient from whom the cells were derived, or for production of muscle tissue for consumption as meat, satellite cells are the ideal choice. With regard to the production of muscle grafts, cells would need to be harvested from the patient in order to prevent immune rejection upon reimplantation, which necessitates the use of satellite cells as this will involve post-natal specimens. With regard for the cultivation of muscle tissue for consumption, the use of a post-natal donor herd would be far simpler than large-scale use of embryos, and is less likely to raise ethical concerns among consumers. Their main advantage is that they can be harvested from postnatal muscle biopsies, whereas myoblasts would need to be harvested from embryos, which are far more difficult to source than simple muscle biopsies, and may raise ethical concerns amongst patients and / or consumers. However, the process of isolating primary satellite cells from existing muscle tissue is labour intensive and costly [43] . The work presented in this thesis utilises an immortalised myoblastic cell line (C2C12) rather than primary satellite cells. Cell lines have the capacity for a vast number of doublings, potentially unlimited, in contrast with primary cells which have a finite capacity for proliferation [11, 43-45]. Since repeatedly taking biopsies from relevant tissue and isolating cells of finite proliferative capacity would place a substantial drain on time and resources, many research studies concerning tissue engineering utilise immortalised cell lines as model cells. Mouse-derived C2C12 myoblasts are used as model myogenic progenitor cells in a vast number of such studies, including the work presented in this thesis, this ensures comparability of the results. Additionally, as of the time of this work, there is a lack of commercially available livestock-derived immortalised cell lines.

As stated, however, a functional model of in-vitro meat production would utilise satellite cells derived from muscle biopsies from donor herds. This is due to numerous factors including a loss of or alteration cell functions as a result of the processes for generating continuous

cell lines (such as, irradiation and introduction of carcinogens) [44]. For example Alge *et al.* noted that primary retinal epithelial cells exhibited increased expression of proteins involved in key processes such as cell adhesion, migration, and ECM interactions when compared to hTERT cell lines [46]. Additionally, the lack of commercially available, livestock-derived, immortalised cell lines and consumer concern regarding the use of genetically modified organisms (which an immortalised cell line would be) in food are further considerations as to why primary cells would be used in the final model of cultured meat over cell lines.

In summary, due to their cost-effectiveness, potentially unlimited proliferative potential, and ease of use, cells of the immortalised C2C12 line are to be used in research to assess the viability of potential biomaterials and scaffold designs for the culture of muscle-tissue. Production of the consumable meat would be done using primary cells, specifically satellite cells isolated from muscle biopsied taken from livestock donor herds.

1.4 Scaffolds for muscle-tissue culture

1.4.1 General function of the scaffold

In order to understand the role of the scaffold in this process, one may study the gold-standard scaffolds produced and used by the cells themselves *in vivo*, that being the aforementioned ECM [11]. The most obvious role of the ECM is to provide a structural framework on which adherent cells may grow, in the same way construction scaffolding provides a framework to support the construction of a building, and for a time this was thought to be the sole function of the ECM [47]. It has since become clear that the molecular structure of the ECM initiates cell signalling pathways via associations with their transmembrane receptors, and these signalling pathways govern a vast array of cellular processes from proliferation to apoptosis [12, 47], and immobilise growth factors [48]. With this in mind, scaffolds produced and used in vitro must have the capacity to provide a structural framework for cells and molecular properties which can initiate the correct signalling pathways of adhered cells.

An important aspect of muscle-tissue culture is the production of aligned myotubes, as this facilitates the contractile abilities of the muscle [9, 11, 49]. Differentiating myoblasts can be induced to form myotubes in alignment with one another by modifying the topography of the scaffold. For example, Aviss *et al.* and Choi *et al.* induced the formation of aligned myotubes

by producing electrospun nanofiber matrices where the fibres exhibited a high degree of alignment, as opposed to randomly aligned fibres [9, 49].

1.4.2 Gold-standard biomaterials for muscle-tissue culture

As stated, the ECM represents the gold-standard bioscaffold produced in vivo. It is no surprise, therefore, that the various biomaterials which form the ECM are well-suited for production of scaffolds in vitro. Three distinct layers have been characterised in the ECM of skeletal muscle [50]: the epimysium: which encases the complete muscle, the perimysium: which encases bundles of myotubes, and the endomysium: which encases individual myotubes [50]. The ECM is composed of various proteins:

Collagen is the most notable biomaterial for use in tissue culture, being the most prominent protein of the extracellular matrix and indeed the mammalian body, accounting for 25% of all proteins in the body [11]. There are many types of collagen; types I, II, III, V, and IX have a fibrous morphology [11, 51], and types I and II are most prominent collagens in skeletal muscle ECM [50].

Fibronectin is another notable protein of the ECM. It is a glycoprotein dimer composed of two subunits joined by a disulphide bridge [11, 51]. It is not naturally fibrous, but cell-binding can cause it to become so, formation of additional disulphide bonds connect dimers and lead to the formation of insoluble fibronectin fibrils [11, 51]. Each of the dimers are composed of domains, which contain modules that facilitate associations with other fibronectin dimers (as described), binding to cell surface adhesion receptors, as well as binding to heparin, collagen, and laminin to facilitate organisation of the ECM [11, 50-52].

Also present in skeletal muscle ECM is laminin [50, 51], specifically in the basal lamina [11, 50]. Laminin-1 is composed of three chains, α, β, and *γ*, which intertwine in a helix before separating [11, 51]. The α chain of laminin as well as the coil-structure of the protein are able to bind to cell-surface integrins [11, 50], and the α chain in particular has been noted to be integral in the formation of myotubes [50].

Also notable are gelatin and Matrigel, neither of which are present in the ECM, but are derived from ECM proteins. Gelatin is formed from hydrolysis of type I collagen [51, 53], and Matrigel is a blend of basal laminar proteins including laminin and type IV collagen [54].

The individual components of the ECM have the capacity to support cell growth: For example, Bardouille *et al.* cultured C2C12 myoblasts to differentiated myotubes on Petri dishes coated with collagen [55]. Chaturvedi *et al.* cultured C2C12 myoblasts to differentiated myotubes on type I collagen and fibronectin [50]. Chaturvedi *et al.* also, however, demonstrated that the complex assembly of these various components provides an optimal scaffold on which myogenic cells may be cultured: they found that although collagen and fibronectin supported proliferation and formation of myotubes to a degree highly comparable to that on the decellularised ECM, myotubes formed on the decellularized ECM exhibited a higher degree of alignment, and that the decellularized ECM appeared to induce activation of genes associated with differentiation to a more efficient degree than collagen or fibronectin alone [50]. Wilschut *et al.* in particular, compared myoblastic cell culture on all of the above-mentioned materials [52]. They noted that all were able to support the culture of myoblasts to differentiated myotubes [52]. However, there was an apparent variance in the efficiency with which this was accomplished: the cells cultured on Matrigel appeared fully confluent after 3 days. Those on collagen and gelatin appeared to be near-confluent, cells on fibronectin showed a moderate degree of proliferation, and laminin samples showed a relatively high amount of empty space on the culture surface [52]. They also analysed the expression of differentiation markers over time on the biomaterials: 2 days after the induction of differentiation, cells on collagen and gelatin showed significantly higher expression of desmin than those on other biomaterials [52]. At the same timepoint, cells on Matrigel and laminin appeared to show the highest expression myosin heavy chain (MYH) 2, and at the 5-day timepoint, cells on Matrigel exhibited significantly higher expression of myogenin than those on other biomaterials [52]. Myotubes formed on these biomaterials also showed an apparent variance in fusion indices: cells on laminin appeared to show the highest fusion indices, followed by Matrigel, gelatin, collagen, and fibronectin at the lowest [52].

1.4.3 Other biomaterials in scaffolds for muscle-tissue engineering

1.4.3.1 Silk fibroin

Silk proteins are produced by a variety of insect and arthropod species. Silk as produced by insects is composed of two proteins: fibroin and sericin [56]. The fibroin forms a fibrillar core, whilst the sericin exists as a gum sheath surrounding the fibroin [56]. Whilst sericin exhibits some degree of cytocompatibility, it is also noted to trigger immune responses [56]. For this reason, sericin is typically removed from the silk, leaving only the fibroin, before the

silk can be used for tissue engineering applications [56]. *Bombyx mori* silk fibroin lacks arginylglycyllaspartic acid (RGD) or similar integrin-binding protein motifs and, therefore, relies on the presence of positively charged amino acid side-chains within its structure to facilitate cell-binding [57, 58]. Specifically, amino acids with positively charged side chains such as poly-L-lysine are able to bind to a thin, negatively charged glycoprotein layer (called the glycocalyx) expressed on the cell surface [57].

Chaturvedi *et al.* produced lyophilised *bombyx mori* silk fibroin sponges for use as bioscaffolds, on which human skeletal muscle myoblasts were observed to proliferate and differentiate into myotubes [59]. They also noted that, when cultured on silk fibroin produced by *bombyx mori*, cells expressed higher levels of the MyoD1 and MYH7 differentiation markers than those cultured in silk fibroin produced by *antheraea mylitta*, whose most highly expressed differentiation markers were actin-alpha-1 (ACTA1) and MYH7 [59].

1.4.3.2 Chitosan

Chitin, commonly derived from crustacea, is the second most abundant polysaccharide in nature after cellulose [60, 61]. Its repeating unit is a ring of carbon and oxygen with hydroxyl side-chains, as well as an acetyl group connected to the main unit by a nitrogen bridge [60]. When chitin is reacted with alkalis or acids, the acetyl groups can be converted to amine groups, at which point the biomaterial is referred to as chitosan [60, 61]. The amount of acetyl groups converted to amine groups is expressed as a percentage of the total initial acetyl groups, termed the degree of deacetylation (DDA%) [61, 62]. Freier *et al.* noted that the degree of deacetylation has a direct impact on chitosan's biocompatibility; they found that chitosan samples of higher DDA% were able to maintain cultures of dorsal root ganglion neurons with higher degrees of viability [63]. Although chitosan, as a polysaccharide, has no inherent protein structures with which to bind cell-expressed integrins, it is able to adsorb serum-proteins such as fibronectin [64, 65].

Hajiabbas *et al.* produced hydrogels from a blend of chitosan and gelatin, on which they were able to culture muscle-derived cells [66]. They noted that proliferation of these muscle-derived cells occurred on gels containing 4% chitosan (w/v), but not on gels containing 2% or 6% chitosan [66]. Ruini *et al.* produced fibrous chitosan scaffolds on which they cultured C2C12 myoblasts [67]. They noted positive proliferation over time, which was enhanced on scaffolds whose fibres were aligned [67].

1.4.3.3 Alginate

Alginate is a biomaterial used in the formation of hydrogel scaffolds (to be discussed). It is a polymer derived from the Phaeophyceae class of algae [68]. The repeating units of the alginate polymer chain are D-mannuronic acid and L-guluronic acid [69]. Alginate lacks the ability to directly bind cells, having no structures which can associate with cell integrins, and lacking the ability to adsorb serum proteins as chitosan does [70]. Therefore, studies involving the use of alginate as a scaffold commonly exploit the polymer's carboxyl groups in order to covalently attach integrin-binding protein motifs such as RGD [70-73]. The presence of L-guluronic acid within the structure of alginate is what enables it to form hydrogels; at points in the polymer chain where the L-guluronic acid residues are found in sequence, they form diamond-shape protrusions [74]. Divalent cations, most commonly calcium (but not magnesium), can then be applied to displace the monovalent sodium ions within the alginate's structure [74]. The diamond-shaped double-L-guluronic acid structures of different polymer strands align in parallel, creating pockets in which the divalent calcium ions facilitate aggregation of a large number of monomers [74, 75]. This 'encasement' of the calcium ions is the reason this crosslinking mechanism has been termed the "egg-box model" [74, 75].

Rowley *et al.* produced alginate hydrogels, functionalised with RGD-containing peptide chains, for the culture of C2C12 myoblasts [70]. The cells seeded onto unmodified alginate exhibited minimal attachment, whereas cells were able to adhere to the functionalised alginate, and showed a high degree of spreading after 24 hours [70]. The cells also showed the ability to proliferate, with the population density on functionalised alginate rising from approximately 1×10^4 cells to approximately 8×10^4 cells over 72 hours [70]. Encapsulation of cells within alginate gels can also be applied for the purposes of cell maintenance and transport, as described by Swioklo and Connon [76]. For example, Wright *et al.* used alginate to produce hydrogels in which corneal and limbal epithelial cells were encapsulated [77]. This alginate was oxidised, by way of reaction with sodium periodate, to varying degrees [77]. It was noted that an increase in degree of oxidation (from 2% to 5%) resulted in an increased number of viable cells extracted from the gels after 3 days of culture [77].

1.4.3.4 Synthetic materials

As previously mentioned, synthetic polymers are another category of biomaterials from which scaffolds can be produced. Ceramics, the third category, are not typically used for soft-tissue culture. Two examples of commonly used synthetic materials used in scaffold design are Poly(lactic-*co*-glycolic acid) (PLGA) and polycaprolactone (PCL).

Poly(lactic-*co*-glycolic acid) is a polymer composed of two substances: glycolic acid and DL-lactic acid, both of which terminate in hydroxyl groups, thus enabling polymerisation via condensation reactions [78]. It its monomer form, caprolactone is composed of a ring of 6 carbons and one oxygen, with a double-bonded oxygen protrusion [79]. Polymerisation of caprolactone generally involves ring-opening induced by any of a variety of catalysis, which results in a linear carbon chain with a singularly bonded oxygen atom at the terminal, which in turn can form links with other repeating units [80].

Choi *et al.* synthesised fibrous, composite scaffolds of type I collagen and PCL in order to culture human skeletal mesenchymal stem cells to myotubes [9]. Scaffolds have been produced from PLGA alone, such as the fibrous scaffolds of Aviss *et al.* onto which myoblasts were able to grow [49].

1.4.4 Scaffolds for muscle-tissue culture

1.4.4.1 Fibrous scaffolds for muscle-tissue culture

Aviss *et al.* produced electrospun fibres composed of PLGA, with diameters ranging from 0.1 – 1.8 μm, which were able to support the growth and differentiation of C2C12 myoblasts [49]. They also noted that, when the fibres were produced with uniform alignment, there was a significantly higher fusion index on the fibres than on glass slide controls [49]. Zhang *et al.* also produced electrospun fibres of PLGA which supported culture of C2C12 myoblasts [81]. Their fibres exhibited diameters ranging from 0.2 – 1.1 μm in the case of random-oriented fibres, and 0.1 – 0.8 μm in the case of aligned fibres [81]. Sirivisoot and Harrison produced electrospun nanotubes composed of polyurethane carbon, alongside fibres of polyurethane [82]. The conductive nature of the former scaffold allowed for electrical stimulation of the adhered C2C12 myoblasts, which led to enhanced degrees of fusion into myotubes [82]. Choi *et al.* produced electrospun fibres composed of a blend of PCL and collagen, and showed that proliferation of human skeletal muscle cells was unchanged when compared to that on TCP controls [9]. Riboldi *et al.* produced electrospun

fibres from the commercially available biomaterial DegraPol [83]. They demonstrated that cells were able to proliferate on these fibres to a degree comparable to that on DegraPol slides and that, when scaffolds were coated with Matrigel, differentiation of C2C12 myoblasts occurred [83].

Hollow-fibre membranes as used by Ellis *et al.* for example, have been produced via wet-spinning [15, 84]. These hollow fibres were produced from blends of PLGA and polyvinyl alcohol (PVA), and appear (from images) to have held diameters of over 500 μm [15, 84]. Flat (non-fibrous) wet-spun membranes were analysed for their cytocompatibility and showed an ability to support cell growth comparable to that of TCP [15]. Later, these fibres were noted to have the ability to allow perfusion of a model serum protein, bovine serum albumin [84].

1.4.4.2 Particulate scaffolds for muscle-tissue culture

Molnar *et al.* noted that myogenic-cell proliferation appeared reduced when cells were cultured on commercially available Cytodex-3 or Biosilon microcarriers (composed of dextran and polystyrene, respectively) as opposed to culture plate surfaces [85]. Nevertheless, they noted that the satellite cells cultured in microcarriers were able to proliferate, differentiate, and form 3-dimensional aggregates [85]. Verbruggen *et al.* cultured bovine-derived myoblasts on microcarriers, and noted that cells cultivated on microcarriers expressed less differentiation markers than those cultured on the surfaces of well-plates [16]. However, they were able to confirm that the myoblasts cultured on microcarriers did indeed differentiate, and fuse into myotubes [16]. Kankala *et al.* produced porous microcarriers which C2C12 myoblasts were able to adhere to, and penetrate [86]. These C2C12 myoblasts exhibited subsequent proliferation, and the expression of differentiation markers such as myosin heavy chain after 7 days [86]. Torgan *et al.* used commercially available microcarriers to culture C2C12 myoblasts, and noted that the cells were able to proliferate, express differentiation markers, and form 3-dimensional aggregates [87]. Bardouille *et al.* cultured C2C12 myoblasts on a variety of commercially available microcarriers composed of various materials, of which collagen-coated Cytodex beads were noted to be the most effective at supporting myoblastic growth, with cells growing to confluence and differentiation on the beads' surfaces [55].

The aforementioned microcarriers of Kankala *et al.* were produced via microfluidic flow focusing, and exhibited a diameter range of 280 – 370 μm (with the highest incidence of particles in the 320 – 330 μm range) [86]. Huang *et al.* produced microparticles from egg

proteins using microfluidics (however, rather than a T-shaped arrangement of channels, their capillaries were coaxially aligned with the continuous phase flowing around the tip of the disperse phase's needle) with the addition of a heating element [88]. Their microparticles had radiuses ranging from 175 – 215 μm, with the highest incidence of particles in the 195 – 200 μm range [88], and it was noted that HepG2 cells were able to grow on the microcarriers' surface [88]. Luetchford *et al.* used microfluidic flow focusing to produce microcarriers composed of silk fibroin and gelatin with mean diameters varying from approximately 350 – 150 μm, depending on the flow rate ratios of the continuous and disperse phases [89]. It was further noted that these microcarriers could support the growth of mesenchymal stem cells, with varying efficiencies depending on the ratios of silk fibroin and gelatin [89].

1.4.4.3 Gelatinous scaffolds

Hydrogels are another basis of bioscaffold design prevalent in tissue engineering. Though they can also be formed into fibrous or particulate scaffolds, their fundamental structure is distinct from the solid scaffold designs described previously. Hydrogels are formed when polymers in an aqueous solution are crosslinked, resulting in an insoluble polymer matrix with a high water content [90, 91]. The fibrous polymer network as well as the high water content provide an environment that mimics traits of the ECM [92].

To cite examples of hydrogels formed from the previously discussed biomaterials, Gouviea *et al.* synthesised collagen hydrogels functionalised using chains of arginine, glycine, aspartic acid, and serine (RGDS), which in turn were connected to the collagen using N-(fluorenyl-9-methoxycarbonyl) [93]. The hydrogels themselves were formed by allowing collagen solutions to polymerise at 37˚C [93]. They found that cell (human corneal stromal fibroblast) cultures on unmodified collagen gels showed a viability of approximately 60% after 5 days of culture, and that those on the RGDS-functionalised collagen gels at the same timepoint held a significantly higher population viability approximately 80% [93]. Mi *et al.* produced collagen gels by photochemical crosslinking, wherein collagen was treated with riboflavin and exposed to ultraviolet light to induce crosslinking, and they noted that these gels were able to support the growth of limbal epithelial cells [94]. As previously mentioned, Wright *et al.* produced hydrogels of alginate, which was oxidised by reacting with sodium periodate [77]. The alginate was crosslinked using calcium chloride, and some samples included type IV collagen [77]. They encapsulated limbal and corneal epithelial cells within these gels at densities of 3 x 10^5 cells, and were able to extract live cells after three days [77]. Azab *et al.* produced chitosan hydrogels by crosslinking the biomaterial using

glutaraldehyde for the purpose of drug delivery [95]. Kim *et al.* synthesised silk-fibroin hydrogels by blending aqueous silk fibroin solution with polyaspartic acid solution, and leaving the mixture at room temperature for 24 hours, after which they noted gelation had occurred [96]. They seeded the scaffolds with human mesenchymal stem cells at densities of 5 x 10^6 cells per scaffold [96]. After 6 weeks of culture, they obtained a minimum of approximately 10000 cells per mg of scaffold, and a maximum of approximately 16000 cells per mg of scaffold, depending on the ratio of silk fibroin to polyaspartic acid [96].

Hydrogels have also been applied to myogenic cell culture. As previously mentioned, Rowley *et al.* produced alginate hydrogels functionalised by the addition of RGD-containing protein motifs, and demonstrated the ability of C2C12 myoblasts to adhere, spread, and proliferate on these gels [70]. Mooney and Rowley would again produce functionalised alginate hydrogels, this time comparing alginates high in L-guluronic acid and alginates high in D-mannuronic acid [97]. They noted that C2C12 myoblasts cultured on the former exhibited enhanced proliferation compared to the latter, and to alginates which contained equal amounts of both residues [97]. They also noted what appeared to be extensive myotube formation on the functionalised alginate gels with higher amounts of L-guluronic acid [97].

1.4.4.2 Scaffold characteristics

An ideal bioscaffold will bear structures which can bind to integrins expressed on the surface of cells, which are the primary class of cell-surface receptors that facilitate adhesion to the ECM [11, 98]. These transmembrane structures are connected to the actin cytoskeleton of the cell, as well as various other structures, and they represent the first step in many cell-signalling pathways [11, 51]. Particularly notable, integrins of the β1 and β3 varieties are noted to bind to collagens, fibronectin, and laminin, among others [51]. To cite just a few examples of the many ways in which ECM proteins can bind integrins, fibronectin and laminin are able to bind cells using chains of RGD within their structure [11]. This RGD motif is perhaps the most notable integrin-binding protein motif, with over half of the documented integrins having the capacity to bind it [99]. The coil section of laminin is also able to bind to α6β1 and α7β1 integrins [51]. Collagens have been noted to bind to integrins via more complex protein motifs such as chains of glycine, phenylalanine, pyrrolysine, glycine, glutamic acid, and arginine (GFOGER), as well as chains of glycine leucine, phenylalanine, glycine, glutamic acid, and arginine (GLOGER), and also chains of glycine, alanine, serine, glycine, glutamic acid, and arginine (GASGER), which bind to integrins α1β1 and α2β1 [98].

The mechanical properties of the scaffold are also of importance with regard to cell culture. For example, Wells notes that stiff matrices induce proliferation in various types of liver-derived cells [100]. When focusing on hepatocytes specifically, stiff matrices induce proliferation but inhibit differentiation, and the inverse is true on softer matrices [100]. Foster *et al.* cultured cornea-derived epithelial cells on collage, and found that the expression of yes-associated protein (YAP) increased in correlation with substrate stiffness [101]. It was further demonstrated that cornea-derived epithelial cells express higher levels of the differentiation factor bone morphogenetic protein 4 (BMP4), and that the same cells on softer collagen scaffolds showed enhanced proliferation and expression of proliferation markers such as β-catenin [102]. With particular regard to myogenic cell culture, Griffin *et al.* noted that increased scaffold stiffness enhances spreading of myogenic cells [103]. Additionally, they noted that whilst formation of myotubes was not affected by scaffold stiffness, myotube striation was [103]. Specifically, the relationship between striation percentage and the elastic modulus of the scaffold exhibited a bell-curve trend; striation was most pronounced when scaffolds held elastic moduli in the mid-range, specifically 12 – 15 kPa, which is the elastic moduli noted for myotubes themselves [103].

Also of importance is the manner in which cells are seeded onto scaffolds after they have been produced. Dynamic seeding is preferable to static seeding, as it facilitates a greater degree of cell attachment [21]. For example, Vunjak-Novakovic *et al.* compared poly-glycolic acid (PGA) scaffolds seeded under static conditions in a Petri dish, to the same seeded under dynamic conditions in a stirred-flask (wherein the liquid inside was agitated), and found that scaffolds seeded under the latter conditions showed greater cell population densities over time than those seeded under static conditions [24]. Wendt *et al.* demonstrated a dynamic-seeding technique that further improved cell attachment; fluxing cell suspension through the pores of a scaffold not only resulted in significantly more viable cells than observed on those seeded under static or stirred-flask conditions, but also a significant increase in the distribution uniformity of these cells (again, in comparison to both static and stirred-flask seeding) [25].

1.5 Bioreactors for muscle-tissue culture

In their review of expansion bioreactors for the production of cultured meat, Allan *et al.* provide numerous examples of studies using various designs of bioreactors for the expansion of skeletal muscle cells [19]:

Molnar *et al.* used a high-aspect-ratio-vessel (HARV), a rotating-wall vessel design of bioreactor, in order to analyse the culture of rat-derived satellite cells in a simulated micro-gravity environment [85]. They highlighted the strength of the vessel design, in that it is able to produce a dynamic internal environment whilst maintaining low shear-stresses on cell cultures [85]. Torgan *et al.* also utilised the rotating wall vessel design in their culture of C2C12 myoblasts on commercially available microcarriers, they noted decreased amounts of contractile proteins myosin and trypomyosin in cells cultured in the rotating wall vessel compared to those cultured in Teflon bags, which were used as control vessels [87]. The bovine-derived myoblasts cultured on microcarriers by Verbruggen *et al.* were grown in a stirred-tank vessel [16].

Bioreactors must also be able to produce mechanical stimuli akin to those the tissue cultures would experience in vivo; those for muscle tissue culture should aim to produce tensile stress forces and induce contractile forces in the cells [23]. Bhumiratana *et al.* provide an overview of bioreactor designs which accommodate mechanical stimulation into their design [23]: Lu *et al.* for example, designed a bioreactor system in which the cell culture matrix is suspended as a column between two vertical pillars, one of which can be pulled and rotated to induce longitudinal stress on the cell culture matrix [104]. A relatively early and simple example of a bioreactor with the ability to provide electrical stimuli to cells cultured within can be found in the design of Berger *et al.* wherein two electrodes are placed into the culture medium contained within a standard culture flask, and noted that stimulation in this way prevented loss of contractile function in the cells [105]. Milica *et al.* also studied the effects of electrical stimulation to induce contraction in cardiomyocytes, by placing precultured cells into a glass chamber with parallel-aligned electrodes, and noted that stimulated cells appeared to show increased expression of proteins such as myosin heavy chain after 8 days of culture compared to unstimulated controls [106].

1.6 Tissue engineering for cultured meat

The biotechnology model of cultured meat, also referred to as in-vitro meat or clean meat, utilised the principles of tissue engineering in order to produce meat for general consumption. In this model, illustrated in figure 1.05, myogenic cells are harvested from donor herds and cultured in vitro into skeletal muscle tissue [107].

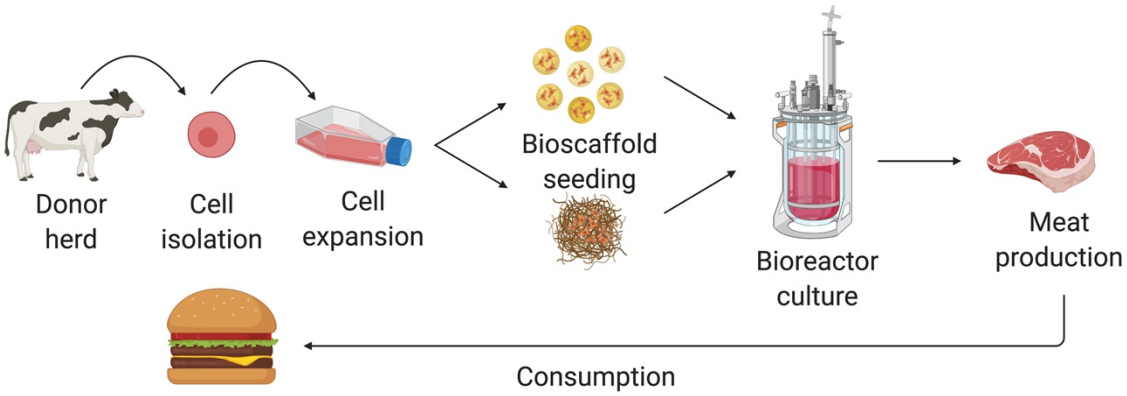

Figure 1.05: Overview of the tissue engineering process for cultured meat applications. Created with Biorender.com.

Highlighting the potential for innovation in the field of cultured meat in their book "The *in vitro* Meat Cookbook", van Mensvoort and Grievink speculate on the possible downstream, blue-sky implications of the successful development of cultured meat biotechnology [108]. They postulate, among many other things, that cultured meat may provide a slaughter-free means of producing pet food, particularly for obligate carnivores such as felines [108]. Also that dehydrated cultured meat could be used for disaster relief applications [108]. They note that cultured avian liver could provide *foie gras* without the ethical concerns associated with the current methods by which *foie gras* is produced, and that on-the-bone meat products could be provided by use of 3D printed skeletal structures [108].

Though research into this biotechnology is in its early stages, notable progress has been made: the first cultured meat burger was produced by Dutch researchers led by Dr Mark Post and eaten in London in 2013 [109]. This was made by way of a process which relied heavily on animal-derived materials, and $50,000 were subsequently invested into additional research into an animal-free system by which cultured meat could be produced [109].

1.6.1 The environmental implications of meat production

The environmental impacts of conventional meat production are significant, and so the need for alternatives to conventional meat is clear. The total area of ice-free land on Earth is cited as approximately 13.4 x 10^9 hectares [110]. The rearing of livestock for meat production is noted to use 30% of global ice-free land [1], which would represent an area of approximately 402 x 10^6 hectares: enough to cover the United Kingdom (over 24 x 10^6 hectares [111]) more than 16 times over. Conventional meat production contributes to 18% of global

greenhouse gas emissions, more than all forms of global transportation combined [1], and also required 8% of the Earth's fresh water [1]. By the year 2050, global meat consumption is estimated to be double that of what it was in 1999 [1], and of course the environmental impacts of conventional meat production will increase proportionally. It has been postulated that the United Kingdom alone will experience a shortage of farmland as early as the year 2030 [111]. Additionally, concerns have long been raised over the ethicality of practices such as factory farming prevalent in the meat industry, as well as ethical concerns over the practice of animal-slaughter in general [112]. Considering the aforementioned doubling in meat consumption by the year 2050 [1], these concerns are likely to become exacerbated. As stated, the need for alternatives to conventional production of meat is highly apparent.

Research into the development of a cultured-meat-production system is still in its early stages; the year 2020 would have seen the 6th International Scientific Conference on Cultured Meat [113]. Due to the emergent nature of the field, it is difficult to estimate the environmental impact of the final product. Nevertheless, there have been attempts to do so. Tuomisto and De Mattos produced a study in which the environmental impact of meat production was compared to a theoretical model of cultured meat [1]. In this study, it is proposed that cyanobacteria will be cultured in ponds and hydrolysed (with an assumed yield of 50% biomass) to produce feeding stock for cell cultures [1]. The assumed end product is a mince-like mass of cultured meat whose protein content is equal to 19% of the total mass, and that this product is produced using a 1000 litre stirred-tank bioreactor which can be filled to 80% capacity, and requires 60 days to produce 1000 kg of cultured meat [1]. With these parameters in mind, Tuomisto and De Mattos postulate that production of 1000 kg of cultured meat would require less than 60% of the energy used to produce an equal mass of slaughter-derived beef, less than 10% of the water and land, and would produce less than 10% of the greenhouse gas emissions (all in comparison to slaughter-derived beef) [1]. The theoretical cultivation of cyanobacteria as cell-feed was included in these estimations, this cultivation accounted for 23% of the total energy usage of the cultured meat system, as well as 28% of the greenhouse gas emissions and 17% of the water use [1]. The greenhouse gas emissions in cultured meat production were postulated to be different from those in conventional meat production in that they are produced by electrically powering the bioreactors, whereas the majority of greenhouse gas emissions in conventional meat production are from livestock [1]. Waste products of the cultured meat process in this model are noted to be 75% of the cyanobacteria biomass, 50% of which is lost during hydrolysis (but can be repurposed), and a further 50% of the remaining biomass is metabolised by the muscle cells into carbon dioxide or lactate [1].

In a subsequent study, published 3 years after the first, Tuomisto *et al.* consider the impact of hydrolysed wheat or corn instead of hydrolysed cyanobacteria as feeding stock (with an assumed 2 kg of wheat or corn required to produce 1 kg of cultured meat), and the use of a hollow-fibre bioreactor instead of a stirred-tank bioreactor [114]. This had the effect of increasing the energy use of cultured meat to slightly above that of beef, and increased the water use of cultured meat to approximately 50% that of beef [114]. This increased energy requirement appeared to be due to the bioreactor design, which would need additional heating elements [114]. The increase in water requirements is noted to be due to an updated methodology in how the water footprint was calculated, though it is also notable that the water requirements vary as the assumed feeding stock is changed (water requirements were more than doubled for corn versus cyanobacteria, but reduced for wheat versus cyanobacteria) [114]. These studies are optimistic regarding the environmental impact of cultured meat versus conventional meat production, but also highlight the highly speculative nature of such analyses. The theorised environmental impact of cultured meat production will continue to change as research continues.

1.6.2 Serum-free cell culture

As part of Kolkmann *et al.*'s group, Dr Post would also explore the field of serum-free cell culture, with respect to the culture of bovine-derived myogenic cells [115]. They analysed myoblast behaviour in the presence of various commercially available serum-free media, as well as testing combinations thereof, in comparison to standard culture medium which contained fetal bovine serum (FBS) [115]. They noted that it was possible for myoblasts to proliferate in serum-free media containing LipoGro™ additive [115], however they also noted that this proliferation was reduced compared to that of cells cultured in media containing 20% (v/v) FBS [115]. Additionally, they noted that myoblasts cultured in media containing LipGro exhibited adipogenic differentiation [115]. There is much progress yet to be made with regard to myoblastic culture in serum-free conditions.

1.6.3 Adipocyte coculture and heme protein content

This adipogenic differentiation is a notable, though not positive, result, as it highlights downstream challenges the cultured meat biotechnology is likely to face. Though the cultured meat community tends to focus on meat in terms of skeletal muscle culture, slaughter-derived meat is not limited to muscle tissue. Fat is also a notable part of meat [116]. For example, the high fat-content of Japanese Wagyu beef produces a high degree

of marbling in the meat, enhancing the flavour and texture, and results in a highly sought-after steak product which can be sold for high prices [117]. Co-culture of myogenic and adipogenic cells will therefore also be a key area of research in development of cultured meat, but may present further challenges.

The study of Kolkmann *et al.* demonstrate that the lipoprotein solution of LipoGro™ induces adipogenic differentiation in bovine-derived satellite cells [115]. Beloor provide further evidence for this, as they demonstrated that the presence of serum lipid solution, even at concentrations as low as 5 µl per ml of medium, can induce adipogenic differentiation in bovine-derived satellite cells, heralded by an increase in adipogenic genes such as peroxisome proliferator-activated receptor gamma (PPARγ) [118], as well as a lessening in myogenic gene expression such as MyoD and myogenic factor 5 (Myf5) [118]. The formulation of culture medium will be an important consideration in production of cultured meat.

Cell sourcing may also be a consideration with regard to myogenic and adipogenic coculture of satellite cells. Schubert *et al.* for example, demonstrate that satellite cells sourced from mouse rotator-cuff muscles, in comparison to those sourced from mouse gastrocnemium, show lessened expression of myogenic genes such as myogenic regulatory factor 4 (MRF4) and increased expression of adipogenic genes such as PPARγ and fatty-acid-binding protein 4 (FABP4) [119].

Heme proteins are also a factor to be considered in the development of cultured meat. It has been noted that heme contributes heavily to the taste of meat, with Impossible™ foods utilising heme produced by genetically modified yeast to flavour their signature “Impossible Burger”; a plant-based burger substitute noted to bear similarity to meat-based burgers [120]. Simsa *et al.* analysed the effect of haemoglobin and myoglobin on bovine-derived satellite cells, with further consideration to its effect on any resultant cultured-meat product [121]. They noted that myoglobin in particular enhanced the proliferation of bovine myosatellite cells, and that both haemoglobin and myoglobin increased pigmentation in the final tissue construct [121].

These challenges will be present in the hypothetical production of a steak-like meat product, which must be essentially analogous to a cross-sectional cut of muscle tissue. Minced meat and products such as burgers, in contrast, are commonly formed from significant grinding of large quantities of meat, with burger and sausage product being subsequently formed into the appropriate shapes. For the purposes of these products, it may be sufficient to

simply culture skeletal muscle tissue which can be compacted into patties from which to form burgers, sausages, and similar products. Factors such as fat-content could hypothetically be determined afterward, via the addition of vegetable-based fat or plant-derived heme proteins, for example.

1.6.4 Sources of biomaterials and scaffold design

As discussed, myogenic cell culture typically employs animal-derived biomaterials such as collagen, gelatin, or Matrigel. The ideal model for cultured meat would not rely on animal-derived materials, as these would lessen the scalability of the process as well as increase the environmental impact and ethical concerns. Highly renewable plant-based biomaterials would be a more ideal choice. Furthermore, the ideal scaffold would be edible so as to be consumed with the meat culture. Otherwise, the scaffold would need to be removed from the meat before reaching the consumer, which would be a labour-intensive task and would have severe implications for the scalability of the biotechnology.

1.6.5 Scale-up considerations

Allan *et al.* provide a comprehensive review of considerations to be taken into account at various stages of the cultured meat model which relate to the potential for mass production [19]. Optimisation of cellular functions is an immediately obvious consideration, Allan *et al.* note that cells should have an optimised capacity for proliferation (as previously noted in section 1.3.4, primary cells have the disadvantage of limited proliferative capabilities when compared to immortalised cell lines), and they should have an optimised capacity for induced differentiation [19] (for example, as noted in section 1.6.3, myogenic cells from different parts of the body can exhibit differing levels of myogenic gene expression). Media would ideally be specially formulated to optimise these parameters as well [19]. The design of the scaffold is also of vital importance with regard to the potential for scale-up; the design of scaffold directly affects the type of bioreactor which would be used (which, as discussed in section 1.6.1, can have significant effects on the energy requirements of the cultured meat production model) and will affect parameters such as media requirements [19]. The scaffold should also be composed of a material which is constantly available and can be sustainably produced, and should also be edible in order to avoid cell-detachment considerations [19]. Various bioreactor designs have their advantages and disadvantages with regard to scale-up: the hollow-fibre bioreactor is noted to have the potential for achieving particularly high final cell densities [19], but due to heating requirements may necessitate a higher energy input than stirred-tank systems [114]. However, in order to

achieve continuous operation of stirred-tank bioreactors, it would be necessary to incorporate complex cell retention devices [19].

1.7 Aims and objectives

Contributions to the development of cultured meat biotechnology are being made from various sub-fields of tissue engineering research. This work focusses on one such sub-field: the production of scaffolds. As discussed, bioscaffolds used for tissue engineering (and within the field of cultured meat) are usually based on animal-derived ECM proteins, typically collagen [2, 3, 6, 115]. The potential of plant-based bioscaffolds has yet to be fully explored.

It is postulated here that a plant-based scaffold is ideal for the field of cultured meat. Synthetic biomaterials must, of course, be manually synthesised. PCL, for example, is synthesised first of all by the oxidation of cyclohexanone into caprolactone monomers via peracetic acid [80]. The monomers are then subjected to ring-opening polymerisation by one of a variety of chemical processes [80]. With regard to cultured meat, the need to synthesise the material to be used for a scaffold would hamper scale-up potential. Additionally, the selection of synthetic biomaterials that are edible is limited in comparison to naturally occurring biomaterials [122]. It would be far more ideal to harvest a naturally occurring biomaterial. Animal-derived biomaterials such as collagen would fit this criteria, however such biomaterials are derived from mammalian tissue (collagen, for example, is usually obtained from porcine dermis [123]). The biotechnology of cultured meat hopes to alleviate the environmental and ethical concerns of the slaughter industry. The use of an animal-derived scaffold would make the process of cultured meat reliant on the slaughter-industry, and add to the demand thereupon, which would be directly contrary to the aim of cultured meat to lessen the ethical and environmental concerns caused by the slaughter industry. The high degree of renewability associated with plant-derived substances is reflected in price comparisons with animal-derived and synthetic biomaterials. For example, from the supplier Sigma Aldrich, 5 g of polycaprolactone can be purchased for £32.60 [124]. In comparison, 100 g of gelatin can be purchased for £33.40 [125], and 1 kg of cellulose can be purchased for £36.70 [126]. Thus a scaffold produced from plant-based biomaterials would be ideal for the purposes of cultured meat if it were able to support myogenic cell growth and differentiation to a degree comparable to animal-derived or synthetic biomaterials. As stated, this work aims to produce such a scaffold. Aside from being plant-based, characteristics for an ideal scaffold for cultured meat production are given in table 1.

Characteristic	Rationale
The scaffold must be cytocompatible	Cells must be able to adhere to the substrate, and the substrate must be able to facilitate cell proliferation, spreading, and differentiation without exhibiting cytotoxic effects.
The biomaterial must be renewable and readily available	It must be possible to produce the scaffold easily, cheaply, and quickly in order for the cultured meat process to have scale-up potential. The biomaterial should be renewably sourced in order to minimise the environmental impact of the cultured meat process. As stated, this is a distinct strength plant-based biomaterials.
The scaffold must be compatible with bioreactors designs commonly used in tissue engineering	As novel bioreactor design is beyond the scope of this work, it must be possible to utilise the scaffold in existing bioreactor designs. This means that the scaffold must be produced in morphologies such as hydrogels, hollow-fibre membranes, microparticles, or electrospun fibre matrices.
The scaffold should ideally be edible	The scaffold should be edible so as to be consumed along with the cultured meat. If the scaffold were inedible, it would require displacement of the cells before the product can be eaten, which would negatively impact potential for scale-up.
The scaffold should ideally have an elastic modulus of approximately 12 - 15 kPa	As previously noted, the ability of myotubes to develop striations is dependent on the stiffness of the substrate on which they are formed. Specifically, the substrate must have an elastic modulus within the range of 12 – 15 kPa in order for myotubes to develop striations [103], which will optimise

	the induction of contractile forces [11]. This is listed as an ideal characteristic as myotubes will still form on a substrate regardless of stiffness [103].
The scaffold should ideally have topographical features such as parallel grooves	It is noted that topographical features of a scaffold can influence the behaviour of myogenic cells: Random microscale structures on the substrate surface are not noted to exert such an influence, however micropatterned grooves and ridges have been noted to induce cell alignment [127]. Such alignment will be necessary to optimise stimulation of cultured cells, such as by inducing contractile forces or applying tensile forces.

Table 1: Requirements of an ideal scaffold for cultured meat production

The scaffold will be plant-based to as much of a degree as possible. The biomaterial from which the scaffold is formed will be a plant-derived protein or polymer, though there may be cause to investigate cross-material blending. Such avenues of investigation would be based on established literature, and so secondary biomaterials used for blending may not be plant-derived. The intention is, nonetheless, to produce a scaffold composed of only plant-derived biomaterials. Standard procedures will be used for cell culture, therefore cell feeding stock will be standard culture medium (containing foetal bovine serum) and differentiation medium will make use of horse serum. As stated, research into serum-free myogenic cell culture is beyond the scope of this work. Cell displacement during passaging or seeding will be accomplished using trypsin solution (which will also be animal-derived) as is standard laboratory practice. Procedures involving modification of the materials (such as crosslinking) will be carried out using methods and reagents that are standard for the material in question, this is for the sake of comparability of results and for time and cost efficiency, as the primary objective is a plant-based physical scaffold. However, in the interest of producing not only a sustainable scaffold, but doing so by sustainable means, due consideration will be given to animal-free alternatives where possible (if the procedure in question relies on animal-derived reagents). The myogenic cells will, of course, be animal-derived.

With regard to the theoretical model of a complete cultured meat system, the emergent nature of the field makes it difficult to draw concrete conclusions as previously discussed. However, several possibilities exist. Whilst the view expressed herein is that a plant-based scaffold is the ideal choice, there is still the potential for a scaffold constructed from animal-derived biomaterials, synthetic biomaterials, or the use of decellularised ECM which may be obtained from slaughter industry waste. It is generally thought that cell feeding stock will not be animal-derived [115], though this does not necessarily mean it will be plant-derived; as previously discussed, Tuomisto and De Mattos postulate a model in which cell feeding stock is obtained via hydrolysis of cyanobacteria [1], and the London-based company Multus Media are conducting research into producing growth factors for xeno-free media via genetically modified yeast [128]. Even cell displacement may not rely on animal-derived substances; the Newcastle-based company CellulaREvolution conduct research into peptides which facilitate the self-detachment of cells [128]. There are also other means to facilitate cell detachment without relying on animal-derived reagents, such as TrypLE (a recombinant enzyme) or the detachment of cells using shear forces [19].

Though the production of the bioscaffold is noted to be a crucial and intrinsic stage of the cultured meat process [19], there are still challenges to be overcome in other important fields (some of which have already been discussed in section 1.6) which are beyond the scope of this work: the proliferative capabilities of primary cells must be optimised [19], research into optimised cell sourcing from other livestock species is being conducted [128], serum-free culture of myogenic cells has yet to be achieved to a satisfactory degree [115], there remains room for exploration in alternative to animal-derived serum such as cyanobacteria lysate [1], challenges remain present regarding the coculture of adipocytes alongside myocytes [19], and innovations continue to be made in bioreactor design and optimisation [10, 19].

1.7.1 Biomaterials of focus

1.7.1.1 Carrageenan

Carrageenan, like alginate, is seaweed-derived polysaccharide (though it is found in red seaweed, in contrast to the brown seaweed from which alginate is derived) [14]. It is water soluble, and can be used to produce hydrogels when ionically crosslinked (usually potassium ions) [129]. With regard to their potential as a bioscaffold (particularly compared to alginate), carrageenans are able to interact with protein motifs associated with cell-

binding: carrageenan gels have been shown, for example, to inhibit the herpes simplex virus 2 (HSV-2) from entering human cells by binding and blocking the viral motifs used to facilitate cell-entry [130]. These motifs are, in turn, noted to facilitate cell-entry by associating with membrane-bound proteoglycans [131].

Zhang *et al.* produced hydrogels of carrageenan and poly(vinyl alcohol), and noted that the adhesion of chondrogenic cells was improved in correlation to the amount of carrageenan included in the scaffold [132]. Mihalia *et al.* produced carrageenan fibres in which human epithelial cells were encapsulated and retrieved after 21 days [129]. Pourjavadi *et al.* produced hydrogels composed of chitosan and carrageenan, into which MG-63 human osteocytes were injected [133]. They noted that the cells maintained viability after 21 days of culture [133]. Gaharwar *et al.* produced carrageenan hydrogels by methacrylating the carrageenan before use, enabling gelation via photocrosslinking [134]. Fibroblasts encapsulated in these gels were also able to maintain their viability [134]. There appears to be room for exploration with regard to the interactions between myogenic cells and carrageenan hydrogels.

1.7.1.2 Zein

Zein is a protein found in abundance within the endosperm of corn [135, 136]. It is the most abundant protein within corn, accounting for just under half of the total protein content of the kernel [135, 136]. A notable characteristic of zein is its hydrophobicity, and solubility in aqueous alcohol solutions [135, 136].

Yang *et al.* produced electrospun fibres from blends of zein and gelatin, onto which human periodontal stem cells were seeded [137]. They noted that gelatin enhanced cell proliferation on these scaffolds, but the zein-only controls were nevertheless able to support cell proliferation well [137]. Tu *et al.* produced porous zein scaffolds, which were seeded with mesenchymal stem cells and implanted into the thigh muscle pouches of nude mice. They noted bone formation 12 weeks after implantation [138]. Jing *et al.* utilised 3D printing technology to synthesise scaffolds from blends of zein and PCL [139]. They noted that, within the first 3 days of H1299 human lung cancer cell culture, cell population densities were higher on scaffolds containing zein, and that this increase was further enhanced in scaffolds of higher zein content [139]. Lian *et al.* produced membranes from hydroxyapatite and zein, onto which mesenchymal stem cells were seeded. Similar to the study of Yang *et al.* they noted that cell proliferation was increased in correlation with the amount of the non-

zein material, but that zein-only controls were still able to facilitate cell growth to a satisfactory degree [140]. As with carrageenan, there appears to be room for exploration with regard to myogenic cell interactions with zein scaffolds.

1.8 Summary

Tissue engineering is a multi-disciplinary field with the overall aims of applying principles of biological sciences and engineering to the repair or even the production of biological tissues. The production of muscle-tissue, specifically, begins in vivo with embryonic myoblasts. These myoblasts proliferate, spread, and then fuse to form multi-nucleated myotubes, which may be regarded as a complete differentiated skeletal muscle cell. In post-natal muscle, myosatellite cells with the ability to renter the proliferative state may be found in the basal lamina of the myotubes, and these would be the ideal cells to use for muscle-tissue engineering, as they can be easily harvested from adult specimens via muscle biopsy. However, many studies use myoblastic cell lines as model cells. Scaffold design is a crucial stage in tissue culture. The scaffold forms the physical framework on which cells adhere, initiating cellular signalling pathways via the binding of integrins and through their mechanical properties. In vivo, the ECM forms the gold-standard bioscaffold. It is composed of proteins such as collagen, fibronectin, and laminin, and is largely fibrous. Many studies researching the culture of myogenic cells utilise these animal-derived biomaterials in order to produce scaffolds capable of efficiently facilitating their adhesion, growth, and differentiation. Scaffolds may be produced in the form of particles, fibre matrices, and hydrogels, to cite notable examples. These scaffold morphologies can be applied to various design of bioreactor, which provides the physiological environment that the cells require. Cultured meat aims to produce muscle tissue *in vitro* for the purposes of human consumption, and carries significantly reduced environmental and ethical implications compared to conventional meat production. Although a cultured meat burger has been produced, there is still progress to be made. For the purposes of cost-effectiveness, scalability, as well as environmental and ethical implications, the model of cultured meat production would rely on animal-based biomaterials (with the exception of cells) as little as possible. This requires progress to be made in areas such as serum-free cell culture, and biomaterial sources for scaffold design. This work focuses on the latter; an ideal scaffold for cultured meat would avoid animal-derived biomaterials, and also be edible. This is to ensure that the scaffold does not have to be removed before consumption of the meat cultured thereon. Biomaterials of focus in this work are carrageenan, which can be formed into hydrogel scaffolds, and zein, which can be formed into solid protein scaffolds.

Chapter 2 – Methodology

2.1 Cell-based methods

The methods presented in section 2.1 concern experimental procedures involving the handling of cells.

2.1.1 Cell culture and maintenance

All non-sterile liquids were sterilised using a 0.2 µm syringe filter [Fisherbrand™ 15206869] before use with cells, or any materials which were to be used with cells.

2.1.1.1 Standard culture conditions

Cells were maintained in T75 culture flasks (Thermo fisher 156472), in Dulbecco's Modified Eagle's Medium (DMEM; Sigma D5796-500ML) supplemented with 10% (v/v) FBS (GIBCO 10500-064) and 1% (v/v) Penicillin-Streptomycin solution (P/S; Sigma P4333-100ML): hereafter "culture medium", which was warmed to 37˚C before being in contact with live cells at any time. Flasks were kept in a Sanyo MCO-18AIC incubator at 37˚C and under 5% CO_2.

2.1.1.2 Passaging and seeding

Phosphate buffered saline (PBS) solution was prepared by taking a known volume of mH_2O and adding 1 tablet of PBS (Oxoid BR0014G) per 100 ml of mH_2O. This PBS solution was autoclaved before use.

1 L of working trypsin solution was prepared by adding 100 ml of 10X trypsin stock solution (Sigma 59427C) and 10 ml of 2% (w/v) aqueous ethylenediaminetetraacetic acid (EDTA; Sigma E9884), to 890 ml of PBS solution. This working trypsin solution was aliquoted and frozen until required.

Cells were washed with PBS solution pre-warmed to 37˚C. 3 ml of working trypsin solution was added, whereupon the flask was returned to the incubator and left for 15 minutes. The surface of the flask interior to which the cells were adhered was then washed thoroughly with culture medium, and the cell suspension was triturated to break up any cell aggregates.

The cell suspension was centrifuged at 1500 rpm for 5 minutes (Fisher accuSpin™ 400). The supernatant was discarded, and the cell pellet was resuspended in 10 ml of culture medium.

At this point, if cells were to be seeded, the material on which this was to take place was sterilized for 30 minutes using a Bioquell ABS1200UV ultraviolet (UV) lamp. The number of cells present in the suspension was calculated using a haemocytometer, and the appropriate amount of cell suspension was pipetted onto the material. For the experiment relating to data presented in figure 4.01, cell seeding density was 2500 cells / cm^2. For all other experiments involving cell culture, cells were seeded at a density of 5000 cells / cm^2.

If cells were to be passaged, then 0.5 ml of cell suspension was added to 9.5 ml of culture medium to give a 1:20 dilution of cell suspension, which was then stored and maintained as per section 2.1.1.1.

2.1.1.3 Freezing for long-term storage

Freezing medium was prepared by adding dimethylsulphoxide (DMSO; Sigma D8418-500ML) to culture medium to a concentration of 5% (v/v). Cells were trypsinised and centrifuged as per section 2.1.1.2, the pellet was resuspended in 1 ml of freezing medium and the cells counted as per section 2.1.1.2. The cell suspension was then diluted with additional freezing medium to achieve a total cell density of $1x10^6$ cells / ml. Cell suspensions were placed into cryotubes, which were in turn placed into a Mr Frosty™ freezing container [Nalgene 5100-0001], and stored at -80˚C overnight in a KM-DU73Y1E ultra-low temperature freezer. The cryotubes were then transferred to a liquid nitrogen container where they were stored until required.

2.1.1.4 Differentiation of myoblasts into myotubes

Cells were cultured, as per section 2.1.1.1, to confluence. They were then cultured in differentiation medium, composed of DMEM supplemented with 2% (v/v) horse serum (Sigma H1270-100ML) and 1% (v/v) P/S (hereafter “differentiation medium”), for 1 week. Experiments involving zein in which this procedure was used were carried out with cells cultured on glass coverslips, which in turn were maintained in 6-well plates. Experiments involving silk fibroin in which this procedure was used were carried out in 6-well plates.

2.1.2 Experimental assays

2.1.2.1 Cell-staining for enhanced imaging

2.1.2.1.1 Hoechst 33342 staining

Hoechst 33342 (Invitrogen H21492) was prepared in mH_2O to a concentration of 10 mg / ml, and stored at -20˚C until required. The stock Hoechst solution was diluted to 2 µg / ml in PBS solution. This working Hoechst solution was applied to cells and left, protected from light, for 15 minutes at room temperature. Cells were then washed with PBS and imaged using a Leica DMI 4000 B fluorescence microscope. Experiments in which this procedure was used were carried out in 6-well nunclon delta well plates. For some (where stipulated), cells were cultured on glass coverslips, which were maintained in 6-well plates.

2.1.2.1.2 CellTracker™ Green CMFDA staining

CellTracker™ Green 5-chloromethylfluorescein diacetate (CMFDA) (Thermo Fisher C2925) was dissolved in DMSO to a concentration of 10 mM. This stock solution was further diluted to a working concentration of 5 µM in DMEM supplemented with 1% (v/v) P/S (hereafter “serum-free medium”). The working solution was applied to cells and left for 30 minutes at 37˚C and 5% CO_2. The working CellTracker solution was removed, cells were washed with serum-free medium, and fresh serum-free medium was applied. Cells were imaged using a Leica DMI 4000 B fluorescence microscope. Experiments in which this procedure was used were carried out in 6-well nunclon delta well plates.

2.1.2.1.3 Fluorescein diacetate staining

Fluorescein diacetate (Acros Organics 191660050) was dissolved in acetone (VWR BDH chemicals 67-64-1) to a concentration of 5 mg / ml and this stock solution stored at -20˚C until required. The stock solution was added to serum-free medium to a concentration of 8 µl / 5 ml. The working solution was applied to cells for 5 minutes at room temperature, protected from light, and then imaged using a Leica DMI 4000 B fluorescence microscope. Experiments in which this procedure was used were carried out in nunclon delta 24-well plates.

2.1.2.2 Resazurin metabolic assay

Resazurin sodium salt (Sigma R7017) was added to PBS solution to a concentration of 0.15 mg / ml. This stock resazurin solution was kept protected from light at 4˚C until required, whereupon it was added to culture medium to a concentration of 10% (v/v). Cells were incubated in this working resazurin solution for 2 hours at 37˚C and 5% CO_2. 100 µl of solution was then transferred to individual wells of a 96-well plate (Thermo fisher 167008) and analysed using a BMG FLUOstar Omega plate reader (540 nm excitation and 590 nm emission). This was repeated at various timepoints to assess cell proliferation. Where stated, this procedure was carried out in nunclon delta 6-well plates, or on cells cultured on glass coverslips, which were maintained in nunclon delta 6-well plates (alongside TCP controls also in 6-well plates). Otherwise, experiments in which this procedure was used were carried out in nunclon delta 12-well plates.

2.1.2.3 Cell differentiation analysis

Cells were cultured under differentiation conditions as per section 2.1.1.4. After 1 week in differentiation medium, cells were fixed using -20˚C methanol (Alfa Aesar L13255) for 15 minutes. Blocking buffer was prepared using serum-free medium supplemented with 1% (v/v) goat serum (Sigma G9023-10ML) and 0.1% (v/v) Triton X-100 (Sigma X100-100ML). The fixed cells were treated with the blocking buffer for 1 hour at room temperature and then washed with PBS solution. Mouse monoclonal anti-myosin primary antibody (Sigma M4276-.2ML) was added to fresh blocking buffer to a concentration of 1:1000 from the as-supplied concentration, and incubated with the cells overnight at room temperature. Cells were then washed with PBS solution. Goat anti-mouse Alexa Fluor 488 secondary antibody (Life technologies A11001) was added to fresh blocking buffer to a concentration of 1:1000 from the as-supplied condition. Cells were incubated with secondary antibody solution for 3 hours at room temperature, protected from light, and washed with PBS. Cells were then counterstained with Hoechst 33342 as per section 2.1.2.1.1, and imaged using a Leica DMI 4000 B fluorescence microscope. Experiments involving zein in which this procedure was used were carried out with cells cultured on glass coverslips, which in turn were maintained in 6-well plates. Experiments involving silk fibroin in which this procedure was used were carried out in 6-well plates.

2.2 Biomaterials-based methods

The methods presented in section 2.2 concern experimental procedures involving the handling of biomaterials.

2.2.1 Production of carrageenan scaffolds

2.2.1.1 Macroscopic beads, fibres, and discs

κ-carrageenan powder (Sigma 22048) was dissolved in milliQ water at 80˚C to a concentration of 2% (w/v). KCl (Sigma P9333) was dissolved mH_2O at room temperature to a concentration of 5% (w/v).

To produce carrageenan discs, the carrageenan solution was cast into multiwell plates (specific sizes varying by experiment, to be given in subsequent sections) and allowed to cool. 2 ml was used for 12-well plates, 1 ml for 24-well plates, and 0.5 ml for 48-well plates. The discs were frozen at -80˚C for 3 hours in a KM-DU73Y1E ultra-low temperature freezer, and lyophilised using a MicroModulyo-230 freeze-drier. The 5% (w/v) aqueous KCl crosslinker solution was applied to the dried carrageenan discs and left for 1 hour at room temperature. To produce macroscopic carrageean beads, 10 ml of the carrageenan solution was added dropwise, using a plastic 10 ml syringe (BD Plastipak 302188) topped with an 18-gauge needle (Adhesive Dispensing Ltd AD718100) to 100 ml of the 5% (w/v) KCl solution, and left for 1 hour at room temperature. To produce wet-spun carrageenan fibres, the needle was immersed in the 5% (w/v) KCl solution and 10 ml of carrageenan solution was extruded directly into the crosslinker (again using a plastic syringe). This process is illustrated in figure 2.01.

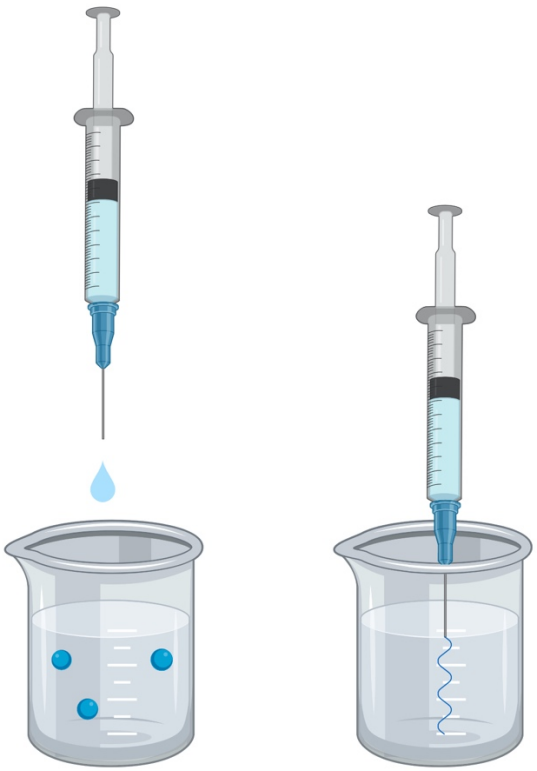

Figure 2.01: Production of carrageenan beads (left) and fibres (right). Created with Biorender.com.

2.2.1.2 Microparticles

2% carrageenan solution was prepared as per section 2.2.1.1. The carrageenan solution was placed into a plastic 10 ml syringe (BD Plastipak 302188) topped with a 23-gauge needle (Adhesive Dispensing Ltd AD725100). The needle was inserted into a purpose built, 3D-printed, airflow-channelling apparatus, which in turn was connected to a pressurised N_2 gas supply. The carrageenan was manually pumped through, and nitrogen (N_2) gas was simultaneously pumped though at a pressure of 0.5 bar. This was carried out for 5 minutes, and the particles were collected in a 100 ml solution aqueous 5% (w/v) KCl (in 200 ml glass beaker) and allowed to crosslink for 1 hour at room temperature. This apparatus design is illustrated in figure 2.02. Details of the 3D-printed apparatus design are given in figures 2.03 – 2.04.

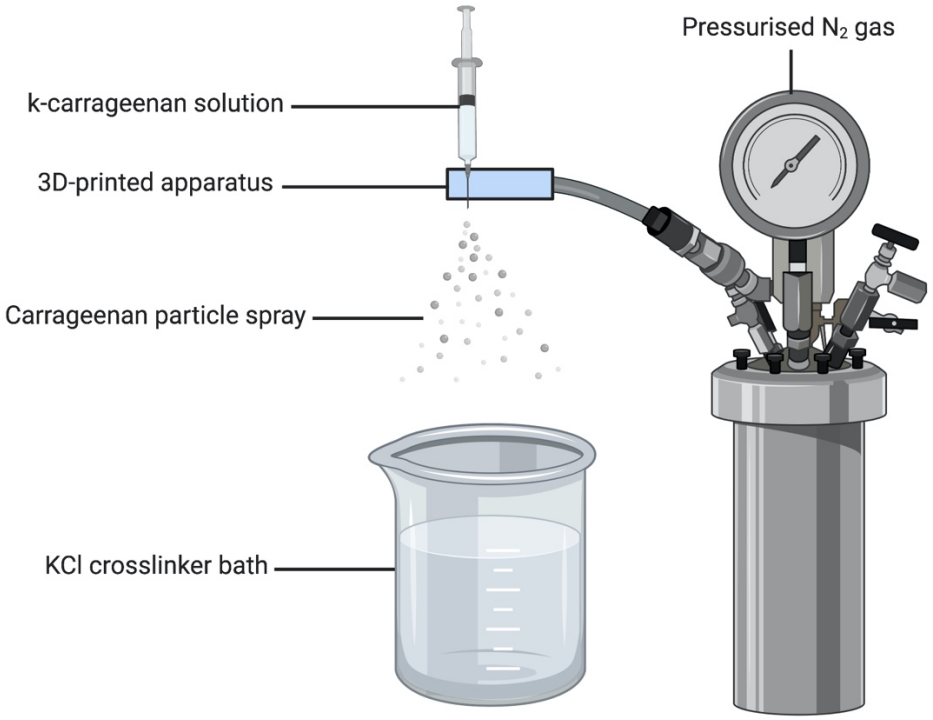

Figure 2.02: Schematic of the air-blowing procedure for producing carrageenan microspheres. Created with Biorender.com

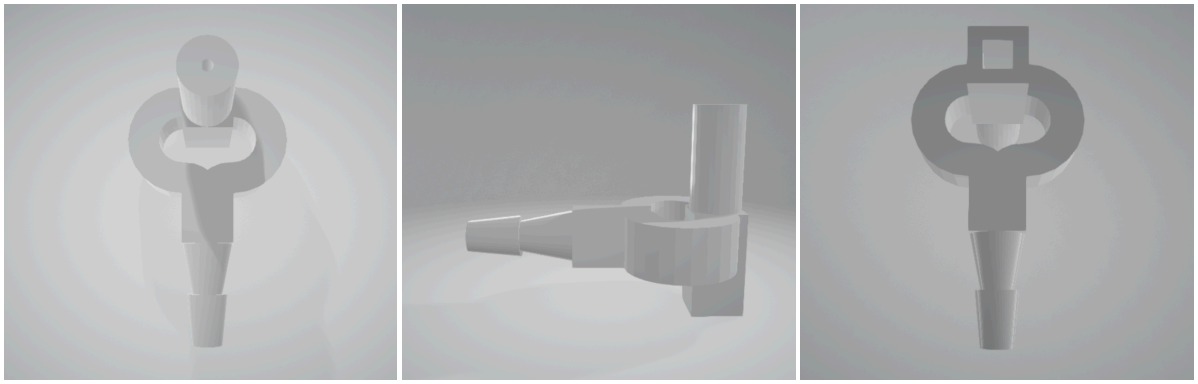

Figure 2.03: Modelling images of the 3D-printed apparatus used for production of carrageenan microparticles via air blowing.

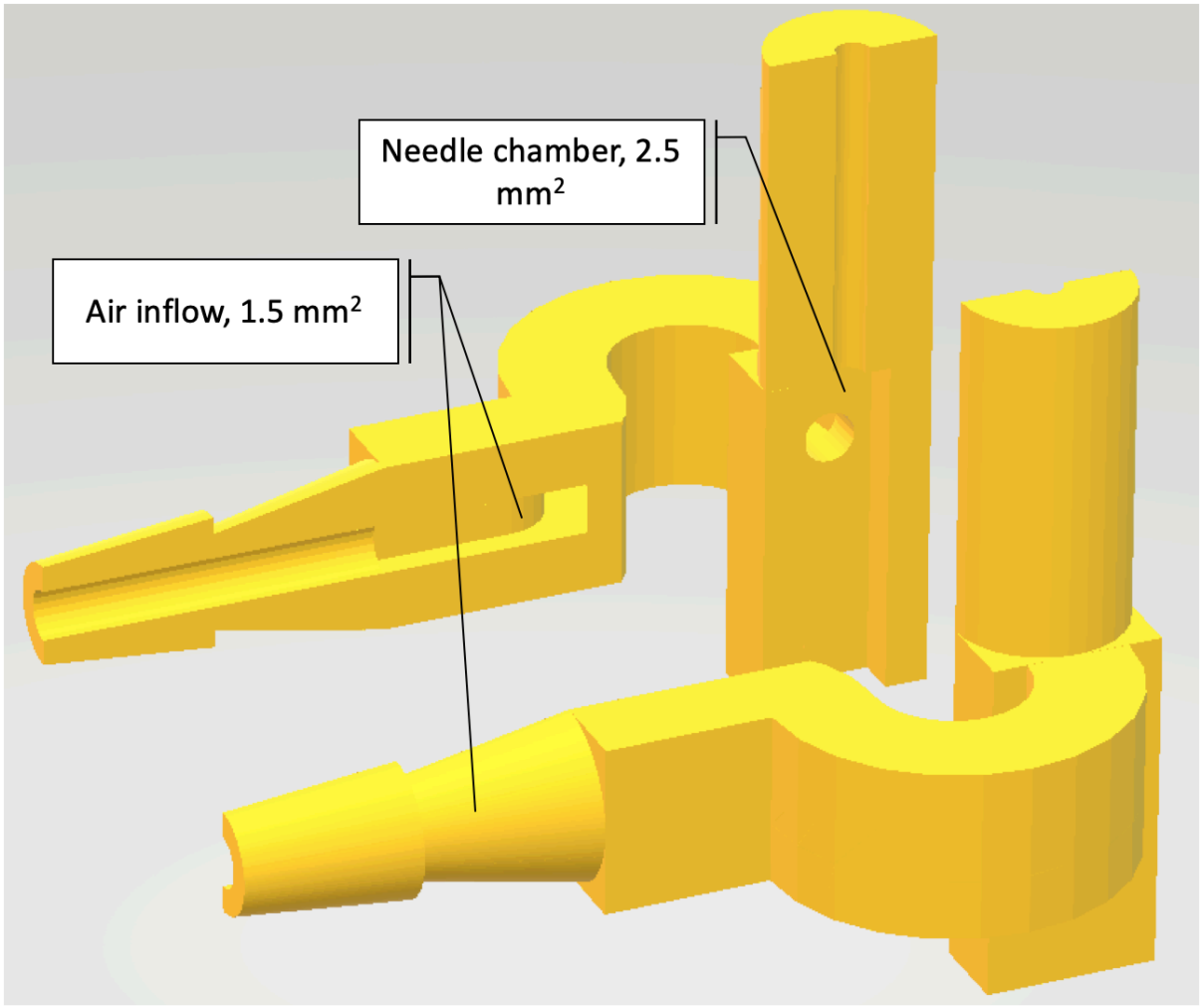

Figure 2.04: Design schematic of the 3D-printed apparatus used for production of carrageenan microparticles via air blowing. The chamber surrounding the needle has a horizontal cross-sectional area of 2.5 mm^2. The air-flow inlet splits into two channels, whose vertical cross-sectional area is 1.5 mm^2.

2.2.2 Stabilisation of carrageenan scaffolds

2.2.2.1 Manipulation of formation and environmental parameters

To analyse their effect on scaffold stability, the standard conditions outlined in section 2.2.1.1 were varied individually:

- Carrageenan concentration was varied between 0.5% (w/v) and 4% (w/v). This experiment was carried out using 12-well plates, and the average starting mass of the scaffolds was 1.9 ± 0.09 g.

- KCl concentration was varied between 2.5% (w/v) and 10% (w/v). This experiment was carried out using 24-well plates, and the average starting mass of the scaffolds was 0.8 ± 0.1 g.

The scaffolds were incubated in PBS solution at 37˚C and 5% CO_2, and their wet mass (after blotting with tissue paper to remove excess buffer or medium) was measured over time to ascertain the degree of degradation.

Scaffolds were also maintained in DMEM at 37˚C and 5% CO_2, and again their mass was measured over time. This was compared to that of scaffolds maintained in PBS. These experiments were carried out in 48-well plates, and the average starting mass of the scaffolds was 0.3 ± 0.1 g.

Later, scaffolds were also exposed to resazurin working solution (prepared as per 2.1.2.2) for 2 hours daily, and their mass was also measured over time and compared to scaffolds maintained in PBS and DMEM. These experiments were carried out in 48-well plates, and the average starting mass of the scaffolds was 0.2 ± 0.05 g.

Coated scaffolds (the procedure by which these were produced given in subsequent sections) were also analysed for degradation in this manner. These experiments were carried out in 24-well plates, and the average starting mass of the scaffolds was 0.7 ± 0.4 g.

2.2.2.2 Surface coating

2.2.2.2.1 Chitosan-coated carrageenan

Chitosan (Sigma 448869-50G) was deacetylated as per section 2.2.4, and dissolved in a 1% (v/v) solution of aqueous acetic acid (BDH 10001CU) to a concentration of 1% (w/v). Carrageenan discs (prepared as per section 2.2.1.1, in 24-well plates) were placed in new 24-well plates to which 1 ml of the chitosan solution was applied. The discs were left for 1 hour at room temperature for the chitosan to adsorb to the carrageenan surface. The chitosan solution was then removed, and the discs were washed thoroughly with mH_2O: each disc was immersed in 1 ml of mH_2O for 5 minutes at room temperature, which was then aspirated and replaced with fresh mH_2O of the same volume, and this was repeated as needed. After 3 washes, 1 ml of DMEM was applied to the wells and left for 5 minutes

at room temperature. The pH indicator (phenol red) of DMEM would turn yellow in the presence of any remaining acetic acid. When the DMEM did not show any signs of colour change after 5 minutes, it was determined that the scaffolds had been sufficiently washed.

To produce chitosan-coated carrageenan microspheres, chitosan solution was prepared as above, and KCl was added to a concentration of 5% (w/v). This resulted in an aqueous acetic acid solution of 1% (v/v) containing 1% chitosan (w/v) and 5% KCl (w/v). 2% (w/v) carrageenan solution was air-blown as per section 2.2.1.2, using 100 ml of this chitosan-KCl solution in a 200 ml glass beaker as the crosslinker bath.

2.2.2.2.2 Layer-by-layer chitosan-coating of carrageenan discs

κ-carrageenan was dissolved to 2% (w/v) concentration in mH_2O at 70˚C. 1 ml of this solution was placed into each well of a 24-well plate, the remainder was adjusted to pH 8 with aqueous sodium hydroxide (NaOH) solution of 0.1 M concentration**.** The pH 8 carrageenan solution was also plated out into a 24-well plate using 1 ml per well. The solution in the well-plates were allowed to gel (thermal induced) at room temperature, and crosslinked with 5% (w/v) KCl in mH_2O for 1 hour at room temperature, using 1 ml of KCl solution per well. The charged (pH 8) discs were:

1. Soaked in pH 8 aqueous NaOH of 0.1 M concentration, at room temperature, to ensure they were properly charged, using 1 ml of NaOH per well.
2. Washed for 5 minutes in distilled water (dH_2O) at room temperature.
3. Soaked in 1% (w/v) chitosan (which had been previously deacetylated as per section 2.2.4) solution, in 25% (v/v) acetic acid at room temperature (the higher concentration compared to standard was to give the solution a pH value of 2).
4. Washed again with dH_2O for 5 minutes at room temperature.
5. Soaked in the pH 8, 2% (w/v) aqueous κ-carrageenan solution for 20 minutes at 37˚C (the temperature used was to ensure the carrageenan solution did not gel).
6. Washed again with dH_2O for 5 minutes at room temperature.
7. And the process was repeated as needed.

The uncharged discs were divided into two sets. One set was coated with 1% (w/v) chitosan (deacetylated as per section 2.2.4) in 1% (v/v) acetic acid for 1 hour as per section 2.2.2.2.1, and the other was left untreated. All discs were washed with mH_2O: 1 ml of mH_2O was applied to each well and left for 5 minutes at room temperature, after which the mH_2O was aspirated and replaced with fresh mH_2O. DMEM was again used to confirm all remaining acetic acid had been removed; 1 ml of DMEM was applied to the wells and left for 5 minutes

at room temperature, when there was no yellow colouration observed (due to the phenol red pH indicator) samples were considered sufficiently washed. Samples generated from this procedure included carrageenan discs which were:

- Charged – Uncoated
- Charged – One chitosan coat
- Charged – Two chitosan coats, with one carrageenan coat in between
- Uncharged – Uncoated
- Uncharged – One (uncharged) chitosan coat

The process is illustrated in figure 2.05.

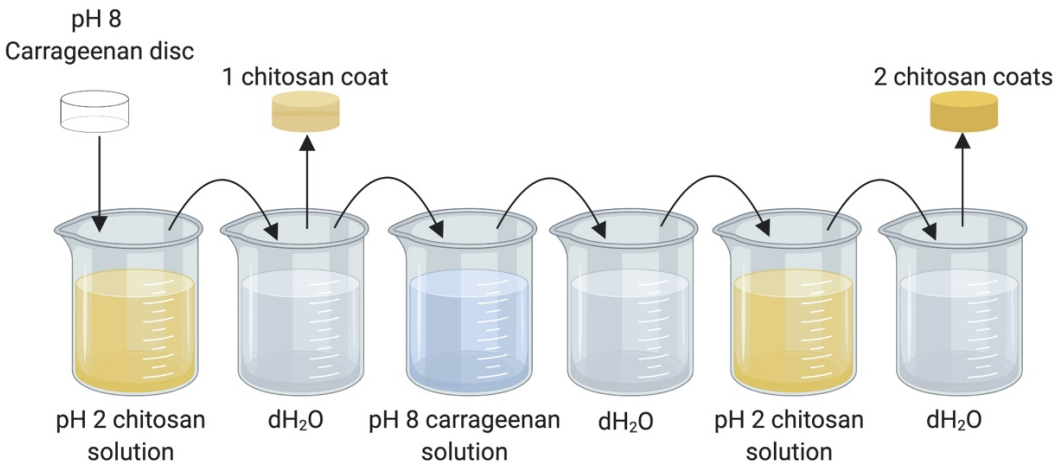

Figure 2.05: Process for layer-by-layer chitosan-coating of carrageenan discs. Created with Biorender.com.

2.2.2.2.3 Silk-coated carrageenan

Aqueous silk solution was prepared as per section 2.2.3.1 and diluted to a concentration of 1% (w/v) in mH_2O. Carrageenan discs (prepared as per section 2.2.1.1, in 24-well plates) were placed in new 24-well plates, to which 1 ml of the silk solution was applied, and left for 1 hour at room temperature. The silk solution was then removed, and replaced with 1 ml of 90% (v/v) aqueous ethanol (VWR 64-17-5), which was left for 1 hour at room temperature to insolubise the silk. The aqueous ethanol solution was removed and 1 ml of mH2O was applied to each well to wash the samples, the mH_2O was left for 5 minutes at room temperature before being replaced with fresh mH_2O, and this washing procedure was thrice repeated.

2.2.2.2.4 Production and coating of alginate discs

Sodium alginate (Sigma, A1112-100G) was dissolved in in mH_2O to a concentration of 5% (w/v). This solution was plated into nunclon delta 12-well plates, and using 1 ml of alginate solution per well. The solution was frozen at -80˚C for 3 hours, and subsequently lyophilised in a MicroModulyo-230 freeze-drier. The dry alginate discs were crosslinked with 1.5% (w/v) aqueous calcium chloride ($CaCl_2$) solution (Sigma, 442909-1KG), using 1 ml per well, for 1 hour at room temperature. These alginate discs were then divided into 3 sets.

Set 1 was left uncoated.

Set 2 was coated in chitosan as per section 2.2.2.2.1: Chitosan (Sigma 448869-50G) was deacetylated as per section 2.2.4, and dissolved in a 1% (v/v) solution of aqueous acetic acid (BDH 10001CU) to a concentration of 1% (w/v). The alginate discs were placed in new 24-well plates to which 1 ml of the chitosan solution was applied. The discs were left for 1 hour at room temperature for the chitosan to adsorb to the alginate surface. The chitosan solution was then removed, and the discs were washed thoroughly with mH_2O: .each disc was immersed in 1 ml of mH_2O for 5 minutes at room temperature, which was then aspirated and replaced with fresh mH_2O of the same volume, and this was repeated as needed. After 3 washes, 1 ml of DMEM was applied to the wells and left for 5 minutes at room temperature. The pH indicator (phenol red) of DMEM would turn yellow in the presence of any remaining acetic acid. When the DMEM did not show any signs of colour change after 5 minutes, it was determined that the discs had been sufficiently washed.

Set 3 was coated in silk fibroin as per section 2.2.2.2.3: Aqueous silk solution was prepared as per section 2.2.3.1 and diluted to a concentration of 1% (w/v) in mH_2O. The alginate discs were placed in new 24-well plates, to which 1 ml of the silk solution was applied, and left for 1 hour at room temperature. The silk solution was then removed, and replaced with 1 ml of 90% (v/v) aqueous ethanol (VWR 64-17-5), which was left for 1 hour at room temperature to insolubilise the silk. The aqueous ethanol solution was removed and 1 ml of mH2O was applied to each well to wash the samples, the mH_2O was left for 5 minutes at room temperature before being replaced with fresh mH_2O, and this washing procedure was thrice repeated.

2.2.3 Silk

2.2.3.1 Purification of silk fibroin from *Bombyx mori* silk cocoons and formation of silk fibroin films

A 2 litre solution of 0.02 M sodium carbonate (Na_2CO_3) (Sigma S2127-500G) was prepared, and heated to 100˚C. Twelve *Bombyx mori* silk cocoons were cut into small pieces and boiled in the solution for 1 hour. The silk pieces were then washed five times with dH_2O for 10 minutes per wash, using boiling water for the first wash. The silk pieces were then dried by having any excess water squeezed out between sheets of blue tissue (until no dampness was observed in the tissue), then left to air dry at room temperature overnight.

A 9 M aqueous solution of lithium bromide (LiBr) (Alfa Aesar, 13408) was prepared, and the degummed silk fibroin was dissolved therein, at 60˚C, to a concentration of 10% (w/v). The LiBr-silk solution was then subjected to dialysis in SnakeSkin™ tubing with 3.5 kDa molecular weight cut-off (Thermo Fisher, 68035) against dH_2O.

The resultant aqueous silk solution was either diluted to a desired concentration or subjected to lyophilisation using a MicroModulyo-230 freeze-drier and stored as a solid. Films were formed from the aqueous silk solution by diluting it to a concentration of 1% (w/v) in mH_2O, and placing into a nunclon delta 12-well plate (using 1 ml per well) and allowing to dry at room temperature. 90% (v/v) aqueous ethanol solution was then applied to induce conversion to type II silk fibroin, and render the protein insoluble in aqueous solution (using 1 ml of aqueous ethanol solution per well, which was left for 1 hour at room temperature). The aqueous ethanol was removed and silk films were washed thrice with 1 ml of mH_2O per well, for 5 minutes per wash. The films were again allowed to dry for 1 hour at room temperature. For differentiation experiments involving silk fibroin, the films were formed in 6-well plates using 3 ml of silk solution per well.

2.2.3.2 Production of silk fibroin microparticles

Microfluidic flow focusing was employed in order to produce silk fibroin microparticles. Silk fibroin solution was prepared as per section 2.2.3.1 and diluted to 3% (w/v) in mH_2O. The silk solution was used as the disperse phase. Initial attempts (where stated) used vegetable oil as the continuous phase, and a collection bath of methanol. Subsequent attempts, where stated, used a continuous phase comprised of oleic acid (Alfa Aesar A16663), methanol

(Alfa Aesar L13255), and Span 80 (Sigma S6760), in ratios of 73:25:2, respectively, and a collection bath composed of 50:50 methanol and continuous phase. In both cases, the solutions were pumped through a purpose-made, 3D-printed apparatus (made using an Ultimaker 2+ 3D printer), as illustrated in figured 2.06 – 2.07. The flow rates were used at a ratio of Q_o (outer phase flow rate) = Q_i (inner phase flow rate) x 40 (where Q_i = 0.015 ml / min). The particles were filtered using a 100 µm cell strainer [Fisherbrand™ 11517532] and transferred to 100% methanol, where they were left for 1 hour before being transferred to another bath of methanol, again being left for 1 hour. This process was repeated one more time before the particles were imaged under white light microscopy using a Leica DMI 4000 B microscope. The flow rates were also varied to $Q_o = Q_i$ x 20, and $Q_o = Q_i$ x 10.

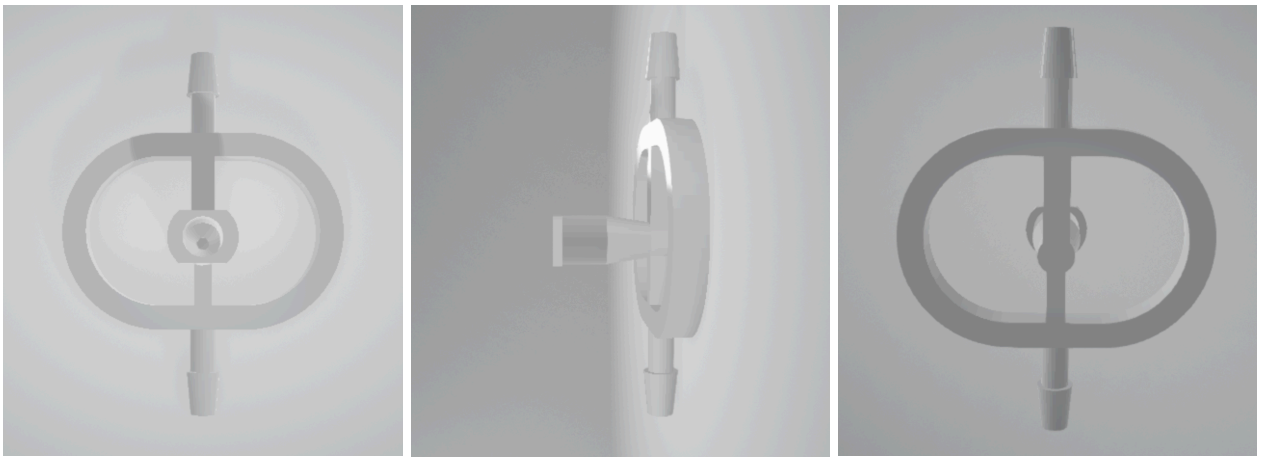

Figure 2.06: Modelling images of the 3D-printed apparatus used for microfluidic flow focusing in production of silk fibroin microparticles.

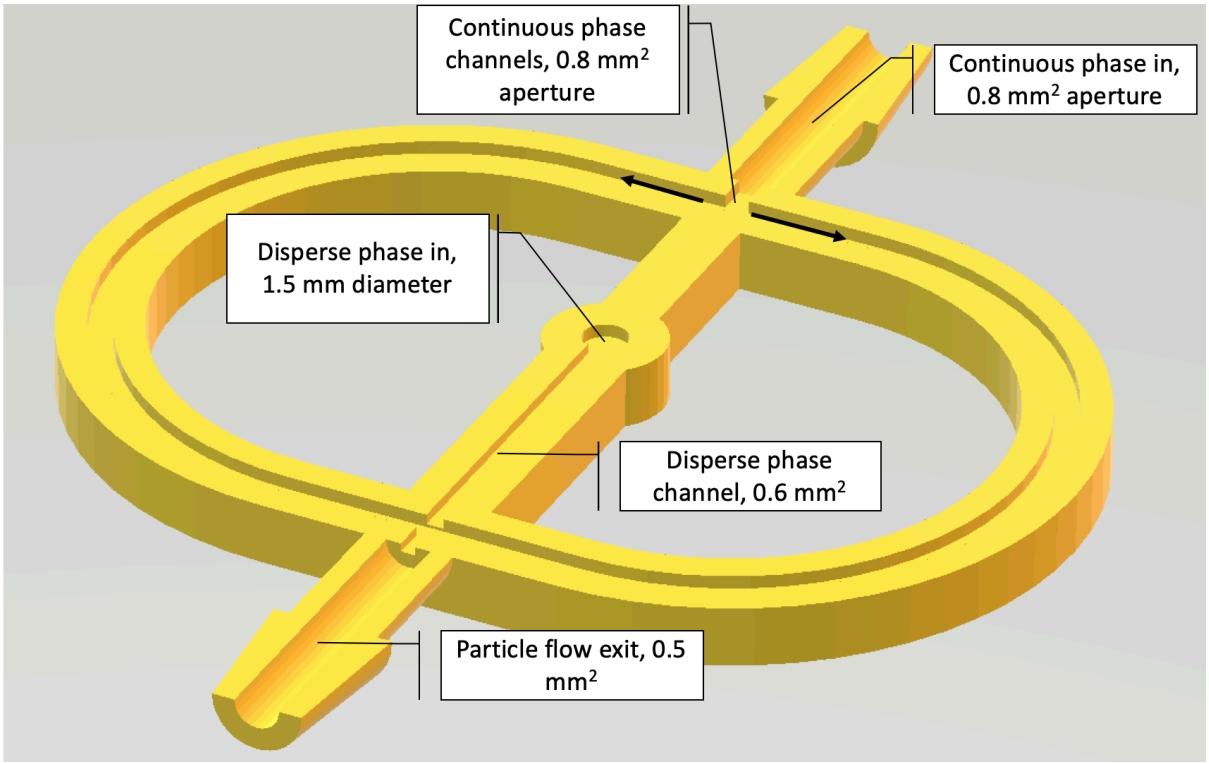

Figure 2.07: Design schematic of 3D-printed apparatus used for microfluidic flow focusing in production of silk fibroin microparticles.

2.2.4 Deacetylation of chitosan and formation of chitosan films

45% (w/v) aqueous NaOH (Sigma 221465) was prepared. Chitosan (Sigma 448869-50G) was placed in rounded-bottom flasks, and the NaOH solution was added so the chitosan was present as a concentration of 10% (w/v). Three samples were prepared in this manner. The air was removed from the flasks and replaced with gaseous N_2 and the flasks then purged with N_2 a further three times in this manner to ensure a purely N_2 internal atmosphere. The flasks were heated to 90˚C and the N_2 was continuously pumped through and allowed to exit via an escape needle. The apparatus design is illustrated in figure 2.08. The three samples were each heated for varying lengths of time: 30 minutes, 60 minutes, and 90 minutes. In order to determine the DDA%, chitosan was dissolved at 10 mg / ml in D_2O acidified with concentrated HCl. ^1H nuclear magnetic resonance (NMR) spectra were recorded at 70˚C on a Bruker Acance III spectrometer by Dr Tim Woodman.

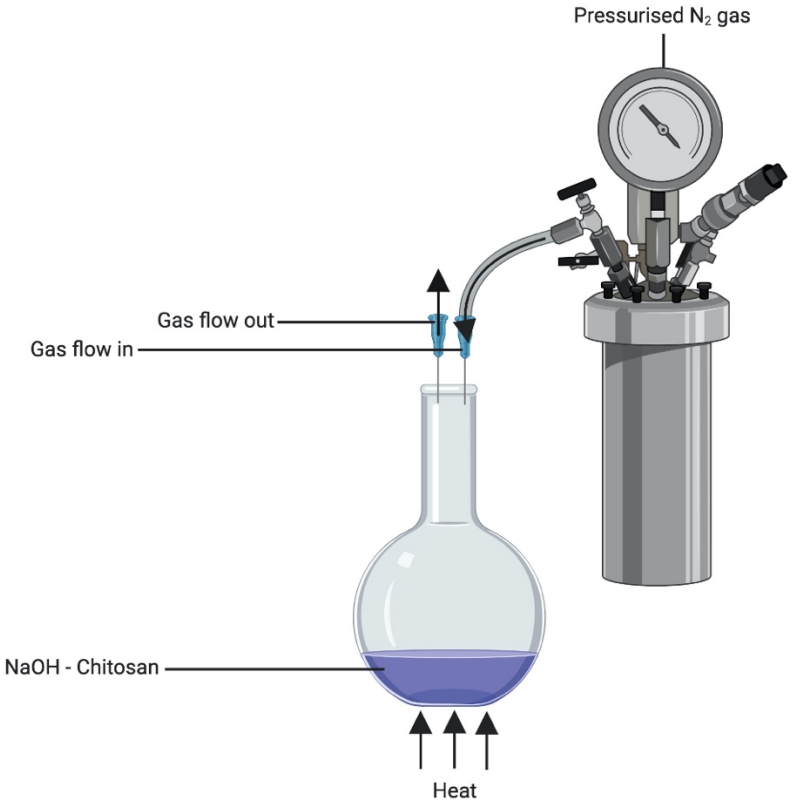

Figure 2.08: Apparatus for deacetylation of chitosan in NaOH under nitrogen atmosphere. Created with Biorender.com.

In order to prepare chitosan films for cell-seeding, chitosan samples were dissolved in 1% (v/v) aqueous acetic acid, to a concentration of 1% (w/v). The solutions were placed into nunclon delta 12-well plates, using 1 ml of solution per well, and allowed to dry at room temperature.

2.2.5 Zein

2.2.5.1 Production of zein films

Zein powder (Sigma Z3625-500G or Acros Organics A0347340) was dissolved in 70% (v/v) aqueous ethanol to a concentration of 1% (w/v). The solution was cast into wells of multi-well Nunclon delta plates (sizes varying depending on experiment, to be stated in subsequent sections) and allowed to dry at room temperature. For 12-well plates, 1 ml of zein solution was used. For 24-well plates, 500 µl of solution per well was used. For 48-well plates, 250 µl of solution per well was used. Alternately, where stipulated, zein films were formed on glass coverslips by placing 200 µl on the coverslip, spreading evenly using the

edge of another coverslip, and allowing to dry at room temperature. An initial experiment was conducted to analyse C2C12 proliferation on Sigma-brand zein versus Acros-brand zein (chapter 4, figure 4.01). All subsequent experiments used Sigma-brand zein.

2.2.5.2 Mechanical testing of zein films

Zein powder (Sigma Z3625-500G) was dissolved in 70% (v/v) aqueous ethanol to a range of concentrations (w/v): 1%, 5%, and 10%. The solutions were cast separately into silicon moulds and allowed to dry at room temperature. These films were either left dry or hydrated via immersion in DMEM overnight at 37˚C. The films were removed from the moulds and cut into 5 cm x 2 cm (length x width) rectangular strips. Films were then subjected to dynamic mechanical analysis in a Mettler Toledo DMA1, analysis was carried out over a period of 28 seconds at 37˚C, using a fixed offset force of 0.5 N and an oscillating force of 0.2 N, with a displacement amplitude of 10 μm at a frequency of 1 Hz. Data was automatically collected using STARe software.

2.2.5.3 Production of zein microparticles via microfluific flow focusing

Three zein solutions were prepared, wherein zein (Sigma Z3625-500G) was dissolved in 70% (v/v) aqueous ethanol to 1% (w/v), 5% (w/v), and 10% (w/v). These zein solutions were used as the disperse phases. Vegetable oil containing 0.1% (v/v) Span 80 was used as the continuous phase for all conditions. The solutions were placed into 10 ml plastic syringes and pumped (using a Cole Parmer 78-9100C syringe driver) through a purpose-made, 3D-printed, crucifix device, made using an Ultimaker 2+ 3D printer, into a collection bath of 100 ml mH_2O. The flow rates were used in ratios of $Q_o = Q_i \times 40$, $Q_o = Q_i \times 20$, and $Q_o = Q_i \times 10$. Q^i was maintained at 0.05 ml / min. The collection solution was placed into a phase separation funnel, allowed to separate for 1 hour at room temperature, and the oil was discarded. The aqueous particle suspension was filtered through a 70 μm cell strainer [Fisherbrand™ 11597522] and subsequently washed thrice: 100 ml of mH_2O was added to the filtered particles and left for 5 minutes at room temperature, this was then repeated twice more. 500 μl of this aqueous suspension was applied to a glass cover slide and thinly spread thereon, and the particles were subsequently imaged under white light microscopy using a Leica DMI 4000 B microscope. The 3D printed apparatus design in illustrated in figures 2.09 – 2.10.

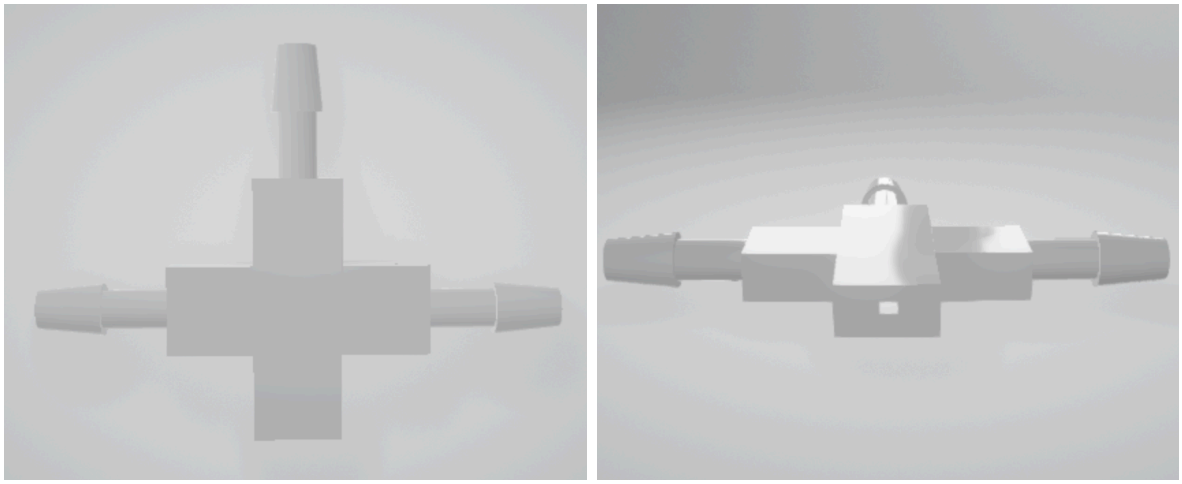

Figure 2.09: Modelling images of the 3D printed apparatus used for generation of zein microparticles via microfluidic flow focusing.

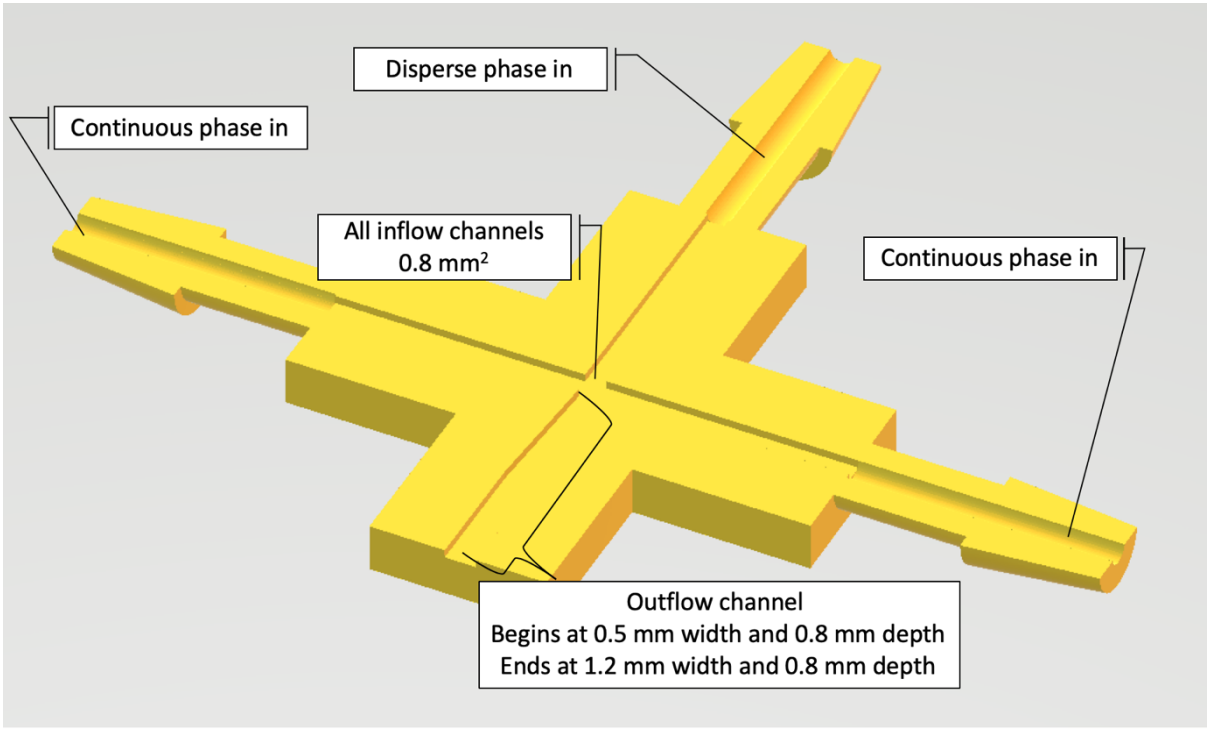

Figure 2.10: Design schematic of the 3D printed apparatus used for production of zein microparticles via microfluidic flow focusing.

2.2.5.4 Production of zein microparticles via emulsification precipitation

400 ml of vegetable oil was heated to 70˚C in a 500 ml glass beaker. Tween 20 (Sigma P1379-500ML) was added to a concentration of 1% (v/v) and mixed thoroughly. 50 ml of 3% (w/v) zein dissolved in 70% (v/v) aqueous ethanol was added. The solution was stirred for 30 minutes at 600 RPM, then placed on ice. 200 ml of chilled mH_2O was added, and the

solution was stirred at 600 RPM for 30 minutes. The collection solution was placed into a phase separation funnel, allowed to separate for 1 hour at room temperature, and the oil was discarded. The aqueous suspension of particles was filtered through a 70 μm cell strainer [Fisherbrand™ 11597522] before washing thrice: 100 ml of mH_2O was added to the filtered particles and left for 5 minutes at room temperature, this was then repeated twice more. 500 μl of this aqueous suspension was applied to a glass cover slide and thinly spread thereon, and the particles were subsequently imaged under white light microscopy. Q_i was maintained at 0.05 ml / min.

The process was repeated using stirring speeds of 300 RPM and 10 RPM.

2.2.5.5 Production of wet-spun zein fibres

Zein was dissolved in 50:50 chloroform-methanol (Alfa Aesar 32614 and L13255) to various concentrations (1%, 5%, 10%, and 15% w/v). The solution was pumped into 500 ml of mH_2O (in a 500 ml glass beaker) through an 18-gauge (Adhesive Dispensing Ltd AD718100) or a 27-gauge needle (Adhesive Dispensing Ltd AD727050), using a Cole Parmer 78-9100C syringe driver, at various flow rates between 1 and 50 ml / hr.

2.2.5.6 Production of electrospun zein fibres

Dry zein powder was dissolved in 70% aqueous ethanol to a concentration of 20% (w/v). These solutions were pumped through a plastic syringe (BD Plastipak 302188), topped with a 27-gauge needle (Adhesive Dispensing Ltd AD727050), at a rate of 0.5 ml / hr using a Cole Parmer 78-9100C syringe driver. A voltage of 20 kV was applied to the needle using a Genvolt high voltage power supply. A purpose-built collector comprising of a wooden block, wrapped in copper wiring, and covered with aluminum foil, was earthed and used to retrieve the electrospun fibres. In some instances (for visualisation of fibres via white-light microscopy) glass cover slides were affixed to the collector and the fibres were thusly collected on glass.

Where stated, attempts were made to produce aligned electrospun fibres by using spaced, parallel electrodes as collectors, as described by Li *et al.* [141]. In this instance, a glass cover slide was placed across the collectors in order to image the fibres.

2.2.5.7 Stabilisation of electrospun zein fibres

Electrospun mats (prepared as per section 2.2.5.6) were punched into discs of 1.9 cm^2 diameter using a cork borer. These mats were initially maintained in PBS for varying lengths of time (1 – 7 days), and later batches were treated in various ways as described below. After treatment, the discs were soaked in distilled water: each disc was placed into a well of a 24-well plate, to which 1 ml of dH_2O was added, and their surface areas measured over time using ImageJ image analysis software (NIH, Bethesda, MD, USA; http://imagej.nih.gov/ij).

2.2.5.7.1 EDC / NHS crosslinking

2-ethanesulfonic acid (MES) buffer (Alfa Aesar H56472) was prepared to a concentration of 0.05 M, at pH 5.4. 1-Ethyl-3-(3-dimethylaminopropyl)carbodiimide (EDC) (Alfa Aesar A10807) and N-Hydroxysuccinimide (NHS) (Alfa Aesar A10312) were dissolved in the MES buffer, acetone or ethanol, each in amounts of 1.731 g EDC and 0.415 g NHS per gram of protein. When applied to electrospun discs, the electrospun discs were placed into 24-well plates, and appropriate amount of crosslinker solution (determined by the mass of the sample) was added to each well and left for 1 hour at room temperature. This procedure was also applied, where stated, to zein films formed in 12-well plates as per section 2.2.5.1. The crosslinker solution was removed and replaced with 1 ml dH_2O which was left for 5 minutes at room temperature, this washing procedure was repeated as necessary. DMEM was used to ascertain when samples had been sufficiently washed: after 3 washes, 1 ml of DMEM was applied to each well and left for 5 minutes at room temperature. When no yellow colouration (owing to the phenol red pH indicator) was observed after 5 minutes, the samples were consideref sufficiently washed. 1 ml of dH_2O was then applied to each well, and the plates were left at room temperature. The electrospun mats were analysed for reduction in surface area over time using ImageJ software (NIH, Bethesda, MD, USA; http://imagej.nih.gov/ij). This procedure was also later carried out using 10% and 1% of the aforementioned crosslinker concentrations.

2.2.5.7.2 Citric acid crosslinking

Treatment with citric acid occurred before electrospinning. For this, citric acid (Sigma C0759-500G) was dissolved in 70% aqueous ethanol to a concentration of 9% (w/v). Zein powder was then dissolved in this solution to a concentration of 50% (w/v). The solution

was left for 48 hours at room temperature, before being diluted to 25% (w/v) with additional 70% aqueous ethanol to lessen the viscosity. This procedure was carried out at room temperature. The solution was then electrospun as per section 2.2.5.6. Discs of known area were punched from the mats using a cork boarer. These discs were then heated to 90 ˚C for 1 hour to induce crosslinking. Other samples were left unheated as controls. Electrospun zein mats formed from zein solution which were aged for 48 hours were used as super-negative controls. The discs were then placed into wells of 24-well plates, to which 1 ml of dH_2O was added. Samples were maintained at room temperature and analysed for reduction in surface area over time using ImageJ software (NIH, Bethesda, MD, USA; http://imagej.nih.gov/ij). Samples aged with citric acid as above

2.2.5.7.3 UV treatment

After electrospinning as per section 2.2.5.6, electrosun mats were exposed to UV light using a Bioquell ABS1200UV lamp for 2 hours on each side. Discs were then placed into wells of 24-well plates, to which 1 ml of dH_2O was added. Samples were maintained at room temperature and analysed for reduction in surface area over time using ImageJ software (NIH, Bethesda, MD, USA; http://imagej.nih.gov/ij).

2.2.5.8 Preparation of electrospun zein nanofibres for scanning electron microscopy (SEM) analysis

Samples of electrospun fibre mats were cut into small square pieces (no greater in size than 2 cm^2). The samples were placed on aluminium stubs and anchored in place with double-sided tape. Thin strips of the same tape were used to anchor down any raised sides or corners of the samples. The stubs were placed in a tin container with a punctured lid, which was stored under vacuum overnight. The following day, the samples were removed from the vacuum and coated with gold using an Edwards Sputter Coater S150B. The samples were then imaged under SEM using a JEOL JSM-6480LV scanning electron microscope.

2.2.5.9 Preparation of cell cultures on electrospun zein nanofibers for SEM

DMEM powder (Sigma D5648-1L) was added to premade liquid DMEM at 13.4 g / L to make double-strength medium. The double-strength medium was aliquoted and 25 % electron microscopy grade glutaraldehyde (GDA) (TAAB G011/3) was added to one aliquot at a ratio of 5 ml per 25 ml of double-strength medium. This was diluted 1:1 with milliQ water. Potassium ferrocyanide (TAAB P018) was added to a concentration of 1% (w/v). The culture

medium was slowly aspirated from the cells, and cells were washed with double-strength medium. Cells were then incubated for 2 hours with GDA-potassium ferrocyanide solution at 37˚C and 5% CO_2 before washing once more with double-strength medium. Cells were post-fixed in an aqueous solution containing 1% (w/v) aqueous osmium tetroxide (TAAB O015/1) and 1% (w/v) potassium ferrocyanide for 1 hour in a fume hood at room temperature. Cells were then washed in dH_2O twice for 10 minutes per wash, and stained with 2% (w/v) uranyl acetate [Agar scientific, AGR1260A] for 1 hour, whilst being protected from light. Cells were then progressively dehydrated in aqueous acetone at 50%, 70%, and 90% (v/v), culminating in 100% dry acetone. Immersion in these solutions was performed for 10 minutes at a time, twice for each concentration. A 50:50 solution of acetone and hexamethyldisilazane (HMDS; TAAB H028) was prepared and applied to cells for 15 minutes. HMDS solution was then applied to cells twice, for 15 minutes per application. The HMDS was aspirated off, and the samples were left partially covered in the fume hood for any remaining liquid to evaporate. Cells were then prepared and analysed via SEM as per section 2.2.5.8.

2.3 Statistical analysis

Statistical analysis was conducted using IBM SPSS Statistics for Windows, version 26 (IBM Corp, Armonk, N.Y, USA). A Shapiro-Wilk analysis was conducted to test for normal distribution. A Levene's test of sphericity was conducted to test for equality of error variances, and a Greenhouse-Geisser correction was applied where a lack of sphericity was noted. A p value of < 0.05 was considered statistically significant. A list of analysis techniques used is given overleaf in table 2.

Figure number	Statistical analysis technique
3.10	Log rank (Mantel-cox) analysis of survival with pairwise comparisons
3.11	Two-way analysis of variance (ANOVA) with pairwise comparisons
3.13	One-way ANOVA with Tukey's honest significant difference post-hoc test
3.14	Log rank (Mantel-cox) analysis of survival
3.19	Repeated measures ANOVA with pairwise comparisons
3.20	Repeated measures ANOVA
4.02	Repeated measures ANOVA
4.08	Two sample t-test
5.11	Paired t-test
5.40	Repeated measures ANOVA with pairwise comparisons
5.44	Repeated measures ANOVA

Table 2: List of statistical analysis techniques used, ordered by respective figure numbers

Chapter 3 - Production and Stabilisation of Hydrocolloid Scaffolds

3.1 Introduction

3.1.1 Hydrogels

Hydrogels are formed via the crosslinking of hydrophilic polymers [68, 90]. They are desirable as tissue engineering scaffolds, as their water-content and hydrophilic-polymer composition enable them to mimic the extracellular matrix [91, 92, 142]. Hydrogels have been formed from animal-derived substances for tissue engineering purposes, such as collagen and gelatin [143-145]. However, as discussed in chapter 1, *in vitro* meat production represents a model whereby the ethical and environmental impact of conventional meat production can be significantly reduced, and so this work aims to utilise plant-based materials as much as possible.

3.1.2 Alginate

A popular plant-derived material for use in tissue engineering hydrogels is alginate: a structural biomaterial derived from Phaeophyceae, or 'brown algae' [68, 146]. Alginate is a polymer whose repeating units comprise two monomers: D-mannuronic acid and L-guluronic acid [69]. However, due to alginate's lack of ability to bind cells in its natural form, studies seeking to utilise alginate as a cytocompatible hydrogel must functionalise the alginate, commonly via covalent attachment of cell-binding peptides [70-73]. Such modification is made possible by the carboxyl groups within the polymer's structure [146].

A noted problem with ionically crosslinked alginate hydrogels is the susceptibility of the divalent calcium ions to being displaced by monovalent sodium ions in solution, resulting in a weaker gel [68, 147]. Although physical crosslinking procedures can be applied to hydrogels, these are not without drawbacks. Such procedures may employ toxic reactants [68] such as EDC [148, 149]. Physically crosslinked hydrogels also exhibit different mechanical properties than their ionically crosslinked counterparts: Kong *et al.* for example, showed covalently crosslinked alginate hydrogels to be weaker than those crosslinked via divalent cations, with a significant lowering of the point of failure in tensile stress-strain trials [148]. Zhao *et al.* in their stress-relaxation studies of covalent versus ionic crosslinking of hydrogels, propose that these differing mechanical properties are a result of ionic-

crosslinking bonds being able to break and easily reform under stress, whereas covalent crosslinking bonds are not so adaptable [149].

3.1.3 Carrageenan

An alternative may be found in carrageenan: another seaweed-derived polysaccharide [14]. There are three types of carrageenan that are commonly used, each distinguished (primarily) by the number of sulfonate (OSO_2) groups contained within their repeating units [14], these being:

- K-carrageenan, containing one OSO_2 group
- I-carrageenan, containing two
- Λ-carrageenan, containing three

These structural differences are reflected in the various properties and uses of the various carrageenans. I-carrageenan may be crosslinked by use of calcium ions to form gels, though these gels are not as strong as those formed via potassium-ion crosslinking of κ-carrageenan [14, 150]. Λ-carrageenan, in contrast, will not form a gel in the presence of cations (and is used primarily in the food industry as a thickening agent) [14, 150]. In the case of κ-carrageenan, the monovalent potassium ions serve to cancel out repulsion between the single sulfate groups in each repeating unit, forming an ionic bridge therebetween [151]. Accordingly, ι-carrageenan relies on the divalent calcium cations to accomplish the same with its two sulfate groups per repeating unit. Mu-carrageenan and vega-carrageenan are two additional types of carrageenan that are known to exist, though these are structural precursors of κ and ι carrageenan (respectively) [150]. Carrageenan solutions are also susceptible to thermogelation; Upon heating to temperatures of approximately 80˚C, the polymer chains exist as random coils [152]. When cooled, these random coils will interact to form double helices, and this stage may be induced by temperatures of approximately 50˚C ± 10˚C [152]. These helices may aggregate by way of hydrogen-bonding in order to form gels [152]. K-carrageenan would appear to be the ideal choice from which to produce a hydrogel for tissue-engineering applications, given its capacity to form the strongest, most rigid hydrogels out of the available carrageenan classes.

Carrageenans have been noted to have the ability to associate with protein motifs associated with cell-surface receptor binding, and this is perhaps the key feature that may give them potential over alginate [130]. Carrageenan hydrogels have also been applied to

epithelial cells [129], osteocytes [133], and fibroblasts [134]. Studies concerning myoblastic interactions with carrageenan hydrogels appear sparse, however.

This chapter explores the potential of ionically crosslinked carrageenan hydrogels as bioscaffolds on which to culture muscle tissue.

3.1.4 Aims and objectives

This chapter aims to produce fibrous and / or particulate carrageenan hydrogel scaffolds, which can support the growth and differentiation of surface-seeded and / or encapsulated myogenic cells.

3.2. Results and discussion

Carrageenan gels were produced via ionic crosslinking, wherein liquid carrageenan solution (of 2% w/v concentration, unless otherwise stated) was placed into a 5% (w/v) aqueous KCl solution, either by adding dropwise to form beads or extruding as a stream directly into the solution to form fibres. These morphologies were chosen due to their potential use in bioreactors: stirred-tank, rotating wall, and fluidised bed vessels for beads and fixed-bed, perfusion, or airlift vessels for fibres, for example. Additionally, these morphologies have previously been chosen for cell-culture and tissue-engineering applications [129, 153, 154]. This process was simple and scaffolds were easily produced. Cells were seeded thereon in order to assess their compatibility with the scaffolds. However, it soon became apparent that these carrageenan scaffolds were degrading: losing their gelatinous structure and gradually reverting to a liquid state. This resulted in a loss of surface-seeded cells, and impaired the gels' viability as bioscaffolds. Encapsulation of cells would not, in itself, be an adequate solution to this problem, as the scaffolds liquified too quickly for any meaningful culture to be achieved (based on time taken to proliferate and differentiate into myotubes on TCP). In order to utilise these carrageenan constructs as bioscaffolds, this degradation issue required addressing and correction.

3.2.1 The effect of formation parameters and maintenance conditions on hydrogel stability

3.2.1.1 The effect of carrageenan concentration

The first independent variable assayed was the percentage concentration (w/v) of the carrageenan scaffolds. This was chosen because the carrageenan concentration is the first and most obvious parameter determined in the formation process of carrageenan scaffolds. Additionally, it has been noted that the polymer concentration of hydrogels can have an effect on efficiency of gelation [155]. In particular, Zhang *et al.* noted that the gelation threshold of alginate gels was inversely proportional to the concentration of alginate solution [156]. It was also observed here that, in the case of carrageenan gels formed with a lower carrageenan content (usually 1% w/v or lower), thermally induced gelation took longer to occur than for those gels formed with higher carrageenan concentrations (data not shown). Carrageenan solutions were prepared at various percentage (w/v) concentrations and beads and fibres were formed as per chapter 2 section 2.2.1.1, using KCl crosslinker solution at a standard concentration of 5% (w/v), for 1 hour, at room temperature. The resultant carrageenan scaffolds were then maintained in PBS solution at 37˚C, with their masses being measured at various timepoints, and standardising the data by converting the mass values to a percentage of the initial mass recorded. This data is displayed in figures 3.01 and 3.02. The mean time taken to complete dissolution of the scaffolds is represented in figure 3.03. The maximum mass recorded (denoting the degree of swelling) is shown in figure 3.04.

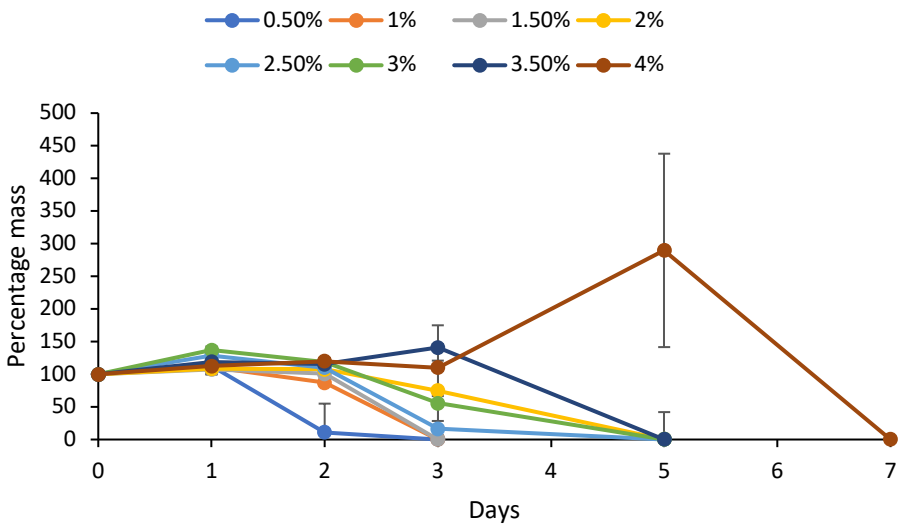

Figure 3.01: Degradation of carrageenan beads of various percentage (w/v) concentration and crosslinked using 5% (w/v) KCl solution, represented as percentage mass of original over time in 37˚C PBS solution. Data represent median ± interquartile range.

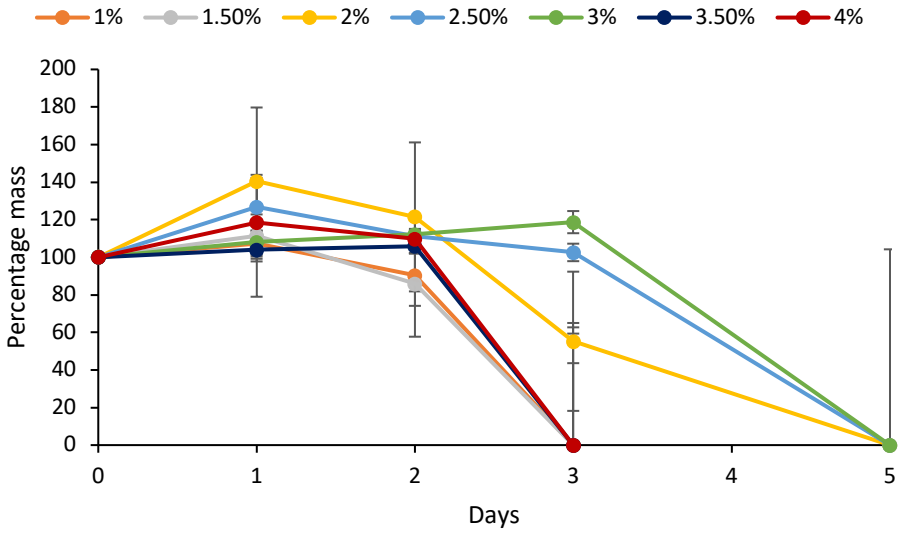

Figure 3.02: Degradation of carrageenan fibres of various percentage (w/v) concentration and crosslinked using 5% (w/v) KCl solution, represented as percentage mass of original over time in 37˚C PBS solution. Data represent median ± interquartile range.

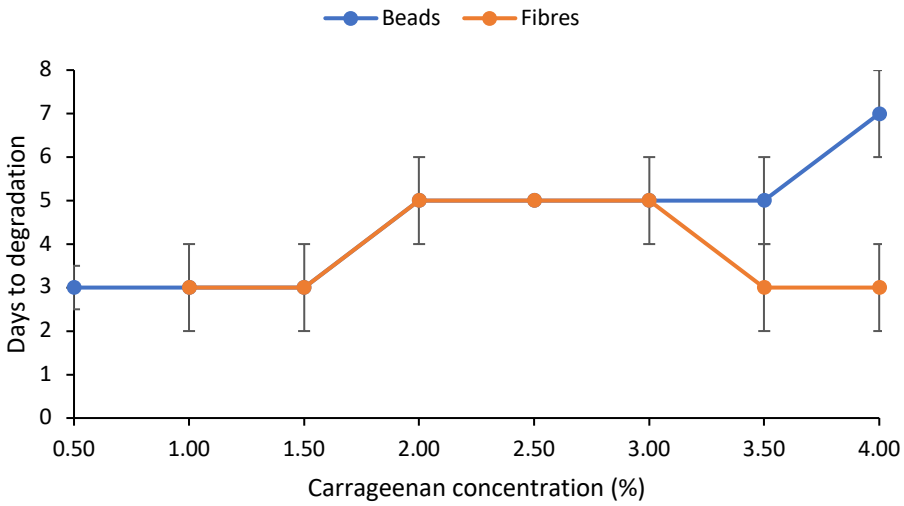

Figure 3.03: Degradation time of carrageenan beads and fibres against percentage (w/v) concentration (crosslinked using 5% (w/v) KCl solution). Degradation time is defined here as the time taken for the sample to reach 0% initial mass, i.e. to become fully dissolved in solution. Data represent median ± interquartile range.

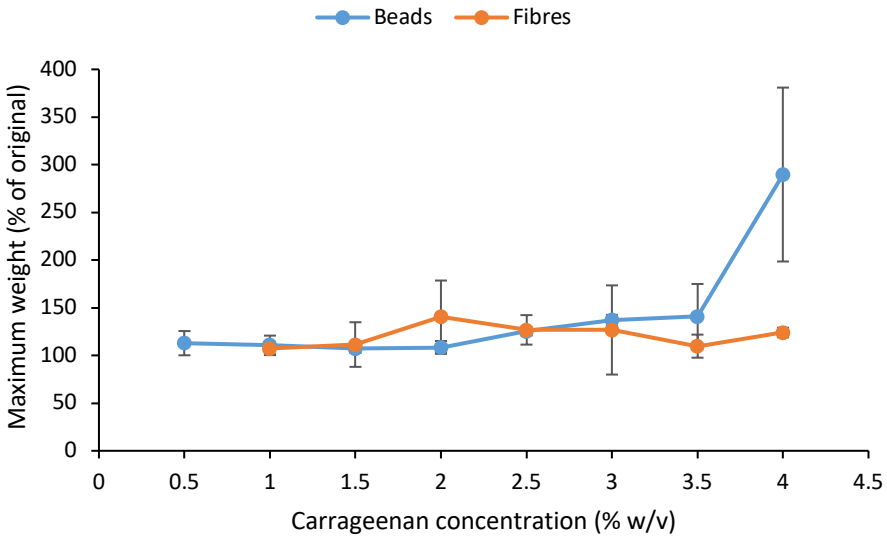

Figure 3.04: The maximum recorded mass of carrageenan beads and fibres of various percentage (w/v) concentration (crosslinked using 5% (w/v) KCl solution). Data represent median ± interquartile range.

Figures 3.01 and 3.03 show a positive correlation between the percentage concentration of carrageenan beads and total degradation time (the time taken until carrageenan scaffolds were irretrievable from the liquid in which they were immersed). This does not necessarily translate to an increase in stability however, as Figure 3.01 also shows that carrageenan

beads of higher concentration experience an increased degree of swelling before degrading. Figure 3.04 analyses this phenomenon in more detail, and shows an exponential relationship between carrageenan concentration and the mass increase of carrageenan beads. This is not unexpected, as other ionically crosslinked hydrogels (such as those composed of alginate) have been shown to experience an increase in swelling when formed with a higher concentration of polymer [157]. A truly stabilised carrageenan scaffold would show an increased degradation time (or ideally, no degradation at all), wherein the scaffolds experience little fluctuation from their initial mass. Although Figure 3.02 does show that the increase in mass does occur in the fibrous scaffolds, Figure 3.04 shows no correlation between this mass increase and carrageenan concentration. Although the results suggest that increasing the carrageenan content of scaffolds may result in a longer degradation time, it cannot be said to improve the stability of the scaffolds.

Figures 3.03 and 3.04 show differences in the general trends of degradation time and swelling (respectively) between beads and fibres. Degradation time for beads appears to show a roughly linear correlation with carrageenan percentage, however degradation time for fibres appears to show no particular correlation (figure 3.03). The degree of swelling appears to increase in an exponential fashion for beads as carrageenan concentration rises, but again no particular correlation between the variables is observed for fibres. This may be due to the higher surface area per unit mass that would be attributable to beads compared to fibres, as this would result in increased contact between the carrageenan and the local environment.

Although 4% (w/v) concentration of carrageenan led to an increase in degradation time, it also led to an increase in the degree of swelling for beads. Therefore, subsequent experiments maintained 2% concentration of carrageenan (w/v) as standard.

As previously stated, the carrageenan concentration is the first variable to appear in the scaffold formation process. The second is the concentration of KCl in the aqueous KCl crosslinker solution, and this was the next variable assayed for any effect on scaffold stability.

3.2.1.2 The effect of crosslinker concentration

It has been shown that crosslinker concentration can indeed have a significant impact on resultant hydrogels, such as their mechanical properties [158, 159]. For example, Jang *et al.* showed that, in the case of alginate hydrogels, increases in the crosslinker concentration

corresponded to exponential increases in the point of failure under compressive stress, and thus the compressive moduli of the gels [159]. Although this study also showed little difference in degradation times of these gels (in fact, little degradation at all over the course of 7 days), it is important to note that this study maintained the gels in distilled water, whereas gels here were maintained in PBS or DMEM (these solutions contain higher concentrations of metal cations, the implications of which are evidenced and discussed in section 3.2.1.3). It was hoped that greater amounts of KCl would facilitate a greater amount of crosslinking within a specific length of time, and so this was assessed next to ascertain if carrageenan scaffolds could be stabilised by increased crosslinker concentrations. The effect was measured, as before, by soaking carrageenan scaffolds (formed from 2% w/v carrageenan solution as per chapter 2, section 2.2.1.1), crosslinked using various crosslinker concentrations as per chapter 2, section 2.2.2.1) in PBS solution at 37˚C, and measuring their mass at various timepoints, and standardising the data by converting the values to a percentage of the initial mass recorded. This data is shown in figures 3.05 for beads and 3.06 for fibres. The mean times taken for complete degradation is shown in figures 3.07. The degree of swelling, represented as the maximum mass recorded, is shown in figure 3.08.

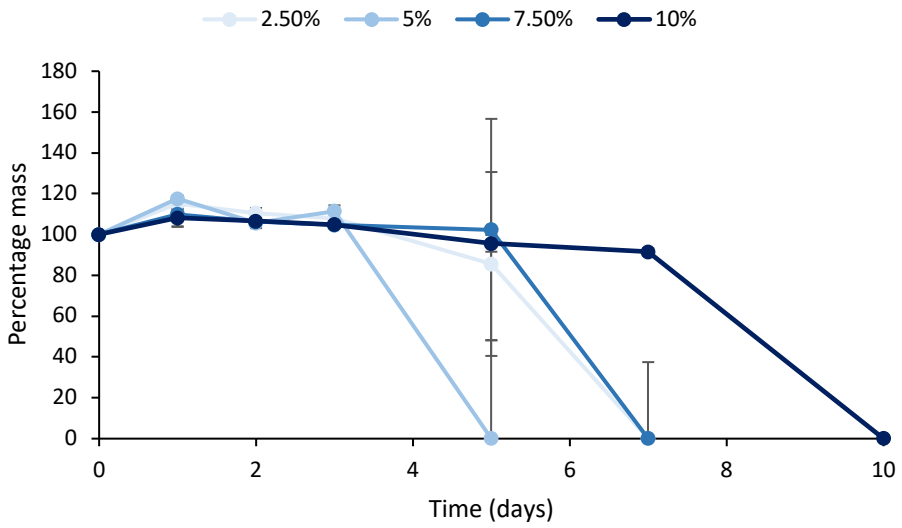

Figure 3.05: Degradation of carrageenan beads in 37˚C PBS, formed using various percentage (w/v) concentrations of KCl crosslinker and a constant carrageenan concentration of 2% (w/v), represented as percentage mass of original over time in 37˚C PBS solution. Data represent median ± interquartile range.

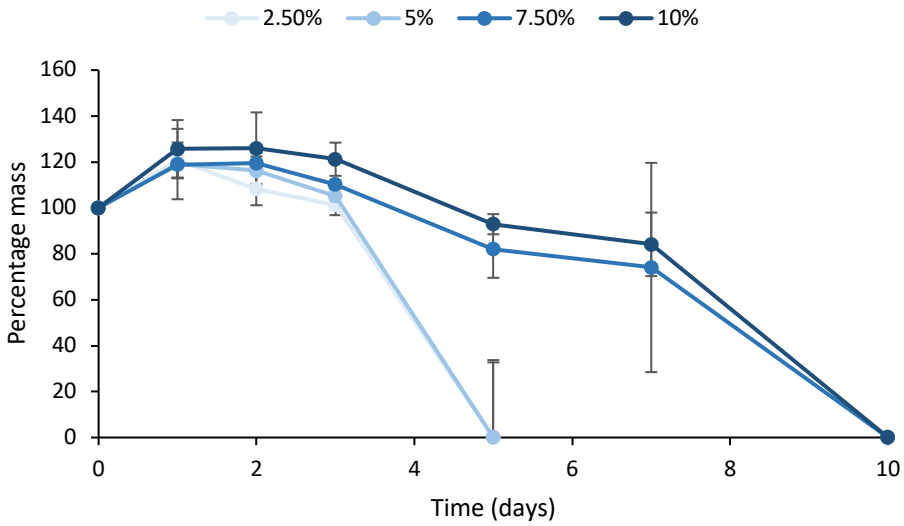

Figure 3.06 Degradation of carrageenan fibres in 37˚C PBS, formed using various percentage (w/v) concentrations of KCl crosslinker and a constant carrageenan concentration of 2% (w/v), represented as percentage mass of original over time in 37˚C PBS solution. Data represent median ± interquartile range.

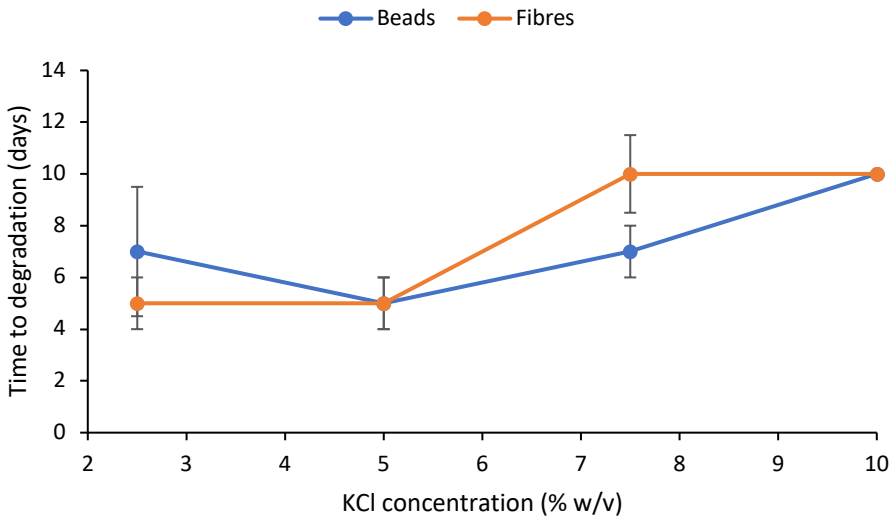

Figure 3.07 Degradation time of carrageenan beads and fibres in 37˚C PBS, formed using various percentage (w/v) concentrations of KCl crosslinker and a constant carrageenan concentration of 2% (w/v). Data represent median ± interquartile range.

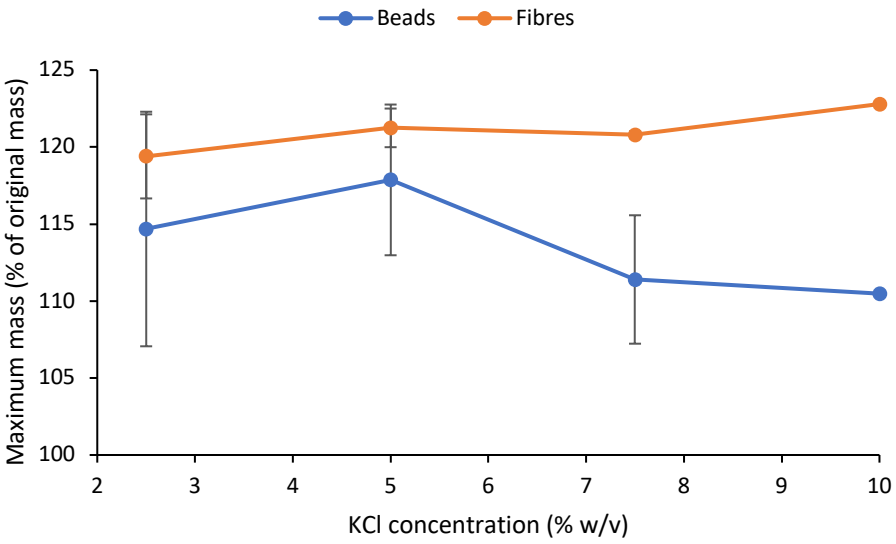

Figure 3.08: The maximum recorded mass of carrageenan beads and fibres in 37˚C PBS, formed of various percentage (w/v) concentrations of KCl crosslinker and a constant carrageenan concentration of 2% (w/v). Data represent median ± interquartile range.

These attempts appear to be largely unsuccessful. There appears to be a positive correlation between crosslinker concentration and mean degradation time of carrageenan fibres, however this correlation does not appear to be present in the case of carrageenan beads (figure 3.07), and the crosslinker concentration does not appear to be correlated with the degree of swelling in either case (figure 3.08). This was unexpected, as it has been shown that an increase in crosslinker concentration results, at least, in a lessening of the degree of hydrogel swelling [90, 160]. It may be that, in the case of beads, even the minimum amounts employed in this experiment were sufficient to produce a saturation of crosslinks.

3.2.1.3 The effect of liquid type and hydrogel morphology

It was hoped that growth of a cell monolayer on the surface of the scaffold may impart some degree of stability, indeed the use of cell adherence as a method for physically crosslinking hydrogels has been postulated [68]. To this end, carrageenan discs were produced as per chapter 2, section 2.2.1.1. Cells were seeded thereon but showed no meaningful proliferation on these discs (data not shown). However, it was noted that these discs persisted in solution far longer than the bead or fibre variants. Since the attempt to cultivate cells on these discs involved them being kept in cell culture medium as opposed to PBS, it was unknown whether the increase in degradation time was attributable to the scaffold morphology or the choice of immersion liquid. Therefore, these factors were treated as

separate variables and analysed independently. The change in mass over time is shown in figure 3.09. The mean degradation times are shown in figure 3.10. The degrees of swelling are shown in figure 3.11.

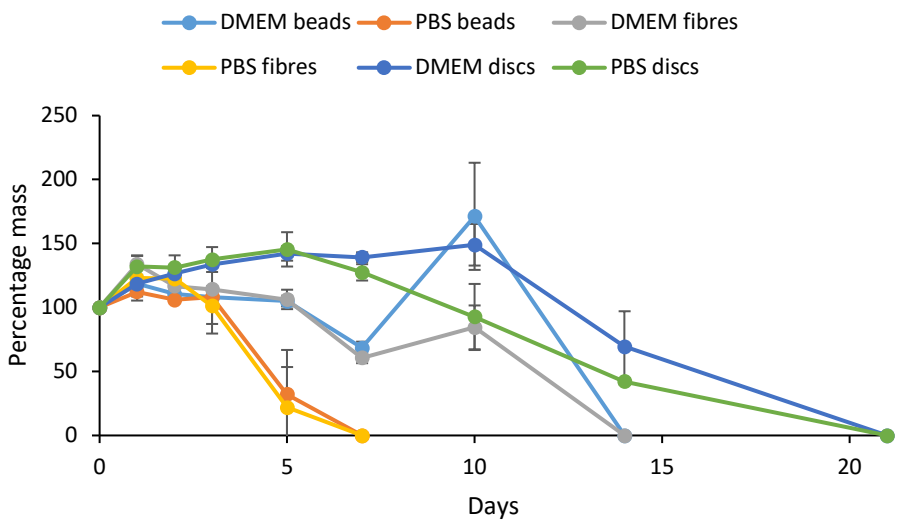

Figure 3.09: Degradation of carrageenan beads, fibres, and freeze-dried discs, in 37˚C PBS versus 37˚C DMEM. Represented as percentage mass of original over time in solution. Data represent mean ± standard error.

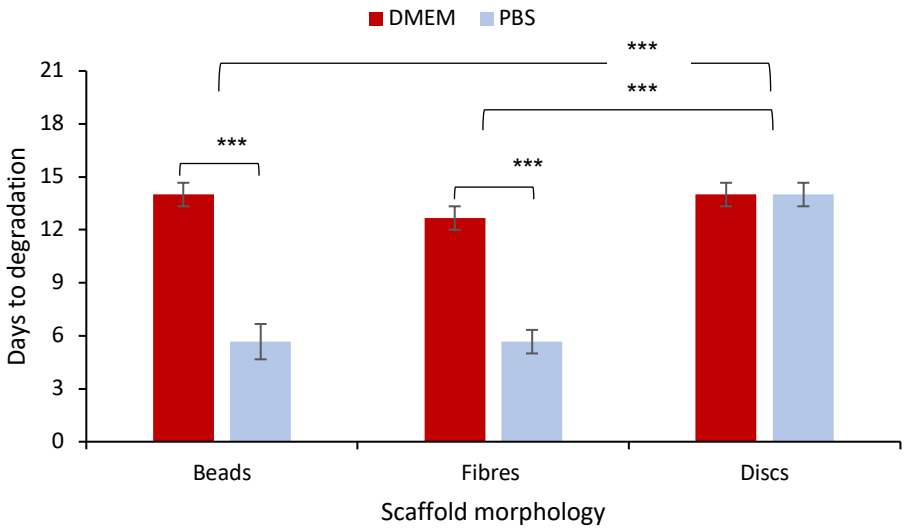

Figure 3.10: Days to complete degradation of carrageenan scaffolds in 37˚C PBS versus 37˚C DMEM. Data represent median ± interquartile range. ***p < 0.001

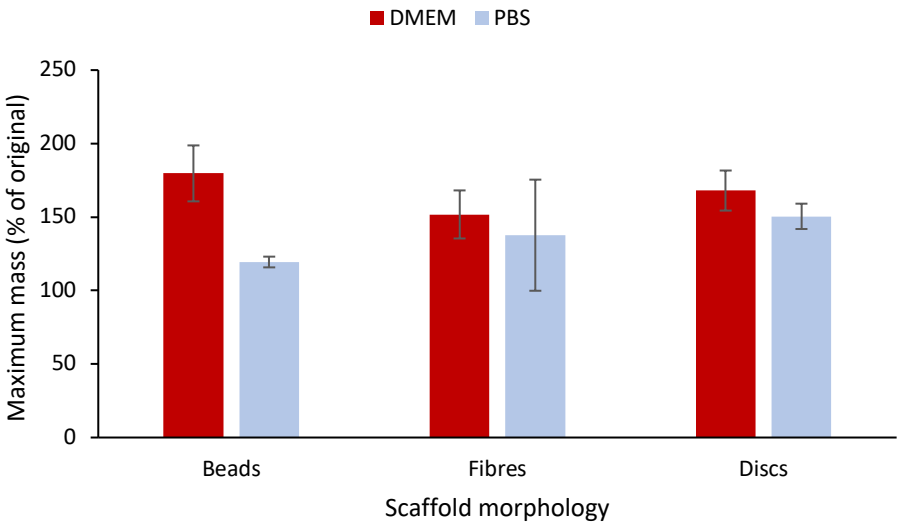

Figure 3.11: Degree of swelling of carrageenan scaffolds in 37˚C PBS versus 37˚C DMEM, represented as maximum recorded mass as a percentage of initial mass. Data represent median ± interquartile range. **p < 0.01

Figures 3.09 and 3.10 show that the disc morphology has a significantly lengthened degradation time in comparison to beads and fibres ($p < 0.001$ for both comparisons). Beads and fibres however, were not noted to exhibit significantly different degradation times to each other ($p = 0.518$). Scaffold degradation time was increased in DMEM (as opposed to PBS) for all scaffold morphologies for beads and fibres: the degradation time of beads was noted to be significantly lengthened when maintained in DMEM versus PBS ($p < 0.001$), and the same was true for fibres ($p < 0.001$). The degradation time for discs was not noted to be significantly different when maintained in DMEM versus PBS ($p = 0.082$).

These results strongly suggest that scaffold morphology and the liquid in which scaffolds are maintained both have significant, independent effects on the time taken for the scaffolds to degrade. The lyophilisation stage included in disc formation is likely the cause of this, as it is the only aspect of the formation process omitted for beads and fibres. From what is known of carrageenan gelation mechanisms, this may be caused by a reduction in space between helices as water is sublimed from between them under vacuum, which would then facilitate more effective and thorough interactions between the helices and K^+ ions.

Figure 3.11 provides evidence that scaffold morphology does not affect the degree of swelling: there was no significant difference in the maximum mass of scaffolds of differing morphologies within the same liquid type ($p > 0.05$). The liquid in which the scaffolds are maintained (DMEM versus PBS) however, was noted to have a significant effect on scaffold

swelling: the maximum mass of scaffolds in PBS versus those in DMEM was noted to be significantly different ($p < 0.01$).

Since the degree of swelling does not appear to be significantly reduced in the disc morphology (compared to beads and fibres), it cannot be said that scaffolds thusly formed are stable. However, the significant increase in degradation time for discs versus beads and fibres is clear and pronounced, and this effect is consistent across results for scaffolds kept in DMEM and in PBS. To summarise the effects of scaffold morphology, carrageenan discs (crosslinked after lyophilisation) are shown to degrade more slowly than beads or fibres. Furthermore, although the disc morphology did not show a significant reduction in degree of swelling, there was no significant increase in the degree of swelling either (in comparison to data shown in figures 3.01 – 3.04, where lengthened degradation times appeared to come at the cost of increased degrees of swelling. Thus it can be argued that the disc morphologies are more stable than beads or fibres, though they do not yet appear fully stabilised.

In the case of immersion media (DMEM versus PBS), scaffolds show consistently increased degradation time in DMEM (though not of statistical significance in the case of discs). Analysis of the degree of swelling showed that the maximum mass of the scaffolds was significantly reduced for scaffolds of all morphologies maintained in DMEM as opposed to PBS. Therefore, it can again be argued that the use of DMEM imparts a degree of stability to the scaffolds.

As previously stated: carrageenan solutions can exist in a variety of structures depending on the temperature, and presence of cations [152]. After thermogelation, an additional structural change is triggered by further cooling in the presence of cations (such as potassium) [152], which bind to the negatively charged organosulfate groups of the repeating units of the carrageenan polymer chains [150], thereby negating the electrostatic repulsion between these groups [151] and facilitating ion-dipole intermolecular force bonding between polymer chains [161]. Hydrogen bonds also form between hydroxyl groups on the polymer chains, facilitating the aggregation of the helices into a supramolecular lattice [152]. It is well known that when ionic salts are exposed to water molecules, the electrostatic forces between the two cause the former to become dissociated, releasing cations and anions. Thus, exposure of carrageenan to an aqueous KCl solution allows for the free K^+ ions to associate with the negative organosulfate groups of the carrageenan polymer chain.

It is known that ionic displacement leads to degradation of ionically crosslinked alginate hydrogels [68, 147], specifically calcium ions being displaced by local sodium ions in cell medium [162]. It is also noted that alginate hydrogels can be dissolved by use of chelation agents, such as EDTA [163] or sodium citrate [77, 162, 164], whereby the calcium ions maintaining the gelatinous structure are isolated and prevented from interacting with the surrounding polymers. The results shown here provide evidence this ionic-displacement phenomenon also takes place ionically crosslinked carrageenan hydrogels. As previously mentioned, the gelation temperature range in which the random coils join to form double-helicies can have a lower-threshold of 40˚C [152], which may appear dangerously close to the incubator's internal temperature of 37˚C. However, it is noted that κ-carrageenan shows a higher melting temperature than gelation temperature, owing to its lesser amount of negatively charged groups (compared to ι-carrageenan), which would keep it stable at temperatures associated with cell-culture conditions [165].

Also, given the incubator's constant internal temperature of 37˚C, a variance in temperature between the DMEM vs PBS experiments can be dismissed as a causal factor for the difference in degradation rates.

It is noted that acidic pH can catalyse hydrolysis of κ-carrageenan [166]. This minor difference in pH is unlikely to be attributable to the difference in degradation times, especially as they both fall within the neutral range.

The elimination of pH or ambient temperature differences as causal factors for the increased degradation time in DMEM vs PBS leaves chemical factors as the only likely explanation. It was initially speculated that displacement reactions occurring between the ions crosslinking the carrageenan, and those in solution, were causing a gradual weakening of the gel structure. It is consistently noted in literature that the use of Na^+ ions produces weaker carrageenan gels than those produced through the use of K^+ ions [161] [167], it has also been shown that this translates to a lowering of sol-gel and (more importantly, in this case) gel-sol transition temperatures [168]. If the K^+ ions in κ-carrageenan gels were gradually replaced with Na+ ions, it would likely lead to a gradual lowering of gel-sol temperature, which would result in the gelatinous carrageenan scaffolds degrading into solution.

As previously mentioned, an attempt was made to cultivate cells on the surface of the carrageenan gels in the hopes that a monolayer adhering thereto would help to physically hold the scaffold together. When an attempt was made to track the growth of these cells via a resazurin metabolic assay (as per chapter 2, section 2.1.2.2), it was observed that the

scaffolds degraded even more quickly. This apparent deleterious effect of resazurin on carrageenan hydrogels was analysed in more detail as described in chapter 2, section 2.2.2.1. The mass over time is shown in figure 3.12, the degree of swelling is shown in figure 3.13, and the mean degradation time is shown in figure 3.14. It was initially thought that this provided evidence for a role of sodium ions in destabilising the gels, as the resazurin compound is itself a sodium salt. However, further consideration renders this conjecture highly unlikely, and will be discussed further.

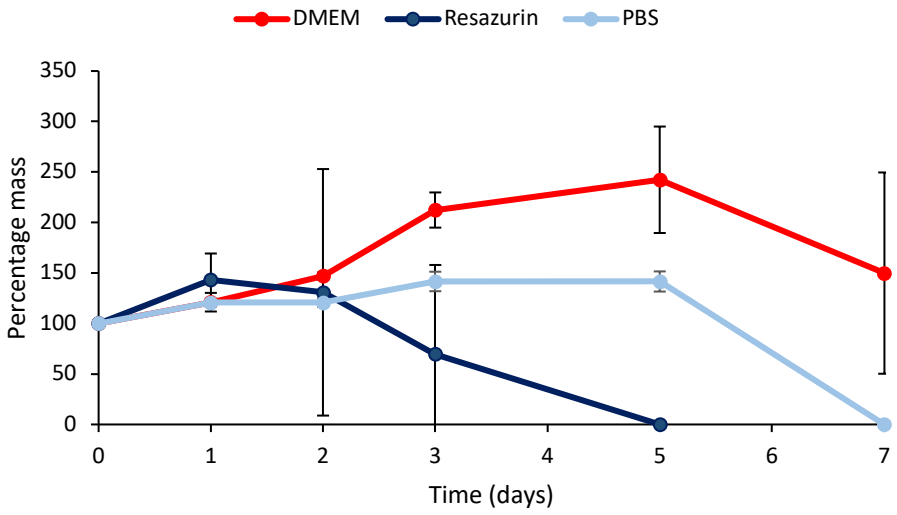

Figure 3.12: Percentage mass over time of carrageenan scaffolds in 37˚C DMEM, 37˚C PBS, and 37˚C DMEM exposed to resazurin sodium salt solution for 2 hours per day. Data represent median ± interquartile range.

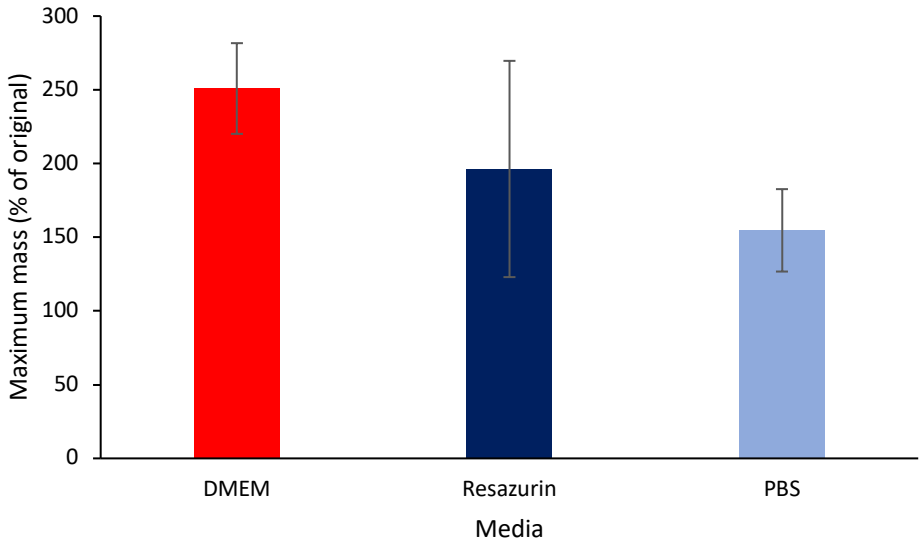

Figure 3.13 Maximum percentage mass (degree of swelling) of carrageenan scaffolds 37˚C DMEM, 37˚C PBS, and 37˚C DMEM exposed to resazurin sodium salt solution for 2 hours per day. Data represent median ± interquartile range.

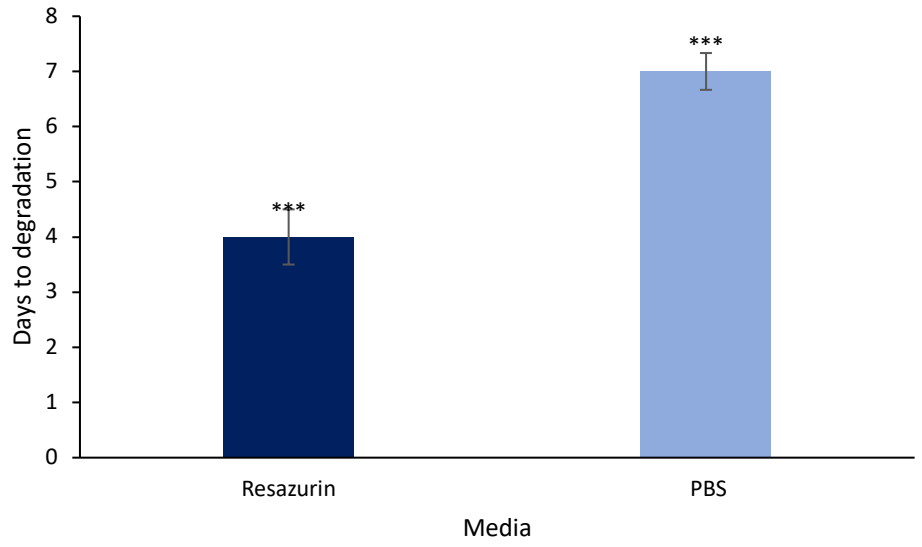

Figure 3.14: Time to degradation of carrageenan scaffolds in 37˚C DMEM versus 37˚C DMEM exposed to resazurin sodium salt solution for 2 hours per day. Data represent median ± interquartile range. **p <0.001.

The carrageenan scaffolds showed significantly faster degradation ($p < 0.001$) when kept in DMEM but exposed to resazurin for 2 hours daily than those kept in PBS (figure 3.14). As the experiment was halted before the samples in DMEM degraded, statistical analysis on degradation times could not be performed between these samples and those exposed to resazurin, but it is observable that these samples degraded at a slower rate than the PBS

and resazurin samples. There was no significant difference between degree of swelling (maximum mass) of scaffolds between media ($p > 0.05$ for all comparisons). The manufacturer specifications show the resazurin to be an organic sodium salt, with the sodium ion bound to the resazurin's negative oxygen ion.

Given the manufacturer specifications for both Sigma D5795 DMEM and Oxoid BR0014G 'Dulbecco A' PBS, the inorganic salt content and concentrations of the two can be compared (Table 3).

	Oxoid BR0014G PBS	**Sigma D5796 DMEM**
NaCl	6.4 g/L	6.4 g/L
KCl	0.16 g/L	0.4 g/L
NaH_2PO_4	0.92 g/L	0.109 g/L
KH_2PO_4	0.16 g/L	-
$CaCl_2$	-	0.265 g/L
$Fe(NO_3)3 \bullet 9H2O$	-	0.0001 g/L
$MgSO_4$	-	0.09767 g/L
$NaHCO_3$	-	3.7 g/L

Table 3: A comparison of the inorganic salt content of Oxoid BR0014G PBS versus Sigma D5795 DMEM, based on manufacturer specifications.

A comparison of ion content, in terms of molarity, between these three solutions is given in table 4.

	PBS	**DMEM**	**Resazurin**
Sodium	117.18 mM	110.89 mM	111.52 mM
Potassium	3.33 mM	0.81 mM	1.06 mM
Calcium	-	2.39 mM	2.39 mM
Magnesium	-	0.811 mM	0.811 mM
Iron	-	0.25 µM	0.25 µM

Table 4: Molar concentrations of cations in Oxoid BR0014G PBS, Sigma D5796 DMEM, and working resazurin solution. Data extrapolated from manufacturer specifications.

The reactivity series of metals places potassium as the most reactive, sodium as the second-most reactive, calcium as the third, magnesium as the fourth, and iron as the seventh (after aluminium and zinc) [169]. On a one-to-one basis, sodium will be unable to displace potassium. However, this does not completely preclude the possibility of sodium ions displacing the potassium ions. Indeed after sodium alginate is dissolved into aqueous solution, calcium ions readily take the place of the more reactive sodium ions [170]. The comparatively high concentrations of sodium ions present in PBS, DMEM, and resazurin working solutions must be taken into account, thus the gradual replacement of potassium ions in carrageenan gels with sodium ions may well be the cause of destabilisation.

The molar concentrations of sodium ions presented in table 2 are likely too small to be of significance, with a variance of less than 0.0063 M between the highest and lowest sodium content. Yet, there were significant differences in the stability of gels maintained in these three solutions: samples exposed to resazurin were shown to degrade more quickly than those maintained in PBS or DMEM, and samples maintained in PBS degraded more slowly than those in DMEM (figures 3.13 and 3.14). The DMEM solution contains a wealth of additional substances besides the ionic salts, and it may be possible that one or more of these imparts a degree of stability to the carrageenan gels, such as weak surface adsorption of serum-proteins, or polar molecules interacting with the ions in solution preventing them from disrupting the carrageenan crosslinking. The resazurin solution is, of course, only distinguished from the other two solutions by its resazurin content. There may be a possible mechanism by which phenoxazine-type organic molecules, such as resazurin, also destabilise the integrity of ionically crosslinked hydrogels.

With regard to the lyophilisation approach, the length of time required to produce carrageenan discs was much greater than that for beads and fibres, sometimes by as much as 72 hours (owing to the freezing and lyophilisation stage). Since a scaffold for commercial meat production would ideally be simple and time-efficient to produce, it was felt that this comparatively huge increase in the time taken to produce the scaffold (a matter of hours versus days, representing an increase by a factor of more than 10x) made the practice of freeze-drying inefficient for cultured meat applications.

However, reflecting on previous results, it was decided that all scaffolds would be subsequently kept in DMEM and the use of PBS for this purpose would be discontinued.

3.2.2 Surface-coating of hydrogels

Manipulation of gel-formation conditions and environmental maintenance conditions showed some effect on gel stability, however the desired degree of stability was not achieved. Therefore, focus was shifted to modification of the gels themselves after they were produced. To this end, chitosan and silk were selected for use as surface coatings in the hopes that such coating would impart stability to the gels.

A crucial attribute of any surface-coating applied to a scaffold intended for cultured meat is biodegradability and edibility, which are demonstrated by both chitosan [171] and silk fibroin [172]. In order to properly adhere to the carrageenan gels, the coatings would need to contain polar regions within their molecular structure. The non-repeating amino acid chain at the carboxy-terminal end of the silk fibroin protein chain contains a number of basic amino acids, them being nine pairs of arginine and lysine [58], which contain positively charged regions. Chitosan may contain a wealth of positively charged amine groups within its structure which can become protonated at acidic pH [173, 174]. However, this is dependent on the DDA: chitosan is typically harvested from crustacea as chitin, which lacks the aforementioned amine groups in favour of acetyl groups [175]. The chitin must be treated under alkaline conditions in order to achieve deacetylation [175], wherein the acetyl groups are converted to amine groups: the degree to which this is achieved is expressed as the chitosan's DDA%. This is an important aspect of chitosan with respect to its application in tissue-engineering, as the DDA% has been shown to positively correlate with chitosan's ability to support cell binding and proliferation [176]. The mechanics of this relationship will be discussed in further detail in section 3.2.2.2. The cytocompatibility of chitosan has not escaped researchers: Cai *et al.* were able to produce a porous, lyophilised chitosan scaffold which was able to maintain L929 fibroblasts and bovine carotid endothelial cells, depending on pore size and release of growth factors [177]. Foster *et al.* were able to show that chitosan of high DDA% was able to support proliferation of olfactory ensheathing cells [176]. Ji *et al.* produced chitosan hydrogels which supported proliferation of GM388 fibroblasts, and were able to increase the degree to which cells infiltrate the gel by manipulating pore size [178].

The cytocompatibility of silk fibroin has also been well-documented. For example, Mandal *et al.* were able to produce lyophilised silk scaffolds on which human primary dermal fibroblasts would proliferate [179]. Sakunphanitphan *et al.* were able to proliferate SCAP cells on sill fibroin hydrogels [180]. Carrasco-Torres *et al.* were able to maintain KaCaT

keratinocytes on composite silk fibroin / polyethylene oxide electrospun scaffolds [181]. Interestingly, all three of these independent studies noted a decrease in cytocompatibility as the percentage concentration of the silk fibroin protein increased.

It is no surprise then that both silk and chitosan have been utilised as modifiers for hydrogel scaffolds: the carrageenan fibres of Mihaila *et al.* were surface-coated with chitosan, and the alginate beads of Patil and Singh were blended with silk fibroin, for instance [129, 154].

3.2.2.1 Deacetylation of chitosan

Chitosan-coating of carrageenan had been previously employed in attempts to stabilise the gels and improve cytocompatibility, however these attempts failed on both counts (data not shown). After NMR analysis of the stock chitosan ("Reaction time 0 min" as seen in figure 3.19) showed it to have a much lower DDA% than stated by the supplier, it was decided that these experiments would be repeated after the stock chitosan had been further deacetylated as per chapter 2, section 2.2.4. Samples were then dissolved to 10 mg / ml in D_2O acidified by concentrated HCl, followed by ^1H NMR analysis by Dr Tim Woodman, also as described in section 2.2.4. The molecular structure of acetyl groups is illustrated in figure 3.15. The NMR analysis of these samples, as well as the stock chitosan, are given in figures 3.16 and 3.17, where data are expressed in parts per million downfield from $SiMe_4$ as an internal standard. The extrapolated degrees of deacetylation for the samples are given in figure 3.18. The equation by which the integrals from NMR are converted into DDA% is given in equation 1.

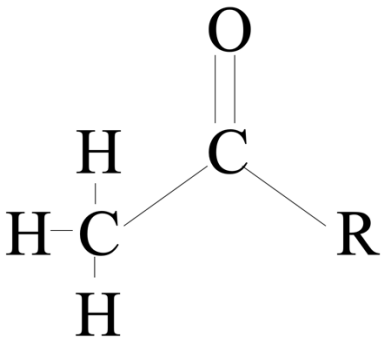

Figure 3.15: Molecular structure of the acetyl group. The NMR records the magnetic resonance of the hydrogen nuclei (protons).

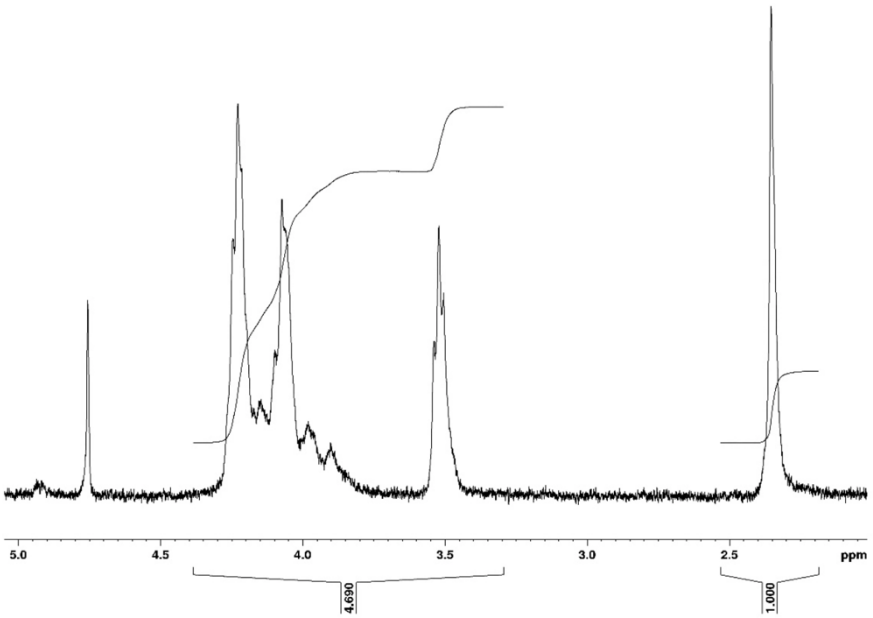

Figure 3.16: ^{1}H NMR spectrum of stock chitosan samples.

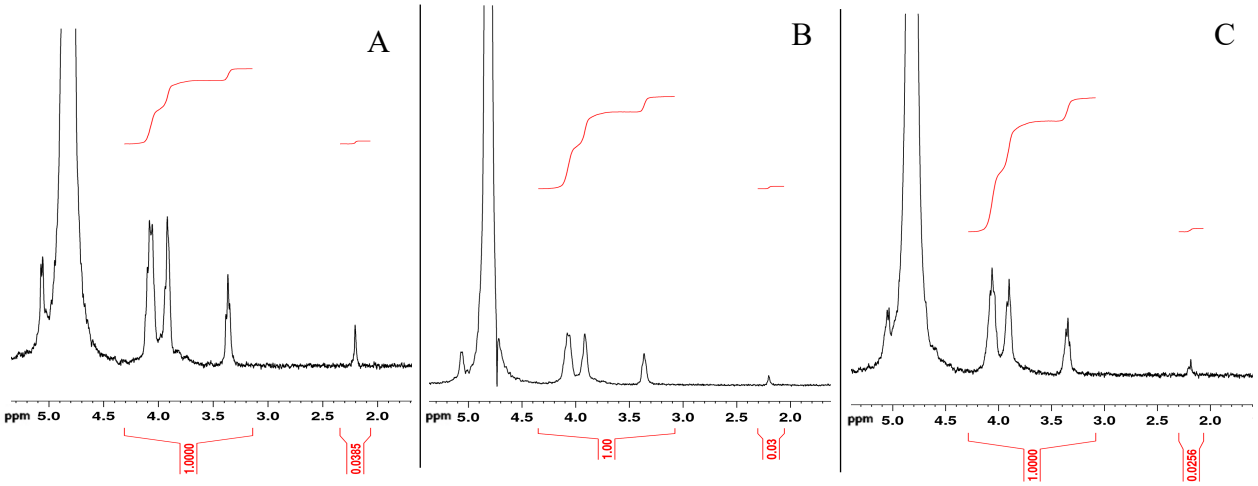

Figure 3.17: ^{1}H NMR spectrum of chitosan samples reacted with 45% (w/v) NaOH solution at 90˚C for A: 30 minutes. B: 60 minutes. C: 60 minutes. Peaks between 2.0 and 2.5 ppm represent hydrogen nuclei of CH_3 groups (which in turn belong to acetyl groups). Peaks between 3.0 and 4.5 ppm represent nuclei of hydrogens 2 - 6 of the monomer.

$$DDA_{\%} = \left(1 - \frac{I_{ac} / 3}{I_{H2\text{-}6} / 6} \right) X\ 100$$

Equation 1 [182]: DDA from the magnetic resonance of various hydrogen nuclei in chitosan. I_{ac} refers to the integral of hydrogen nuclei associated with CH_3 in acetyl groups [182]. $IH_{2\text{-}6}$ refers to the integral of hydrogens at positions 2 – 6 (as well as 6') in the monomer [182].

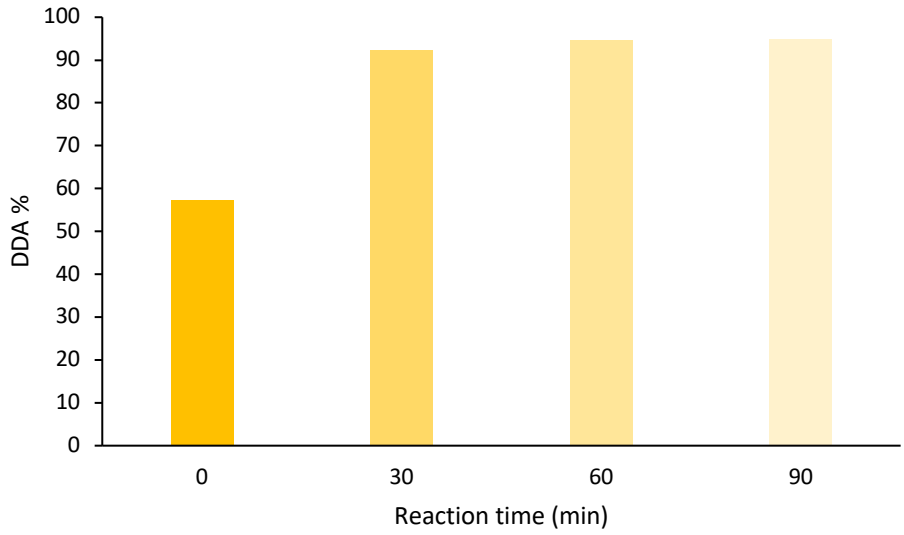

Figure 3.18: Degree of deacetylation (DDA%) of chitosan samples, heated with NaOH solution under nitrogen atmosphere for various lengths of time.

The deacetylation process appears to have been highly successful. As expected, DDA shows positive correlation with reaction time (figure 3.18). The trend of this correlation is also in line with literature, where the increase plateaus when reaching high values, meaning increasing the reaction time is unlikely to yield a high enough increase in DDA to justify the time consumption. For this reason, it was decided that 60 minutes would subsequently be used as a standard reaction time when manually deacetylating chitosan. The unmodified chitosan showed a low DDA by the standard of controls used in literature.

Hussain *et al.* noted a maximum DDA% value of 85.85% even after 8 hours of treatment [61] (over 5 times longer than the maximum reaction time here). This study also appeared to show a slower rate of deacetylation, with DDA for the earlier-noted sample increasing roughly at a rate of 4% per hour, which is substantially slower than the results shown here where samples rose by over 30% DDA in 30 minutes. Prashanth *et al.* achieved a comparable value of 88.8% DDA using the same NaOH concentration, but in an eight of

time (1 hour) [183]. However, this study maintained the reaction at 100˚C, 20˚C higher than that conducted by Hussain *et al.*. Indeed, Chang *et al.* cite reaction temperature as the most critical variable in producing high DDA samples, and was able to produce DDA's well into the high-90% range using a high temperature of 133.78˚C. This study also used a high concentration of NaOH (51.89%) also citing this as a highly important factor [175].

Yuan *et al.* were able to achieve an excellent DDA% of 99.68% using 45% NaOH at 90˚C for 2 hours [62]. From this study, it is particularly noticeable that the method by which DDA is determined can have a substantial effect on the value; the same sample which gave the aforementioned value of 99.68% DDA under ultraviolet-vis spectrophotometry also gave a value of 86.68% when analysed via acid-base titration [62]. Studies tend to use various methods of confirming DDA, and these methods are not necessarily consistent between studies, making comparisons less reliable. The results shown here (figures 3.16 and 3.17) were obtained by way of NMR analysis. The previously mentioned study of Prashanth *et al.* as well as that of Freier *et al.* also analysed their samples using NMR [63]: the maximum DDA attained in 2 was markedly lower than even the least efficient result shown here (88.8% versus 92.3%) despite being carried out for 90 minutes longer and at a temperature 10˚C higher. However, Freier *et al.* were able to produce samples of 99.5% DDA with only a 30-minute increase from the maximum reaction time shown here, but at a temperature of 110˚C.

The samples showed higher DDA values than anticipated, which was a positive result. However, an increase in temperature may serve to further optimise the procedure. The use of various techniques to determine DDA rather than the exclusive use of NMR (figures 3.16 and 3.17) would have served to make the results more comparable to other studies, which would help to contextualise the importance of the experimental conditions. But as the goal was simply to confirm an increase in the DDA of the chitosan for the purposes of cytocompatibility (rather than raising it to any particular target value), it was decided that analysis by NMR was sufficient.

This variance depending on experimental technique may also explain the surprising lower value obtained for DDA% of the stock chitosan (52%) when compared to the estimate of 75-85% provided by the manufacturer. It was communicated by Sigma Aldrich that the stock chitosan's DDA% was ascertained by way of titration. This would likely be either acid-base or potentiometric titration [62], which would limit the sensitivity of the procedure to that of the pH meter or voltmeter (respectively). In a worst-case scenario, the use of coloured indicators in acid-base titrations, if used to determine DDA%, may indicate that the end-

point of the procedure was determined qualitatively rather than quantitatively. The volume of titrant contained in a droplet (as titration procedures often add the titrant solution to the analyte dropwise) would also represent a margin of error in a titration procedure to determine DDA%. Reflecting on the principles of NMR, it would seem to be a far more precise technique than titration. NMR operates by inducing a shift in energy at the sub-atomic level, triggering a change in the orientation of nucleic spin [184]. The exact quantity of energy required to induce this effect is determined not only by type of atomic nucleus, but by the surrounding electrons as well [184]. This enables detection of the exact molecular group in which the nuclei are found. This allows for direct detection of acetyl groups in the molecular structure of the chitosan samples, and quantification thereof, rather than relying on their effecting ambient pH or potential difference. Thus, the NMR-based result of 57% DDA for the stock chitosan samples (figure 3.18) is likely to be more accurate than those obtained by the manufacturer by way of titration.

3.2.2.2 Cytocompatibility of chitosan

In order to determine whether this increase in DDA% translated to an increase in cytocompatibility, chitosan films were prepared as per chapter 2, section 2.2.4. Cells were then seeded on the resultant chitosan films and their growth was tracked by way of resazurin metabolic assay, as per chapter 2 section 2.1.2.2.

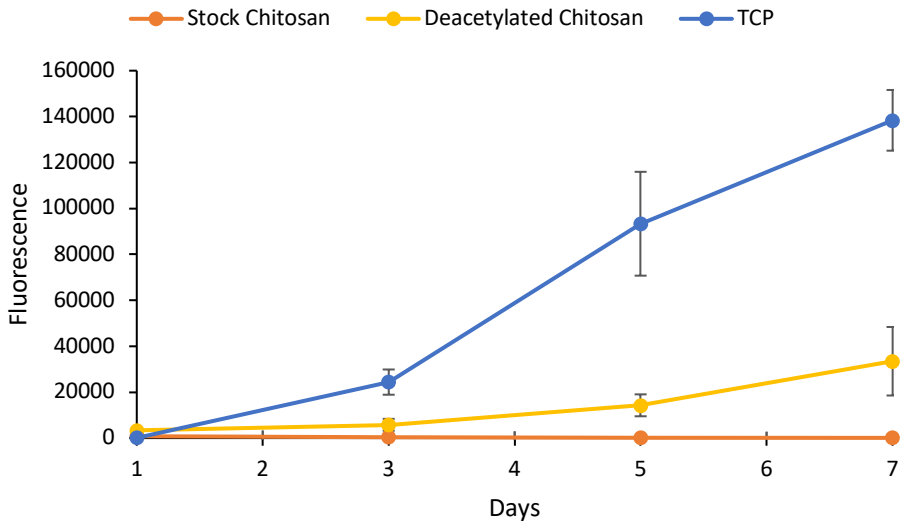

Figure 3.19: C2C12 cell proliferation on chitosan samples (stock versus 60-minute sample as seen in figure 3.18) and TCP, measured by way of resazurin metabolic assay. Data represent median ± interquartile range.

The results appear positive. The deacetylated chitosan samples appeared to show an increased degree of cytocompatibility compared to their unmodified counterparts (figure 3.19); the general upward trend in fluorescence over time is immediately obvious for deacetylated chitosan samples compared to the flatline associated with the stock samples, and this difference was determined to be of statistical significance ($p = < 0.05$). The cytocompatibility of the two chitosans were, however, both shown to be inferior to TCP controls. Fluorescence readings from stock chitosan samples and deacetylated samples were both shown to be significantly different to those of TCP samples ($p < 0.001$ for both comparisons).

The apparent increase in cytocompatibility for the deacetylated samples compared with the stock samples is not altogether unexpected. Although chitosan is a polysaccharide, it has the capacity for adsorption of cell-binding peptides (normally present in serum) to its surface [64, 185], such as fibronectin [65]. This is likely facilitated by the amine groups within the chitosan structure, as these would not only have the ability to join with peptide-bound carboxylic acid groups, but the positive charge of the amine groups (especially at acidic pH) [173, 174]. This would explain why cytocompatibility of chitosan increases with DDA%, as higher a DDA% denotes a greater number of amine groups present to facilitate the binding of serum proteins, which in turn allow chitosan to bind cells. It was hoped that the deacetylated samples would show higher cytocompatibility than seen in figure 3.19, given that the stock samples exhibited a DDA% of below 60% compared to the >90% exhibited by deacetylated samples (figure 3.18). However, as previously mentioned, DDA% readings can vary with the experimental technique employed to obtain them, and studies primarily focusing on DDA% typically make use of more than one technique in order to acquire a more reliable set of results with regard to degree of deacetylation. Use of additional techniques may show the mean DDA% of chitosan samples presented herein to be lower than that measured by NMR only, and so there may be room for further optimisation of the deacetylation procedure, which would in turn further improve cytocompatibility.

It is known that the isolation of chitin begins with deproteination, wherein potentially allergenic peptides are separated from the polysaccharide, and demineralisation, wherein calcium carbonate is removed from the chitin [60]. The manufacturer gives no specifications as to the purity of the chitosan [186]. However the presence of residual calcium carbonate is unlikely to have significant cytotoxic effects [187]. The effectiveness of deproteination can vary widely depending on the specific parameters used [60], and studies concerning deproteination do not appear to specify what peptides are being removed [60, 188, 189], making speculation as to the potential effects of protein content in the chitosan difficult.

3.2.2.3 Cytocompatibility of silk fibroin

As previously mentioned, the cytocompatibility of silk has been consistently demonstrated in literature. In order to reconfirm this cytocompatibility before its application to increase that of carrageenan gels, silk fibroin was degummed and formed into films as per section 2.2.3.1. Cells were then seeded as per chapter 2, section 2.1.1.2, and proliferation was tracked by way of resazurin metabolic assay in a 6-well plate as per chapter 2, section 2.1.2.2. The results are given in figure 3.20.

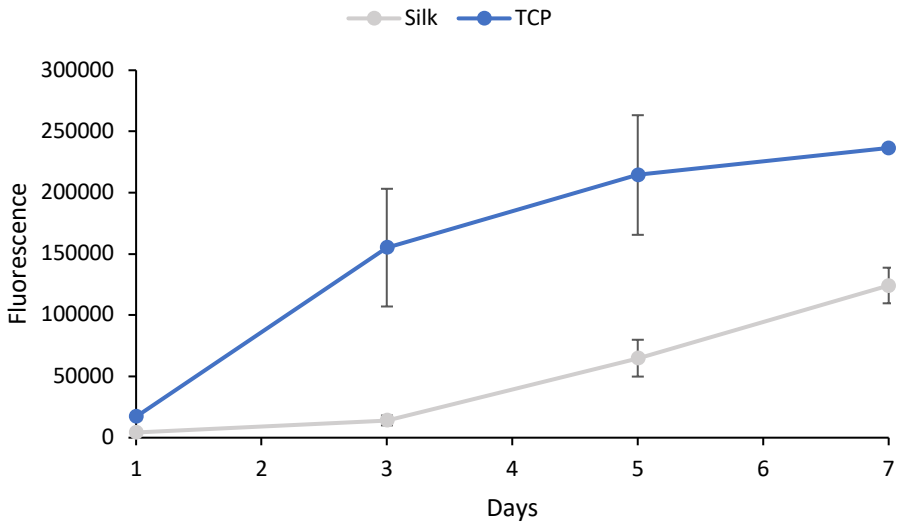

Figure 3.20: C2C12 cell proliferation on degummed, lyophilised silk fibroin discs versus TCP, measured by way of resazurin metabolic assay. Data represent median ± interquartile range.

Silk fibroin films showed positive cytocompatibility, though still inferior to TCP (figure 3.20). Fluorescence from silk samples were significantly lower than those from TCP ($p < 0.001$). These results are further discussed in chapter 4. Comparing these results to those shown from chitosan shown in figure, silk fibroin appears to be the superior biomaterial in terms of facilitating cell growth.

It is unlikely that any significant amount of ethanol remained on the silk films after washing and drying. Tapani *et al.* tested the cytotoxic effects of ethanol on various types of cells over time. They noted that a concentration of 15% (v/v) ethanol would have a total cytotoxic effect on F9 cells after 10 minutes of exposure, this was reduced to a partial cytotoxic effect as concentration was lowered to 10%, and no effect was observed at 5% [190]. Not only was the silk washed thrice which would heavily dilute any remaining trace amounts of ethanol, but the remaining liquid was subsequently allowed to dry (as per chapter 2, section

2.2.3.1). The manufacturer note that the evaporation residue for the ethanol is a maximum of 5 parts per million [191]. Thus it can be reasonably assumed that a negligible amount of ethanol, if any, remained on the silk films after washing and drying and would not have impeded cell growth.

As noted in chapter 2, section 2.2.3.1, an $NaCO_3$ concentration of 0.02 M was used to degum the silk. This translates to a w/v concentration of 0.212%. Dou and Zuo measured the effect of various $NaCO_3$ concentrations on the degumming of silk [192]. Silk degummed with even the minimum $NaCO_3$ concentration of 0.005% (w/v) (for 30 minutes) appeared to exhibit complete removal of sericin, SEM analysis showed fibrous strands of silk fibroin without any visible sericin gum surrounding them [192]. Therefore, it is unlikely that the degumming parameters used here ($NaCO_3$ concentration of 0.02 M or 0.212% w/v, and a boiling time of 1 hour) left any residual sericin in the silk films that could have affected cell growth thereon. Though it was noted in the study of Dou and Zuo that as $NaCO_3$ concentrations increased from 0.05% to 0.5%, the silk fibroin fibres exhibited a small degree of structural damage as a result of the degumming procedure, with the fibres appearing slightly cracked and frayed [192]. This effect was observed to be much more severe when NaCO3 concentration rose to 5% [192]. It is conceivable, therefore, that the $NaCO_3$ concentration of 0.2% (w/v) and 1 hour of boiling time may have caused minor damage to the silk fibroin, though the fibres were subsequently dissolved and formed into dry films from regenerated solution, rather than the cells being grown on the fibres themselves, and so this is also unlikely to have significantly impacted results.

In order to determine whether these cells would form myotubes, the cells on silk films were cultured to differentiation as per chapter 2, section 2.1.1.4, and stained as per chapter 2, section 2.1.2.3 (without Hoechst counter-staining). This procedure was not carried out on chitosan due to the lessened degree of proliferation (figure 3.19), meaning more time would be required in order to culture the cells to confluence. The resultant myotubes are shown in figure 3.21.

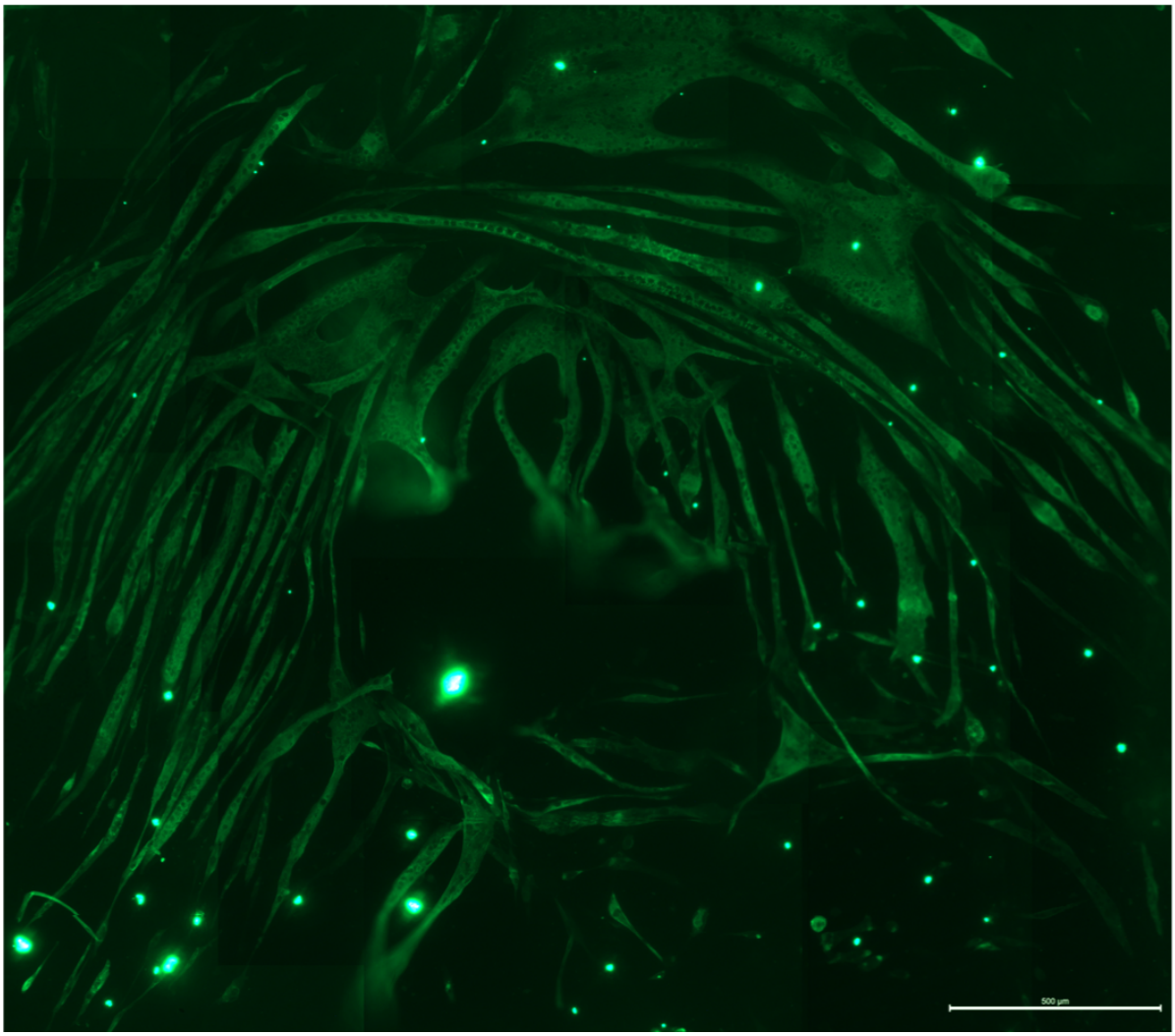

Figure 3.21: Confirmation of C2C12 myoblastic differentiation on silk fibroin discs, visualised via immunostaining for myosin heavy chain. Scale bar represents 500 μm.

The presence of myotubes on silk fibroin (figure 3.21) is a positive result, especially considering the lack of cell-binding motifs that would commonly be found in ECM proteins, which also govern signalling of various cell functions, including differentiation [193-196]. However, silk fibroin has been shown to initiate extracellular signal-regulated kinases (ERK) signalling pathways by inducing phosphorylation [197]. A downstream substrate of ERK, focal adhesion kinase (FAK) [198] is noted to play a crucial role in myotube formation, as its inhibition completely impairs myoblastic fusion [199].

3.2.4.4 The effect of coating on degradation

It is noted in literature [129] that the surface-coating of carrageenan hydrogels serves to impart stability, reducing both the swelling and degradation effect. Carrageenan discs were coated in deacetylated chitosan (as per chapter 2, section 2.2.2.2.1), and silk fibroin (as per

chapter 2, section 2.2.2.2.3). These scaffolds were analysed for degradation as per chapter 2, section 2.2.2.1. The decrease in mass of the coated gels over time is shown in figures 3.22 to 3.23, the mean degradation times in figure 3.24, and the degree of swelling in figure 3.25.

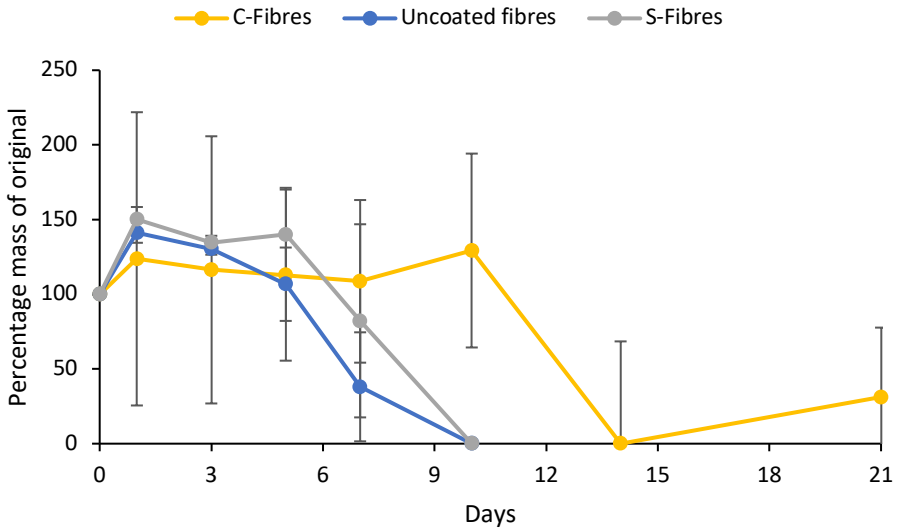

Figure 3.22: Degradation of carrageenan fibres coated in various ways over time in 37˚C DMEM. C-fibres refers to chitosan-coated samples. S-fibres refers to silk-coated samples. Uncoated fibres refer to uncoated controls. Data represent median ± interquartile range.

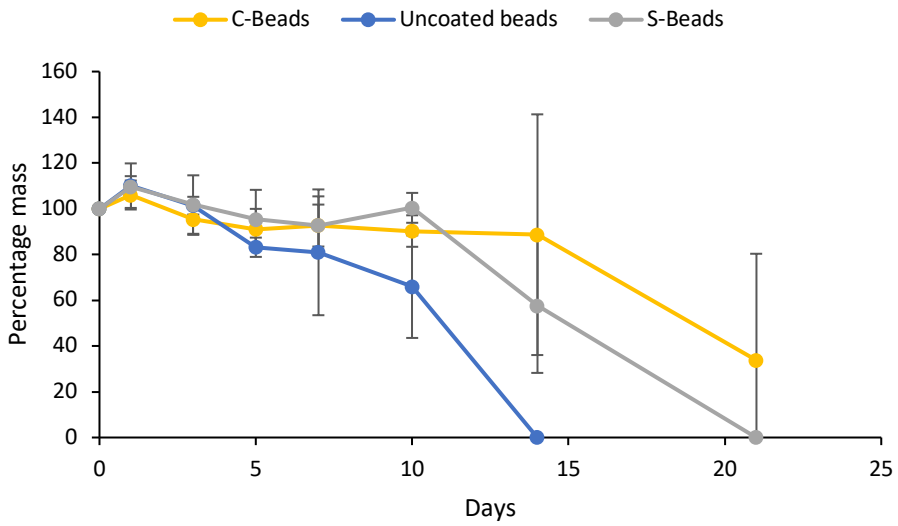

Figure 3.23: Degradation of carrageenan beads coated in various ways over time in 37˚C DMEM. C-beads refers to chitosan-coated samples. S-beads refers to silk-coated samples. Uncoated beads refer to uncoated controls. Data represent median ± interquartile range.

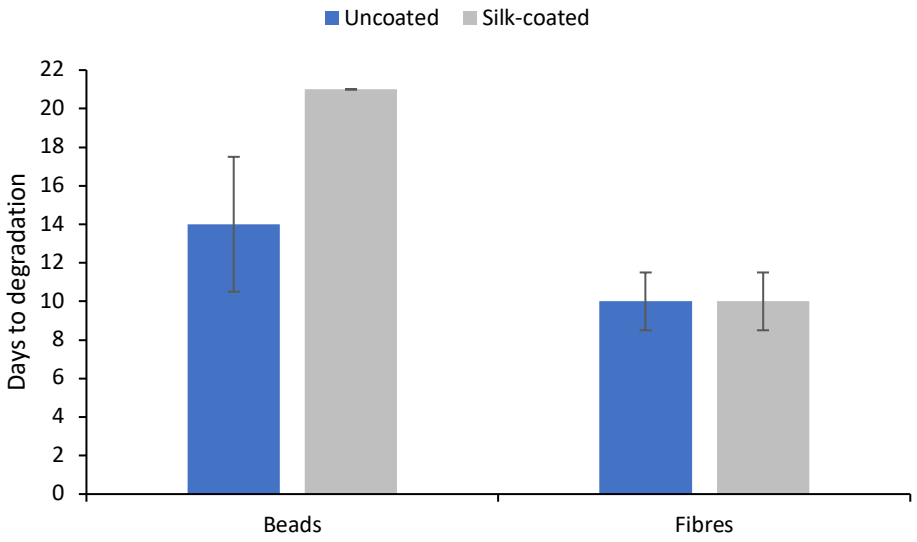

Figure 3.24: Degradation time of uncoated and silk-coated carrageenan beads and fibres in 37˚C DMEM. Data represent median ± interquartile range.

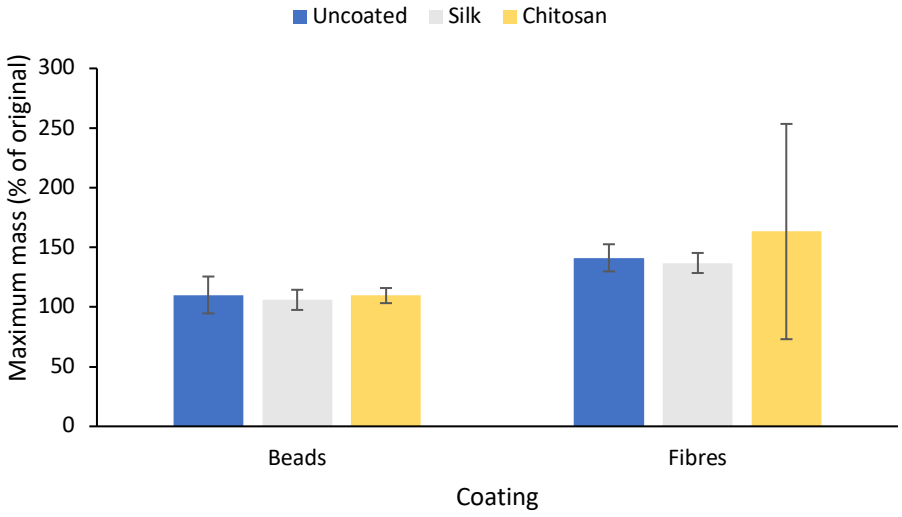

Figure 3.25: Maximum mass (degree of swelling) of uncoated ("U"), silk-coated ("S"), and chitosan-coated ("C") carrageenan beads and fibres in 37˚C DMEM. Data = median ± interquartile range.

Figures 3.22, 3.23, and 3.24 show a clear increase in degradation time for scaffolds coated in silk and chitosan, compared to the uncoated controls. The chitosan-coated samples in particular remained gelatinous even at the 21-day mark (as such, it was not possible to calculate their mean degradation time, which is why these values are missing from Figure 3.24). Figure 3.25 shows the mass increase of each sample, including the uncoated controls. The effect appears consistently reduced in beads versus fibres for all coating conditions. The results for chitosan-coated beads are particularly noteworthy, with their mean maximum mass being only 106.4% of the initial value. Indeed, it has been elsewhere

reported that chitosan-coating reinforces carrageenan hydrogel scaffolds, preventing their swelling and enhancing their stability [129].

Silk-coated beads also showed a sizable increase in degradation time compared to uncoated controls (and even to silk-coated fibres, which did not appear to degrade any more slowly than the uncoated controls) without causing an increase in mass-gain. With optimisation, this may also represent a potential method for producing stable carrageenan scaffolds.

The binding of chitosan to carrageenan can be explained by the fact that chitosan contains in its structure a wealth of O-H and N-H bonds (the former being favoured 3:1), enabling formation of intermolecular hydrogen-bonding [129]. In addition to this, the amine group is observed to become protonated at acidic pH [173], thus bearing a positive charge. This positive charge and capacity for formation of hydrogen-bonding is attributed to chitosan's ability to adhere to carrageenan without the aid of additional agents [174] [129], as the positively amine groups of the chitosan readily associate with the negatively charged organosulfate groups of the carrageenan [200] [201], though the efficiency of adherence can be furthered by the use of glutaric acid and glutaraldehyde [202].

It is also observed that the anime groups of the chitosan become more highly protonated at lower pH [173], and this increase in positive charge can be used to encourage stronger adhesion [173]: it was noted that chitosan adheres to mica films most strongly at pH 3. Trends that may also offer insight into the binding mechanics of chitosan include chitosan's reluctance to form cohesive bonds with other chitosan polymer chains, unless contact time is prolonged. The authors of this particular study offer the conjecture that this denotes a need for chitosan molecules to be specifically oriented in order to form cohesive associations. Further evidence of this theory is given by mica-bound chitosan showing no capacity for cohesion with additionally added chitosan layers until maximum adhesion efficiency with the mica surface has been achieved [173]. This reluctance to form cohesive bonds is shown to escalate into repulsive forces when pH is raised to alkaline levels [173].

As previously discussed, silk fibroin contains amino acid residues which have positively charged regions, which in turn facilitate adsorption to carrageenan via the anionic organosulfate groups. This effect is likewise seen in the interactions between silk fibroin and eukaryotic cells, due to the negatively charged sialic acid expressed on the cell-surface membrane [203]. After the silk fibroin has been adsorbed onto the carrageenan surface, the subsequent treatment with organic solvents dehydrates the fibroin and triggers a structural

conversion from the alpha-helix form to beta-sheets, which are more structurally stable and insoluble in water [204]. It has been theorised that the carbonyl oxygens of silk fibroin form weak bonds with sodium ions (and that this effect can also cause the conversion from alpha-helix into beta-sheet) [205] which may provide a possible mechanism by which silk-coating causes a substantial increase in the stability of carrageenan gels in comparison to uncoated controls. Though the effect of silk-coating on gel stability is clearly inferior to that provided by chitosan-coating.

It may therefore be that a positively charged coat provides some degree of repellent force against positively charged ions, preventing them from penetrating the surface of the gel and disrupting the ionic crosslinking. This may also help to explain the higher efficiency of chitosan-coating (with regard to stabilisation) than that of silk-coating; each repeating monomer of the chitosan chain contains an amine group which, as previously discussed, grants the polymer its positive charge [173]. Polar amino acids within the silk fibroin peptide chain are likely to be far more sparse. Indeed, examination of the predicted amino acids coded for in 5' end repetitive coding region of complementary DNA (cDNA) clones of silk fibroin heavy chain, as given by Mita *et al.* show only 1 positively charged [11] amino acid residue (arginine) among a chain of 494 residues [58]. However, it may also be that the network of surface-adsorbed polymers provides anchorage, which physically holds the gel together. This would also fall in line with there being less positively charged groups in silk fibroin, as it would result in more sporadic adsorption points across the gel surface, and so the silk fibroin would be less able to physically hold the gel together.

3.2.2.5 Cytocompatibility of surface-coated carrageenan gels

The cytocompatibility of silk fibroin and deacetylated chitosan have been demonstrated. The next step was to ascertain whether this effect was maintained when the materials were applied to carrageenan gels. In order to do this, carrageenan gels were coated (separately) with chitosan and silk fibroin as per chapter 2, section 2.2.2.2. Cells were then seeded on the coated gels as per chapter 2, section 2.1.1.2. Given the previously demonstrated effect of resazurin solution on the carrageenan gels (figures 3.12 – 3.14), cytocompatibility was instead ascertained by staining the cells with fluorescein diacetate (as per chapter 2, section 2.1.2.1.3) and manually counting under fluorescence microscopy (with the exception of TCP, on which cells were could be seen with white-light). Staining was conducted just 5 minutes before visualisation, therefore the staining procedure would not have downstream effects on cell proliferation which would affect the results, which are given in figures 3.26 and 3.27.

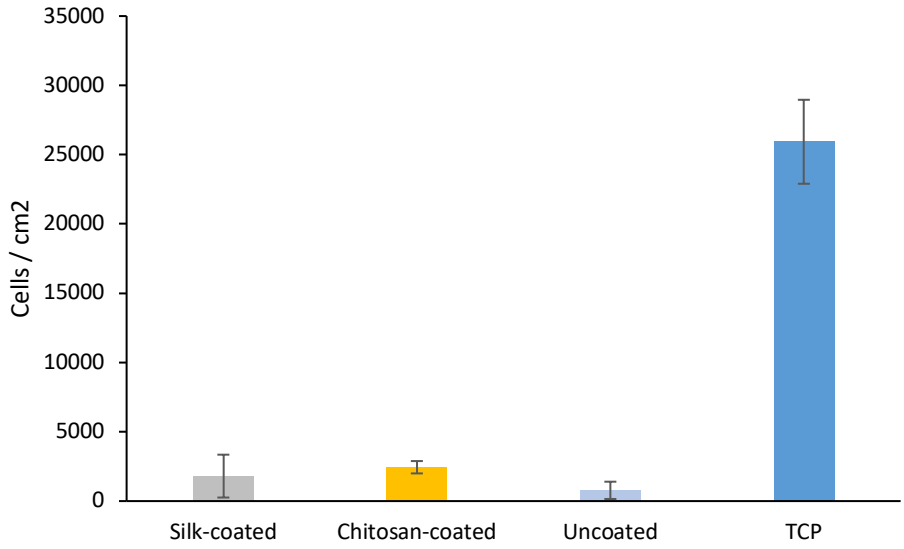

Figure 3.26: C2C12 cell-counts on coated and uncoated discs of carrageenan gels versus TCP. Cells stained by way of fluorescein diacetate and visualised via fluorescence microscopy. Data represent median ± interquartile range.

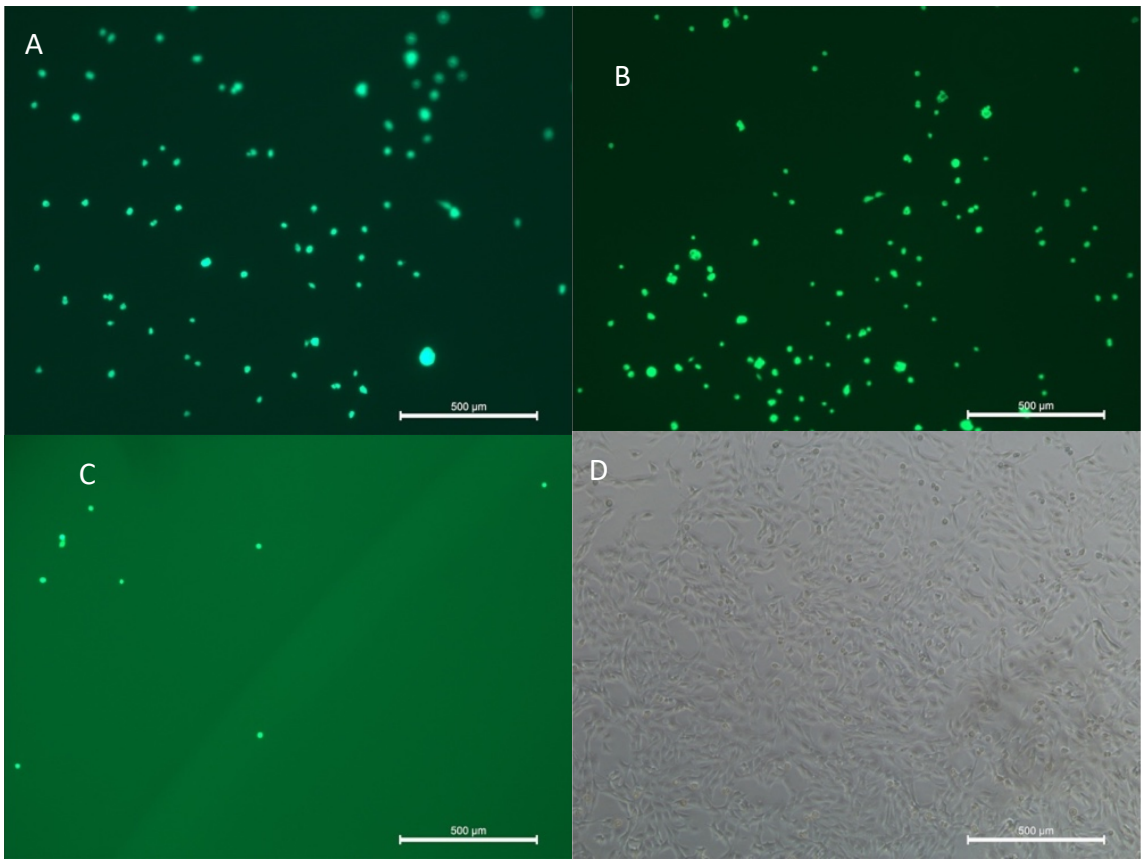

Figure 3.27: Representative images of C2C12 cells on coated and uncoated carrageenan discs, as well as TCP, 3 days after seeding. Cells stained by way of fluorescein diacetate and visualised via fluorescence microscopy. A: Chitosan-coated, B: Silk-coated, C: Uncoated, D: TCP. Scale bars represent 500 µm.

It was necessary to stain cells seeded on carrageenan discs, as they could not be easily distinguished from the scaffold under white light or phase contrast microscopy. Those seeded on TCP were are easily observable under phase contrast. The stained cells were imaged immediately after the staining procedure was carried out, and the TCP controls were contained in the same plate (and so were subject to the same environmental conditions as the cells to be stained, with the exception of the actual stain). The coated carrageenan gels appeared to show higher cell-counts after 3 days than the uncoated controls, suggesting that the coating procedures enhanced the cytocompatibility of the carrageenan gels. However, the cell-counts on the coated samples (both silk and chitosan) were vastly inferior to that on TCP. The fact that the coating procedures did not have the desired effect (or at least, not to the desired degree) of facilitating cell attachment may be explained by the factors governing adsorption of the materials to the carrageenan gels. As previously stated, the positively charged amine groups of the chitosan allow the material to associate with the negatively charged organosulfate groups of the carrageenan, as well as serum-proteins which allow adherence of cells. With the amino groups of the chitosan already engaged with the carrageenan, this may hamper their ability to associate with serum-proteins which in turn would diminish their cytocompatibility. This is also not dissimilar to associations between carrageenan and silk fibroin, wherein positively charged amino acid residues may associate with the negative carrageenan. Arginine, for example, is a positively charged amino acid [11] which is, of course, integral to model RGD motif's ability to bind cells. If such amino acids in cell-binding ligands were associated with the negatively charged carrageenan, it may prevent cells from accessing them.

Shen *et al.* found that layer-by-layer assembly of a charged silk fibroin / alginate scaffold increased cytocompatibility far beyond that of silk fibroin alone [206]. The technique was adapted for applications to carrageenan gels: the carrageenan was charged by way of pH adjustment (using sodium hydroxide). Chitosan was also given a higher positive charge by lowering the pH (accomplished by increasing the acetic acid concentration of the aqueous acetic acid solution in which the chitosan was dissolved). Charged but uncoated discs were produced, as well as those with one layer of charged chitosan, and finally a three-layer coat of chitosan-carrageenan-chitosan. Cells were seeded and allowed to proliferate for 3 days before imaging under fluorescence microscopy. Representative images are given in figure 3.28.

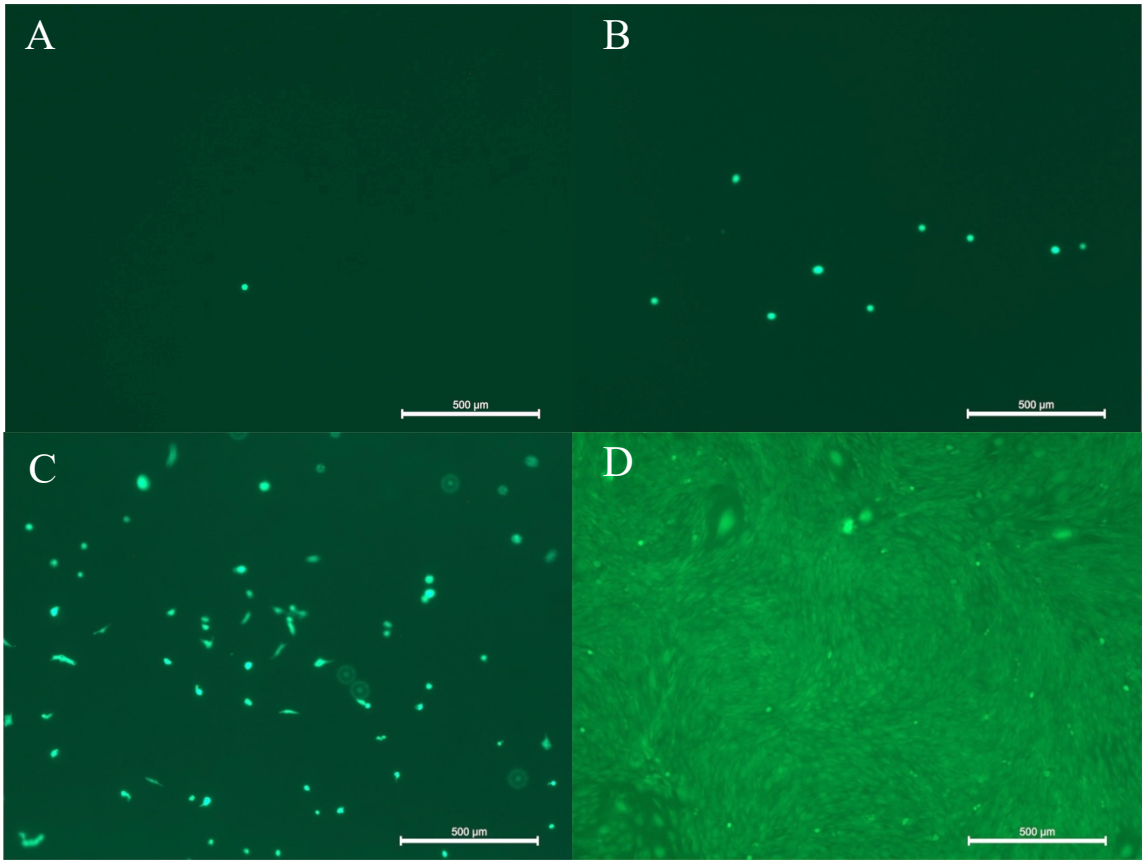

Figure 3.28: Representative images of C2C12 cell populations on carrageenan discs, A: uncoated, B: chitosan-coated, and C: coated with multiple layers of chitosan via layer-by-layer assembly. TCP controls also given (D). Cells stained using fluorescein diacetate and visualised under fluorescence microscopy.

The results appear positive (figure 3.28). Cell density appeared to increase with the addition of chitosan, and then increase further with additional layers. Furthermore, cells on the three-layer coated samples appear to show less rounded-morphology, indicating that some degree of cell-spreading may have taken place. However, these increases did not compare to the cell densities on TCP.

The manufacturer notes that the kappa-carrageenan (Sigma 22048) contains less than 11% potassium, less than 3.5% calcium, and less than 2% sodium, with a moisture content of less than 12% [207]. It is also noted that the product contains a minority (though undefined) amount of iota-carrageenan [207]. Furthermore, the pH of the product is given as being between 7.5 and 10.5 [207]. The slightly alkaline pH and presence of alkali metals are likely due to the process of extracting carrageenan from red seaweed which is typically done using alkaline solutions, such as potassium hydroxide [14], and alkaline solutions such as sodium hydroxide can be used to convert one type of carrageenan to another [208]. Though

these alkaline metals are present in DMEM, they are present in comparatively smaller amounts as seen in table 3. It can be extrapolated from the concentrations of the inorganic salts that the DMEM contains 0.255% (w/v) sodium, 0.003% (w/v) potassium, and 0.01% (w/v) calcium. As stated, the concentrations of these alkaline metals in the carrageenan are noted to be higher [207]. Garland *et al.* investigated the cytotoxic effects of these alkaline metals (as part of inorganic salts). They noted that, when chloride salts of sodium, calcium, and potassium were applied to cells in millimolar concentrations, only salts containing sodium resulted in a lessened degree of cell viability and attachment [209]. It may therefore be possible that the sodium content of the carrageenan negatively impacts the ability of cells to adhere and remain viable on the surface of carrageenan gels. The process of forming a hydrogel scaffold from the carrageenan powder involved exposure to KCl solution, it is therefore possible that residual KCl remained associated with the hydrogels after gelation. As noted however, this is unlikely to have impacted cell attachment or viability [209].

3.2.2.6 Surface-coating of alginate

The primary rationale for choosing carrageenan over alginate was the latter's inability to bind cells in its normal form. However, since carrageenan gels required surface modification in order to prevent their degradation, this rationale was weakened. Cell growth was therefore, briefly assayed on alginate discs, formed and coated as per chapter 2 section 2.2.2.2.4. Cells were seeded as per chapter 2, section 2.1.1.2, and their proliferation was tracked by way of resazurin metabolic assay as per chapter 2, section 2.1.2.2. The results are given in figure 3.29.

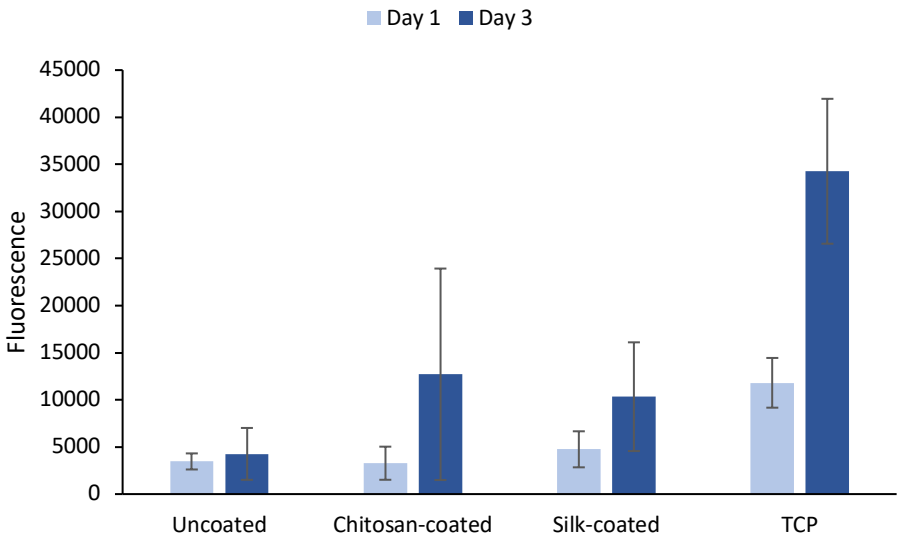

Figure 3.29: C2C12 cell-proliferation on coated and uncoated alginate discs, versus TCP, measured by way of resazurin metabolic assay. Data represent median ± interquartile range.

Again, the results (figure 3.29) suggest that the surface coating improved cytocompatibility compared to the uncoated gels (which, as expected, appeared to show no cell growth of any kind after 3 days). Information regarding purity or potential contaminants is not given by the manufacturer [210], however potential contaminants of improperly purified alginate are noted to include proteins, lipopolysaccharides, and nucleic acids [211]. The process of this surface-coating was relatively simple, especially when compared to the conventional practice of coupling RGD and similar protein motifs to the polysaccharide, which involves costly and hazardous reagents such as EDC and NHS [212, 213] and the peptide itself if purchased from a manufacturer. With optimisation, surface-coating or cross-material blending may represent a more efficient means of functionalising alginate gels than covalent attachment of cell-binding protein motifs. Indeed, silk / alginate blends have been used as scaffolds for mesenchymal stem cell culture [154, 214].

3.2.2.7 Air-blown, surface-coated carrageenan microbeads

Although there are still obstacles to overcome in the use of carrageenan hydrogels to support cell culture, progress has been made with regard to stabilisation of these carrageenan gels, and there may be wider-scope downstream implications for these stabilised hydrogels such as cell encapsulation for therapeutic delivery or preservation [76], or drug delivery [215, 216]. With this in mind, the possibility of rapid-generation of stabilised carrageenan microparticles was explored: carrageenan solution was sprayed into a

collection bath of crosslinker solution as per chapter 2, section 2.2.1.2. The resultant droplets gelled into microparticles, whose size distribution is shown in figures 3.30 – 3.32.

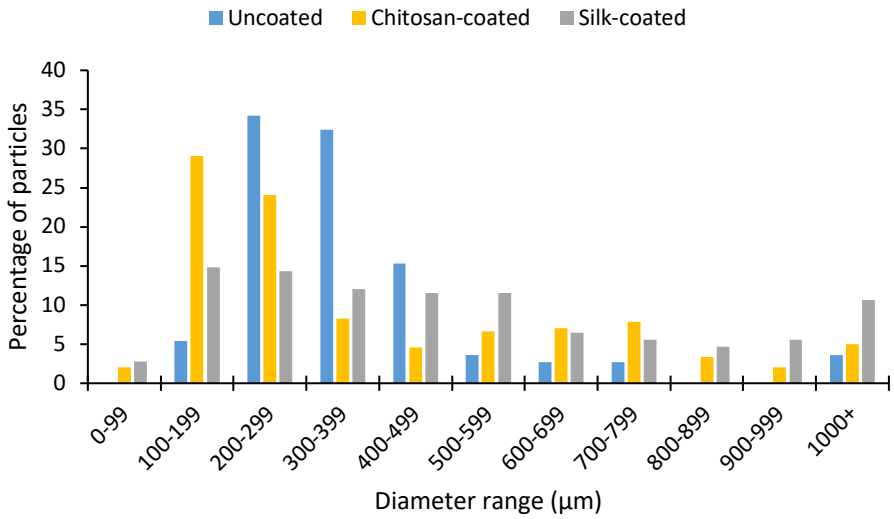

Figure 3.30: Size distribution of surface-coated carrageenan particles, produced by air blowing. Data represent individual observations.

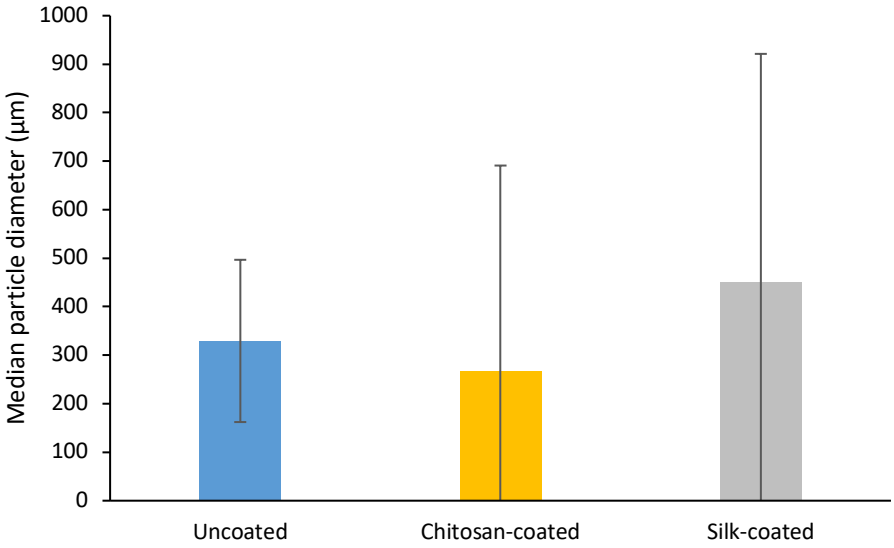

Figure 3.31: Median diameter of surface-coated carrageenan particles, produced by air blowing. Data represent median ± interquartile range.

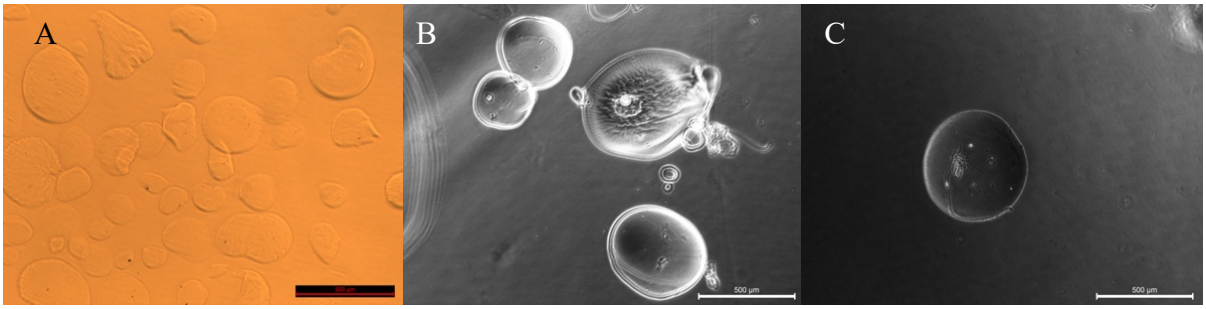

Figure 3.32: Representative images of surface-coated carrageenan gel particles produced by air blowing. A: Uncoated, B: Chitosan-coated, C: Silk-coated. Scale bars represent 500 μm.

Due to an error in the experimental procedure, the coated samples were imaged under phase contrast microscopy whereas the control samples were imaged under white light microscopy. However the particles are clearly visible under both conditions, and diameters of the particles are easily measured. The resultant particles were generally spherical in shape (figure 3.32). The vast majority of particles were less than a millimetre in diameter (figure 3.30) with mean diameters of around 400 – 500 μm, depending on surface-coating. This would appear to make this method of generating carrageenan particles unsuitable for drug delivery, as hydrogel particles for this purpose are produced with diameters in the nanometer range [215-217]. They may be applicable to cell encapsulation techniques, however. This will be discussed further in section 3.3.4. Most importantly, if the obstacles with regard to surface-seeding can be overcome, these particles would be of sufficient size to be applied to this end.

Even after extensive work, carrageenan gels capable of supporting the growth of myoblastic cell cultures had not been produced, although progress had been made with regard to stabilising the carrageenan gels. Focus therefore was shifted to a protein-based biomaterial which could be formed into solid scaffolds.

3.3 Further work and wider implications

3.3.1 Analysis of disruptive substances

The data shown in figures 3.10 and 3.11 have curious implications. It remains highly likely that sodium ions disrupt the ionically crosslinked carrageenan hydrogels, gradually replacing the potassium links with weaker sodium links. However, given the hastened

degradation time of gels exposed to resazurin working solution for only 2 hours per day versus those exposed only to PBS or DMEM, it was expected that the resazurin working solution would have the highest sodium content, i.e. that degradation time would correlate with sodium content. The resazurin working solution presented an anomaly in this regard. Whilst DMEM had the lowest sodium content, and the longest degradation time for gels maintained therein, and PBS showed a shorter degradation time in line with its higher sodium content compared to DMEM, resazurin working solution exhibited the shortest degradation time despite its sodium content falling between that of DMEM and PBS. It may be beneficial to explore this in further detail, perhaps by maintaining carrageenan gels in solutions of deionised water with gradually increasing concentrations of sodium chloride added thereto. If this produced the expected correlation between sodium content and gel degradation times without the presence of additional substances, it would concretely demonstrate the role of sodium ions in destabilising carrageenan gels. It would also be beneficial to expose carrageenan gels to phenoxazines under controlled conditions in order to ascertain whether this class of organic molecule plays a role in destabilising the gels.

3.3.2 Topographical micropatterning

The carrageenan hydrogels used here had no designed topographical features. It is noted that topographical features (microscale or nanoscale structures on the substrate surface) influence the behaviour of cultured cells [218], thus the introduction of such structures on the surface of the carrageenan gels may serve to improve cytocompatibility. For example, Lam *et al.* demonstrated that the introduction of wave patterns (with peaks ranging from 3 – 12 μm distance from each other) on silicone substrates [219]. They noted that the presence of these wave structures induced alignment in cultured myoblasts, and that waves whose peaks were 6 μm apart did this to the most effective degree [219]. Two notable techniques by which hydrogels may be given topographical features are photolithography and soft lithography [218, 220]. In order for photolithography to be applicable, the hydrogel must have the capacity for photocrosslinking. This capacity is exploited by designing an opaque mask with the desired topographical pattern included as transparent sections [218]. This mask is applied to the hydrogel precursor and as the light shines through the mask, the hydrogel is photocrosslinked according to the pattern of the mask, and so topographical features are formed on the surface of the gel [218, 220]. Soft lithography usually involves a polydimethylsiloxane construct, which can be designed with the inverse of the desired topographical pattern and then applied to the hydrogel precursor [218, 220]. When polymerised, the construct is removed, leaving the hydrogel surface imprinted with the topographical pattern [218, 220]. Other forms of soft lithography involve forming the

hydrogel within the topographical features of the polydimethylsiloxane construct, which can then be applied to the surface of an existing substrate [218, 220].

3.3.3 Potential for non-animal-based coatings

The obvious drawback to these stabilisation methods is that they employ animal products, and the focus of this research is to produce a largely (or preferably, wholly) plant-based scaffold.

3.3.3.1 Fungal sources of chitosan

Although the primary source of chitin is from crustacean exoskeletal structures [60], the substance is not limited to shellfish, plant-based sources of chitin have been noted; it has been observed that some edible mushrooms deviate from the norm for fungi and plantae in that they contain the polysaccharides glycogen and chitin, as opposed to cellulose and starch [60, 221, 222]. The process by which chitin is isolated is the same in either case. The biomass is washed thoroughly and pulverised. Chitin is then disassociated from surrounding proteins in a step termed deproteinization, usually via treatment with high-temperature sodium hydroxide. Subsequently, the chitin may be separated from surrounding minerals, such as calcium chloride. This demineralisation step employs acids, most commonly hydrochloric acid [60]. Chitin content can vary greatly depending on the source; even amongst shellfish the chitin content (as a percentage of the total biomass) has been noted to vary from 13% - 42% [223]. This is likewise true for fungal chitin, the chitin content of the whole fruit body of Amycel's 3015 shiitake strain of mushroom was noted to be 4.95% [224], and *Lactifluus vellereus* was observed to contain 11.4% chitin per dry mass [222]. Chitin is not limited only to fully cultivated mushroom fungi; chitin has also been isolated from fungal mycelia, where the highest yield was noted as 41.3% chitin per dry biomass [225]. The deacetylated derivative, chitosan, has also been observed to be biologically produced in fungal cells; a study reported a maximum of 14% chitosan per dry mass produced from *Rhizopus oryzae*, with a relatively high DDA% of 87.9% [226]. Though shellfish have, on mean, a higher chitin content than fungal alternatives [60], scaled-up cultivation of suitable species of mushroom may be a more environmentally friendly method by which chitin can be produced, which would be an advancement in-line with the some of the aims of cultured meat production, and so mushroom / fungal chitin / chitosan may represent an alternative to shellfish-derived chitin from which a stabilised, plant-based carrageenan scaffold may be developed. Additionally, it has been speculated that the

isolation process of chitin may be enhanced (with respect to the environmental impact) via employing protease enzymes in leu of the sodium hydroxide in the aforementioned deproteinization stage, and enzymes such as trypsin or pepsin have been proposed for this purpose [60]. Various protease enzymes have been noted in a number of edible mushroom species, including caspase varieties, ingensin, and chymotrypsin [227]. There may be scope for a model in which both chitin / chitosan and protease enzymes may be obtained from mass-production of mushrooms, and these proteases utilised to further lessen the environmental impact of the chitin-isolation process, already lessened by the switching of fungal production rather than shellfish farming.

3.3.3.2. Cellulose as an alternative to chitosan

Chitin is known to be the second most abundant polysaccharide in nature, with the most abundant being cellulose [188, 228]. Like chitosan, cellulose is a structural polysaccharide [184]. Despite being composed of glucose chains, similar to starch or glycogen, it is not used primarily as a glucose storage polysaccharide as are starch and glycogen [184]. This is due to the repeating units in cellulose being joined by an oxygen bridge between the beta-1 carbon of one unit, and the number 4 carbon of the other (whereas the links between repeating units in starch or glycogen are formed between the number 4 alpha-1 carbons) [184]. This means that while storage polysaccharides such as glycogen and starch take on a curved structure, cellulose is able to assemble in the form of a long straight chain [184]. These chains can then align with each other and associate via intermolecular hydrogen bonding [184, 228], facilitated by hydroxyl groups; each repeating unit of cellulose has three hydroxyl groups, whereas those of chitosan have two hydroxyl groups and one amine group [229, 230]. Given that oxygen is slightly more electronegative than nitrogen, this would mean cellulose has a higher capacity for hydrogen-bonding than chitosan. This, in turn, may mean that cellulose would adhere to the surface of carrageenan hydrogels more effectively than chitosan, and should provide effective shielding against ions which may interfere with the crosslinking of the carrageenan gel.

Cellulose is a difficult polysaccharide to dissolve. It is insoluble in water, unless the solution is taken to extreme pH levels [228]. The mechanism of cellulose dissolution is poorly understood, as the few solvents in which it will dissolve do not have distinguishing attributes in common [228]. This insolubility is an important trait also seen in chitosan, which will dissolve in weakly acidic solutions but not in water. Cellulose, like chitosan, would not redissolve into culture medium after being used to coat a hydrogel.

3.3.4 Silk fibroin from other sources

As previously mentioned, not all forms of silk fibroin lack RGD motifs. Talukdar *et al.* for example, showed that cardiomyocytes exhibited significantly higher metabolic activity on *Antheraea mylitta* silk fibroin than on *bombyx mori* silk fibroin [231]. An exploration of silk fibroin from various species may result in coatings which further increase the cytocompatibility of the coated carrageenan gels.

3.3.5 Cell encapsulation and gel porosity

Surface-seeding appeared unsuccessful. However, there is precedent for successful culture of cells by encapsulation within carrageenan gels. Mihalia *et al.* particularly, were able to culture endothelial cells within chitosan-coated carrageenan fibres [129]. It is generally understood that cell encapsulation within hydrogels is accomplished by suspending the cells in the polymer solution, with subsequent crosslinking to induce gelation [232]. Indeed, this is the cited approach used in studies concerning cell encapsulation within carrageenan hydrogels [233, 234]. This was attempted, but cells showed no signs of proliferation (data not shown). This approach involved mixing carrageenan solution (with as low % concentration as would allow the solution to remain liquid in a 37˚C water bath) with an equal volume of DMEM cell suspension. An initial concern was that, since this effectively halved the carrageenan concentration of the final solution, an excessively low carrageenan content was to blame. Or that excessive heat from the carrageenan solution led to cell-damage, though the temperature was little above 37˚C. However, upon reflection, porosity and pore size present themselves as possible causal factors for this inability to support encapsulated cell proliferation. It was also noted that, once encapsulated, cells could no longer be stained using CellTracker Green CMFDA dye (data not shown), and staining prior to encapsulation was required in order to visualise the cells once inside the gel. This may indicate that either cells are killed immediately upon encapsulation, or the gels lack the pore size to allow the CMFDA dye to penetrate the gels and reach the cells. It was also observable that the carrageenan gels retained the red colouration of DMEM after immersion therein. This may indicate that the phenol red component of DMEM is able to enter the gel. Given that the molecular weight of Celltracker Green CMFDA dye is 464.8 g/mol [235], and that of phenol red is 376.4 g/mol [236], this may provide a very rough indication of the gels' pore size. If the pores of the carrageenan gels were only of sufficient diameter to accommodate molecules of < 464.8 g/mol but > 376.4 g/mol, it would preclude many vital nutrients and peptides from penetrating the gel and thus starve the cells of these critical

substances, as well as preventing the exit of cellular waste products. Wright *et al.* for example, noted that pore size of their alginate hydrogels was increased via oxidation, and this (along with decreased stiffness) enhanced the viability of encapsulated corneal epithelial cells [77]. Ji *et al.* noted that by increasing the pore size of chitosan hydrogels, cells were able to remain viable at increased depths [178]. Further work may seek to clearly ascertain the degree of porosity and pore size in the carrageenan gels by scanning electron microscopy, in order to determine whether this is the causal factor for the lack of encapsulated cell proliferation. If a lack of porosity or insufficient pore size were confirmed, porogen-leaching techniques would likely be the best method by which to create larger pores, for example Kim *et al.* produced macroporous alginate scaffolds by addition of sodium chloride (NaCl) crystals of diameters ranging from 100 – 300 μm, which were then leached during the ionic crosslinking stage [237]. This may also warrant further consideration of the lyophilisation approach discussed in section 3.2.1.3, as it may aid in generation of larger pores to facilitate infiltration of surface-seeded cells.

With further regard to cell encapsulation: as previously mentioned, cells could not be stained with CellTracker Green CMFDA dye once encapsulated within carrageenan gels. Cells stained beforehand retained their rounded shape and green fluorescence indefinitely after encapsulation, without further staining, indicating no proliferation had taken place (data not shown). However, this may indicate a retention of viability despite immobilisation, in which case cell encapsulation within carrageenan gels may represent a means for hypothermic storage of cells, as described by Constantinescu and Connon who successfully maintained viability of adipose-derives stem cells in alginate at relatively low temperatures [164]. Alginate gels have also been applied in this way to human mesenchymal stem cells as well as mouse embryonic stem cells [238]. In order to ascertain whether or not this is the case, gels would need to be maintained between 4˚C and 23˚C in serum-free conditions, and cells analysed for their ability to proliferate, spread, and differentiate after release, as done in the aforementioned study [164]. In contrast however, the use of chelators to dissolve the gels may not be necessary; the release of cells from carrageenan gels could be achieved by simple heating, depending on the carrageenan concentration. Encapsulation could, similarly, be achieved by cooling a suspension of cells in carrageenan solution, leading to thermal gelation. If carrageenan gels can indeed be applied for the immobilisation and hypothermic preservation of cells, they could be further applied for wound-treatment purposes [162].

3.4 Concluding remarks

Carrageenan hydrogels are easy to produce, and the method by which this is accomplished is highly time-efficient. The stabilisation of these gels, however, is more complicated. Increasing the carrageenan concentration of the scaffolds did result in a longer degradation time, but also increased the degree of swelling. Increasing the KCl crosslinker concentration had no effect on the degradation time of beads, but appeared to translate into increased degradation time for fibres. The concentration of KCl crosslinker did not appear to correlate (either positively or negatively) with the degree of swelling for beads or fibres.

It was noted that allowing the scaffolds to gel by cooling, with subsequent lyophilisation before the crosslinking stage, did cause a significant increase in stability (as denoted by the time taken to degrade). This did not appear to substantially increase the degree of swelling, as these lyophilised disc scaffolds showed a maximum mass significantly higher than beads alone, and then, only when maintained in DMEM. Thus, the lyophilisation stage did appear to impart stability to the carrageenan gels. The reason for this increased stability was theorised to be a decrease in space between the carrageenan's molecular chains during lyophilisation, allowing for more thorough crosslinking when exposed to KCl solution. However, this stage increased the time taken to produce the scaffolds by many times. Additionally, while this technique was easily applicable to discs (being allowed to cool in multi-well plates), the same could not be said for beads or fibres. There was no suitable container to allow the carrageenan solution to cool whilst in droplet or fibrous shapes, and such a mould would be difficult to construct. It was attempted to form carrageenan beads and fibres in cold (4˚C) water, but this proved ineffective (data not shown). It may be possible to induce thermal gelation for the bead and fibre morphologies using solvent solutions which could be chilled to temperatures below the freezing point of water, whilst remaining in liquid form, or in liquid nitrogen. However, this would lessen the cost-effectiveness of the procedure by a wide margin. It was therefore concluded that the lyophilisation approach, while successful, would not be suitable for large-scale scaffold production.

Coating the carrageenan gels in other biomaterials, namely chitosan and silk, proved to be the most effective means of stabilisation out of those attempted. While silk-coating resulted in higher stability, chitosan-coating was more effective; chitosan-coated scaffolds remained gelatinous even after 21 days in 37˚C DMEM, showing no sign that they would degrade in the near-future. This increase in stability was theorised to be a result of the polar nature of the coating materials, as the polar regions would attract ions present in the solution and

prevent them from interfering with the ionic forces that hold the gel together. The drawback to these results were that they were produced via the use of animal-derived biomaterials. As previously stated, this work aims to minimise the use of animal-based materials in order to make the process as ethically and environmentally viable as possible. Further work in this area and for this purpose may, therefore, investigate non-animal-derived biomaterials as potential coatings for carrageenan gels.

Carrageenan gels are easy to produce, but appear susceptible to destabilisation via sodium ions in solution. Surface-coating of the gels with chitosan would seem to represent an efficient means of correcting this issue. However, the gels appear unable to support growth of surface-seeded cells. Cell encapsulation within surface-coated gels may be a potential avenue by which carrageenan can be developed into a functional scaffold for myoblastic cell culture. The primary strength of carrageenan hydrogels with regard to cultured meat applications is the time and cost-efficiency of producing scaffolds: essentially requiring only the polymer solution and a crosslinker bath, though its significant drawback is the lack of a satisfactory degree of inherent biocompatibility without the need for modification.

Chapter 4 – Cytocompatability of Edible Protein Biomaterials

4.1 Introduction

4.1.1 Gold-standard protein biomaterials

As discussed in chapter 1, extracellular matrix proteins represent the gold-standard with regard to choice of biomaterials in tissue engineering scaffolds. The ECM forms the cells' native environment *in vivo*, and is responsible for providing not only mechanical support, but also initiates signalling pathways regulating a variety of vital cell functions such as adhesion and differentiation [193-196]. It follows that bioscaffolds are often modelled after the ECM, or incorporate such substances into their design.

Collagen is perhaps the most notable component of the ECM, being the most abundant protein in the body and being present in many different isoforms [196]. Perhaps the most critical isoform is type I collagen, the knockout of which is noted to have lethal consequences [195]. Another primary component of the ECM is fibronectin, a dimer protein which facilitates binding of cells to the ECM, and also the assembly of many ECM components [196]. Knockout of the fibronectin domain 1 (FN1) region is noted to be lethal [195]. Elastin is another example of an integral ECM component whose knockout is noted to be lethal [195]. Elastin, as the name implies, determines mechanical properties of the ECM such as elasticity [196].

Although not present *in vivo*, gelatin is a biomaterial used in tissue engineering derived from ECM, specifically from the hydrolysis of collagen [53]. Although showing limited cytocompatibility alone, its incorporation into cross-material bioscaffolds has been shown to increase their cytocompatibility [89, 137, 239]. Another example of an ECM-derived biomaterial used in tissue engineering [240, 241] is Matrigel, which is a composite of laminin, collagen type IV, and enactin, extracted from Englebreth-Holm-Swarm mice tumours [54].

As discussed in chapter 1, however, an ideal scaffold for cultured meat applications would be plant-based in order to achieve the desired renewability as well as edibility, and to prevent cultured meat from relying on by-products of current livestock processing practices.

4.1.2 Zein as a biomaterial

As discussed in chapter 1, a renewable and environmentally friendly scaffold would be ideal for large scale production of cultured muscle tissue. A plant-based material is the obvious choice to fulfil this criteria. Zein is a protein found in abundance within the endosperm of corn kernels, accounting for nearly half of the kernel's total protein content. It is notable for its solubility in aqueous alcohol solutions rather than water (due to a high ratio of non-polar amino acids), which was what led to its initial discovery [135]. Despite poor nutritional value, zein is of course edible, being an intrinsic component of corn kernels. Being edible, renewable, and easily purified from corn via solvent extraction [135], zein is a particularly attractive candidate from which to produce bioscaffolds for cultured meat purposes.

Zein films have been shown to bear good cytocompatibility: with films being able to support attachment of both liver cells and fibroblasts, these films were also demonstrated to be composed of particles with diameters in the nanometer range [242]. Lian *et al.* showed that composite membrane scaffolds of hydroxyapatite and zein were able to support attachment and proliferation of bone-marrow mesenchymal stem cells, and although composite ratios favouring hydroxyapatite were shown to enhance cytocompatibility, pure zein scaffolds were nonetheless able to facilitate cellular adhesion and proliferation as well [140]. Tu *et al.* successfully prepared, seeded, and implanted salt-leached zein scaffolds, and demonstrated their ability to support ectopic bone formation from mesenchymal stem cells *in vivo* (specifically, in nude mice) [138].

4.1.3 Aims and objectives

As discussed in chapter 1: zein is a plant-based, edible protein. This gives it inherent potential as a biomaterial from which to produce scaffolds for large-scale muscle culture for the purposes of consumption. Zein has been noted in literature to be biocompatible, and has been used in tissue engineering scaffolds, though the interactions between zein and myogenic cells seems sparsely documented. This chapter aims to quantify the compatibility of zein with myogenic cells in terms of its ability to facilitate proliferation, spreading, and differentiation of C2C12 myoblasts (as a model cell line), and compare this cytocompatibility to that on gold-standard ECM-based biomaterials.

4.2 Results and Discussion

Zein films were produced (as per chapter 2, section 2.2.5.1) in order to confirm their cytocompatibility before fibrous and particulate scaffolds were produced. An immediate advantage of zein in this regard was the lack of any need to modify the material since zein is a hydrophobic protein only soluble in aqueous organic solvent solutions [135] and is not liable to redissolve in culture media.

4.2.1 Cell proliferation on zein films

Zein powder was obtained from two manufacturers: Sigma Aldrich and Acros Organics. As a first step, cell growth on each of these types of zein was compared with TCP by way of resazurin metabolic assay, as per chapter 2, section 2.1.2.2. The results are shown in figure 4.01.

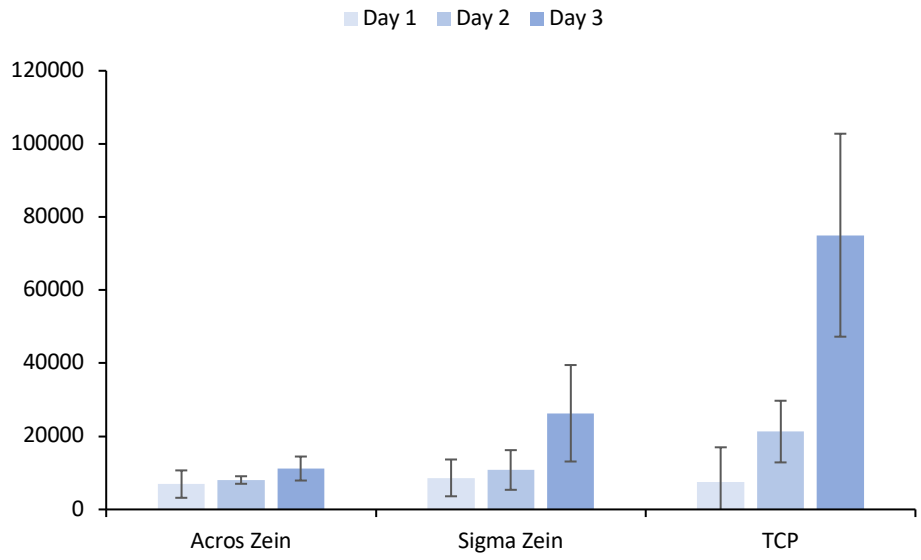

Figure 4.01 A brief assay of C2C12 cell proliferation, measured by resazurin metabolic analysis, on films formed from two different brands of zein versus TCP. Data represent median ± interquartile range.

There appeared to a very slight improvement for cell proliferation on Sigma-brand zein versus Acros-brand zein. Both manufacturers list their product as containing only zein, therefore this difference, if meaningful, cannot be attributed to any additional agent, and would most likely be an effect of variations in the purification process. During experimental procedures, Sigma-brand zein appeared slightly easier to dissolve than Acros-brand zein

(data not shown). There did not appear to be any notable differences otherwise. Sigma-brand zein was used for all subsequent experiments.

Secondly, a more detailed analysis of cell proliferation on sigma zein films versus TCP was conducted, again by resazurin metabolic assay as per chapter 2, section 2.1.2.2.

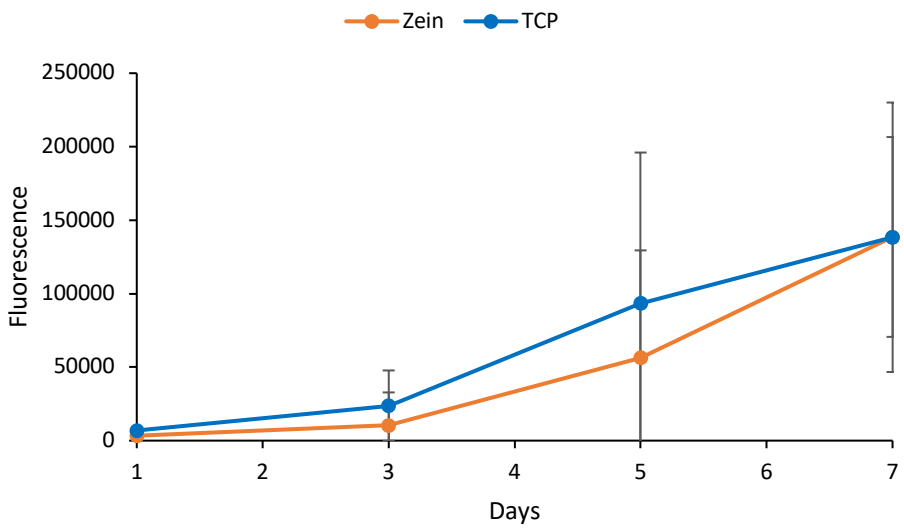

Figure 4.02 C2C12 cell proliferation, measured by resazurin metabolic analysis, on Sigma-brand zein vs TCP. Data represent median ± interquartile range.

Results of cell proliferation on sigma zein films (Figure 4.02) were positive. Growth of cells on zein films increased at a rate comparable to that on TCP; statistical analysis showed that there was no significant difference between the two materials ($p > 0.05$ for all timepoints). This means the cells can be said to grow on zein as efficiently as they do on a material which has been specifically designed to support cell culture. These results are also positive when compared to the proliferation of cells on silk fibroin (chapter 3, figure 3.21), where proliferation was significantly lessened when compared to that on TCP at the 1-day and 7-day timepoints.

Arnesen *et al.* tracked the proliferation of myoblasts on collagen scaffolds by manual cell counts, and the trends observed therein show a similar three-day lag phase to that displayed in figure 4.02 [243]. Subsequently in Arnesen's study, from the end of the lag phase to the final timepoint, cell density increased from approximately 200 cells per field of view to approximately 1200, representing an approximate factor of 6 [243]. Figure 4.02 showed an increase in fluorescence from 56422 after the lag phase, to a final reading of

138575 at the final 7-day timepoint, representing an increase in metabolic activity by an approximate factor of 2.5.

Chaturvedi *et al.* analysed serum-free myoblast culture on fibronectin and type I collagen [50]. It was noted in their study that the lag phase lasted 48 hours, 24 hours shorter than that observed here on zein and in Arnesen's study of type IV collagen scaffolds [243]. After this initial lag phase, cell density rose from 0.5 x 10^5 cells to approximately 2.5 x 10^5 cells within 24 hours [50]. By the 7-day timepoint, the cell densities on type I collagen and fibronectin were approximately 3.5 x 10^5 cells, from their initial seeding-density of 7 x 10^3 cells, using nunclon delta multi-well plates as used in this work [50]. This represents an increase by a magnitude of 50x, and this degree of proliferation is clearly superior to that observed here on zein.

Wilschut *et al.* conducted analysis of porcine muscle stem cells on various ECM proteins [52]. It was noted that cells on type I collagen and gelatin reached near-confluence after 3 days of culture, while those on Matrigel appeared to reach complete confluence in the same timeframe. Those on fibronectin and laminin aggregated into clusters, particularly so on laminin [52]. In contrast, cells on zein reached near-confluence after 7 days of culture.

Proliferation on zein films also appears positive when compared to that on silk fibroin (see chapter 3, figure 3.21), which is also noted to lack RGD or similar gold-standard cell-binding protein motifs within its structure, when obtained from *bombyx mori* [57]. In the absence of these cell-binding motifs, *bombyx mori* silk fibroin relies on its positive charge in order to bind cells [57]. As mentioned in chapter 3, this positive charge is imparted by a number of basic amino acids, such as arginine and lysine [58]. The binding mechanism of cells to zein (to be discussed in section 4.2.2) appears to be superior to that on *Bombyx mori* silk fibroin.

The purity of Acros-brand zein (A0347340) is given by the manufacturer as 91% protein content [244]. The remaining mass is likely to be composed of impurities such as pigments, specifically beta-carotene and xanthophyll [245]. The purity of Sigma-brand zein is not given by the manufacturer [246]. Xanthophyll is unlikely to have any significant effect on cell function, as it is noted to have failed to inhibit the growth of various types of cancerous human cells [247]. Beta-carotene is also noted to lack cytotoxic effects, though the products of its breakdown are noted to exhibit carcinogenicity [248], therefore beta-carotene is also unlikely to have impacted cell function during this work.

Although myogenic cells cultured on zein appear to take longer to reach confluence than those cultured on ECM proteins such as collagen and fibronectin, zein is clearly able to support the proliferation of myoblasts, to the point of confluence, and to a level comparable to positive controls (TCP). This on a plant-based protein, with the inherent renewability and comparative simplicity of production versus animal-based proteins, is a highly positive result.

4.2.2 Cell morphology on zein films

Spreading is a crucial aspect of myogenic cell culture, as the process of cell spreading precedes that of differentiation. Myogenic cells first migrate toward each other [249] before adhering and fusing into myotubes by way of intercellular adhesion proteins expressed on their membrane surfaces [12, 250]. In order to ascertain the degree to which cells are able to spread on zein films, cells were stained with Celltracker Green CFMDA dye and analysed for morphology as per chapter 2, section 2.1.2.1.2. As mentioned in chapter 1, myoblasts experience a change in morphology over time due to rearrangement of their cytoskeleton, giving rise to a more bi-polar and jagged shape [34]. The value for circularity quantifies how close to a perfect circle the cells' shapes are, and as such a lower value for circularity indicates a higher degree of spreading.

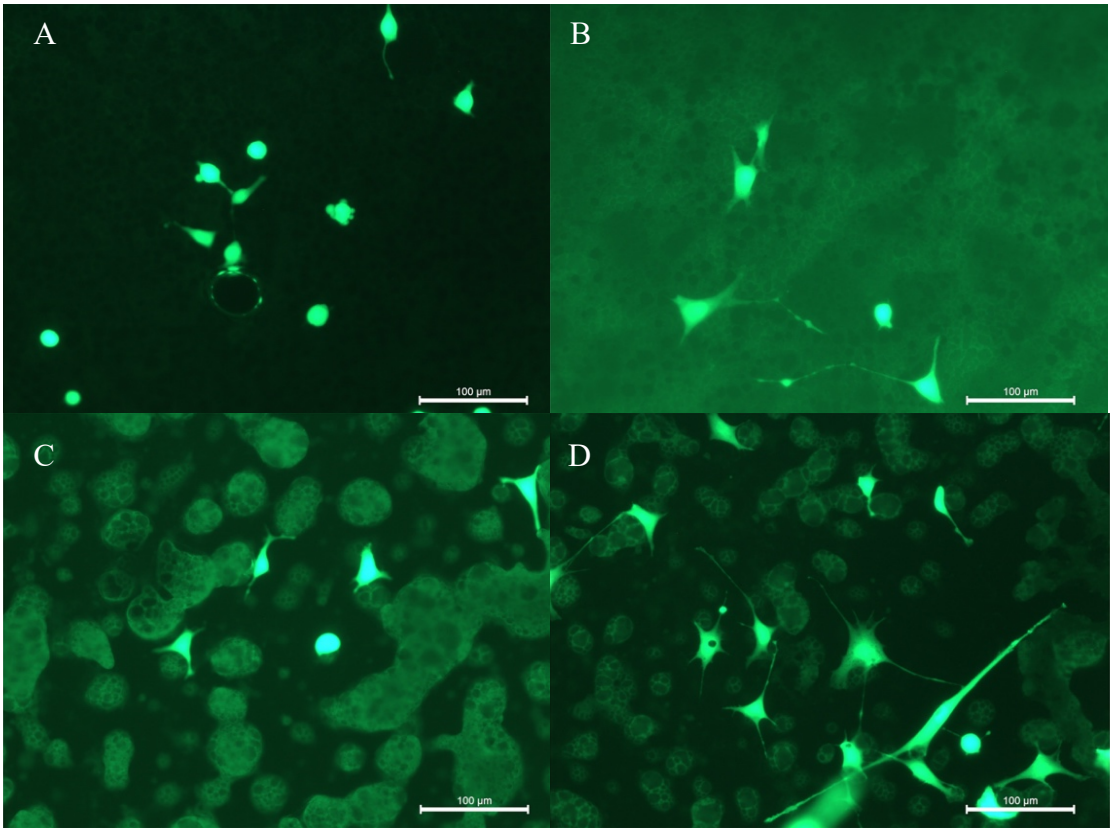

Figure 4.03 Representative images of C2C12 cell morphology on zein films over time. A: 3 hours, B: 24 hours, C: 48 hours, D: 72 hours. Scale bars represent 100 µm.

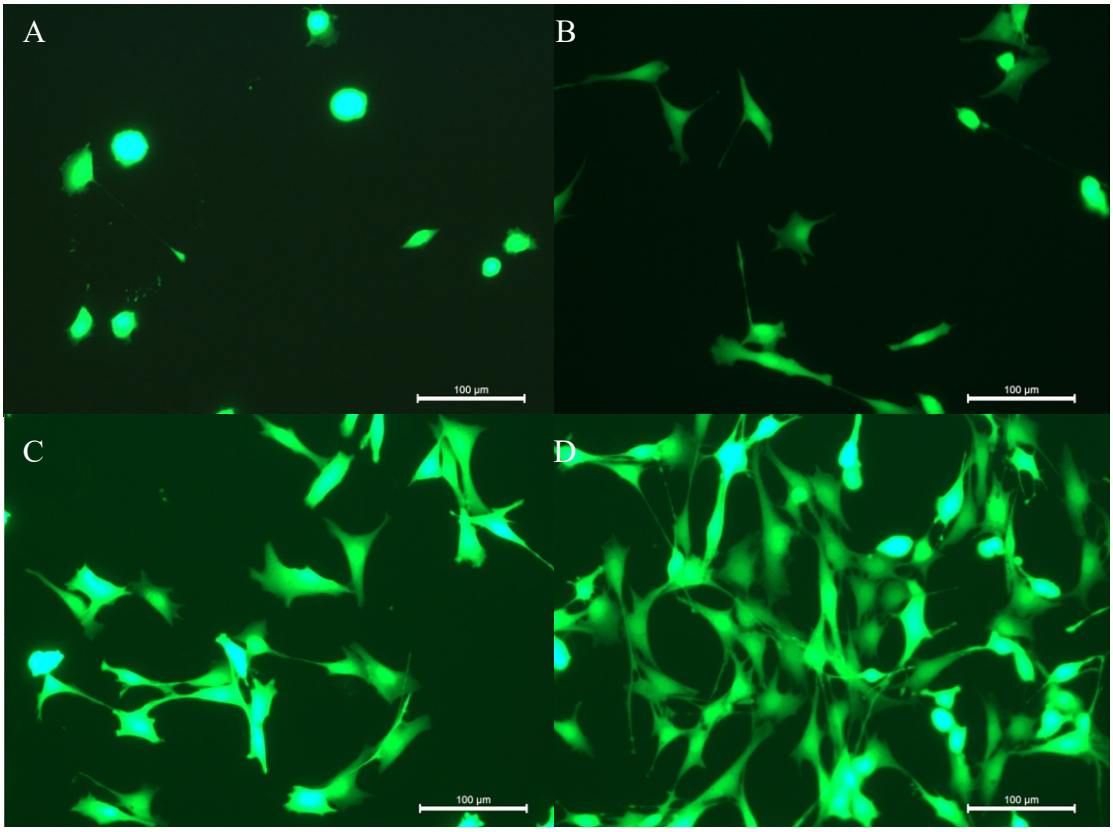

Figure 4.04 Representative images of C2C12 cell morphology on TCP over time. A: 3 hours, B: 24 hours, C: 48 hours, D: 72 hours. Scale bars represent 100 µm.

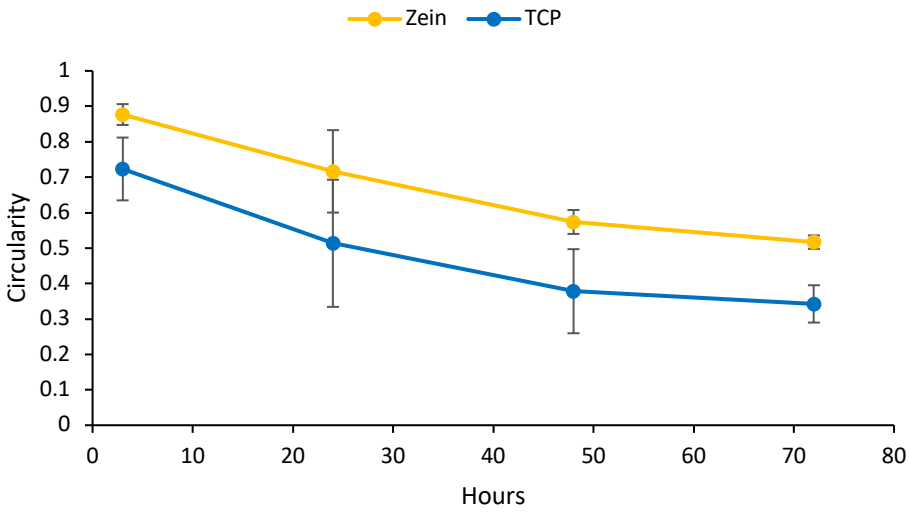

Figure 4.05 C2C12 cell morphology on Sigma-brand Zein films vs TCP, measured using image analysis software after fluorescent-staining of cells. Data represent median ± interquartile range

Cells on zein were shown to spread well over time (Figure 4.05), although the circularity of cells on zein remained above that of cells on TCP at all timepoints ($p < 0.001$). This slightly less efficient degree of spreading can perhaps be explained by an examination of the binding mechanism between cells and zein. Polystyrene is made cytocompatibile by surface

treatment, facilitating adsorption of substances contained in the serum of culture media such as fibronectin and vitronectin [251], both of which contain RGD motifs [252, 253]. These RGD motifs are well known to play a central role in facilitation of cell-binding, with the majority of known integrins having the ability to bind them [99]. However, analysis of the primary structure of zein reveals a lack of RGD motifs, or analogous integrin-target sequences [99, 136, 254]. However, it is notable that zein instead contains an abundance of glutamine residues [254]. Like zein, the 42-kD region of fibronectin has been observed to bind cells despite a lack of RGD or similar integrin-binding motifs [255], and this process is mediated by transglutaminase. The involvement of transglutaminase in cell-binding is convincingly demonstrated: it is noted [256] that osteoblast and fibroblast adhesion to type I collagen is inhibited according to the degree of reduction in transglutaminase expression, and also that the degree of cell adhesion increases in correlation with fibrinogen oligomerisation via transglutaminase [257]. Of course, transglutaminase will not interact with just any peptide containing glutamine, however the factors affecting its affinity for such peptides have been studied [258]. The inclusion of 2 adjacent glutamine residues in the primary structure, the presence of nearby polar and / or charged amino acids, and close proximity of glutamine residues to the N and / or C terminals of the peptide chain, were observed to be factors increasing the affinity of transglutaminase for a peptide [258]. Indeed, zein presents all of these attributes in its primary structure [254]. As well as single glutamine residues, multiple chains of glutamine residues (with the number of residues ranging from 2 to 4) can frequently be found. Charged and polar amino acids can often be seen nearby these repeating units of glutamine; tyrosine, serine, threonine, arginine and glutamic acid are examples thereof which can be found within 3 residues of glutamine-residue chains, and it is not uncommon to even find them adjacent to these glutamine chains [254]. Thus it may be theorised that in the absence of integrin-binding protein motifs, zein's cell-binding is facilitated by transglutaminase. The decreased cell-spreading capacity of cells seeded on zein films as opposed to those on TCP may be explained by the presence of RGD motifs on serum proteins adsorbed onto the TCP surface, as well as transglutaminase-mediated binding afforded by fibronectin [255], whereas cells adhering to zein may, in theory, be constrained to the latter mechanism alone (though adsorption of serum-proteins to zein cannot be discounted without further analysis). Furthermore, integrin-binding plays not only a mechanical role in cell spreading (i.e. providing physical anchorage for the cells), but also a physiological role: specifically, initiation of migration-mediating signalling pathways via the focal adhesion kinases associated with these integrins [259]. However, as previously mentioned, cell-spreading on zein was significantly less-pronounced at only the 24-hour mark.

As previously stated, cell-spreading is a precursor stage to the crucial stage of differentiation in cultivation of muscle tissue, as the cells fuse together to form multinucleated myotubes. The degree to which cells were able to form myotubes was the next aspect of cytocompatibility to be assayed on zein.

4.2.3 Cell differentiation on zein films

Cells were cultured to confluence in culture medium (DMEM containing 10% (v/v) FBS and 1% (v/v) P/S) and then maintained in differentiation medium (DMEM containing 2% (v/v) horse serum and 1% (v/v) P/S) for a period of 1 week. Myosin heavy chain is a notable differentiation marker in myoblasts [260], and so in order to ascertain the efficacy of myotube formation, the myotubes were stained and visualised as per chapter 2, section 2.1.2.3. In this way, not only could the myotubes' length be measured, but the number of nuclei that had become part of a myotube could be expressed as a percentage of the total cell nuclei present hereafter referred to as the fusion index. Zein films were formed on glass coverslips as per chapter 2 section 2.2.5.1, and the cells seeded thereon as per chapter 2, section 2.1.1.2. This was so that the slides could be inverted and placed face down in 6-well plates for effective visualisation. Myotubes lengths and number of nuclei were determined using "ImageJ" analysis software. The range of myotube lengths, as well as the mean myotube length, are given in figures 4.06 and 4.07, respectively. Fusion index is given in figure 4.09.

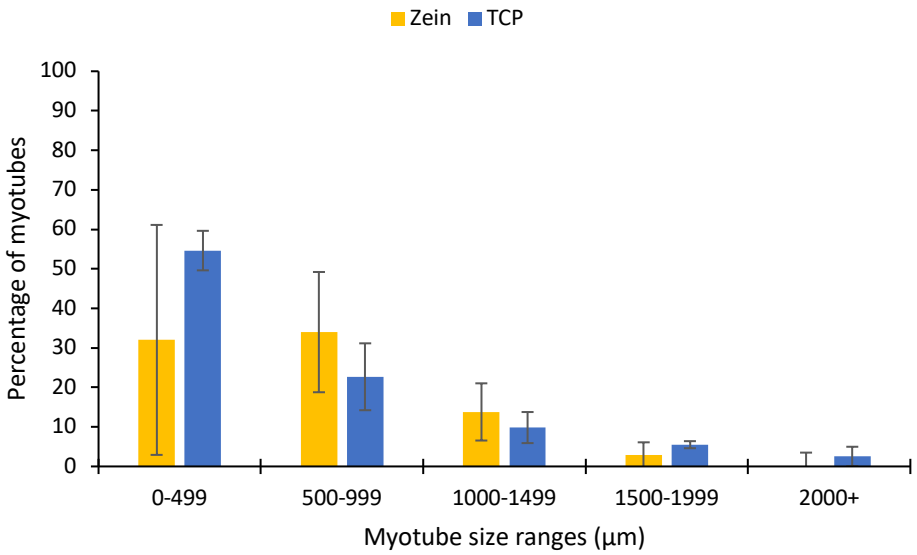

Figure 4.06 Histogram of C2C12 myotube length on zein versus TCP, calculated via image analysis software after fluorescent-staining of myotubes. Data represent median ± interquartile range.

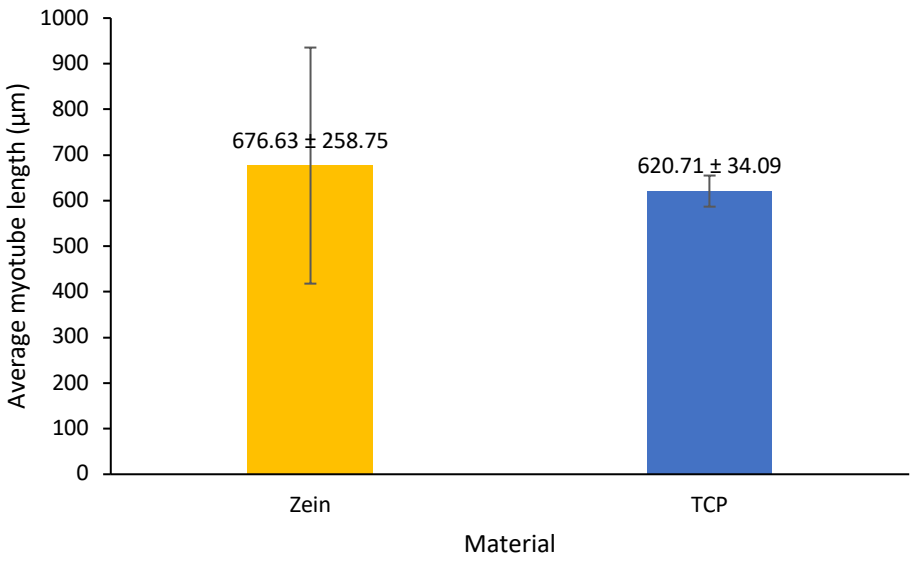

Figure 4.07 Median C2C12 myotube length on zein versus TCP, manually calculated from images of fluorescently stained myotubes via image analysis software. Data represent median ± interquartile range.

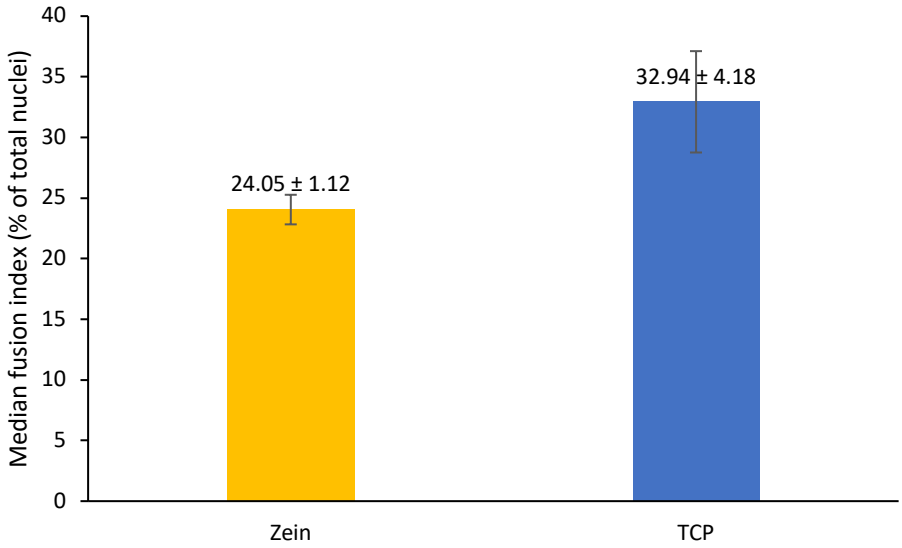

Figure 4.08 Median fusion index of C2C12 myotubes on zein versus those on TCP, manually calculated from images of fluorescently stained nuclei and myotubes via image analysis software. Data represent median ± interquartile range.

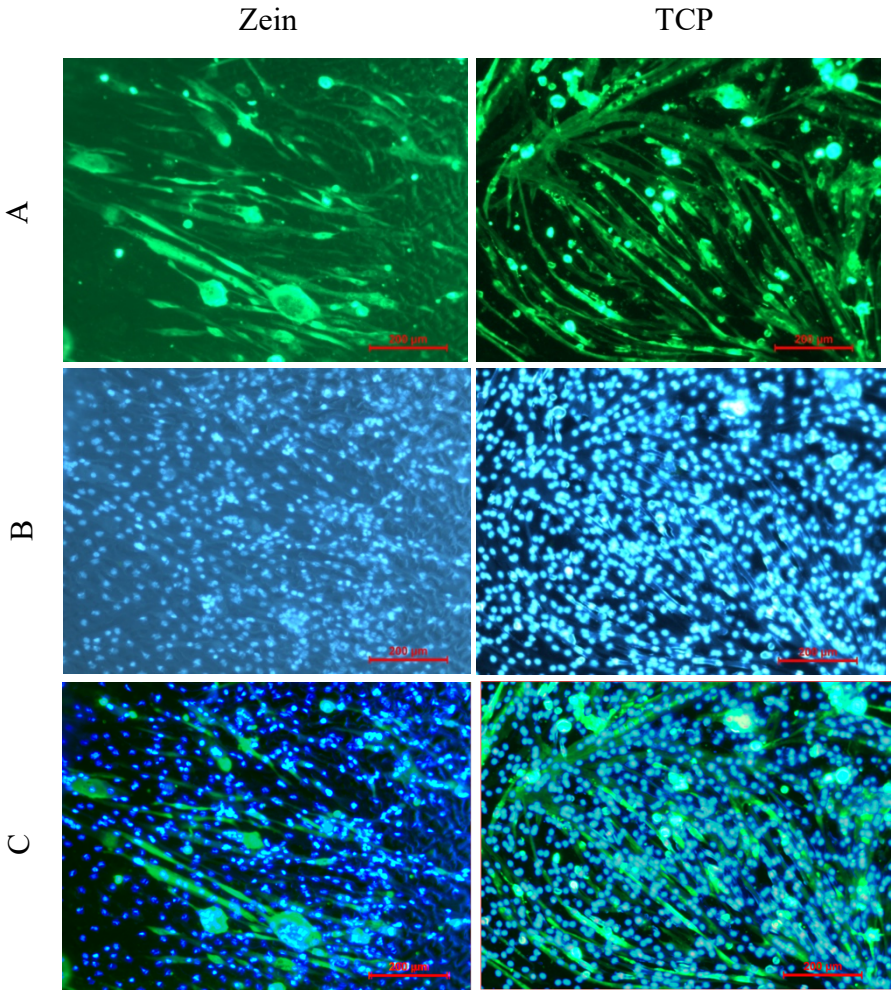

Figure 4.09: Representative images of myotubes and C2C12 cell nuclei on zein (left column) and TCP (right column) following the differentiation of C2C12 cells. A: Myotubes immunostained for myosin heavy chain, B: Hoechst-stained nuclei, C: Composite. Scale bars represent 200 µm.

The fusion index of myotubes on zein was noted to be significantly lower than that of cells on TCP ($p < 0.01$). Additionally, many signalling pathways mediating cellular proliferation and differentiation are intertwined, such as those mediated via Krüppel-like factors, which are in turn associated with ECM interactions [261, 262]. This means that if surface adhesion to the zein were in some way interfering with, or failing to initiate, signalling pathways leading to cellular differentiation, this would likely be reflected by significantly lessened cellular proliferation as well, which was not shown to be the case (figure 4.02). This is a positive result, as it suggests that myoblasts fuse on zein with an efficacy comparable to that on TCP. In all cases, the differences in the degree to which cells are able to carry out critical functions on zein versus on TCP, are not extreme. The fusion index on zein relative to that on TCP appears somewhat inconsistent with the myotube lengths on zein relative to those on TCP. Given that the cells combine their cytoplasm upon fusing, it would follow that

myotubes formed from a larger number of cells (thereby showing a higher fusion index) would also exhibit greater size. However, a large degree of variation was noted for myotube length on zein (figure 4.07). Interestingly, Jeong and Conboy noted that differentiating myoblasts exposed to liposomes of phosphatidylcholine (a component of the cell membrane) produced myotubes of greater length, but reduced fusion index [39]. Kogan *et al.* note that a very specific region of the zein protein (the N-terminal of γ-zein, which is an internal layer of the overall zein complex) is capable of binding to phosphatidylcholine liposomes [263]. As discussed in chapter 1, it has been theorised that phosphatidylserine interactions between the membranes of different myoblasts facilitates membrane fusion as myoblasts join to become myotubes [38], though the precise mechanism is unknown. Given that zein is able to interact with phosphatidylcholine liposomes [263], this may suggest that zein is able induce the same pathways which led to long-but-lesser-nucleated myotubes in the study of Jeong and Conboy where myoblasts were exposed to phosphatidylcholine liposomes [39]. Though the feasibility of this would depend on the specific mechanism by which the phosphatidylcholine liposomes interact with the cell membrane, which has yet to be ascertained.

D'andrea *et al.* in their study of myoblastic interactions with matrices of recombinant elastin-like proteins and type IV collagen, found an mean fusion index of slightly over 30% on human elastin-like polypeptide coated coverslips [264], not far above that noted on zein in figure 4.08 (24.3%). Their study also evaluated myotube length on the same coverslips and observed myotubes ranging up to 500 μm in length [264]. In comparison, myotubes formed on zein were shown to be capable of exceeding 2000 μm in length, with an mean length of 671 μm (figure 4.07).

Gribova *et al.* coated C2C12 myoblasts in layers of fibronectin – gelatin nanofilms with the aim of producing a final composite resembling the ECM, with cells dispersed throughout. Though myotubes were formed, they showed a very low fusion index of less than 2%, rising only to 10% when supplemented with a rho-kinase inhibitor (Y27) [265].

Vaz *et al.* cultured C2C12 myoblasts on cover slips coated with gelatine and fibronectin (separately) [266]. This study expressed differentiation results in terms of nuclei per myotube rather than fusion index. It was noted that myotubes cultured on fibronectin held a mean of slightly over 6 nuclei per myotube, and those on gelatine contained a mean of slightly under 4 nuclei per myotube [266]. This makes comparison difficult, but figure 4.09 appears to show a large ratio of myotubes on zein containing more than 6 nuclei per myotube.

Sotiropoulos *et al.* cultured myogenic cells on Matrigel-coated dishes in order to assay the ability of myoblasts lacking growth hormone receptor to fuse and respond to growth hormone [267]. Although, as expected, the cells lacking growth-hormone receptor (GHR) showed a lessened fusion index, all samples exhibited fusion indices over 80% [267].

Based on review of literature, it appears that relatively low fusion indices arise when cells are cultured on individual ECM proteins [264-266]. This is a highly positive result for zein, showing a capacity to support cell differentiation that is comparable to not only TCP controls (figure 4.08), but to ECM proteins. However, fusion indices that eclipse those on zein can be seen when cells are cultured on matrices of these proteins [267].

4.2.4: Mechanical properties

Stiffness has also been noted to affect the functions of adhered cells; Pelham and Wang, for example, layered type I collagen on acrylamide / bis-acrylamide blends of varying ratios, which allowed for control of stiffness without affecting the biochemical characteristics of the collagen [268]. They found that cells cultured on rigid scaffolds showed higher degrees of spreading but lessened degrees of motility [268]. The relationship between the mechanical properties of a substrate and the behaviour of myogenic progenitor cells has not gone unnoticed; it has been noted that a substrate stiffness between 13 and 45 kPa will enhance myogenic proliferation and differentiation, as well as stimulating release of growth hormones [269]. It is also noted that whilst myotube formation will occur (to varying degrees) on substrates regardless of stiffness, an elastic modulus of approximately 12 kPa is required in order for these myotubes to develop striations of contractile proteins [103].

As a scaffold's mechanical properties is thus known to have a significant effect on myogenic progenitor cells, it was decided that the mechanical properties of the zein films would be analysed. This was done via dynamic mechanical analysis as per chapter 2, section 2.2.5.2, the results of which are given in figure 4.10.

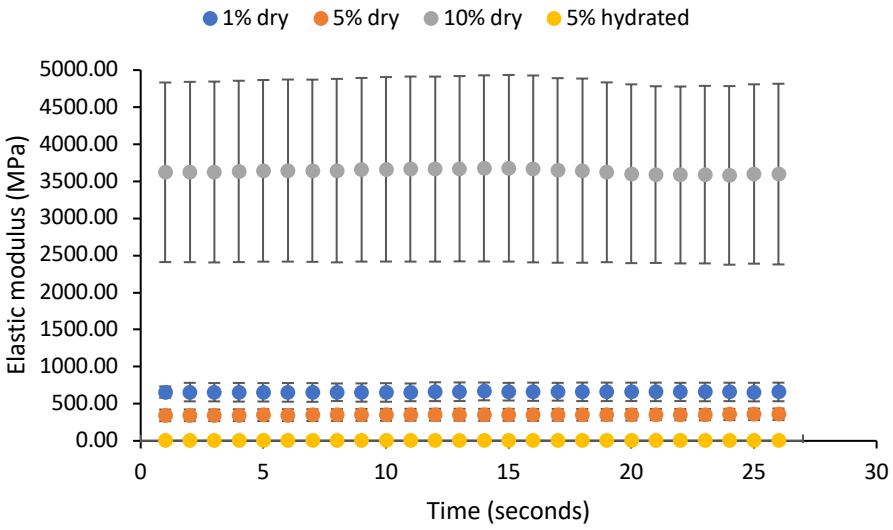

Figure 4.10: Elastic moduli of zein films, formed from solutions of varying concentration (w/v). Data represent median ± interquartile range.

There seemed to be a slight decrease in elastic modulus as zein concentration was increased from 1% to 5% (w/v) . The elastic modulus greatly increased as zein concentration increased from 5% to 10% (w/v). In all cases, the elastic modulus was well above what would be desired, that being an elastic modulus more in line with muscle tissue as noted by Griffin *et al*. [103].

The elastic modulus of 5% (w/v) zein films appeared to be substantially reduced after hydration, decreasing to values ranging between median values of 2.79 ± 2.16 MPa and 5.63 + 5.24 MPa. However, the desired stiffness was still not achieved. The elastic modulus of the hydrated zein films, like the other film samples, was recorded in the MPa range. As previously mentioned, the ideal stiffness of substrates for myogenic cell culture is noted to be approximately 12 kPa [103], and not in excess of 45 kPa [269] (which would correspond to values of 0.012 – 0.045 MPa).

These results highlight potential weaknesses of zein scaffolds. Myotubes cultured on scaffolds bearing such high elastic moduli would not develop striations [103]. As previously discussed, the induction of contractile forces in myogenic cells is beneficial to their cultivation [23]. The absence of striations, due to the excessively high stiffness of the substrate, will lessen the contractile abilities of the myotubes. Though this would not impair the cells' contractile abilities completely; smooth muscle cells retain contractile function despite a lack of striations [270]. Nevertheless, it would be beneficial if the substrate

stiffness were adjusted so as to optimise the cultivation of the skeletal muscle cells. This is discussed further in section 4.3.2.

A second potential weakness of zein highlighted by these results is the plastic deformation under a displacement amplitude of only 10 μm. Powell *et al.* formulated a regiment of stretching patterns which they applied to skeletal muscle constructs (human skeletal muscle progenitor cells encapsulated in Matrigel) [271]. After 8 days of culture, their muscle constructs were subjected to cycles of stretching and relaxation: initially being stretched by 1 mm. This was increased to 2 mm at the 10-day mark, and to 3 mm at the 12-day mark (with the endpoint of the experiment being 16 days) [271]. They noted that the application of this stretching pattern increased the area of the resultant myofibres by 40% in comparison to unstretched controls [271]. Even the lowest displacement amplitude used in the study of Powell *et al.* is 100x larger than that used here (10 μm) which already resulted in plastic deformation. Further work may seek to address this, and this is further discussed in section 4.3.2.

However, the films used in this chapter were produced for the purpose of simply investigating the interactions between myogenic cells and zein as a biomaterial. These films are not the scaffold design that would be used in bioreactors, which are commonly more suited to particulate or fibrous scaffolds [20]. Production of these more complex scaffold morphologies to be discussed in the following chapter may result in changes in the mechanical properties of the scaffold. Ghane *et al.* for example, noted in their study of polyamide-6 that electrospun mats had notably lessened elastic moduli compared to cast films [272].

4.3: Further work and wider implications

4.3.1 Surface topography

It has been noted that surface topography, nanoscale or microscale structures on a substrate surface, can influence the behaviour of surface-seeded cells [127, 273]. Attempts were made to generate data for surface roughness and tensile stiffness of zein films, however these were unsuccessful. Bumps on the surface were too pronounced and were beyond the scope of atomic force microscopy (which is used for nanoscale measurements [274]), indicating that the surface topography of the zein films was at least in the microscale range. Charest *et al.* used a hot embossing technique to create ridges, grooves, and holes on the surface of silicon wafers ranging between 5 μm and 75 μm in size [127]. They noted that C2C12 proliferation was unaffected by surface topography, but that the presence of

ridges and grooves induced cell alignment [127]. The former observation is contested in the study of Zatti *et al.* who noted that the width of micropatterned grooves on polyacrylamide hydrogels correlated to a decrease in mouse-derived myoblastic proliferation and an increase in fusion index for both mouse and human-derived myoblasts [275]. As the zein films were made by simple casting and drying, their topography would be randomly formed and lacking such micropatterned grooves, there would be no expected alignment in the surface-seeded cells, and this is indeed observable in figures 4.03 and 4.09. Jana *et al.* tested the effect of both nanoscale and microscale topography on myoblasts [273]. Similar to Charest *et al.* they noted that microgrooves on their chitosan-PCL films induced cell alignment [273]. However, they also noted a difference in cell alignment induced by microscale topography versus nanoscale topography: cells cultured on aligned nanofibers were aligned and uniformly distributed, whereas those in micropatterned surfaces formed bands of aligned cells [273].

As stated, the topography of the zein films seemed too pronounced for the resolution of atomic force microscopy. Optical profilometry may represent a more suitable technique to characterise the surface of zein films, as the resolution can accommodate microscale structures. For example, Pegg *et al.* used optical profilometry to characterise the surface roughness of their BoneMaster scaffolds, specifically to demonstrate that surface roughness was unchanged and proliferation of osteoblast-like cells was unimpaired after gold sputter-coating, which in turn demonstrates the importance of surface roughness on cytocompatibility [276].

4.3.2: Optimisation of mechanical properties

A common method by which scaffold stiffness may be adjusted is crosslinking [277] [278], however as the scaffold in this case is already excessively stiff without any degree of crosslinking, this approach would not be applicable. Another means of adjusting scaffold stiffness is cross-material blending to varying ratios; the aforementioned study of Pelham and Wang varied the ratios of acrylamide and bis-acrylamide in their scaffolds in order to manipulate the stiffness [268]. Levy-Mishali *et al*. produced composite scaffolds of PLLA and PLGA, the ratios of which were varied in order to manipulate scaffold stiffness [279]. There is scope for applying cross-material blending techniques to zein scaffolds. Alhusein *et al.* were able to produce composite scaffolds of zein and PCL [280], and Yang *et al*. were able to produce blends of zein and gelatin [137]. Incorporation of a soft material such as gelatin may serve to reduce the stiffness of the zein scaffold, though this would be contrary to the aim of producing a scaffold that is plant-based as much as possible. Another gel-based biomaterial such as carrageenan or alginate may hold potential for this application.

The use of a plasticiser may also be a potential means of lowering the stiffness of the scaffold, Lim *et al.* noted that the use of plasticisers resulted in a lowering of the elastic modulus of patented Soluplus films [281]. Plasticisers are not inherently toxic or edible; Sothornvit and Krotcha note that a variety of plasticisers are used in edible film coatings, including sucrose and polyethylene glycol [282], the latter of which was one of the plasticisers employed in the aforementioned study of Lim *et al*. [281].

4.3.3: Potential for serum-free cell culture

Unlike polysaccharide-based biomaterials such as chitosan [64, 65, 185], zein may not have the need to adsorb serum-proteins in order to associate with cells. The field of cultured meat's reliance on animal-derived serum proteins such as FBS, is a notable issue. With this in mind, Kolkmann *et al.* analysed the ability of primary bovine myoblasts to proliferate on diluted Matrigel in the presence of various serum-free media formulations [115]. They noted a lack of myoblastic proliferation when in the presence of DMEM only and that no formula was able to produce cell numbers comparable to those cultured in the presence of growth media, however there was a noted increase in cell number over a period of 6 days for many of the formulae: particularly FBM, Essential8, and TeSR-E8 [115]. They also noted that the lack of serum did not impair the ability of the cells to spread [115]. Given zein's ability to support myoblastic cell functions to a degree comparable to that on TCP, it would be a worthwhile course of investigation to first determine whether zein adsorbs serum proteins and, if so, quantify the degree to which this occurs and assess whether zein can support cell growth in serum-free conditions.

4.4 Concluding remarks

Zein was able to support the proliferation, spreading, and differentiation of myoblasts to a degree comparable to TCP. Zein also appeared to support cell proliferation to a greater degree than silk fibroin (chapter 3, figure 3.21), and this apparent superiority to silk fibroin is especially notable since, like silk fibroin, zein lacks RGD motifs with which to bind cells, and may instead rely on its abundance of glutamine residues in order to facilitate cell adhesion [254]. Nonetheless, zein also appears to compare well to the gold-standard ECM proteins used in literature for the culture of myogenic cells. This is an encouraging result, especially given zein's plant-based nature (as the gold-standard biomaterials used in tissue engineering are commonly animal-derived, as previously discussed). The strengths of zein as a biomaterial for tissue engineering lie in its renewability, ease of processing, and inherent biocompatibility. A clear weakness of zein is its mechanical properties, it is far more stiff than an ideal substrate for cell growth would be, and the threshold for plastic

deformation rather than elastic in hydrated zein films is very low. As discussed however, there is scope for optimisation of zein's mechanical properties,

Of course, a biomaterial film is not compatible with commonly used designs of bioreactors. This may be a potential weakness of zein compared to carrageenan, as the techniques by which more complex scaffolds (such as nanofibre matrices) are produced are more complicated than those for carrageenan (gelation through ionic crosslinking). Methods by which these more complex zein scaffolds may be produced are explored further in chapter 5.

Chapter 5 – Production of Fibrous and Particulate Protein-based Scaffolds

5.1: Introduction:

As stated in Chapter 4, a film on which myoblasts will proliferate, spread, and differentiate is not sufficient for the purposes of producing muscle tissue.. For this purpose, scaffolds must be produced which can be integrated with bioreactor designs. For example, rotating wall vessels and fluidised bed reactors are well-suited to particulate scaffolds [20, 30]. There are also bioreactor designs specifically catered to hollow-fibre membrane scaffolds [10, 27], and electrospun fibre matrices may be suited to the fixed-bed bioreactor design [29]. This chapter explores methods by which fibrous and particulate scaffolds can be produced from protein-based biomaterials whose cytocompatibility has been analysed in previous chapters, with particular emphasis on zein.

5.1.1 The use of fibrous and particulate zein scaffolds

Fibrous and particulate zein structures have been produced in literature, though their potential as scaffolds for cell culture has not gone unnoticed, their common application appears to be toward drug encapsulation and delivery.

With regard to particles, Lau *et al.* produced prednisolone-loaded zein microparticles via phase separation, resulting in particles ranging from just under 400 nm to just over 15 μm in diameter (though approximately half of the particles exhibited diameters of less than 1 μm [283]). They also produced hydrocortisone or mesalazine-loaded zein microspheres via coacervation, which showed diameters in excess of 1 μm but below 13 μm [284]. Jin *et al.* utilised spray-drying to produce lysozyme-loaded zein particles [285], and Farris *et al.* used zein to encapsulate complexes of chitosan and DNA, for use in oral delivery of DNA therapeutics [286]. However, these particles are too small to be used as microcarriers (supporting surface-seeded cells): there is no definitive threshold as to what size of particle constitutes a viable microcarrier, but it is generally estimated to be a minimum of 100 μm [287, 288].

With regard to fibres, Aytac *et al.* produced electrospun zein fibres loaded with thymol and cyclodextrin antibiotics [289], as well as complexes of quercetin and gamma-cyclodextrin [290]. Kayaci and Uyar also encapsulated cyclodextrin within their electrospun zein fibres,

specifically alpha, beta, and gamma-cyclodextrin [291]. Jiang and Yang used citric-acid to crosslink their electrospun zein fibres, which they used to encapsulate diclofenac to a loading efficiency of 58% [292]. Of particular note, Alhusein *et al.* produced electrospun zein fibres, as well as fibres of zein / PCL blends, to encapsulate tetracycline antibiotic (which was contained within the core of a three-layer fibre structure) [293], it was further demonstrated that the release of this tetracycline could not only kill various lines of staphylococcus aureus, but also supported the growth of FEK4 fibroblasts [280].

As stated, the potential of zein scaffolds as substrates for cell growth has been documented. Zein scaffolds have been applied, for example, to the culture of human periodontal stem cells [137], mouse mesenchymal stem cells [138], and human H1299 lung cancer cells [139]. Studies concerning the compatibility of zein scaffolds with myogenic cells appear sparse, however. Therefore this chapter explores methods of producing zein scaffolds, and analysing their potential for use in myogenic cell culture.

5.1.2 Production of fibrous scaffolds

The wet-spinning of hydrogel fibres as seen in chapter 3 involved the extrusion of the polymer solution into a crosslinker bath, which induced gelation and thus formed fibrous hydrogels. It is possible to wet-spin fibres without the prerequisite that they will form hydrogels or even that the coagulation bath be a crosslinker solution; in this case, fibre formation relies on interactions between the solvent in which the polymer is dissolved, and a second solution which is a non-solvent with regard to the polymer, but miscible with the polymer solvent [14, 294]. As the solvent dissolves into the larger volume of non-solvent into which the polymer solution is extruded, the polymer coagulates into fibres [294]. Fibres produced in this manner are fairly large, with wet-spun hollow fibres produced by Meneghello *et al.* for example, exhibiting diameters of many hundreds of micrometers [84]. This large surface area gives them the strength of being able to support a highly dense population of cells.

Nanoscale fibres, though not exhibiting anything close to the surface area of wet-spun fibres, have the advantage of replicating the nanofibrous nature of the ECM [11]. Electrospinning is a technique which relies on electrostatic forces to generate nanofibres from polymer solutions. In this design, a concentrated polymer solution is subjected to high voltage during extrusion [13, 14]. When this electric field is of sufficient strength to overcome the surface tension of the droplet at the spinneret tip, the polymer solution erupts and is stretched into

an ultrathin fibre [13, 14]. The solvent evaporates as the fibre is drawn to a nearby, grounded collector plate [13, 14].

5.1.3 Production of particulate scaffolds

As stated in chapter 1, particulate scaffolds have the advantage of being applicable to a wide range of dynamic culture systems [19, 20], as well as affording the ability to add particles to the culture system as cell populations grow [16].

Emulsification precipitation involves the mixing of two immiscible solutions: a polymer solution and a second (commonly hydrophobic) solution [17]. The mixture is then subjected to mechanical sheer, which causes the polymer to emulsify as microscopic droplets suspended in the hydrophobic phase, which can then be crosslinked or precipitated into solid microspheres, and filtered out of the mixture [17]. Whilst this approach has the benefit of enabling large-scale production of particles in a relatively short timeframe, it has been noted to offer a less-than-ideal degree of control over size distribution over the resultant particles [295].

In contrast, microfluidic flow focusing offers a higher degree of control over the size distribution of particle, but does not afford large-scale production of particles [17]. Microfluidic flow focusing also operates using two immiscible solutions, one of which is the polymer solution [18]. A continuous phase solution of non-solvent is pumped through a T-shaped flow channel, and out of the exit aperture (see section 1.2.1.3). The polymer solution is then pumped in, at a slower flow rate. When the two solutions meet, the disperse phase is isolated as spherical droplets within the continuous phase due to the mechanical sheer exerted upon the former by the latter [17].

Different authors approximate a differing range for ideal cell microcarrier diameter, Yang *et al.* postulate that microcarriers are classified by an approximate diameter of 150 – 200 μm [287], whereas Malda and Frondoza suggest that microcarriers are typically found bearing diameters in the range of 100 – 400 μm [288]. With particular regard to myogenic cell culture, Verbruggen *et al.* analysed myoblast compatibility with three commercially available types of microcarrier [16]. Particularly, they noted that Cytodex 1 (composed of crosslinked dextran and exhibiting a mean diameter of 190 μm), supported proliferation and differentiation of primary bovine myoblasts [16]. They also noted a superior degree of cell attachment on Cellbind and Synthemax II microcarriers, whose diameters were stated to be in the range of 125 – 212 μm, compared to that on the Cytodex microcarriers [16]. Molnar

et al. also report successful culture of satellite cells on Cytodex 3 and Biosilon microcarriers, whose diameter ranges are given as 133 – 215 μm and 160 – 300 μm, respectively [85].

5.1.4 Aims and objectives

This chapter aims to identify a simple method by which fibrous and / or particulate scaffolds may be produced using zein, with potential application to bioreactor designs, and to analyse compatibility of such scaffold morphologies with myogenic cells. Specifically, the ability of myogenic cells to proliferate and differentiate into myotubes.

5.2 Results and discussion

Particulate scaffolds seem easily applicable to a variety of bioreactor designs. As such, development of zein into a particulate scaffold may be the ideal avenue with regard to large-scale production of cultured meat.

5.2.1 Microfluidic flow focusing

The use of microfluidic flow focusing to produce zein particles is not unprecedented; examples include Feng *et al.* who used a disperse phase of zein in aqueous ethanol and a continuous phase of distilled water, resulting in particles with diameters in the low nanoscale range [296]. Feng and Lee also used a disperse phase of zein in aqueous ethanol, but using a continuous phase of soy lecithin, which resulted in nanoparticles as well as microparticles [297]. Man *et al.* [295] are examples of studies which have used the microfluidic flow-focusing technique to produce zein particles. Microfluidic flow focussing, as described in chapter 2, section 2.2.5.3, was therefore employed to produce zein particles. The results of the first attempt, in which the flow rate ratio was $Q_o = Q_i \times 20$, are shown in figure 5.01.

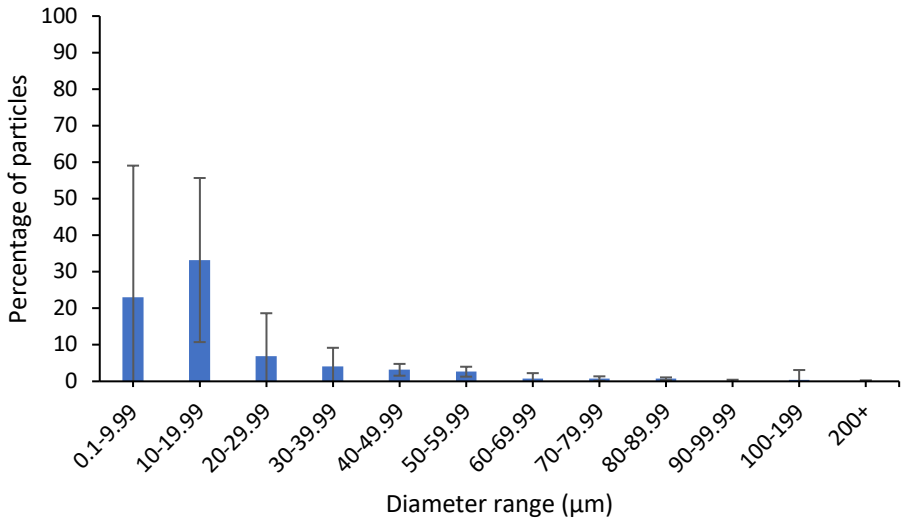

Figure 5.01 Zein particles produced by microfluidic flow focusing. Concentration of the zein solution was 5% (w/v), in 70% (v/v) aqueous ethanol, and the flow rate of the continuous phase relative to the disperse phase was $Q_o = Q_i \times 20$, where Q_o represents the flow rate of the continuous phase, and Q_i represents a disperse phase flow rate of 0.05 ml / min. Data represent median ± interquartile range.

The overwhelming majority of particles produced in this initial attempt (figure 5.01) were too small to accommodate surface-seeded cells; the aim of the experiment was to produce zein microcarriers consistently around 200 µm in diameter, or at least above 100 µm. The size distribution also appears to be quite wide, with particles ranging in diameter from less than a micrometre to over 200 micrometres, though the overwhelming majority are below 50 µm in diameter. As previously mentioned, it is known that particle size is generally inversely proportional to flow rate [89], and so the next series of attempts to generate zein microparticles varied the flow rate (as described in chapter 2, section 2.2.5.3) of the continuous phase in order to ascertain the effect on resultant particle size, as it has been shown that higher continuous phase flow rates result in smaller particles, due to greater shear forces exerted on the incoming disperse phase [89]. The results are shown in figures 5.02 – 5.04.

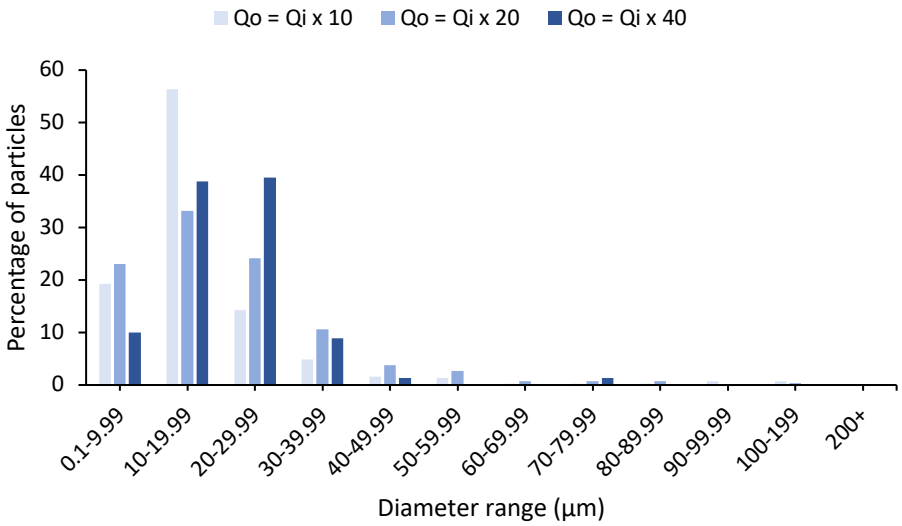

Figure 5.02 Zein microparticles produced by microfluidic flow focusing at various flow rate ratios where Q_i represents a disperse phase flow rate of 0.05 ml / min. Concentration of the zein solution was 5% (w/v) in 70% (v/v) aqueous ethanol. Data represent individual observations.

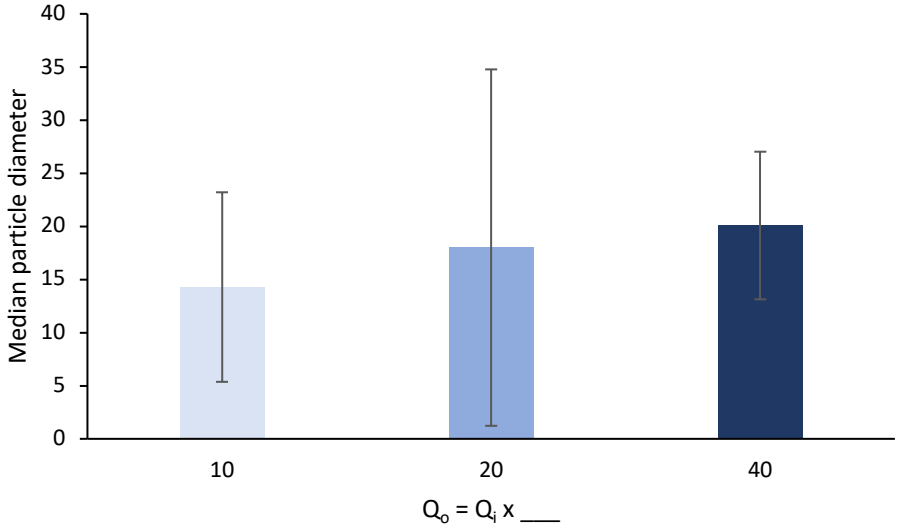

Figure 5.03 Median particle diameter of zein microparticles produced by microfluidic flow focusing. Flow rate of the continuous phase relative to the disperse phase was varied; Q_i represents a disperse phase flow rate of 0.05 ml / min. Zein solution had a concentration of 5% (w/v) in all cases, in 70% (v/v) aqueous ethanol. Data represent median ± interquartile range.

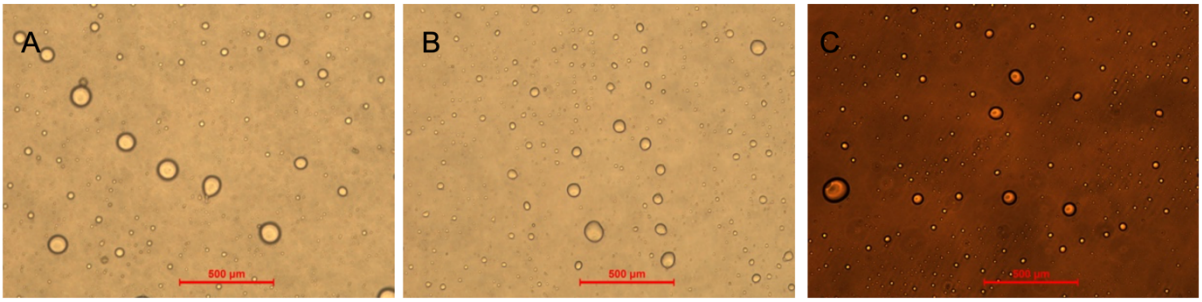

Figure 5.04 Representative images of zein microparticles produced via microfluidic flow focusing with varying flow rates. A: $Q_o = Q_i$ x 10, B: $Q_o = Q_i$ x 20, C: $Q_o = Q_i$ x 40 where Q_i represents a disperse phase flow rate of 0.05 ml / min. Zein solution had a concentration of 5% (w/v), in 70% (v/v) aqueous ethanol. Scale bars represent 500 µm.

All images were captured under white light microscopy, however for unknown reasons the brightness for those representing a flow rate of $Q_o = Q_i$ x 40 was reduced and could not be corrected. However, the particles remain clearly visible. Again, particles were far too small to accommodate surface-seeded cells (figures 5.02 – 5.04), and again, curiously, varying the flow rate did not appear to impact the size of the resultant particles. The next attempt focussed on the percentage concentration (w/v) of the zein solution as the independent variable, since this is noted to be a determining factor in the size of resultant particles [296]. The results of this variance are given in figures 5.05 – 5.07.

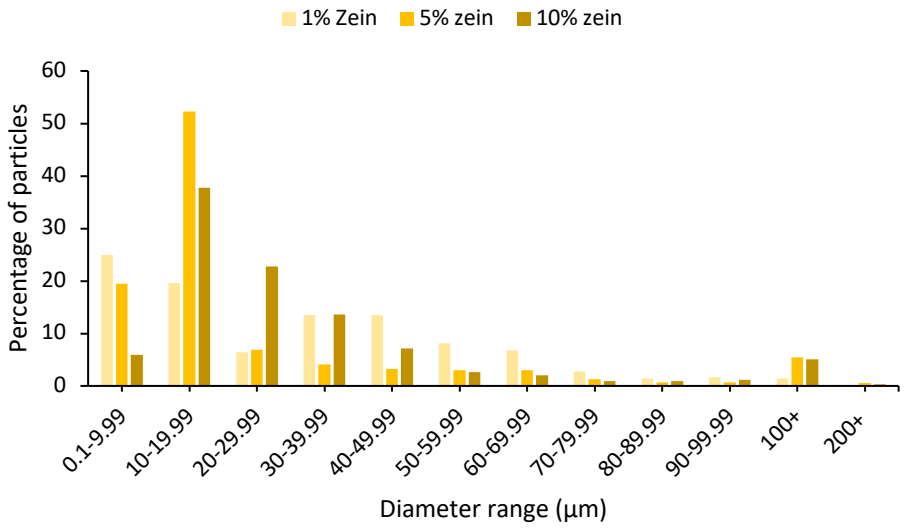

Figure 5.05 Size distribution of microparticles produced via microfluidic flow focusing, $Q_o = Q_i$ x 20 where Q_i represents a disperse phase flow rate of 0.05 ml / min, concentration (% w/v) of the zein solution was varied. Data represent individual observations.

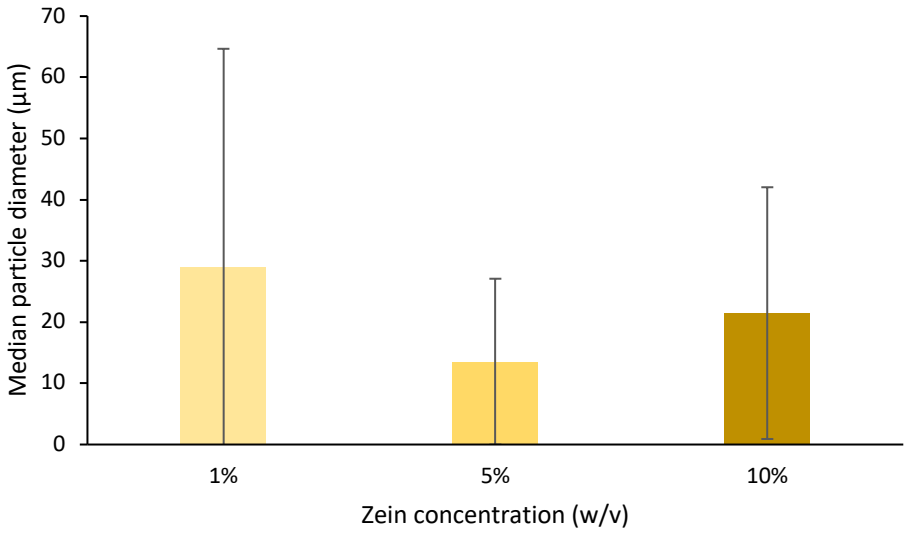

Figure 5.06 Median particle diameter microparticles produced via microfluidic flow focusing, $Q_o = Q_i$ x 20 where Q_i represents a disperse phase flow rate of 0.05 ml / min. Concentration (% w/v) of the zein solution was varied. Data represent median ± interquartile range.

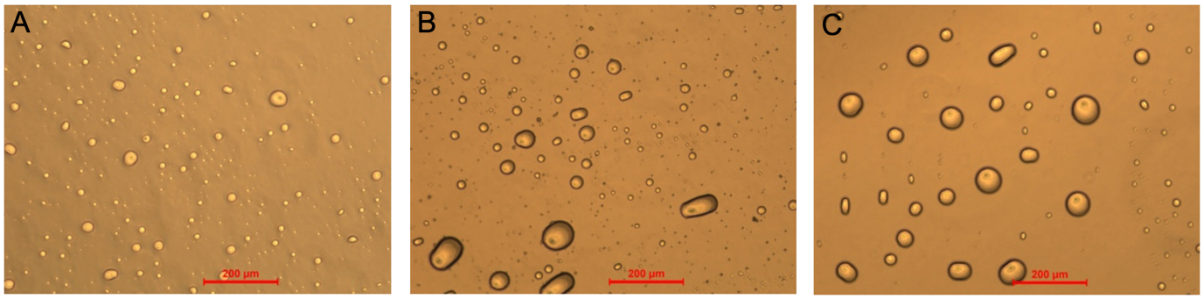

Figure 5.07 Representative images of zein microparticles produced via microfluidic flow focusing. $Q_o = Q_i$ x 20 where Q_i represents a disperse phase flow rate of 0.05 ml / min. Concentration (% w/v) was varied. A: 1%, B: 5%, C: 10%. Scale bars represent 200 µm.

As before, the overwhelming majority of particles lacked sufficient size for cell culture applications (figures 5.05 – 5.07).

It was speculated that further exploration of the continuous phase composition may serve to substantially increase the size of particles. However, other studies using microfluidic flow focusing have also explored such parameters (even using water, zein's most commonly noted non-solvent) as the continuous phase, and the resultant particles are generally found with diameters in the nanoscale range [295-297]. Zein particles produced by Feng *et al.* exhibited diameters of less than 300 nm under all conditions [296], those of Feng and Lee provide images that show particles whose diameters enter the micrometre scale, but still lack the necessary size for cell culture [297], and the zein particles of Man *et al.* held

diameters exclusively in the nanoscale range [295]. Hence, microfluidic flow focusing may not be a technique by which zein microparticles of sufficient size as to support cell attachment can be easily produced, though it may have potential with regard to drug delivery and therapeutic applications. Thus attention was turned to other means by which microparticles can be generated.

5.2.2 Emulsification precipitation

As microfluidic flow focusing failed to produce particles of sufficient size, attention turned to the emulsification precipitation technique. As it is noted that this technique can produce particles with a large size distribution [17], it was hoped that those at the upper end would exhibit sufficient size for cells to adhere to their surfaces. Zein particles were therefore produced by emulsification precipitation as per chapter 2, section 2.2.5.4. The results are shown in figures 5.08 and 5.10.

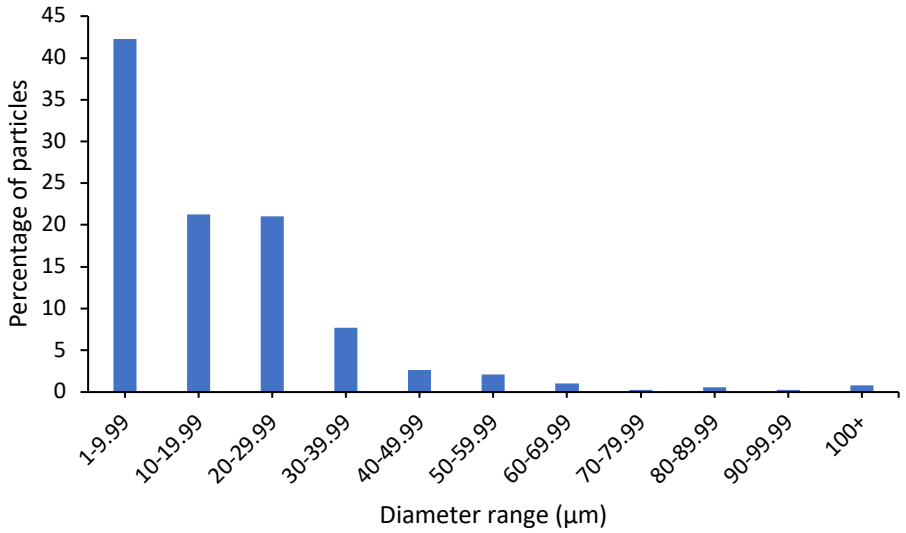

Figure 5.08 Size distribution of zein microparticles generated via emulsification precipitation with a stirring speed of 600 rpm. The zein solution was composed of 3% (w/v) zein in 70% (v/v) aqueous ethanol. The non-solvent phase was composed of vegetable oil and span 80 surfactant. Data represent individual observations.

Again, particles were not of sufficient size. It was decided that mixing speeds would be reduced (as described in chapter 2, section 2.2.5.4), in order to lessen shear stress and increase the size of the resultant droplets.. The results are shown in figures 5.09 and 5.10.

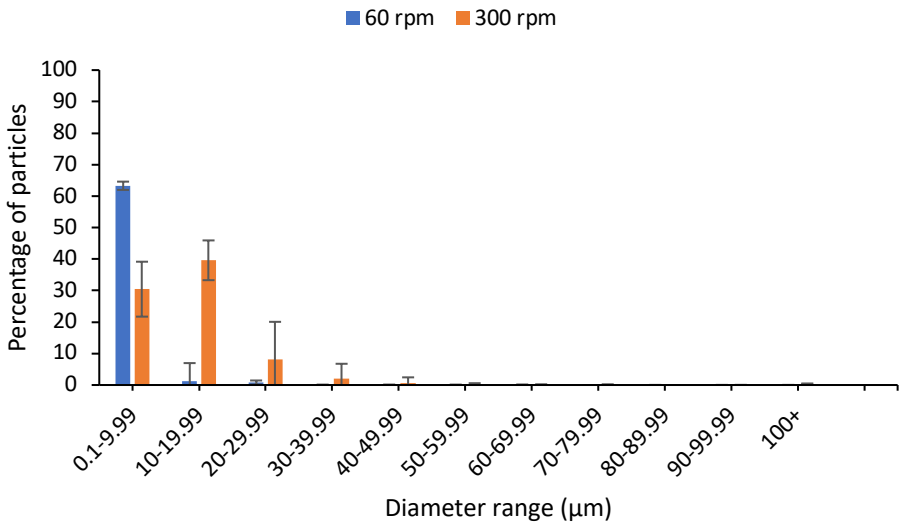

Figure 5.09 Size distribution of zein microspheres generated using slower stirring speeds. The zein solution was composed of 3% (w/v) zein in 70% (v/v) aqueous ethanol. The non-solvent phase was composed of vegetable oil and span 80 surfactant. Data represent median ± interquartile range.

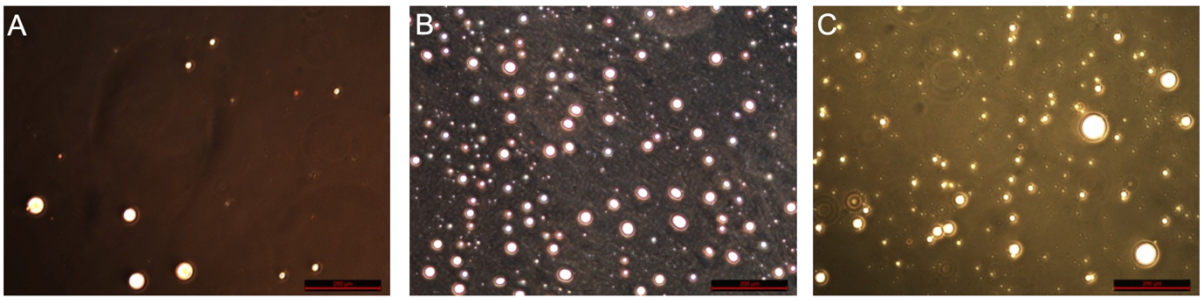

Figure 5.10 Representative images of zein microspheres produced by emulsification precipitation using A: 60 rpm B: 300 rpm, and C: Original stirring speed (600 rpm). The zein solution was composed of 3% (w/v) zein in 70% (v/v) aqueous ethanol. The non-solvent phase was composed of vegetable oil and span 80 surfactant. Scale bars represent 200 µm.

Strangely, the slower stirring speeds appear to have resulted in smaller particles. Speeds of 600 rpm produced microscale particles only (figure 5.08), whereas lower speeds produced some nanoscale particles (figure 5.09). Not only this, but a higher percentage of particles in the lowest size bracket was observed for the slowest stirring speed (figure 5.09). The mean diameters of particles were compared in order to determine whether this trend was significant or the result of random chance, the results of this comparison are presented in figure 5.11.

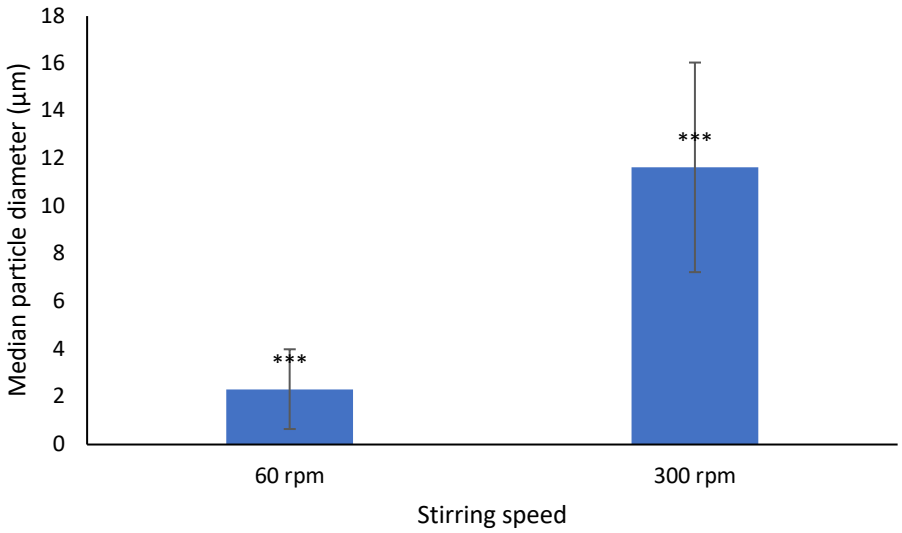

Figure 5.11 Comparison of median microsphere diameter produced using emulsification precipitation with reduced stirring speeds. Data represent median ± interquartile range. ***p < 0.001.

The difference between size distributions of zein particles obtained by emulsification of varying mixing speeds was determined to be of statistical significance ($p < 0.001$). This is an unexpected result, as the technique relies on the generation of sheer forces, which are smaller as stirring speeds are reduced, which should result in larger particles. This may, as in the case of microfluidic flow focussing, be evidence that the non-solvent used (vegetable oil) is not appropriate for the disperse phase. It is also notable that, in the case of microfluidic flow focusing, the size distributions of particles produced using specific flow rates are far from uniform; an extremely high degree of standard error is observable in figure 5.01. Furthermore, variance of the production parameters (flow rate or zein concentration) yielded little difference in the size distributions of the resultant particles (figures 5.03 and 5.06). Most importantly, all microfluidic flow focusing experiments failed to consistently generate a reasonable amount of adequately sized particles. In all cases, the majority of microspheres were below 50 µm in diameter. Since efforts to generate adequately sized zein microparticles were consistently unsuccessful, focus was geared toward the production of fibrous scaffolds instead.

5.2.3 Production of wet-spun zein fibres

As stated in section 5.1, this wet-spinning technique is distinct from that seen in chapter 3 in that this technique relied on the principles of phase inversion commonly exploited to facilitate membrane precipitation, wherein the exchange between the solvent of a polymer solution and a non-solvent results in precipitation of the polymer [298].

Koops *et al.* were able to produce hollow, wet-spun fibre membranes of polyethersuphone and polysulphone by exploiting phase inversion when the polymer solution was extruded into a non-solvent coagulation bath [299]. The fibres (of a few hundred μm in diameter) were made hollow by the extrusion of a bore liquid in the centre of the fibre, and this necessitated their 6-orifice spinneret [299]. Phase inversion wet-spun fibres have been produced without multi-channel spinnerets: Yao *et al.* produced hollow fibre membranes by extruding a polysulfone solution into a water bath [300]. In this instance, the fibres were made hollow by including paraffin oil in the polymer solution, which formed a channel at the centre of the fibre and was subsequently removed by ethanol-treatment [300].

Attempts were made to produce solid (non-hollow) zein fibres, via wet-spinning, which could accommodate surface-seeded cells, as described in chapter 2, section 2.2.5.5. If the procedure were successful, it may be further developed to produce hollow-fibres. Photographs of the results are shown in figures 5.12 – 5.19.

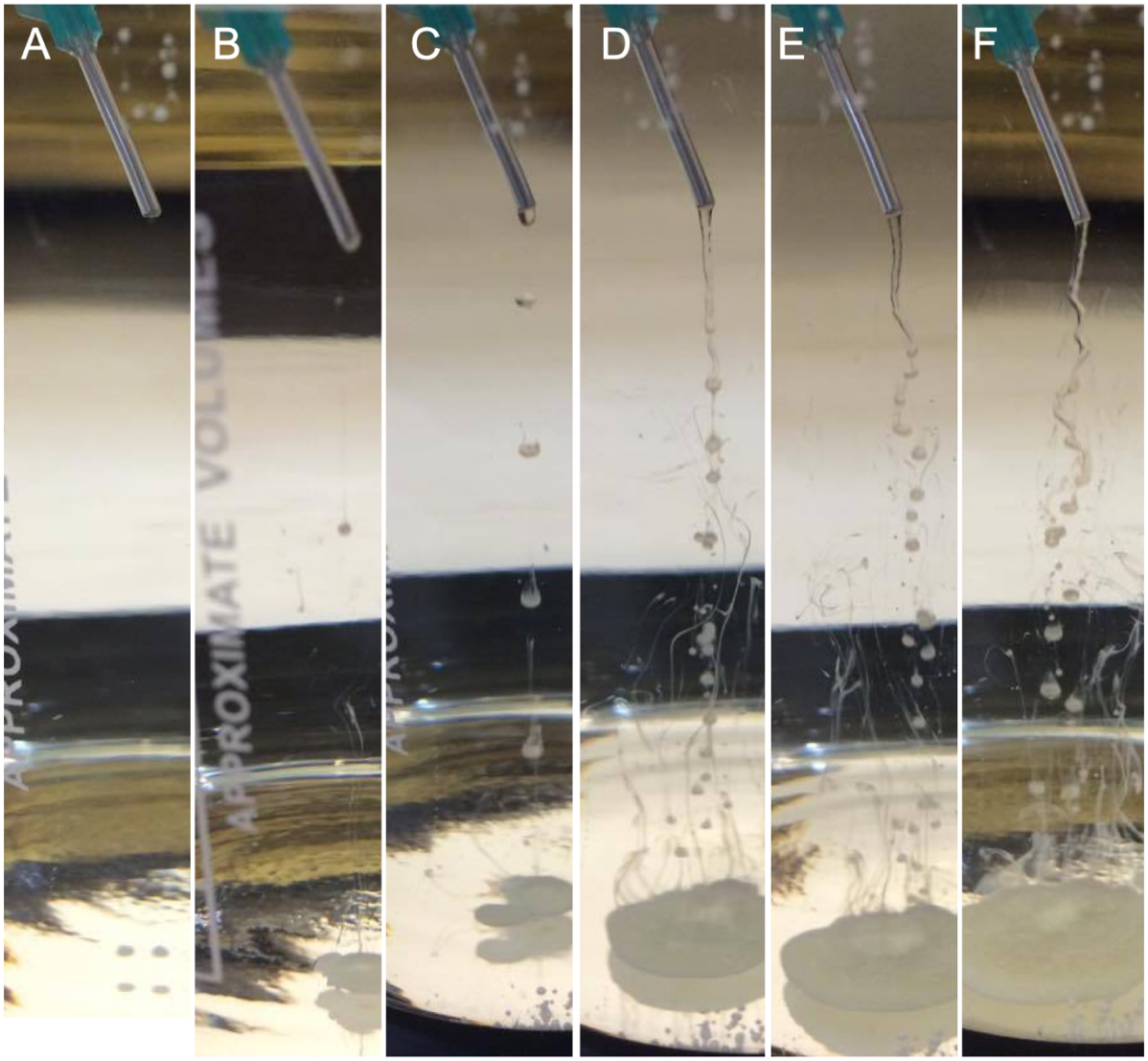

Figure 5.12 Photographs of wet-spinning zein attempts. Using 1% (w/v) zein in 50:50 (v/v) chloroform-methanol, and an 18 gauge needle. Flow rates were A: 1 ml / hr, B: 10 ml / hr, C: 20 ml / hr, D: 30 ml / hr, E: 40 ml / hr, F: 50 ml / hr.

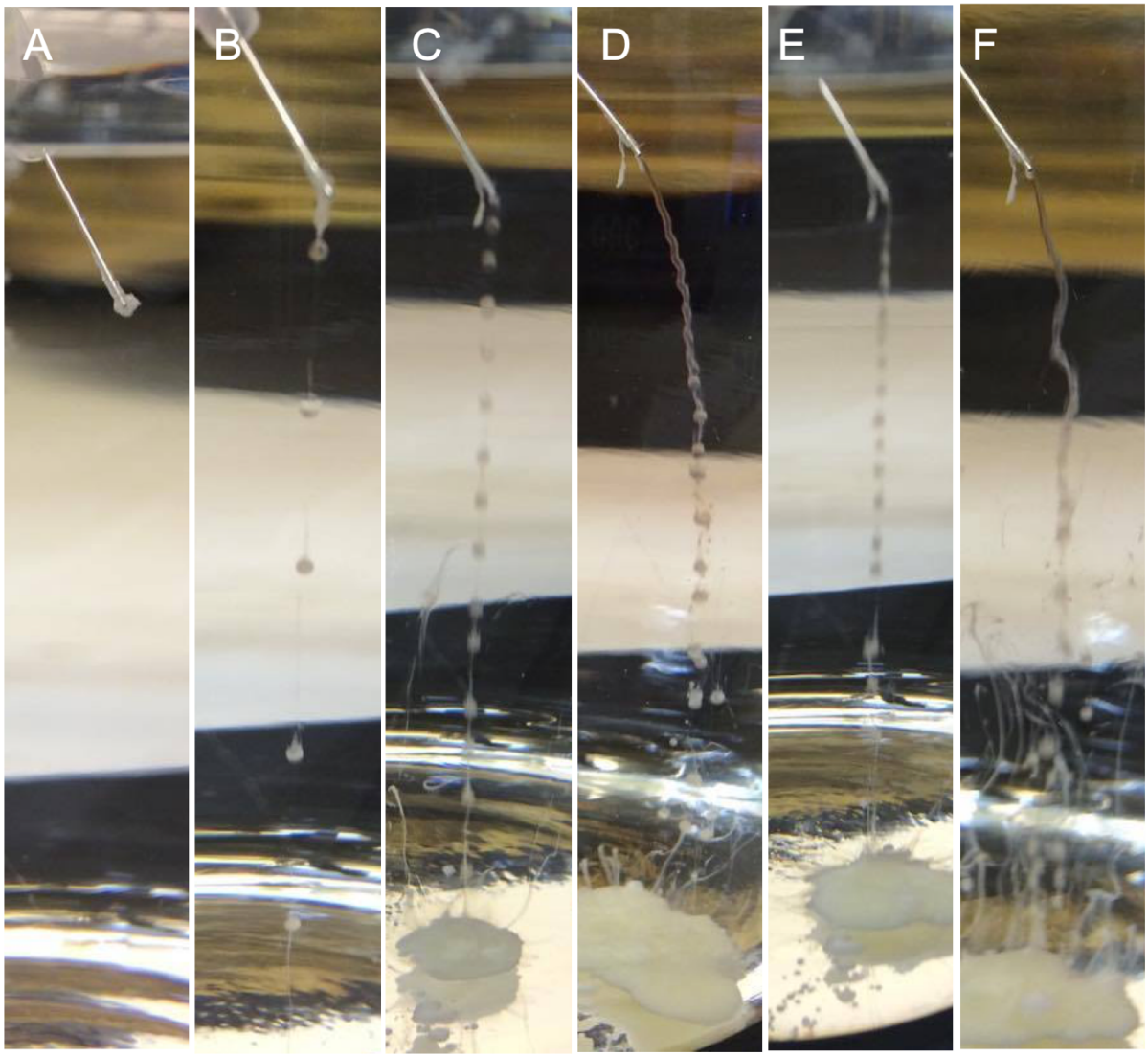

Figure 5.13 Photographs of wet-spinning zein attempts. Using 1% zein (w/v) in 50:50 (v/v) chloroform-methanol, and a 27 gauge needle. Flow rates were A: 1 ml / hr, B: 10 ml / hr, C: 20 ml / hr, D: 30 ml / hr, E: 40 ml / hr, F: 50 ml / hr.

These initial conditions (figures 5.12 and 5.13) failed to produce a sustained jet of zein solution from which a fibre might precipitate. Rather, the zein solution emerged from the needle as a series of droplets. It was theorised that precipitation of the droplet at the needle's edge caused a localised increase in density of zein, which caused a bead-like structure of partially precipitated zein to fall away from the solution stream. As this occurred at all flow rates, the concentration of the zein solution was increased so as to slow this precipitation enough to allow for a sustained stream of zein solution.

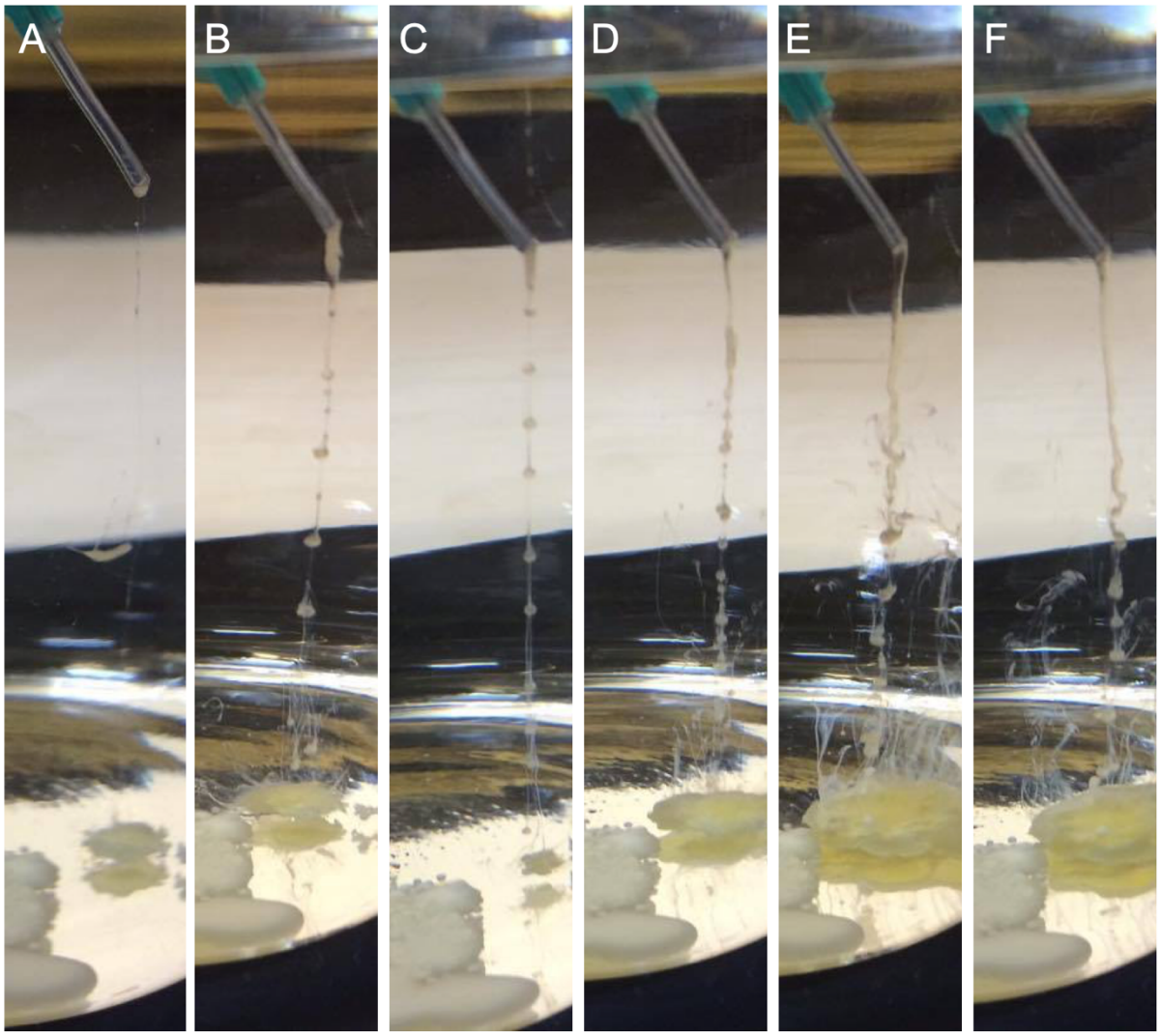

Figure 5.14 Photographs of wet-spinning zein attempts. Using 5% zein (w/v) in 50:50 (v/v) chloroform-methanol, and an 18 gauge needle. Flow rates were A: 1 ml / hr, B: 10 ml / hr, C: 20 ml / hr, D: 30 ml / hr, E: 40 ml / hr, F: 50 ml / hr.

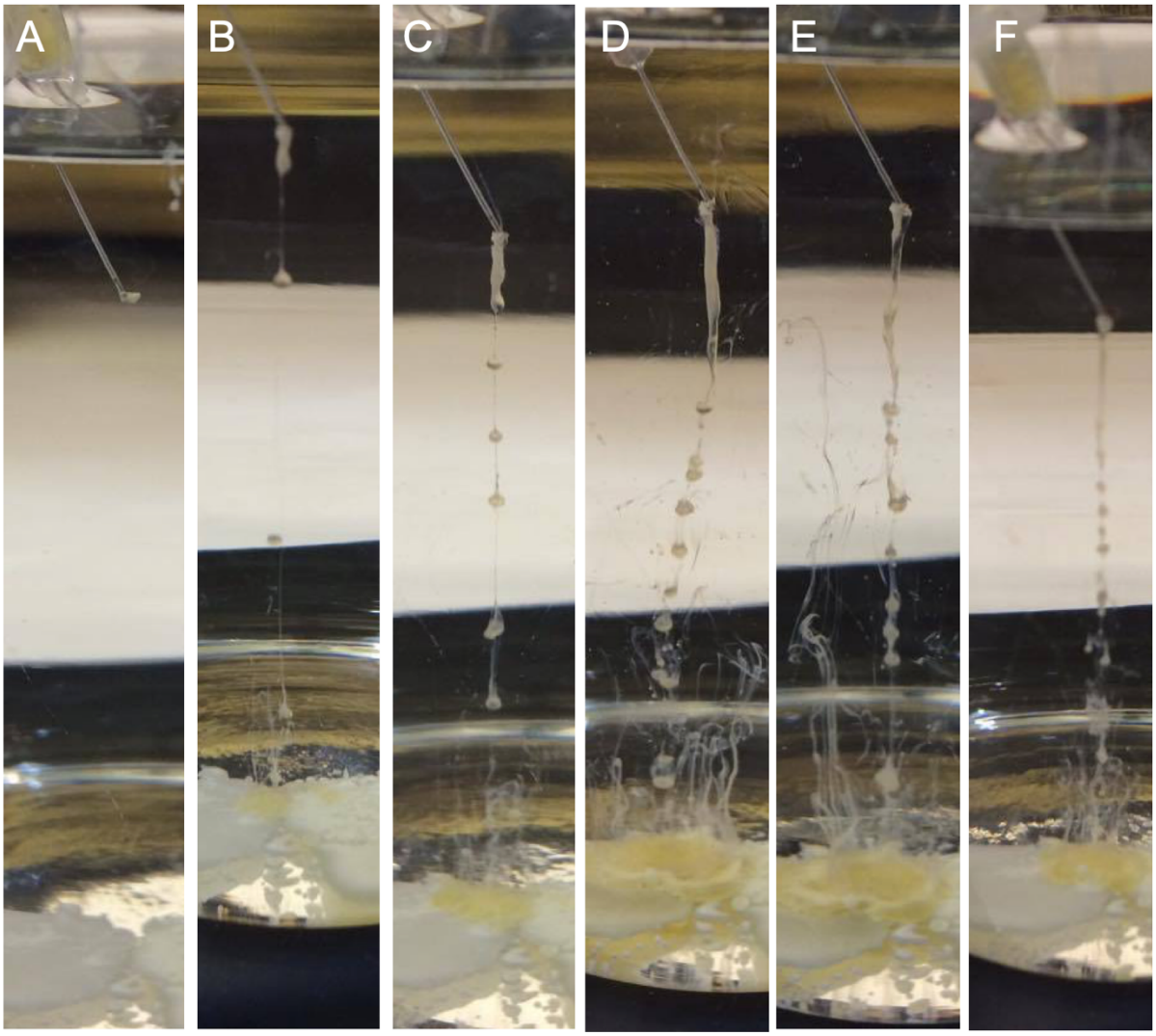

Figure 5.15 Photographs of wet-spinning zein attempts. Using 5% (w/v) zein in 50:50 (v/v) chloroform-methanol, and a 27 gauge needle. Flow rates were A: 1 ml / hr, B: 10 ml / hr, C: 20 ml / hr, D: 30 ml / hr, E: 40 ml / hr, F: 50 ml / hr.

Increasing the concentration of the zein solution to 5% (w/v) appears to have improved results, in that there is the appearance of a sustained stream of zein solution at high flow rates (figures 5.18 and 5.19). However, this stream did not maintain its integrity for long enough and again separated into droplets. Concentration of zein solution was increased further to 10% w/v (figures 5.16 and 5.17) and 15% w/v (figures 5.18 and 5.19).

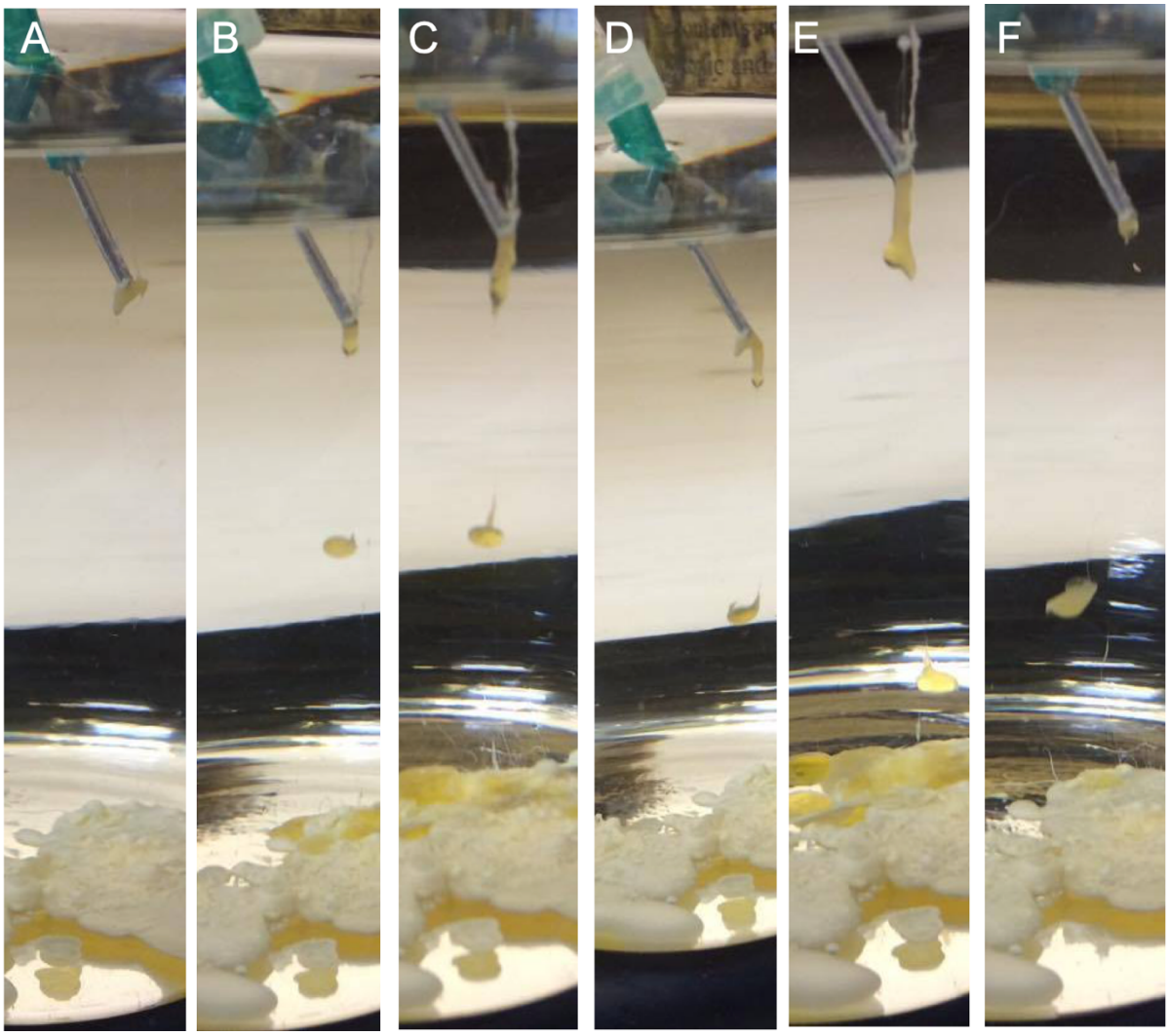

Figure 5.16 Photographs of wet-spinning zein attempts. Using 10% (w/v) zein in 50:50 (v/v) chloroform-methanol, and an 18 gauge needle. Flow rates were A: 1 ml / hr, B: 10 ml / hr, C: 20 ml / hr, D: 30 ml / hr, E: 40 ml / hr, F: 50 ml / hr.

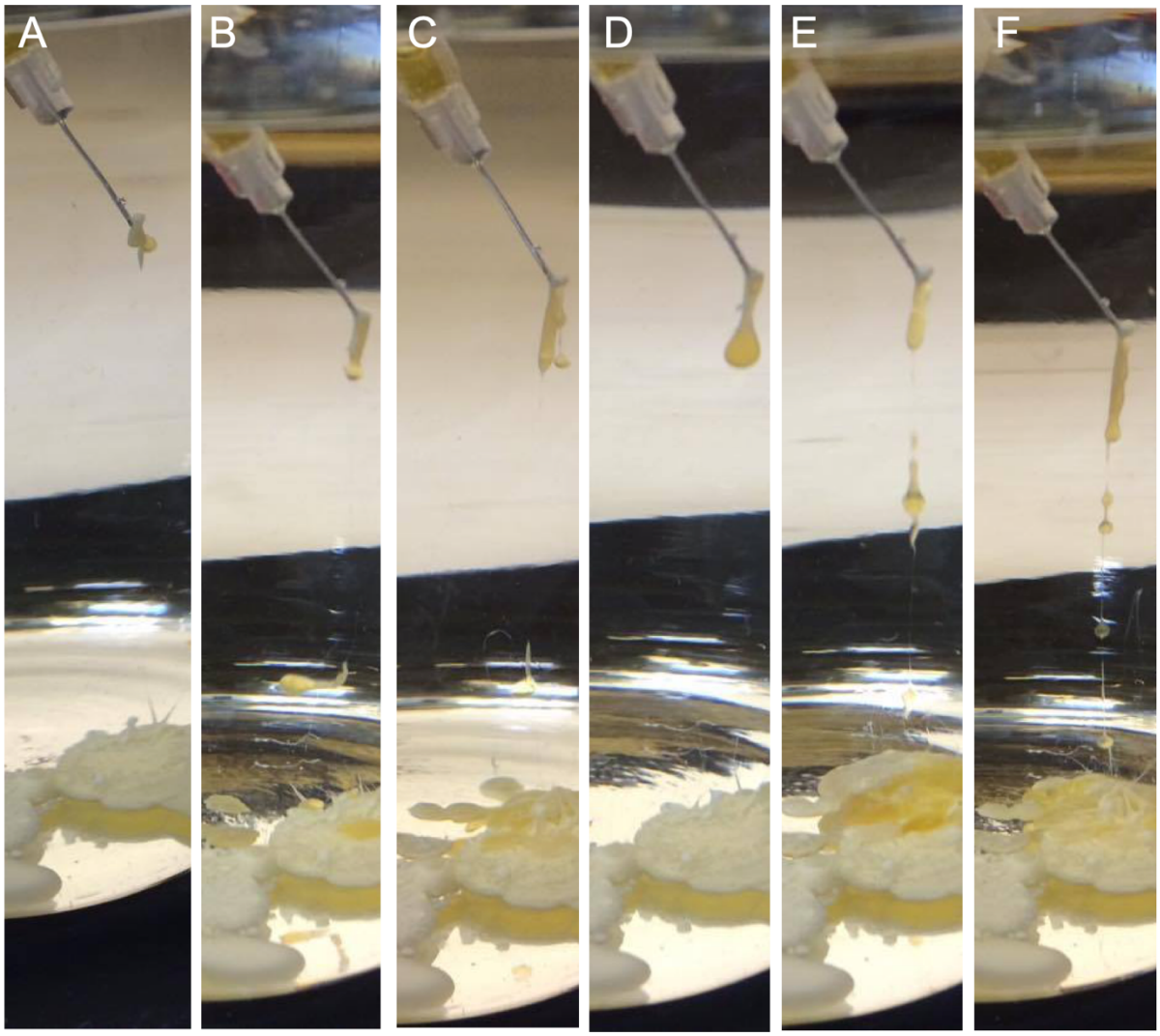

Figure 5.17 Photographs of wet-spinning zein attempts. Using 10% (w/v) zein in 50:50 (v/v) chloroform-methanol, and a 27 gauge needle. Flow rates were A: 1 ml / hr, B: 10 ml / hr, C: 20 ml / hr, D: 30 ml / hr, E: 40 ml / hr, F: 50 ml / hr.

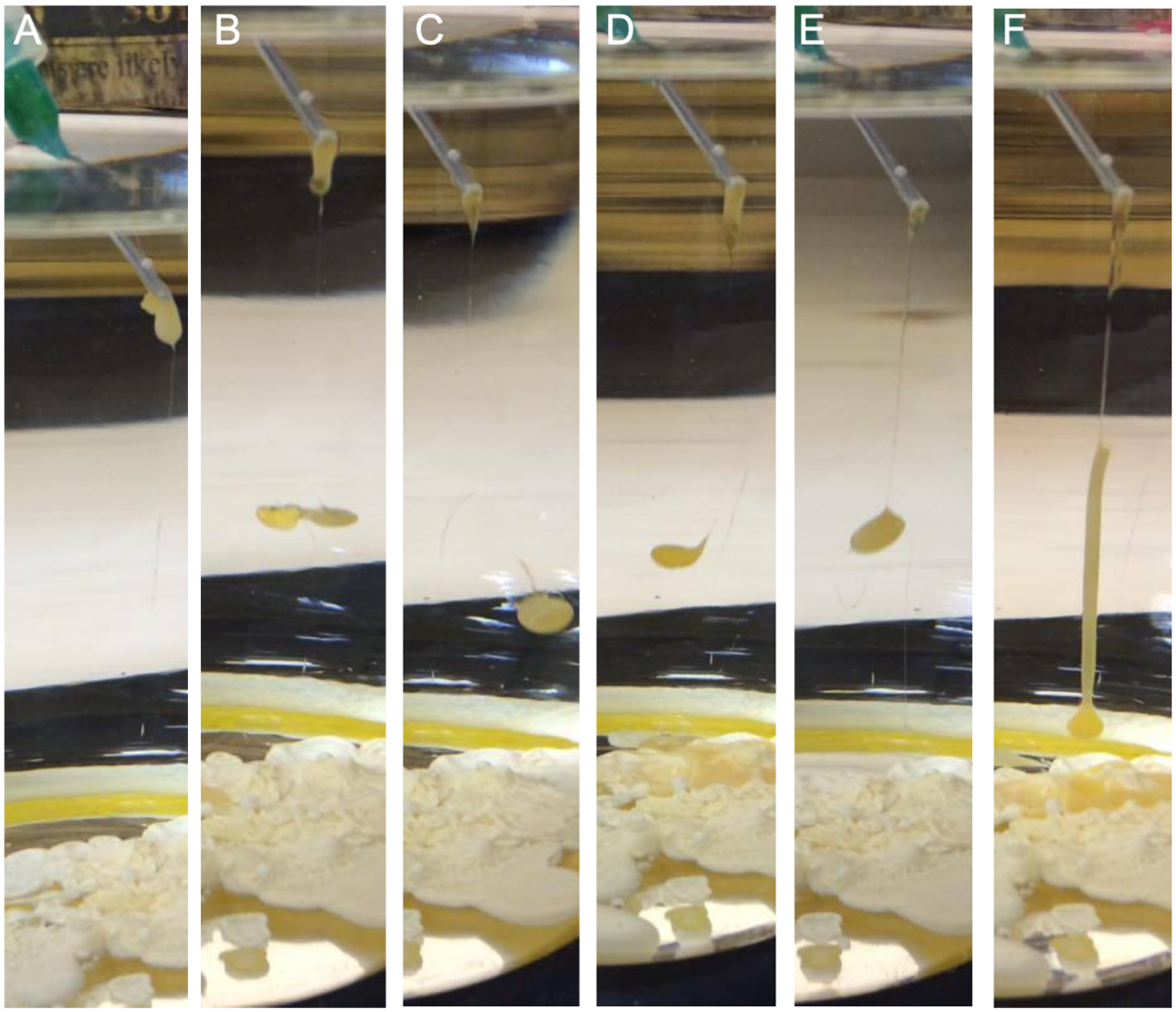

Figure 5.18 Photographs of wet-spinning zein attempts. Using 15% (w/v) zein in 50:50 (v/v) chloroform-methanol, and an 18 gauge needle. Flow rates were A: 1 ml / hr, B: 10 ml / hr, C: 20 ml / hr, D: 30 ml / hr, E: 40 ml / hr, F: 50 ml / hr.

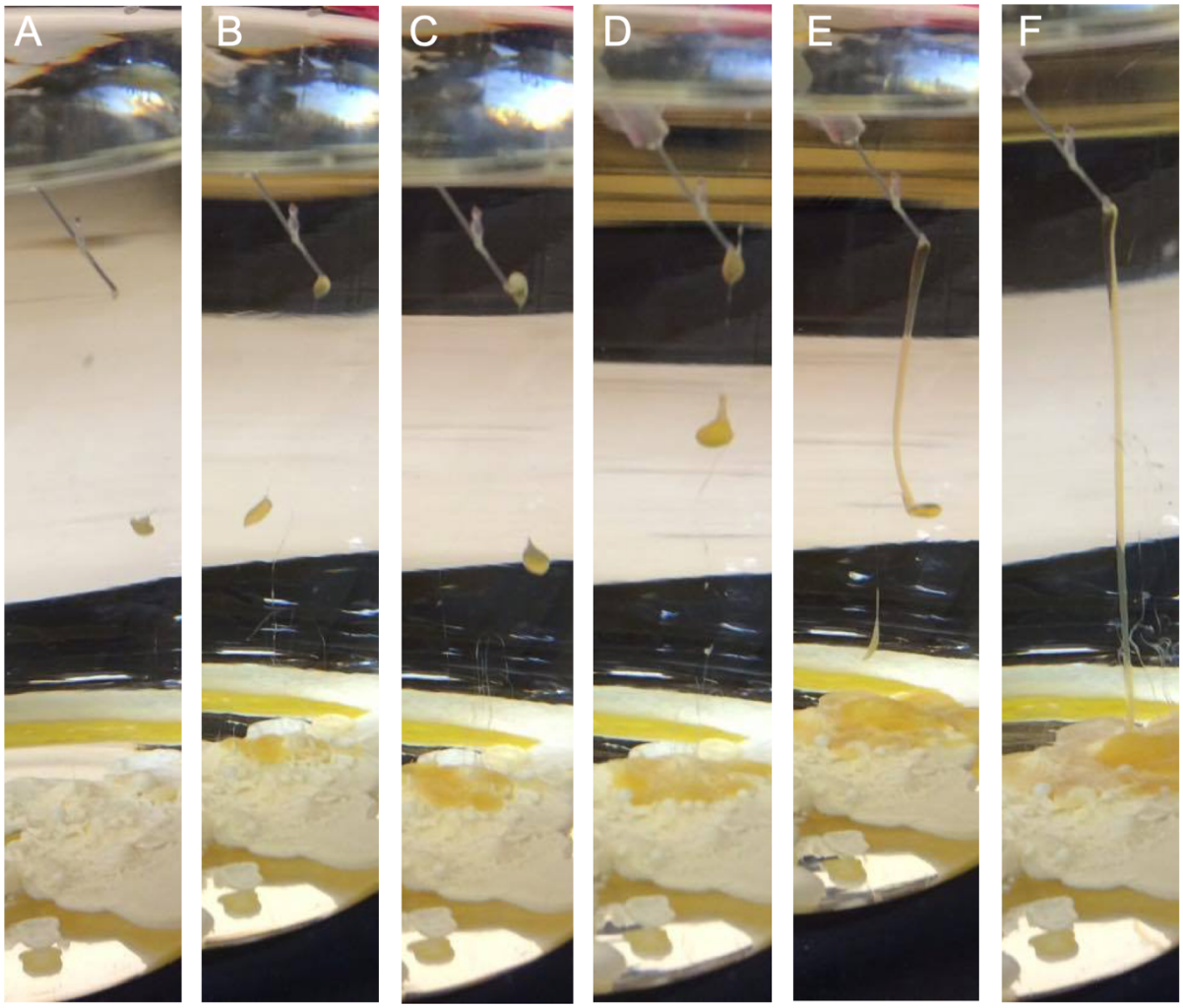

Figure 5.19 Photographs of wet-spinning zein attempts. Using 15% (w/v) zein in 50:50 (v/v) chloroform-methanol, and a 27 gauge needle. Flow rates were A: 1 ml / hr, B: 10 ml / hr, C: 20 ml / hr, D: 30 ml / hr, E: 40 ml / hr, F: 50 ml / hr.

Zein concentrations of at least 15% (w/v), with a flow rate of at least 40 ml / hr, and the use of a 27 gauge needle were required in order for the zein solution to be extruded into the water as a steady stream (figure 5.19). Low concentrations of zein along with low flow rates resulted in the zein solution being extruded as a series of droplets which, if they had precipitated into solid zein, may have represented a means by which zein macroparticles could be produced. However, fully solid zein did not precipitate under any conditions, but remained largely in solution which aggregated at the bottom of the beakers. The colour change observed for these films over time (from a dark yellow to a very pale yellow) may denote precipitation taking place but requiring a greater length of time than that taken to fall from the spinneret to the floor of the vessel. A similar colour change is notable for the zein droplets of low concentration (figure 5.12). The lack of adequate precipitation and hardening is likely due to inadequate solubility of the solvent (chloroform : methanol) in the non-solvent

(water), which is an important parameter in the phase inversion process with regard to precipitation of the polymer [301]. Although methanol shows a high solubility in water, at 1000 mg / ml [302], chloroform does not, showing only 7.95 mg / ml [302]. Chloroform : methanol was chosen as the solvent in this case as it was observed that it could dissolve higher concentrations of zein without thickening to an extreme degree. However, aqueous ethanol may be a better choice of solvent for this application, as it also shows miscibility in water with a solubility value of 1000 mg / ml [302]. The exclusive use of a solvent, or solvents, miscible in water such as ethanol may facilitate precipitation of fibrous or particulate zein membranes in water. Allowing the beads, formed using low concentrations of zein, a greater length of time in water before touching the vessel base (i.e use of a larger vessel) may provide enough time for them to fully precipitate into solid particles. However, it was felt that electrospinning may prove to be less labour-intensive than this wet-spinning approach, and it was therefore decided that this would be explored as a higher priority than refinement of the immersion precipitation attempts.

5.2.4 Production of electrospun fibres

Electrospun zein fibres were successfully produced as per chapter 2, section 2.2.5.6. These fibres were immersed in PBS for varying lengths of time as described in chapter 2, section 2.2.5.7 and imaged under SEM (chapter 2, section 2.2.5.8) to ascertain their stability in aqueous environments. The results of this are shown in figure 5.20.

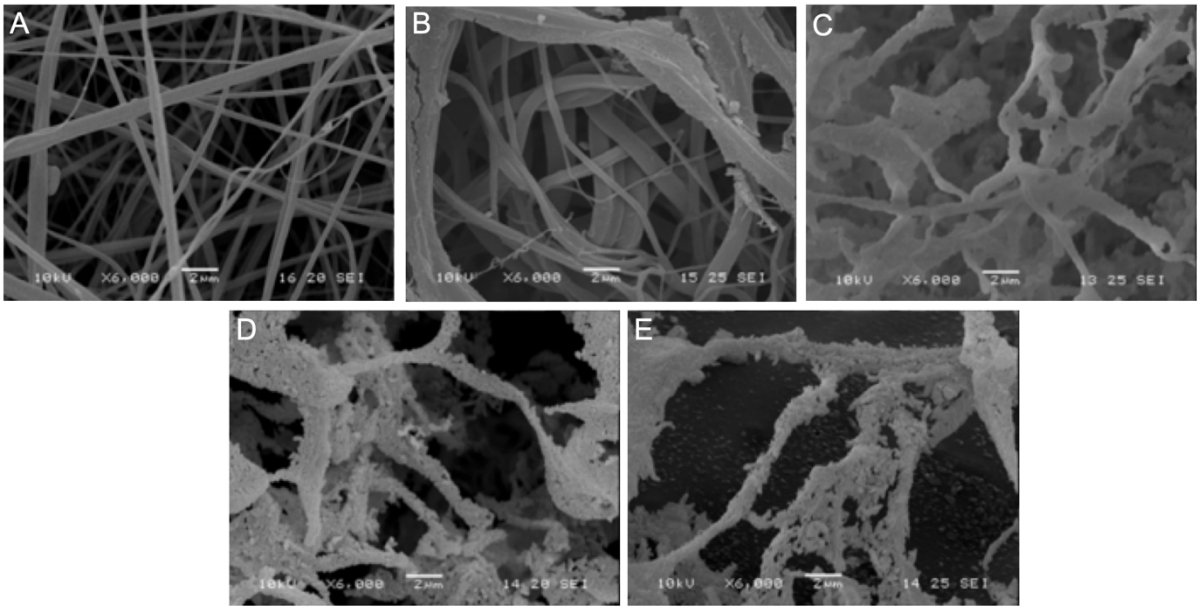

Figure 5.20 Representative SEM images of electrospun fibres after immersion in PBS solution for varying lengths of time. A: Dry, B: 1 day, C: 3 days, D: 5 days, E: 7 days. Scale bars represent 2 μm.

The results appear positive in comparison to other studies utilising electrospun zein fibres, where the fibres collapse into films after exposure to PBS for 7 days [280]. The fibres have, however, clearly swollen, and exhibit a change in texture. It was initially thought that the fibres may be coated in salts from the PBS solution. However, Alhusein *et al.* produced pure-zein electrospun fibres (as negative controls to those blended with PCL), which were immersed in PBS solution and degraded into sheets, not exhibiting this change in surface texture [293]. Furthermore, this change in texture appears to exhibit a gradual onset, which would not be the case if the fibres were simply coated in PBS salts. This may be attributable to Alhusein *et al.*'s use of Acros-brand zein versus the Sigma-brand used here, or it may be a result of lyophilisation: the method by which the samples herein were dried before imaging under SEM. Electrospun fibre mats to be imaged under SEM in subsequent experiments were immersed in water rather than PBS, and allowed to air-dry rather than being subjected to lyophilisation.

5.2.5 Stabilisation of electrospun zein fibres

Electrospun zein fibres were produced under the same conditions as previously described (chapter 2, section 2.2.5.6). In order to prevent this degradation effect when exposed to water, samples were treated in various ways (including EDC / NHS carbodiimide coupling, citric acid crosslinking, and photocrosslinking), and analysed for reduction in surface area over time in water as per chapter 2, section 2.2.5.7. As previously mentioned, the EDC / NHS carbodiimide coupling procedure is less than ideal for use in bioscaffolds due to the toxicity of the reagents, especially here where their presence in the final product would render it inedible. The mechanism involves activation of a carboxylic acid group by the EDC, wherein the EDC is bound to the group forming an unstable intermediate. The EDC is then displaced by the NHS, forming a semi-stable ester, and finally the NHS is displaced by a peptide-bound amine group, thus joining the two peptide chains and leaving the reagents in solution [303]. However, the reagents may be removed by thorough washing of the scaffold with distilled water after the coupling procedure has taken place. Whilst conducting the procedure, it was noted that the presence of the reagents (even in small amounts) caused a colour change in the DMEM, indicating a pH of below 6.4 [304]. The scaffold was determined to be sufficiently washed when no colour change was observed (visually) in the DMEM 30 minutes after application. This technique could be refined by use of colourmetric assays, such as via the FLUOstar omega plate reader used in the previously mentioned resazurin assays, in order to confirm the effectiveness of the washing steps (given that the basic (red-coloured) form is known to bear an absorption peak band of approximately 566

nm [305]). Additionally, carbodiimide chemistry represents a commonly implemented means of covalently joining peptides. As a model technique by which proteins are joined, it warrants analysis in this work alongside other less common protein-coupling techniques.

The citric acid crosslinking procedure used here (chapter 2, section 2.2.5.7.2) was based on the work of Jiang *et al*. [306] who reported the production of water-stable electrospun zein fibres with no apparent cytotoxicity. Citric acid is, of course, edible. The citric acid crosslinking mechanism is distinct from that of carbodiimide chemistry in that the peptides are not directly joined, rather a molecular bridge is formed between them (to be discussed). Although the crosslinked zein showed no evidence of cytotoxicity in the aforementioned study [306], this introduction of additional molecular structures into the protein may result in the generation of potentially harmful substances as the modified protein complex is digested after eating. Thus, if this particular experimental technique showed promise, it may be prudent to analyse the digestion of citric-acid-crosslinked zein *in vitro* (see section 5.3.3).

An additional electrospun mat was subjected to UV treatment in an effort to induce a degree of photocrosslinking (chapter 2, section 2.2.5.7.3). The surface areas of the fibre mats were measured after 24 hours in water, the results of which are displayed in figure 5.21 and 5.22.

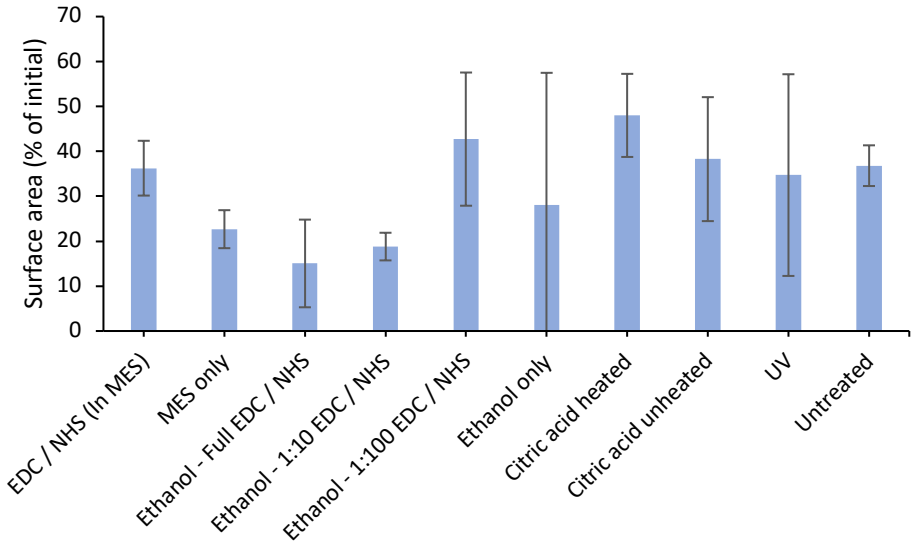

Figure 5.21: Surface area of treated electrospun zein fibre mats 24 hours after exposure to milliQ water, represented as a percentage of the initial surface area. Initial surface area was 1.9 cm^2. Data represent median ± interquartile range.

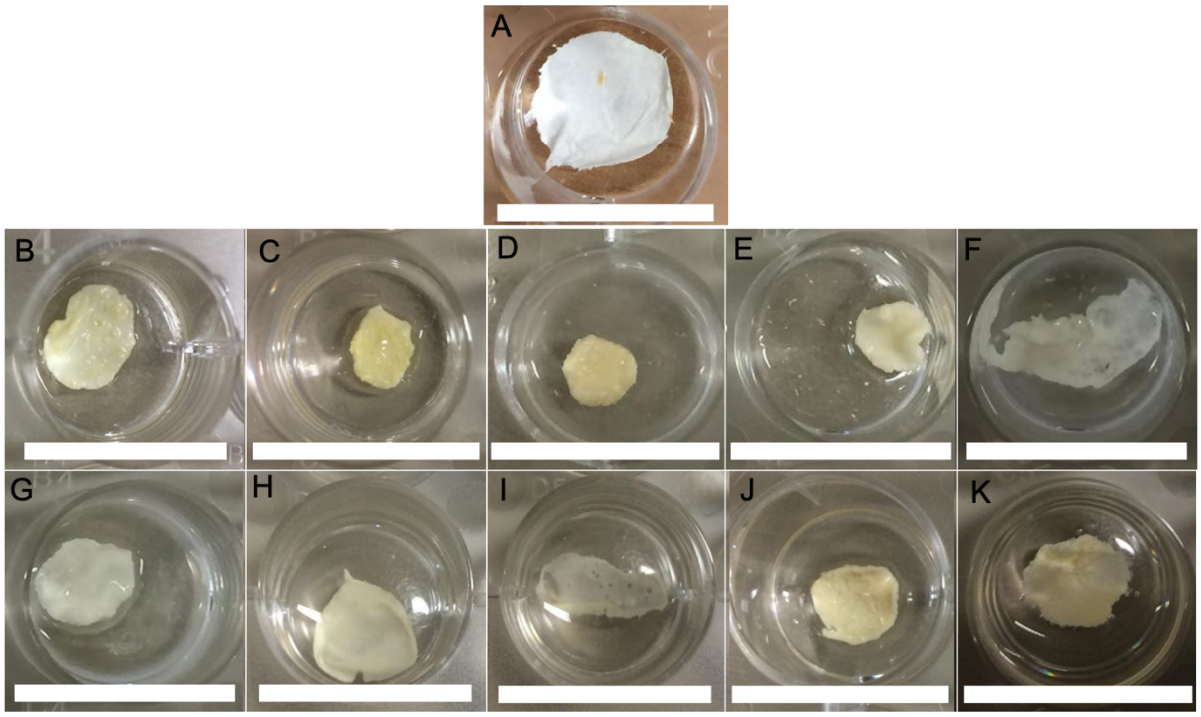

Figure 5.22: Representative images of electrospun zein mats after 24 hours in water. A: Dry B: Treated with EDC/NHS in MES buffer. C: Treated with MES buffer only. D: Treated with EDC/NHS in ethanol. E: Treated with EDC/NHS in ethanol, 10% initial concentration. F: Treated with EDC/NHS in ethanol, 1% initial concentration. G: Treated with ethanol only. H: Aged with citric acid and heat-treated. I: Aged with citric acid, no heat treatment. J UV-treated. K: Untreated. Scale bars (white) represent 1.55 cm.

The citric-acid samples and the samples treated with EDC/NHS in MES buffer showed improved stability compared to other samples, but not in comparison to untreated control samples. In order to determine whether this macroscopic shrinkage was a strong indication of the stability of fibres themselves at the micro / nanoscale, (as opposed to a reduction in porosity of the matrix) SEM analysis was conducted, the results of which are given in figures 5.23 – 5.33. Figures 5.23 – 5.25 show size distribution of the fibres over time. Figure 5.26 shows mean fibre diameter over time. Figures 5.27 – 5.32 show SEM images of the samples at various timepoints.

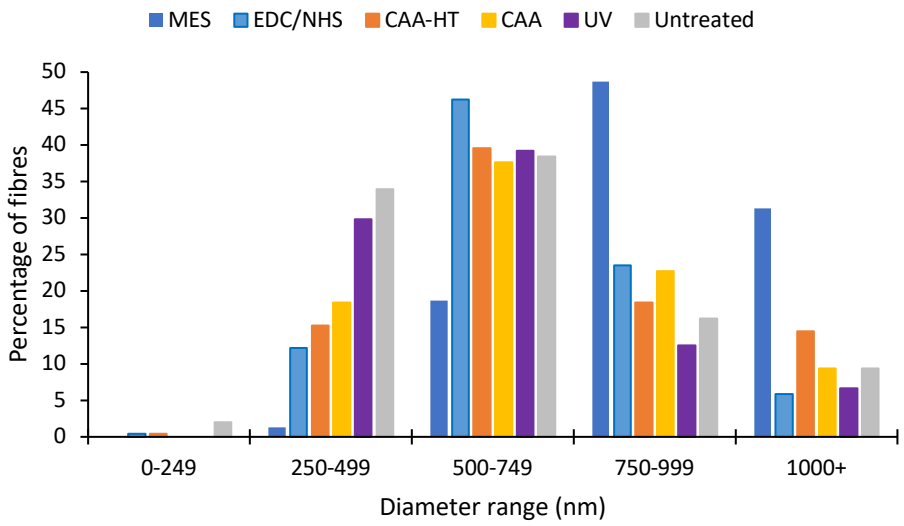

Figure 5.23 Size distribution of treated electrospun zein fibres before exposure to water. “MES” refers to samples treated with MES buffer only. “EDC/NHS” refers to samples treated with EDC and NHS in MES buffer. “CAA-HT” refers to samples aged with citric acid while in solution (“citric acid aged”) with heat treatment after production of fibres. “CAA” refers to samples aged with citric acid without subsequent heat treatment “UV” refers to samples treated with UV light for 2 hours. Data represent individual observations.

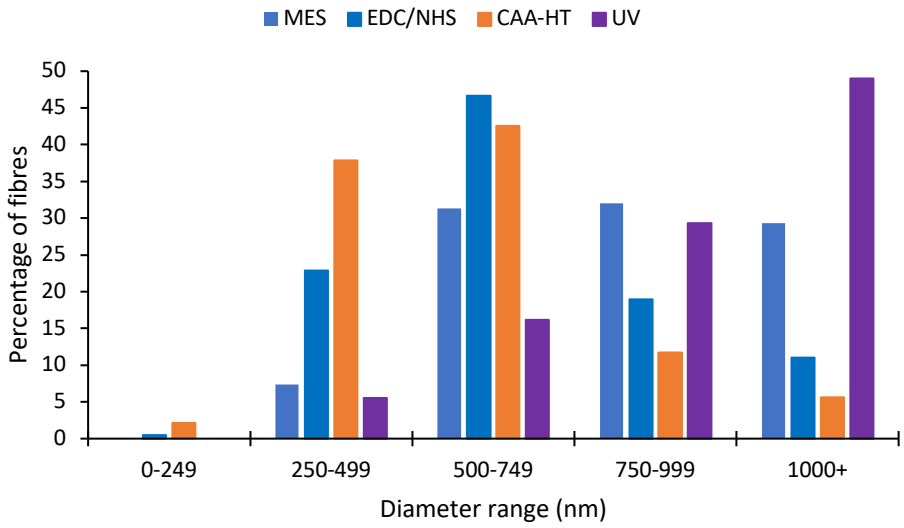

Figure 5.24: Size distribution of treated electrospun zein fibres after 3 days of immersion in water. Treatments from figure 5.20 that are not shown here have lost their fibrous morphology by this point and collapsed into sheets. Data represent individual observations.

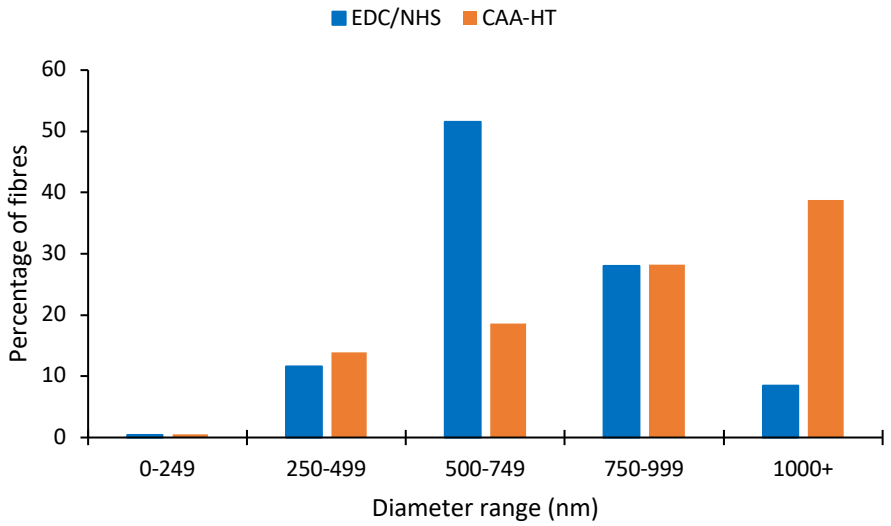

Figure 5.25: Size distribution of treated electrospun zein fibres after 7 days of immersion in water. Treatments from figures 5.20 and 5.23 that are not shown here have lost their fibrous morphology by this point and collapsed into sheets. Data represent individual observations.

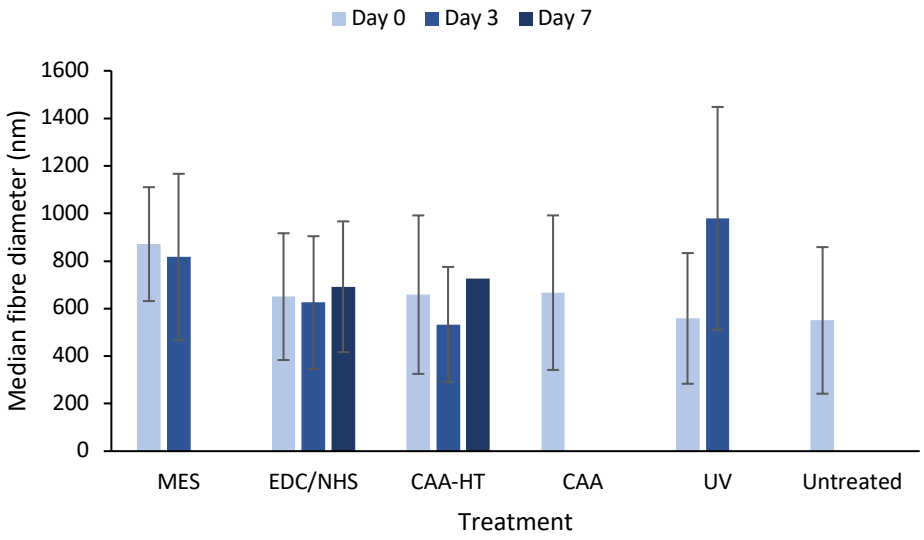

Figure 5.26: Median fibre diameter of electrospun zein fibres treated in various ways, over time immersed in aqueous media. “Day 0” refers to dry fibres before immersion. Data represent median ± interquartile range.

Almost all treatments (including untreated controls) showed the highest prevalence of 500-749 nm diameter fibres at the zero time point (Figure 5.23). This is not the case however, for the MES control samples (treated with MES without EDC/NHS), with fibres having the highest incidence of diameters in the 750-999 nm range. At the 3-day time point, it is observable that there was a dramatic increase in the diameter of UV-treated fibres, the majority thereof having diameters of 1000 nm or more. Untreated controls and citric acid

control samples (non-heat treated) lost their fibrous structure collapsing into films by this time. EDC/NHS and citric acid fibres, however, still show a higher incidence of 500-749 nm fibres than any other size range. Though an increase in citric-acid-treated fibres in the 250-499 nm diameter range is noted at this time (Figure 5.24). By the 7-day time point, only the EDC/NHS and citric-acid treated samples maintain a fibrous structure. EDC/NHS samples still exhibit the majority of fibres in the 500-749 nm diameter range, as they did at the zero time point, suggesting this treatment imparts the highest degree of stability of those assayed. Citric acid samples show a higher incidence of fibres in the upper diameter ranges, with the highest incidence of fibres in the 1000+ nm range. As fibres degrade into a sheet form, an increase in diameter is to be expected, suggesting that the increase in citric acid fibre diameter at the 7-day time point may be the beginnings of degradation (Figure 5.25). The apparent shrinkage in fibre diameter noted at the 3-day time point for the citric acid samples is likely to be the result of random chance. It is notable however that the mean fibre diameter (Figure 5.26) for citric acid samples does not appear to be substantially increased from the value at the zero time point.

The untreated control fibres showed a mean fibre diameter of 643 nm. This is comparable to the aforementioned work of Alhusein *et al.* whose electrospun zein fibres exhibited a mean diameter of 670 nm (± 190 nm) [293]. In contrast, Yang *et al.* produced electrospun zein fibres with a mean diameter of 69 nm (± 22) [137]. This lower fibre diameter is likely owed to the lower concentration of zein solution used (10% w/v, as opposed to the 20% w/v used here), as it has been demonstrated that polymer concentration is positively (and exponentially) correlated with resultant electrospun fibre diameter [307, 308]. With regard to stabilisation, it is immediately notable that samples treated with EDC/NHS, and citric acid (with subsequent heat treatment) not only remain fibrous up to 7 days in water, but also show little increase in fibre diameter during this time. The lack of bars for certain timepoints in other samples indicate that the fibres had collapsed into sheets at this point. These results are illustrated in the representative SEM images displayed in figures 5.27 – 5.33.

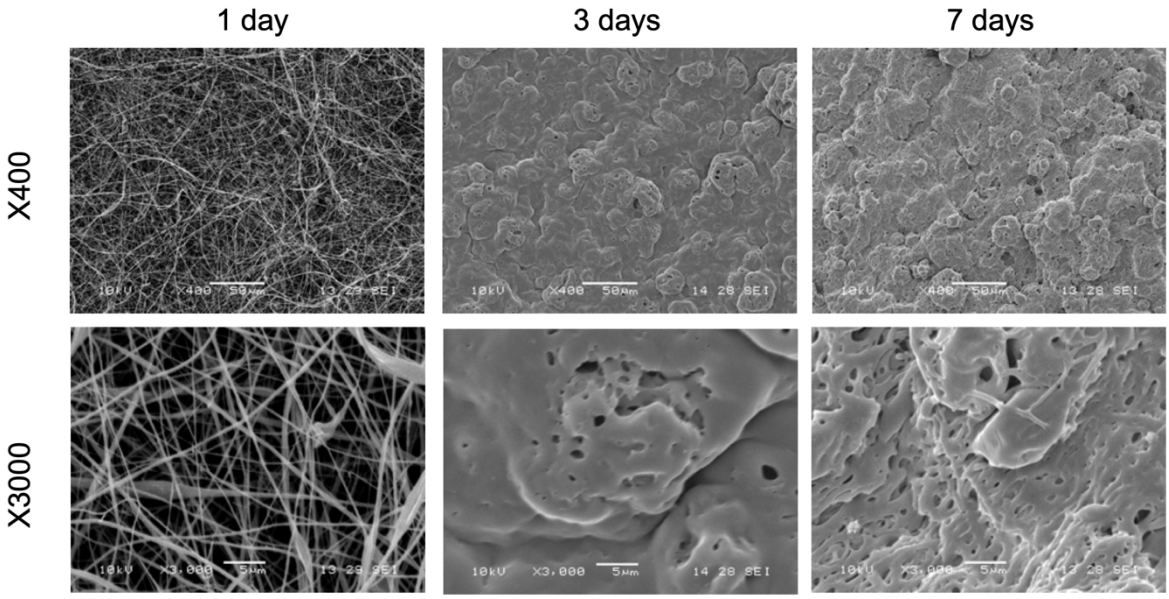

Figure 5.27: SEM images of untreated fibres after being soaked in milliQ H_2O for various lengths of time. Images are given at x400 and x3000 magnification. Scale bars represent 5 μm.

Figure 5.27 represents untreated control samples. It is clear that the fibres have lost their stability and collapsed into sheets as early as 3 days after immersion in milliQ H_2O. These images, in contrast to those presented in figure 5.20, are consistent with those of Alhusein *et al.* [293], where the fibres degrade into sheets after exposure to aqueous media. As Sigma-brand zein is still being used here, it would indicate that the change in surface texture seen in figure 5.20 is the result of the lyophilisation stage. It would also, unfortunately, suggest that those fibres did not retain their fibrous morphology, but rather that the mats were damaged during lyophilisation.

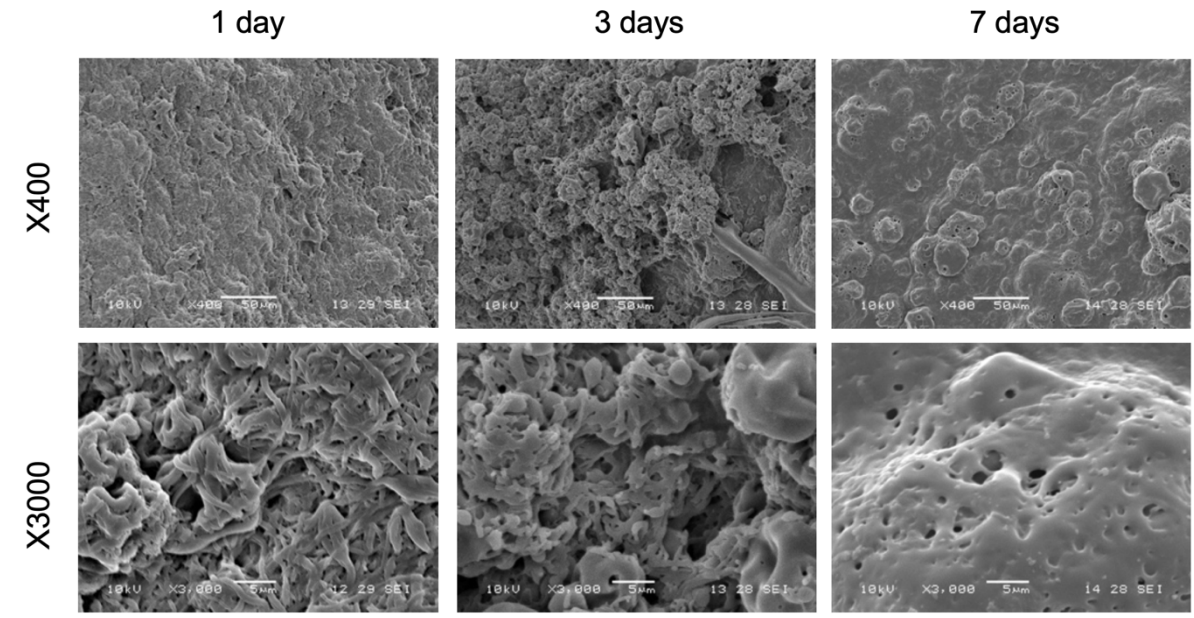

Figure 5.28: SEM images of MES-treated fibres after being soaked in milliQ H_2O for various lengths of time. Images are given at x400 and x3000 magnification. Scale bars represent 5 μm.

Images displayed in Figure 5.28 represent samples which were treated with MES only. These samples represent negative controls for subsequent EDC/NHS treated samples. There is an immediate and obvious change in the appearance of the samples, as the porosity of the fibre matrices appears to have decreased considerably. However, fibres appear to retain their shape up to the 3-day timepoint, despite appearing to form node-like clusters.

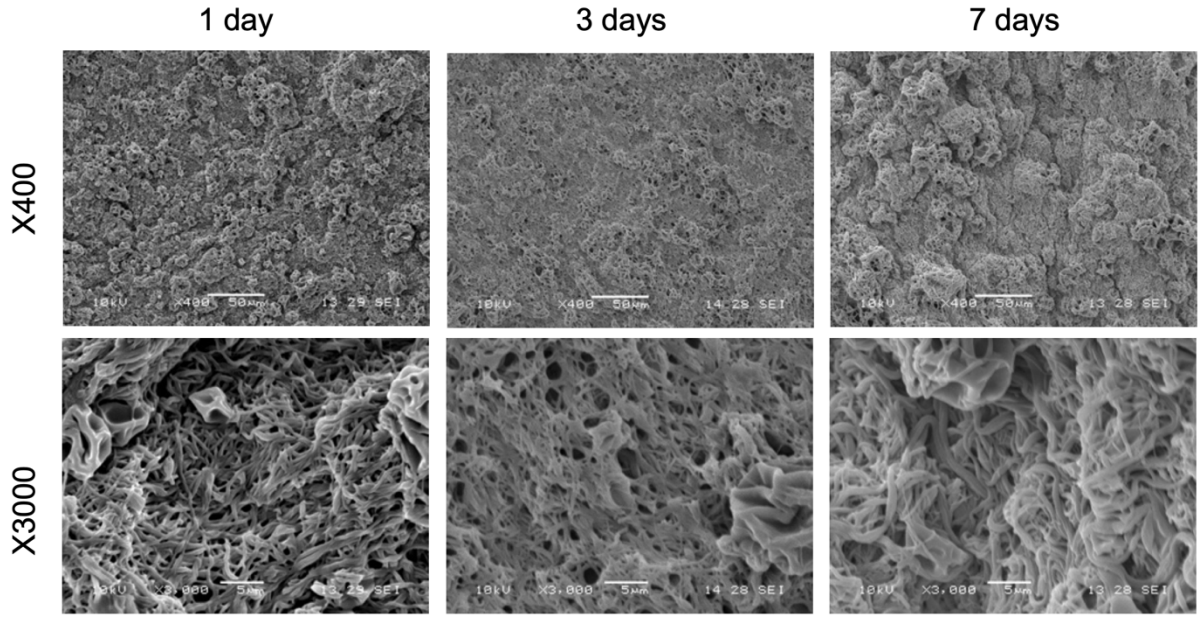

Figure 5.29: SEM images of EDC/NHS-treated fibres after being soaked in milliQ H_2O for various lengths of time. Images are given at x400 and x3000 magnification. Scale bars represent 5 μm.

The images displayed in Figure 5.29 represent samples subjected to crosslinking by way of EDC/NHS treatment, which operates by first binding the carboxylic acid terminal, or free carboxyl group, of an amino acid residue, thus forming an unstable intermediate compound, which may then be stabilised by the replacement of the EDC molecule with NHS, producing an intermediate of higher reactivity. This then facilitates the binding between an amine group terminal of another amino acid or protein chain and the carboxylic acid terminal of the initial protein, leaving the two directly coupled. The effect of this treatment is apparent in that samples appear to show a higher degree of porosity at the 3-day timepoint, and there are less node-like clusters present in the x400 magnification image at this time. These clusters are more prominent at the 7-day timepoint, as is what appears to be a further reduction in porosity. However, the scaffold appears to hold its fibrous structure even after 7 days immersed in water.

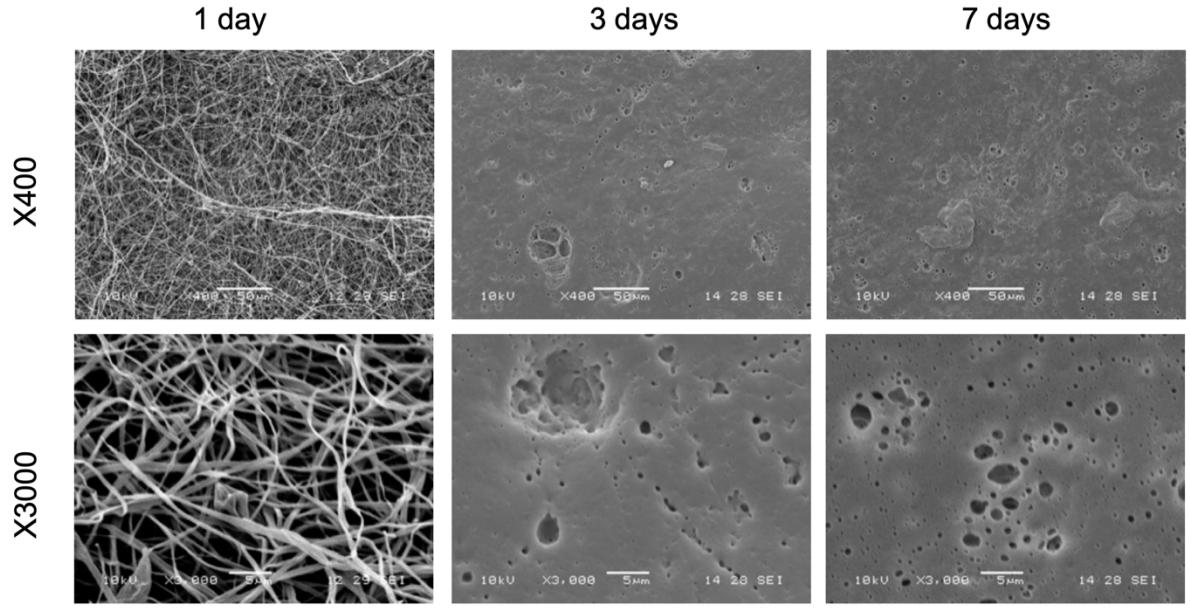

Figure 5.30: SEM images citric acid treated fibres (without heat treatment) after being soaked in milliQ H_2O for various lengths of time. Images are given at x400 and x3000 magnification. Scale bars represent 5 μm.

Images in Figure 5.30 represent controls for citric-acid crosslinking. These samples were formed from zein solutions to which citric acid was added, and the solution aged, but were not heat-treated after electrospinning. Like the untreated, super-negative controls, these samples showed a complete lack of fibres at the 3-day timepoint. The surface of the resultant films also appears smoother than those seen for untreated samples, suggesting that the presence of citric acid without the induction of crosslinking worsens the stability of the fibres.

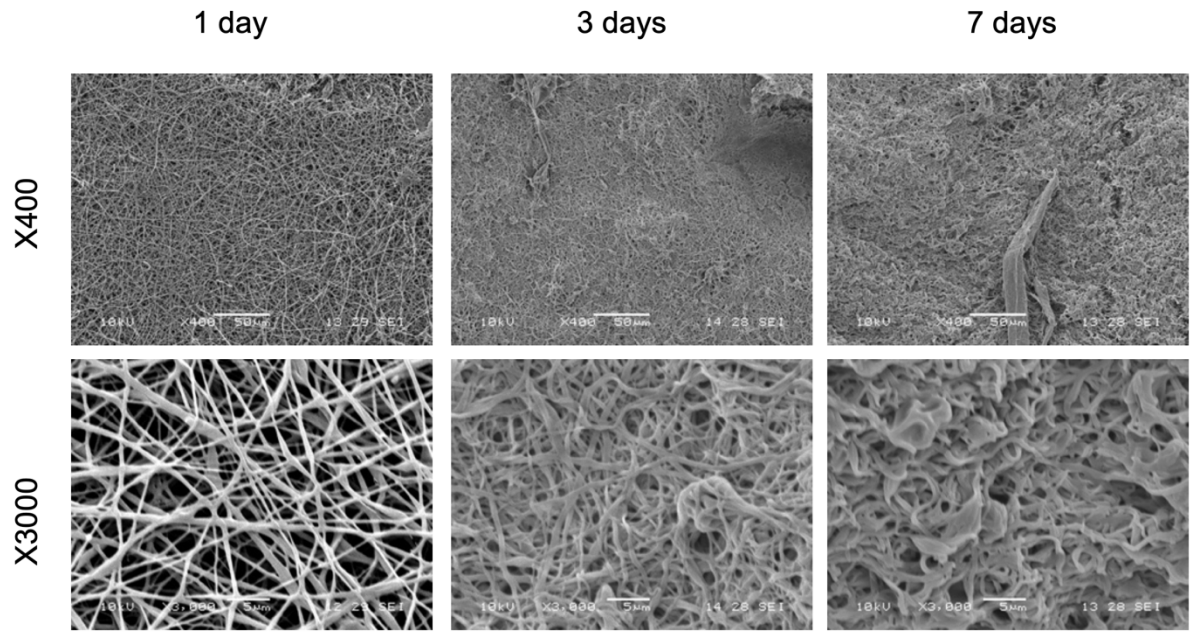

Figure 5.31: SEM images of citric acid and heat treated fibres after being soaked in milliQ H_2O for various lengths of time. Images are given at x400 and x3000 magnification. Scale bars represent 5 μm.

The images in Figure 5.31 represent samples crosslinked using citric acid, with heat-treatment after electrospinning. The mechanism by which this is accomplished is different to that of EDC/NHS treatment. Citric acid contains three carboxylic acid groups, which each have the capacity to bind to anime groups [309], and the amino acid residues in zein contain multiple amine group side chains [310]. In this way, the citric acid is able to react with a maximum of 3 different amino acid residues in the zein protein chains. The effects of this are apparent. Like EDC/NHS-treated samples, the fibres do not collapse into sheets even after 7 days immersed in water. In contrast with EDC/NHS samples, the fibres appear to show less deformation and aggregation at the 3-day timepoint, and only the beginnings of node-like clusters can be observed at the 7-day timepoint. The results displayed in Figure 5.23 show little difference between the initial and final diameters of the fibres associated with these two forms of treatment, but SEM images would seem to suggest that the citric-acid treatment procedure is more effective for the stabilisation of electrospun zein fibres than treatment with EDC/NHS.

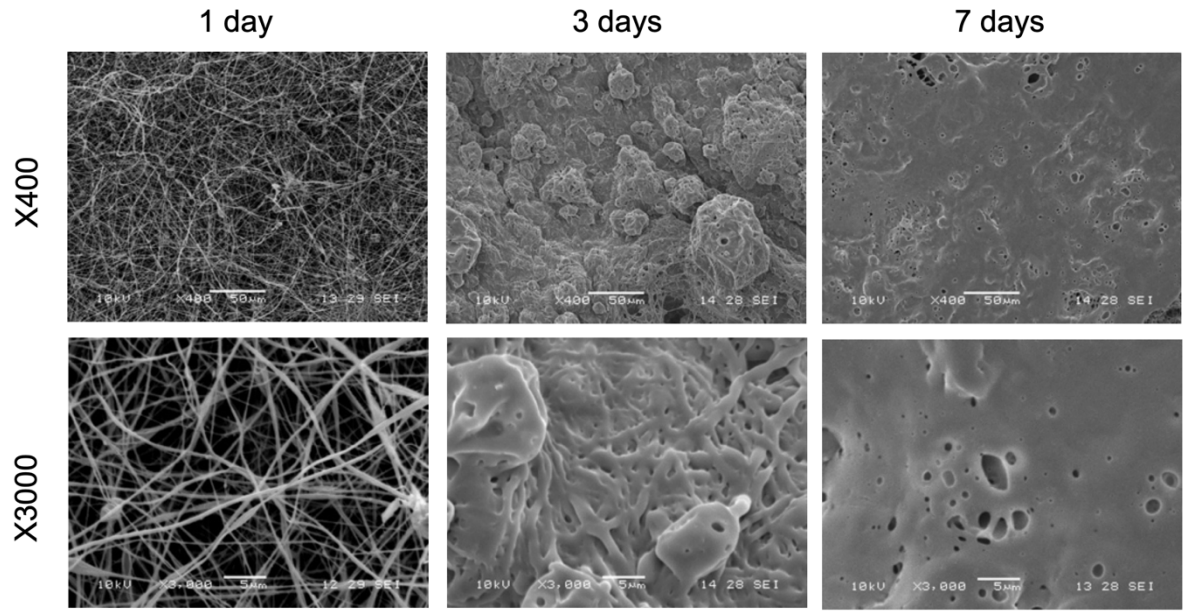

Figure 5.32: SEM images of UV-treated fibres after being soaked in milliQ H_2O for various lengths of time. Images are given at x400 and x3000 magnification. Scale bars represent 5 μm.

Samples treated with UV-light appear to show a marginal improvement compared to untreated samples. Although the fibres are clearly blending together at the 3-day timepoint, it is still possible to identify fibrous structures, whereas a complete lack of fibres was noted at this point for the untreated samples. If this UV treatment is indeed providing a small degree of stabilisation, it may represent a form of crosslinking in which excitation from UV light triggers electron emission from aromatic tryptophan, tyrosine, and phenylalanine amino acids, which are then absorbed by disulphide bridges in the protein chain, ultimately forming thiol groups [311]. It may be that this then allows for formation of new disulphide bonds with other amino acids, producing a crosslinking effect which may have a positive effect on the overall fibre stability.

It appears that samples crosslinked using EDC/NHS, as well as citric acid, effectively stabilise electrospun zein fibres, and prevent them from totally collapsing in the presence of water. The mechanisms of these two crosslinking techniques are markedly different, and the resultant structures of the crosslinked proteins reflect this. EDC/NHS crosslinking leaves the amino acids involved directly joined and operates between one carboxylic acid group and one amine group, whilst the citric acid molecule interacts with up to three amine groups at once, leaving the residues connected by a 6-carbon organic bridge.

Despite citric acid's ability to interact with two amino acid residues simultaneously [312], it appears that the presence of this connecting bridge may result in less-stable fibres than

those directly joined together by EDC/NHS, given the apparent swelling in fibre diameter that begins at the 7-day time point for citric-acid-crosslinked fibres. However, it is also notable that this swelling was not yet severe enough to lead to a noticeable change in mean fibre diameter.

5.2.6 Cytocompatibility of treated electrospun fibre mats

Having produced stabilised electrospun zein fibres, it was then necessary to ascertain whether these crosslinking procedures had an impact on the biomaterial's ability to support cell growth. The effects of the differing crosslinking mechanisms are far more clearly divided in subsequent cytocompatibility experiments. EDC/NHS treatment was the first to be analysed in this way. Zein films were produced and treated with EDC/NHS (chapter 2, section 2.2.5.7.1), then seeded with cells (chapter 2, section 2.1.1.2). Their proliferation over time was tracked by way of resazurin metabolic assay (chapter 2, section 2.1.2.2), the results of which are shown in figure 5.33.

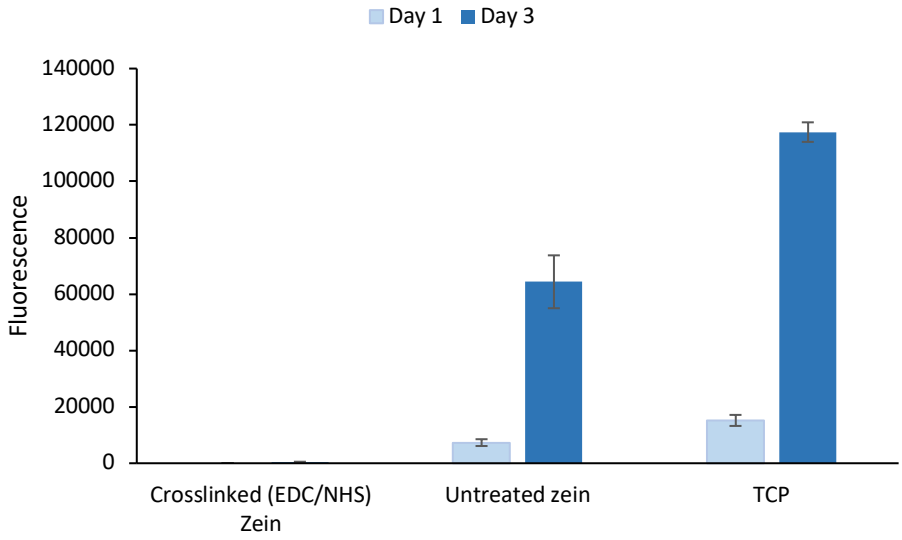

Figure 5.33: C2C12 cell growth on zein films treated with EDC/NHS, versus untreated zein films and TCP. Data represent median ± interquartile range.

From a short-term cell proliferation experiment (Figure 5.33), it is obvious that the EDC/NHS treatment has had a highly detrimental effect on the cytocompatibility of zein. This was conducted on zein films in order to ascertain the effects of the crosslinking on the cytocompatibility of the zein itself as a biomaterial, and (to that end) remove the potential confounding variable of fibre morphology versus films. The zein controls were treated identically to the crosslinked samples with the exception of the EDC/NHS crosslinking

agents. The results show an apparent elimination of any cytocompatibility of crosslinked zein, as opposed to uncrosslinked controls, which show positive cell attachment and growth.

To ascertain the severity of the procedure's effect on the cytocompatibility of zein, this phenomenon was explored in more detail by adjusting the degree of crosslinking (which was done by serial dilution of crosslinker solutions, reducing the concentration of the crosslinking agents by factors of 10 each time whilst maintaining their proportions in regard to the mass of protein) as stated in chapter 2, section 2.2.5.7.2, and analysing fluorescence one day after cell-seeding by way of resazurin metabolic assay (chapter 2, section 2.1.2.2). The results of this are given in figure 5.34.

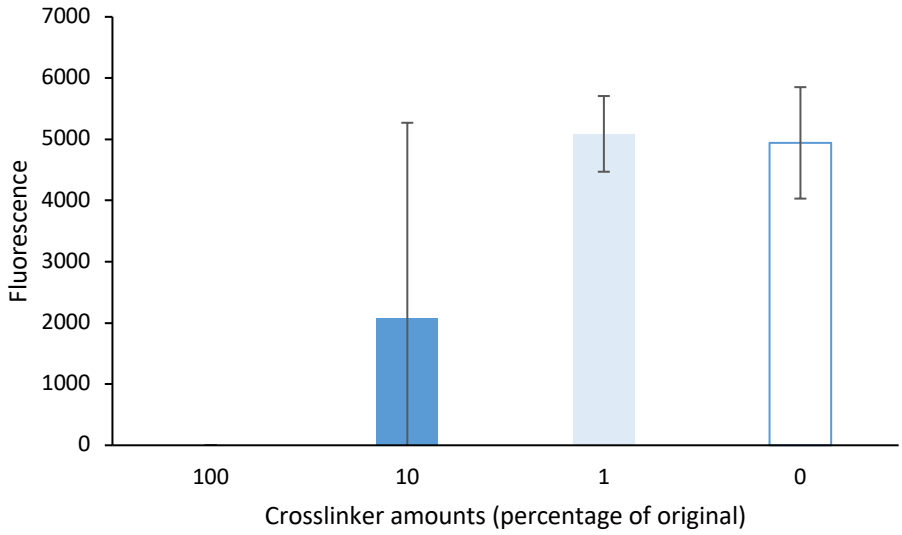

Figure 5.34: C2C12 cell metabolic activity on zein films treated with various amounts of EDC/NHS crosslinker solution, 24 hours post-seeding, measured by way of resazurin proliferation assay. Data represent median ± interquartile range.

There is a noticeable correlation between the degree of crosslinking and cytocompatibility. Cell density after 1 day improves considerably as the degree of EDC/NHS crosslinking is reduced. This is unlikely to be due to residual carbodiimides left in the aqueous environment as samples were separately and thoroughly washed, and the effect is observable across separate experiments. This demonstrates that the cell-binding impairment is likely to be a result of over-crosslinking. However, observation of fibres crosslinked to varying degrees as in figure 5.37 shows that reduction of crosslinking to a point that does not appear to affect cell-binding may result in the loss of the stabilisation effect. Fibres appear stable at 10% of standard crosslinker concentrations, however this still equates almost to a 50% reduction in cell-density after 1 day. These results would be aided by further analysis of cell-growth on these films. For example, if the negative correlation between crosslinker amount and

cytocompatibility were linear, the zein may become unable to support cells when treated with as little as 25% of the original crosslinker concentrations (Figure 5.34).

The effect of other stabilisation treatments on the cytocompatibility of zein films was also explored (Figure 5.35). The results appear positive in regards to cell grown on citric-acid crosslinked films, which show cell proliferation comparable to that on TCP controls. However, there are noticeable anomalies in the data. The untreated controls show what appears to be impaired cytocompatibility, which contradicts all previous data regarding cell growth on zein. This is almost certainly a result of confounding variables during the preparation of the untreated zein films, as well as UV-treated, MES-treated and EDC/NHS-crosslinked, which were all prepared at the same time. The citric acid and respective control samples (zein solutions which were not chemically modified, but allowed to remain in solution for 48 hours before electrospinning, given as “aged controls” in Figure 5.36) were prepared separately and in advance, due the longer length of time required, and appear to be unaffected. All samples were seeded together, and from the same stock of cells, meaning these anomalies are unlikely to be related to any issues therewith.

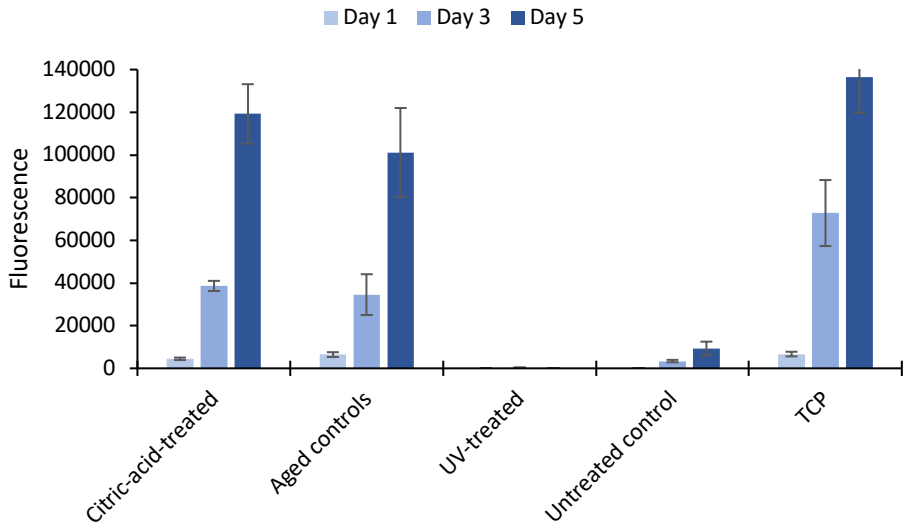

Figure 5.35: C2C12 cell growth on electrospun zein fibres treated by various means. Data represent median ± interquartile range.

Though the reliability is compromised by the presence of anomalous readings, the data (Figure 5.35) demonstrates positive cytocompatibility of citric-acid-crosslinked zein. These citic-acid treated and aged control samples (the latter of which were produced from zein kept in 70% aqueous ethanol solution for the same length of time as the citric acid samples) were prepared separately from all other samples, which is likely the reason they are not affected by whatever variables impaired the UV-treated, and untreated control samples.

The results stand in conflict with the widespread use of EDC/NHS in literature to produce biocompatible scaffolds for tissue engineering applications. Yet they are convincing, not only in the clear and drastic difference between the crosslinked and uncrosslinked zein despite their being otherwise identically processed, but also in that the effect shows correlation with the amount of EDC and NHS used. If EDC and NHS do indeed compromise the mechanisms of cell adhesion to zein (or possibly the initiation of signalling pathways affecting proliferation) whereas citric acid does not, attention is immediately drawn to the differences in their crosslinking mechanisms.

A key difference in these processes is that while both anime and carboxylic acid groups of animo acid residues are involved in the crosslinking process facilitated by EDC and NHS, citric acid will only interact with the amine groups of the proteins, leaving any carboxylic acid groups in the protein unmodified. This would imply that carboxyl groups of animo acid residues may play key roles in some binding mechanisms to cell integrins. To present a model: the RGD protein motif is well-known for its prominent role in integrin-binding, and is capable of binding to many different integrin subunits [99], and indeed, the effect of blocking the carboxylic acid groups on the aspartic acid residue of the RGD is noted to have a significant effect on the motif's cell-binding ability [99]. The significance of the carboxylic acid groups is further highlighted by the effect of substituting the L-aspartic acid residue in the RGD motif for D-aspartic acid [313], which is that the motif is rendered incapable of cell-binding. The only effect of this substitution on the structure of the RGD motif is that the carboxylic acid groups (plus a single CH_2 group in the organic backbone) collectively protrude from the motif at a different angle [314, 315], the position of the attached secondary amine group relative to the rest of the motif would not be affected [314, 315]. Carboxylic acid groups are only found on the aspartic acid residue of the RGD motif, and the fact that a change in their spatial orientation with no changes to the chemical structure of the motif produces such a drastic change in the cell-binding capacity of the motif suggests that these functional groups are of critical importance. Analysis of the RGD binding mechanism provides a context for the assertion that carboxyl groups can play a key role in cell-binding.

As previously discussed, however, the binding mechanism between zein and myoblasts may be facilitated by crosslinking between integrin-bound lysine residues and peptide-bound glutamine residues, crosslinked by transglutaminase. Further analysis of the mechanism by which transglutaminase acts shows that EDC/NHS crosslinking would not interfere therein. In the case of the previously mentioned 42-kD region of fibronectin, transglutaminase is reasoned to facilitate cell-binding by forming a molecular bridge

between integrins (α5ß1 and αIIB3) and peptide-bound glutamine residues [255]. Molecular bridges formed by transglutaminase have been identified to be formed between the γ-carboxamide groups of the peptide-bound glutamine residue and a primary amine group of a peptide-bound lysine group [316]. This mechanism directly contradicts the premise that the decreased cell-binding observed in EDC/NHS-crosslinked zein versus citric-acid-crosslinked zein is a result of the former's interaction with carboxyl groups and amine groups of amino acids in the zein peptide chain, as opposed to citric acid's interaction with zein's anime groups only. As discussed above, zein's transglutaminase-mediated cell-binding properties would involve the γ-carboxyamide groups of the glutamine residues. Thus there is no clear reason why citric acid's lack of interaction with carboxylic acid groups would leave the cytocompatibility of the zein intact. Furthermore, given that EDC/NHS crosslinking interacts with primary amine groups of amino acids, the process would not alter the secondary amines of the carboxamide groups, and so should not compromise the primary structure's ability to form these bonds at all. It may therefore be, that the EDC/NHS mediated joining of the amino acids directly by their carboxyl and amine groups causes some alteration of the secondary or tertiary structure of the protein, making the glutamine residues less accessible to the cell-bound transglutaminase and integrins. Evidence of higher-level structural modification can be found in a side-effect of the EDC/NHS crosslinking process; the crosslinked films appeared to become translucent and colourless, as opposed to the unmodified zein films which remained yellow (Figure 5.36).

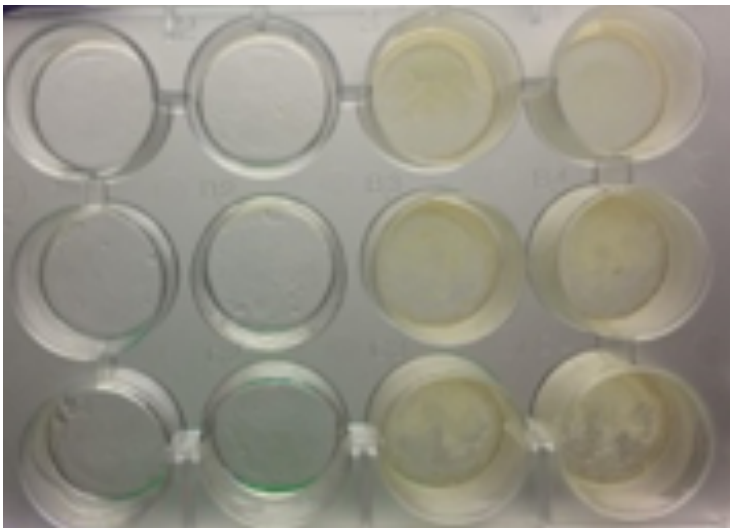

Figure 5.36: Photograph of EDC/NHS crosslinked zein films (left two columns) alongside ethanol-treated zein films (right two columns)

The characteristic yellow pigment of maize (and by extension, zein) arises from the presence of carotenoids, specifically beta-carotene and xanthophyll [245], the structures of which [247, 317] are not found in the functional groups of the well-known 20 amino acids,

and procedures such as supercritical fluid extraction are required to separate it from zein [245]. It may therefore be reasoned that these carotenoids contained within zein are held in place by the secondary or tertiary structure of the protein, and so their release (without employment of additional substances used in decolourisation procedures applied to zein [245]), leading to discolouration of the zein, may be evidence of changes in the secondary or tertiary structure.

In contrast with the direct EDC/NHS crosslinking mechanism, citric acid crosslinking operates via the formation of a the succinic anhydride intermediate, which citric acid is converted to upon heating, and thereafter reacting with amine groups of nearby polymers forming an organic bridge [312]. This allowance for extra space between the functional groups of the amino acids may spare the secondary-structure from any deformations which may be caused by the EDC/NHS mechanism.

To summarise the chemical crosslinking assays, the citric acid crosslinking procedure appears to produce fibres with enhanced stability, and without substantial loss in cytocompatibility. This places the technique above that of EDC/NHS crosslinking in regards to stabilising electrospun zein fibres as, when this technique is employed, the enhanced stability comes at the cost of lessened cytocompatibility. In order to ascertain what effect variance of crosslinking degree (by EDC/NHS treatment) might have on the stability, nanofibres were spun onto glass slides (chapter 2, section 2.2.5.6) and treated with EDC/NHS in the same way as in Figure 5.34. After 3 days of immersion in mH_2O, the fibres were imaged under white-light microscopy (Figure 5.37).

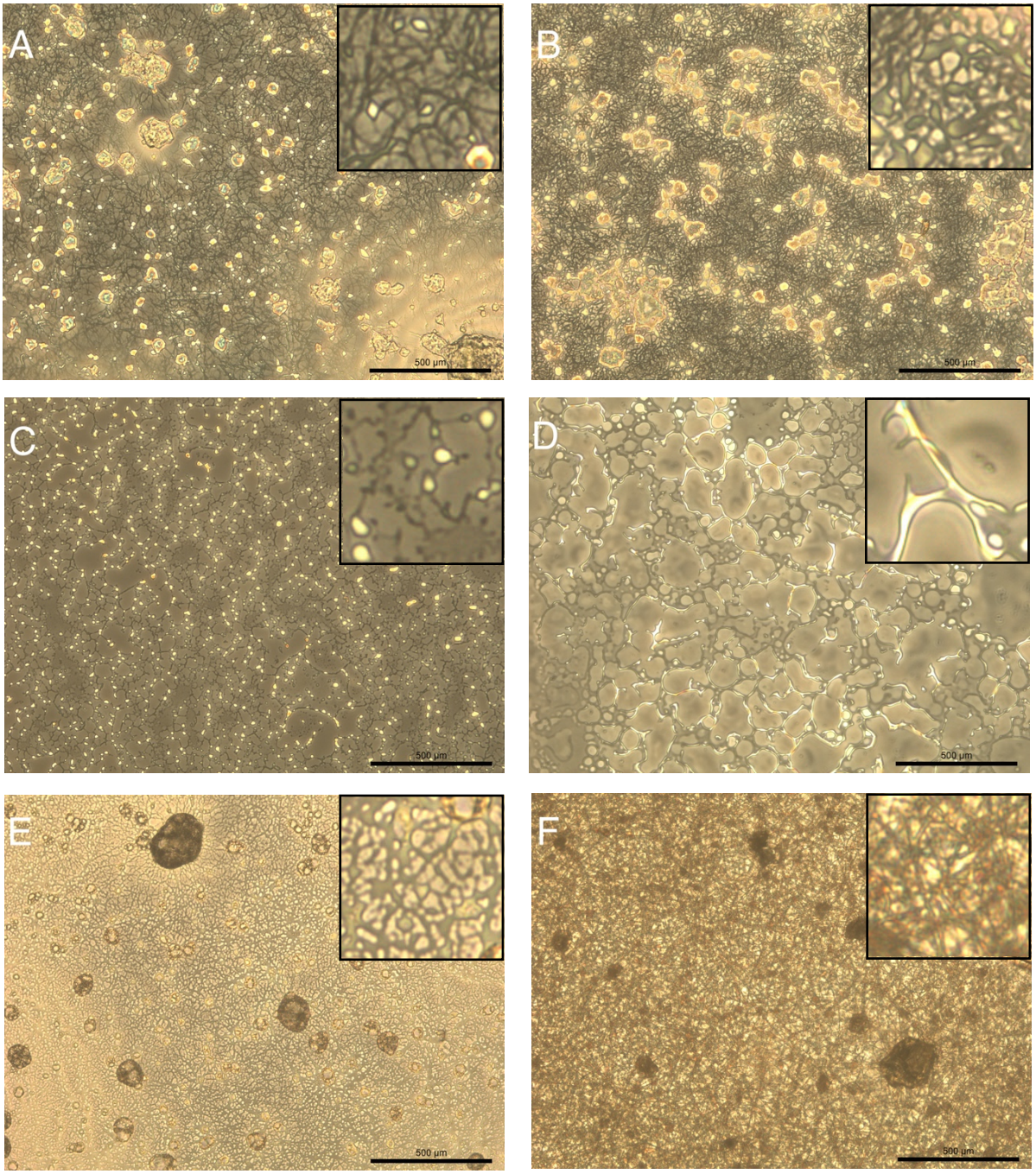

Figure 5.37: Electrospun zein fibres on glass, after treatment with various amounts of EDC/NHS crosslinker solution and immersion in water for 3 days. A: 100% of standard concentration (1.731 g of EDC and 0.415 g of NHS per gram of protein). B: 10% concentration. C: 1% concentration. D: No EDC/NHS, ethanol treated. E: No EDC/NHS treatment, UV treated. F: Untreated, dry. Zoomed inserts are presented in the top right of each image for the respective sample.

This white-light analysis (Figure 5.37) of EDC/NHS-crosslinked electrospun zein fibres shows that there may be room for optimisation for this procedure. Panel B shows that fibres appear stable when treated with 10% of the original EDC/NHS crosslinker amounts, and Figure 5.34 shows that zein crosslinked as such is still able to support cell-growth, albeit to

a lessened degree. Analysis of a finer range of crosslinker concentrations may reveal the value at which fibres are able to hold their morphology for a required length of time with minimal cytocompatibility impairment.

5.2.7 Physical anchorage resulting in stabilised electrospun zein fibres

The white-light analysis of treated fibres shown in figure 5.37 presented an interesting result: the untreated samples did not appear to degrade even after 3 days in water. As previously mentioned, for the purposes of visualisation under white light microscopy, fibres were spun onto glass slides. This apparent stabilisation effect of spinning fibres onto glass was explored in further detail using SEM (figures 5.38 and 5.39).

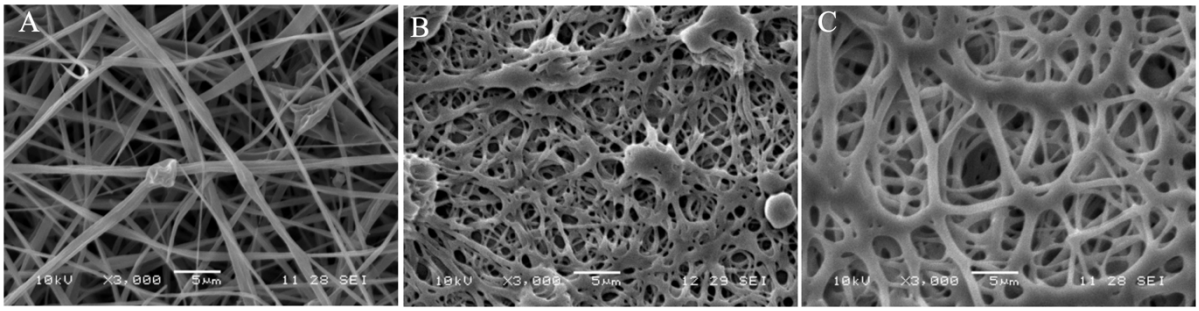

Figure 5.38: SEM of electrospun zein fibres, spun onto glass (otherwise untreated) and soaked in water for various lengths of time. Magnification 3000x. A: Dry, B: 3 days, C: 7 days.

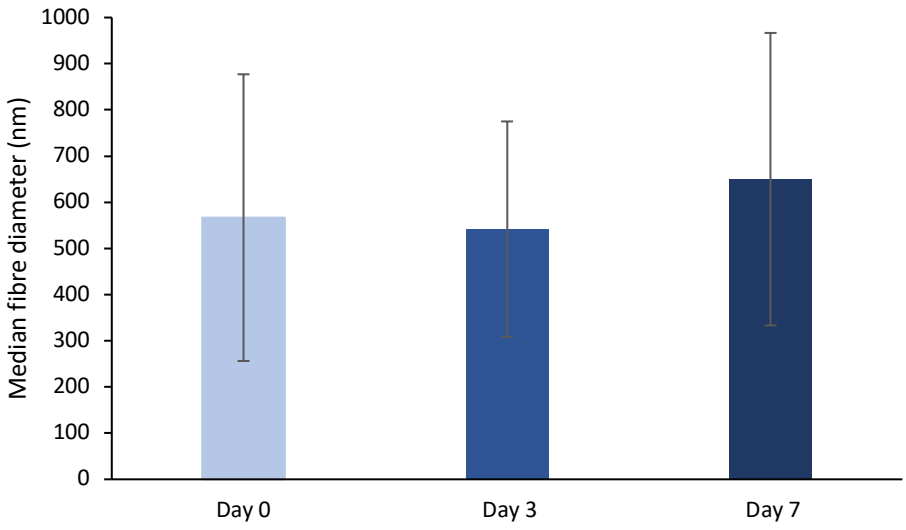

Figure 5.39: Median fibre diameters of zein fibres electrospun onto glass after various lengths of time in water. Data represent median ± interquartile range.

The results were successfully replicated. The electrospun zein fibres on glass appeared to show some degree of swelling after a week in water (Figure 5.39), however they clearly

retain their fibrous structure (Figure 5.38). Also, in comparison with the chemically crosslinked samples wherein the fibres can be seen to aggregate, bend, and entangle with each other (figure 5.29), these fibres appear to maintain their overall structure as a network. Initial speculation entertained the idea that fibres spun onto glass retained their charge. During the electrospinning process, the protein is given a charge at the needle via the electrode, whereupon the molecules are drawn to the collector. On contact with the collector, the protein molecules lose their charge, which travels through the conductive metal and connected grounding wire to earth. Glass however, is an electrical insulator (unless heated, which in this case it was not). The glass cover slides cannot conduct the charge out of the protein molecules, because unlike the ionic lattice of the metal, the atomic structure of glass does not permit the free movement of charge-carrier particles, and this also means that glass cannot be earthed. This may mean that fibres spun onto glass do not lose their charge. However, it is highly unlikely that these fibres would retain this charge during subsequent handling and immersion in aqueous media. It is more likely that the adsorption of the fibre matrix to the glass surface provides anchorage, preventing fibres from being drawn together as porosity is lost, as was the case for every chemically treated sample, the UV-treated samples, and untreated samples (Figures 5.29 – 5.32).

While fibres are drawn into direct physical contact in all chemically and UV-light treated samples, the covalently reinforced structure of the citric-acid (heat treated) and EDC/NHS treated samples allows the fibres to retain their shape. Without this reinforcement, disruption of hydrogen bonding between amino acid residues in the protein by water [318] causes the fibres to lose their structure, and peptide chains associated with separate, individual fibres may form new intermolecular associations, and thus many fibres combine into one large film of zein. In the case of the glass-anchored fibres however, fibres are prevented from coming into contact with each other. Therefore, while some swelling is noted as the plasticising effect of the water takes place, the zein peptides remain confined to their respective fibres, and the overall fibrous configuration is retained.

The next stage after confirming the fibres' stability on glass was to ascertain whether they could also support myoblastic proliferation and differentiation.

5.2.8 Cytocompatibility of physically anchored electrospun zein fibres

Fibres were spun onto glass coverslips (chapter 2, section 2.2.5.6) and cells seeded thereon with coverslips (without fibres) and TCP employed as controls, cell proliferation was

then measured by way of resazurin metabolic assay (chapter 2, section 2.1.2.2) over a period of 7 days, the results of which are displayed in Figure 5.40.

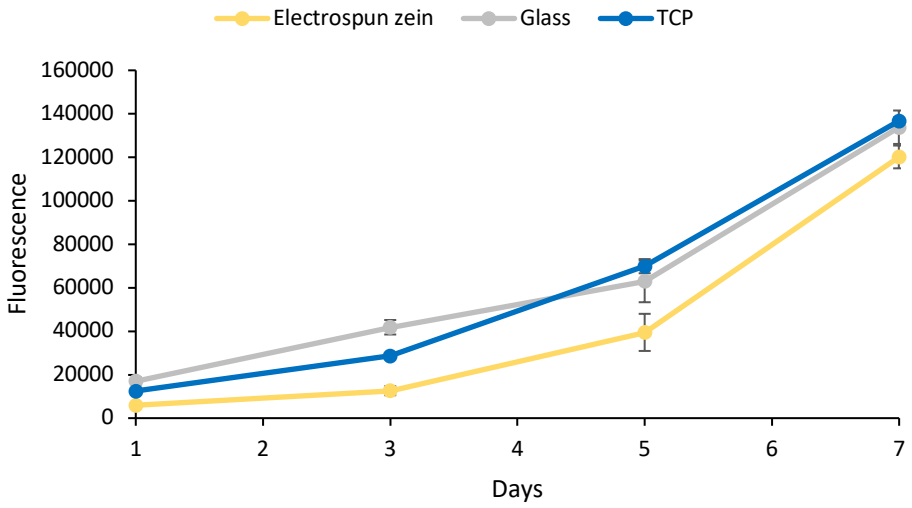

Figure 5.40: Proliferation of C2C12 myoblasts on zein fibres electrospun onto glass versus glass and TCP, measured by way of resazurin proliferation assay. Data represent median ± interquartile range.

The results (figure 5.40) are positive; cells show clear evidence of proliferation on the electrospun zein fibres. This proliferation is slightly less efficient than that observed on the controls. Proliferation on zein fibres was noted to be significantly different to that on glass and TCP ($p < 0.001$ for both comparisons), whereas there was no significant difference between proliferation on glass versus on TCP ($p = 0.142$). As stated in chapter 4, the purity of Sigma-brand zein is not given by the manufacturer, however potential contaminants are likely to be pigments such as beta-carotene and xanthophyll. The process of electrospinning would not introduce any additional impurities or contaminants into the scaffold. A significant difference in cell proliferation between zein fibres and glass provides evidence that the cells are indeed proliferating on the fibres themselves, as opposed to migrating beneath the fibre

matrix and growing on the glass surface beneath. Further evidence for this is provided in figures 5.41 and 5.42.

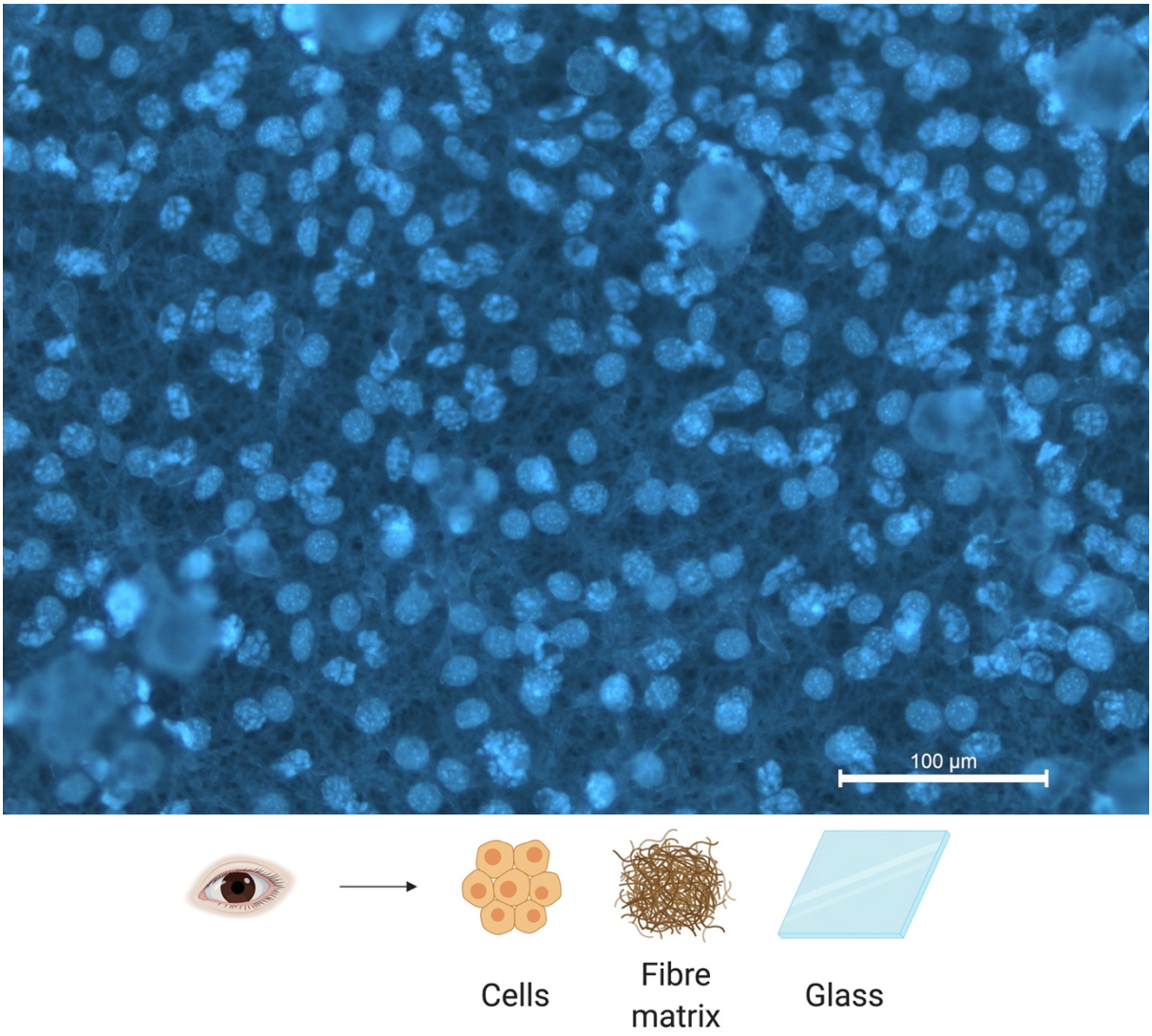

Figure 5.41: Hoescht-stained C2C12 nuclei on electrospun fibres, on glass. Viewed from the top downward: view is of cells, with the fibre matrix farthest away, and the glass slide at the bottom. Scale bars represent 100 µm. Created with biorender.com.

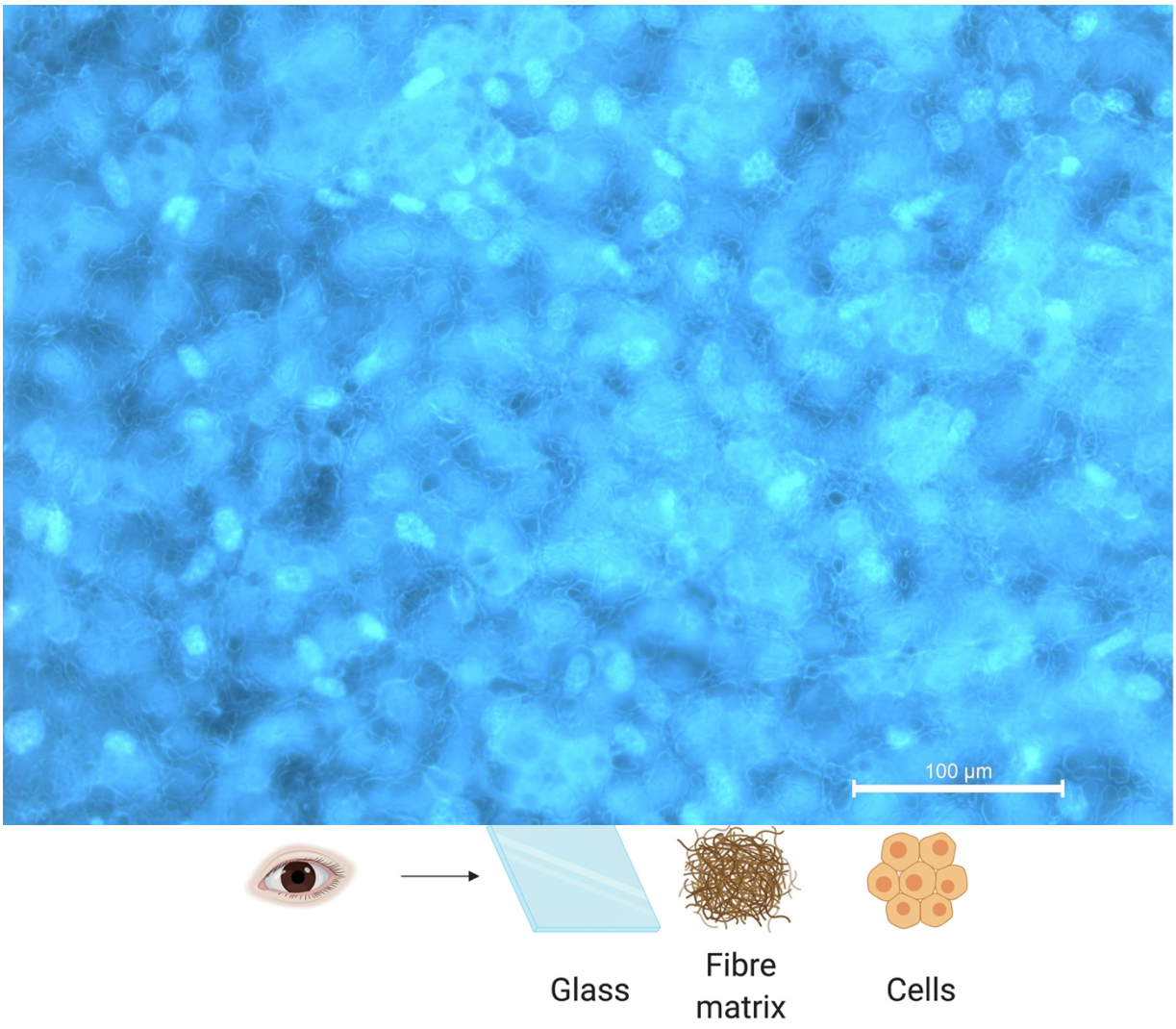

Figure 5.42: Hoescht-stained C2C12 nuclei on electrospun fibres, on glass. Viewed from the bottom upward: looking through the glass, through the fibre matrix, with the cells farthest away. Scale bars represent 100 µm. Created with biorender.com.

Figures 5.41 and 5.42 demonstrate that the cells are indeed growing on and amongst the fibre matrix, as opposed to migrating through it and growing on the glass beneath: the cells are heavily distorted by the thick fibre matrix between them and the lens in Figure 5.42 (which looks up through the glass cover slide), but not in Figure 5.31 (which looks down upon the cells). This is unlikely to be an effect of looking through the glass, as the cover slides were placed onto a glass microscope slide before viewing, and there is no resultant visible distortion in figure 5.41. There is evidence of cell penetration in figure 5.41; a number of nuclei show a series of lines running across them, indicating that these cells have begun to penetrate through pores into intermediate layers of the fibre matrix. Other cells of the

same figure show no such lines, indicating that they reside on the very top layer, at the surface of the fibre matrix. To provide further, more definitive evidence that the cells are in fact adhered to the fibre matrix and not the glass substrate beneath, cells were cultured for one week on electrospun zein fibres (spun and maintained on glass). The samples were prepared and analysed under SEM as per chapter 2, section 2.2.5.9. The results are shown in figure 5.43.

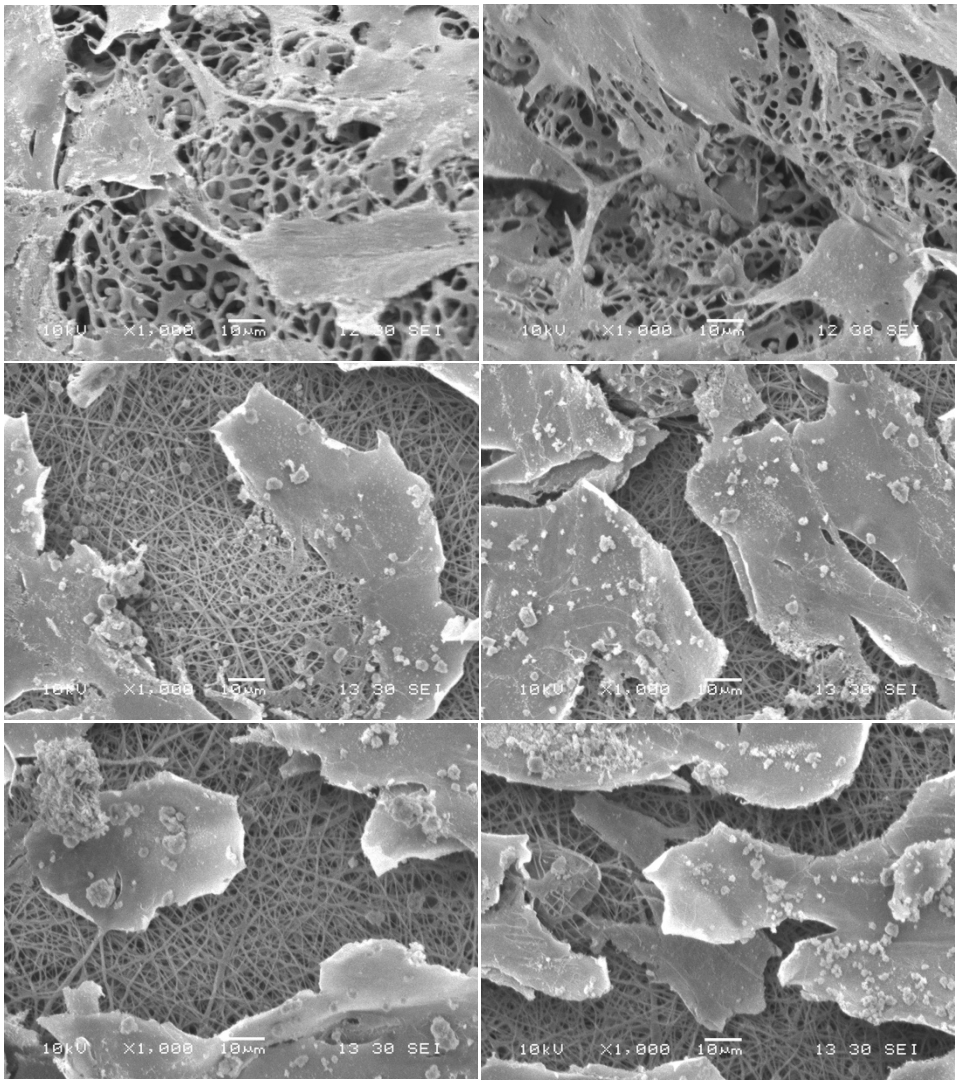

Figure 5.43: SEM of C2C12 myoblasts on electrospun zein fibres, spun and maintained on glass cover slides, after 7 days of culture and fixing by way of GDA and potassium ferrocyanide. Scale bars represent 10 µm.

The cells were cultured to confluence before a harsh fixing procedure which evidently resulted in the cells being broken into plat-like structures. The SEM images displayed in figure 5.43 are very similar in appearance to those of Aviss *et al.* who cultured C2C12 myoblasts on electrospun PLGA fibres and provided SEM images of these cell cultures on the nanofibre matrices [49]. This further demonstrates that the cells are indeed growing on

the fibre matrix. The top row of images shown in figure 5.43 also appear to show a degree of cell penetration into the fibre matrix, suggesting that cells are able to spread and migrate on this scaffold. Also notable is that the second and third rows of images appear to show the fibre matrices as having experience little to no swelling or structural collapse at all (though those of the first row do clearly show signs of swelling, but not to a degree detrimental to their use as scaffolds). It may be that the attachment of cells also imparts a degree of stability to the fibre matrix; it was noted by Lee *et al.* that adherent cells could induce hydrogel formation by crosslinking various polymer chains, as long as these polymer chains had the ability to bind cell-surface adhesion structures [212]. Although this scaffold is composed of dry nanofibers rather than an aqueous suspension of polymer fibres, it is nonetheless plausible that the adherence of cells to various zein nanofibers serves to crosslink the fibre matrix in a similar manner, and thus provides additional stability. As stated, the top row of images in figure 5.43 show that this is not a ubiquitous phenomenon. It may be that this increased stability correlates with the density of locally seeded cells, which would demonstrate the need for a uniform distribution of cells during seeding. Wendt *et al.* note the importance of homogenous distribution of cells when seeding onto a scaffold, and demonstrate how a dynamic seeding approach increases the uniformity of cell distribution onto scaffolds (specifically, by way of fluxing cell suspensions through a porous scaffold) [25]. They also note advantages in seeding high numbers of cells onto a scaffold, such as enhanced differentiation of cardiac cells [25]. If cell adherence to the electrospun fibre matrix does indeed impart additional stability, then this effect may be maximised by seeding high populations onto the scaffolds in dynamic systems, to produce maximal cell coverage with a uniform distribution. Further work may seek to assess whether higher initial-seeding densities of skeletal muscle progenitor cells result in enhanced cell functions as in high-density seeding of cardiac cells [25].

In order to compare the proliferation results on electrospun zein fibres, presented in figure 5.40, to proliferation results on zein films (chapter 4, figure 4.02), the fluorescence of both zein samples was calculated and expressed as a percentage of their respective TCP controls, the results of which are displayed in figure 5.44.

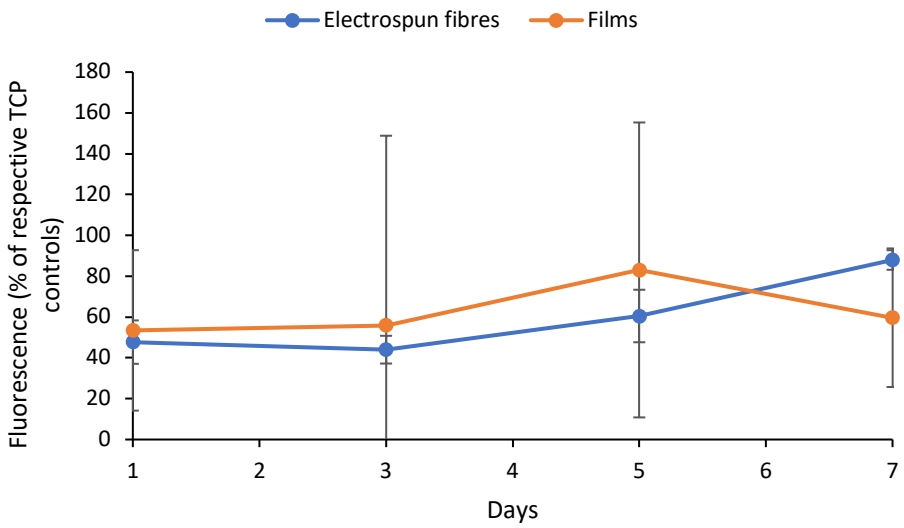

Figure 5.44: C2C12 proliferation on zein films versus electrospun zein fibre matrices, ascertained by way of resazurin metabolic assay and expressed as percentages of the respective TCP controls. Data represent median ± interquartile range.

Statistical analysis of the data presented in figure 5.44 showed there to be no significant difference between electrospun fibres and films ($p = 0.278$). This indicates that electrospun zein fibres are able to support myoblastic cell growth to the same degree as on films. This is a highly positive result; Molnar *et al.* for example cultured myogenic cells on commercially available microcarriers (Cytodex-3 and Biosilon) coated with Matrigel, and noted that proliferation was reduced on these microcarriers in comparison to plates (coated with Matrigel) [85]. In contrast, cells on electrospun zein fibres do not appear to experience a significant reduction in proliferative ability than on zein films. This may indicate that zein has the capacity to outperform Matrigel, a gold-standard ECM-derived mixture of biomaterials, and / or commercially available bioscaffolds, both of which are highly encouraging results.

Anuradha *et al.* produced electrospun matrices from type I collagen and assayed the growth of L6 rat skeletal myoblasts thereon [319]. They noted, in their 3-(4,5-dimethylthiazol-2-yl)-2,5-diphenyltetrazolium bromide (MTT) assay, an increase in optical density from approximately 1.5 (at the start point, 2 days post-seeding) to approximately 2.5 (at the end point, 6 days post-seeding) [319]. The increase in fluorescence on electrospun zein fibres over a similar time period is orders of magnitude greater that the increase in optical density observed on Anuradha *et al.*'s collagen fibres. However, though resazurin and MTT are both reduced by enzymatic activity of cells, even both being reduced by nicotinamide adenine dinucleotide (NADH) co-enzymes [320], the difference in the products of these reactions and the manner in which they are measured (optical density for formazan versus

excitation / emission fluorescence for resorufin [320]) would make direct comparisons between the two (without a calibration curve to clearly define how readings from the two compare) less than fully convincing. The study of Anuradha *et al.* unfortunately does not include a control, which would help contextualise the results both within the study and in comparison to others. Yang *et al.* used a similar procedure, an MTS assay, to quantify proliferation of human periodontal ligament stem cells on electrospun zein matrices, as well as electrospun matrices formed from zein / gelatin blends [137]. They noted an increase in optical density from approximately 0.2 to approximately 0.8 on pure zein fibres between the 1 and 5 day timepoints [137]. They also noted that the incorporation of gelatin, when present in at least a 2:1 ratio to zein (the highest gelatin content of their samples) consistently enhanced cell proliferation on the fibres to a slight but significant degree [137]. This would suggest that although gelatin facilitates cell proliferation on electrospun fibres to a degree higher than that on zein fibres, zein does not fall far behind in this regard, though the difference in cell types, myoblasts versus human periodontal ligament stem cells (HPLSCs), must be taken into account.

Li *et al.* provide a more comparable study, in which H9c2 myoblasts are cultured on electrospun fibres formed from blends of PLGA, gelatin, and elastin, whose proliferation was tracked by way of alamar blue (whose active ingredient is resazurin) against TCP controls [239]. They noted that incorporation of gelatin and elastin into the electrospun fibres, resulted in significantly higher proliferation, compared to TCP, at the final (8-day) timepoint [239]. Before this, any differences were not noted to be statistically significant [239]. In contrast, electrospun zein fibres were able to support proliferation to a degree showing no significant difference to TCP at the final (7-day) timepoint. The degree of proliferation was significantly lower on zein than that on TCP at 2 of the 3 preceding timepoints. This would indicate that myoblasts cultured on electrospun fibres which incorporate ECM proteins into their composition proliferate with greater efficiency than on zein fibres, being able to maintain step with TCP controls and surpassing them at 8 days, while those on zein fibres lag slightly behind TCP controls but equalising therewith at 7 days.

This is still a highly positive result, as myoblastic proliferation on a plant-derived peptide-based electrospun scaffold does not appear drastically reduced compared to that on electrospun scaffolds including ECM proteins. This design of zein scaffold is able to support myoblastic proliferation, using an edible, plant-based, inexpensive biomaterial that needs no further processing after generation of the electrospun nanofibers.

It is not sufficient, however, that cells simply proliferate on the scaffold. For the purposes of muscle-tissue culture, it is necessary that cells are able to differentiate, fusing into myotubes. In order to ascertain whether the electrospun zein fibre matrices were able to facilitate myogenic cell differentiation, cells were cultured to differentiation (chapter 2, section 2.1.1.4), after which they were fixed and immunostained for myosin heavy chain in order to visualise any myotubes present as per chapter 2, section 2.1.2.3. It was confirmed that the cells growing on these electrospun zein fibres were able to differentiate into myotubes (Figure 5.45).

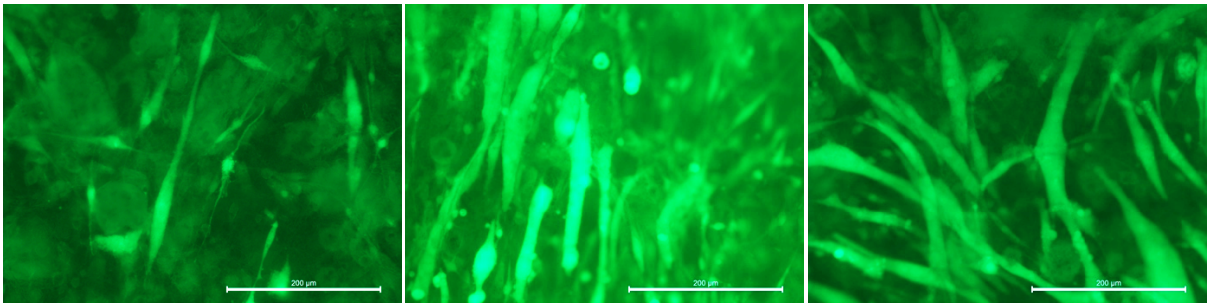

Figure 5.45: Confirmation of C2C12 myotubes on electrospun zein fibres. Scale bars represent 200 μm.

This is also a highly positive result; myoblasts are able to form myotubes, the beginnings of complete muscle tissue, on electrospun zein fibres without the need to incorporate animal-derived proteins. This makes zein comparable to other, more commonly used biomaterials such as PLGA [49], PCL [9], poly-L-lactic acid (PLLA) [321], and collagen [9, 321], in terms of its ability to facilitate the formation of myotubes on electrospun fibre matrices. Further work may seek to quantify the efficiency of myotube formation, in terms of fusion index, in comparison to electrospun fibre matrices formed from other biomaterials (particularly those derived from ECM).

Observable in figure 5.45 is a lack of alignment amongst myotubes. It is important to induce alignment in myotubes as seen in vivo, where aligned myotubes bundle together to form fascicles, which in turn align and cluster together to form complete muscle [322]. Therefore, attempts were made to generate aligned electrospun fibres as described in chapter 2, section 2.1.1.4. The results of these attempts are shown in figure 5.46.

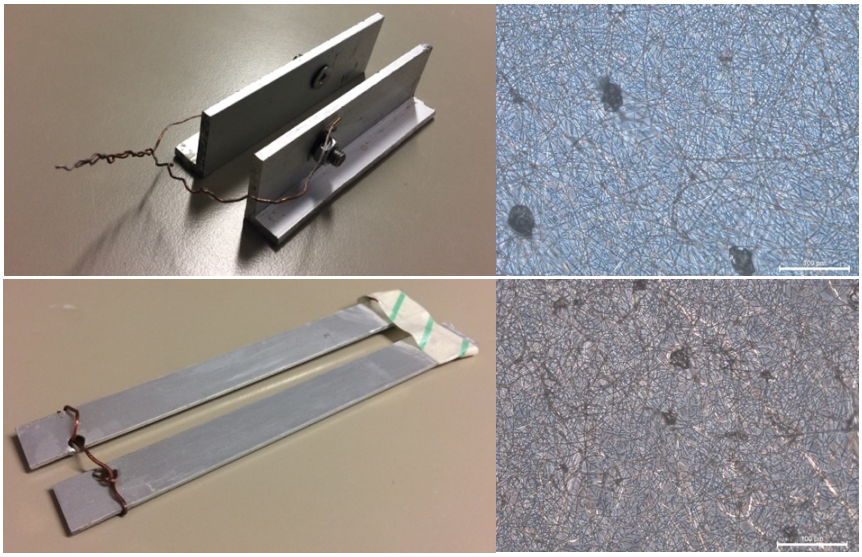

Figure 5.46: Attempts to generate aligned electrospun fibres by using spaces, parallel collectors. Left: photos of collector apparatus. Right: White-light microscopy of resultant nanofibers. Scale bars represent 100 μm.

Unfortunately, neither apparatus was able to collect aligned electrospun fibres. The white-light microscopy images presented in figure 5.46 clearly show matrices with random fibre alignment. This may be due to the use of the glass cover slide: Li *et al.* point to the introduction of the gap in the collector assembly as the causal factor for fibre alignment [141], and the placement of the glass cover slide bridges this gap. However, the insulative nature of the glass would mean that this does not necessarily 'join' the two collectors. Nevertheless, this particular method of aligning nanofibers would present problems with regard to scale-up; Teo *et al.* note that this technique is constrained by its lack of capacity to produce thickly layered mats (whilst maintaining alignment of fibres), as well as the distance between the collectors [323]. There are, however, other methods by which aligned electrospun fibres can be collected, to be discussed further in section 5.3.4.2.

5.3 Further work and wider implications

5.3.1 Other means of scaffold production

An alternative procedure by which fibrous scaffolds can be produced is dry-spinning [14]. In this model, the polymer solution is extruded as a jet through a column, into which hot air is blown [14]. The heat from the air causes the solvent to evaporate, resulting in a solid fibre of the polymer, which can be collected using a winding spool [14]. This technique has been

used, for example, to produce silk fibroin fibres [324, 325]. Spray-drying is a technique by which microparticles can be produced, operating on principles very similar to those of dry-spinning; a spray of polymer solution is rapidly dried with hot air, resulting in a powder-like spray of dried polymer microspheres [326]. These techniques may be applicable to the production of zein scaffolds, given zein's solubility in aqueous alcohol solutions, which would exhibit relatively low evaporation temperatures.

5.3.2 Mechanical analysis and optimisation

It was noted from handling that the electrospun mats seemed much more flexible than the films described in chapter 4. It was also noted, again from handling, that they were more easily pulled apart. Mechanical analysis should be conducted to confirm whether the electrospun mats do indeed exhibit reduced stiffness and tensile strength in comparison to films. A reduction in stiffness would be beneficial, as the films were noted to have excessively high elastic moduli. Reduced tensile strength may present potential issues when applying tensile forces to cell-laden scaffolds to provide mechanical stimuli to cells.

It is noted that, in a porous protein-based scaffold, the presence of microparticles of the protein can affect the mechanical properties of the overall scaffold [327, 328]. Purwanti *et al.* formed gels from whey protein isolate, as well as whey protein isolate microparticles (insolubilised by way of heating until denaturation of the protein occurred) [328]. They noted that gels whose total protein concentration was comprised of a higher percentage of microparticles exhibited reduced stiffness [328]. Rajkhowa *et al.* applied a very similar technique to their salt-leached silk fibroin scaffolds [327]. They noted that loading their porous scaffolds with silk fibroin microparticles increased the yield strength of the scaffold, and that this increase correlated with the degree of particle loading [327]. For this technique to be applicable to zein scaffolds, it would be necessary to produce insoluble zein microparticles. Malumba *et al.* noted that drying corn kernels at high temperatures (up to 130˚C) resulted in a significant reduction in the yield of zein obtained by solvent extraction [329]. It may therefore be possible to produce insoluble zein microparticles, and use them to produce stronger, more flexible electrospun zein mats.

5.3.3 Digestion analysis of crosslinked zein

As previously mentioned, the citric acid crosslinking technique differs from that of EDC / NHS crosslinking in that the citric acid method results in the peptides being bridged, rather than directly joined. This modification may result in potentially undesirable products after

digestion, and so it may be prudent to analyse the digestion of citric-acid-crosslinked zein *in vitro*. Bronhorst and Singh [330], for example, produced simulated saliva by mixing mucin glycoprotein, alpha-amylase enzyme, sodium and potassium chloride, and sodium carbonate in deionised water (at neutral pH). They also produced simulated gastric juice by mixing mucin, pepsin enzyme, and sodium chloride in deionised water (whose pH was adjusted to 1.8 – 2.0 via addition of hydrochloric acid). The products of digestion could then be analysed under NMR spectroscopy in order to detect any potentially harmful organic structures.

5.3.4 Further analysis and development of microparticles

Given the small size of zein microparticles generated by microfluidic flow focusing when using vegetable oil as the continuous phase, as well as those produced by emulsification precipitation, these techniques may be applicable to drug encapsulation (which, as mentioned in section 5.1, appears to be the major focus of studies utilising zein as a biomaterial). Although these techniques would require refinement, as microparticles for drug encapsulation are commonly found in the nanoscale size range, and many of the microparticles produced for zein exceeded 1 μm in diameter. If the mean size of these microparticles could be reduced (while maintaining a narrow size distribution), they could be produced from a solution of protein mixed with therapeutic agents, and analysed for their release-profiles in physiological conditions.

It may also be prudent to investigate other cytocompatible, protein-based biomaterials for their ability to produce adequately sized microcarriers for surface-seeding of cells. To this end, preliminary experiments were conducted to produce silk fibroin microcarriers, as silk fibroin microparticles have demonstrated the ability to interact with cells. Nisal *et al.* for example, produced silk fibroin microparticles by extruding droplets of silk fibroin into a methanol coagulation bath; their microparticles held diameters well in excess of 100 μm and were able to support the growth of osteoblasts [331]. Li *et al.* produced silk fibroin microparticles via electrospinning, which resulted in a series of connected beads, with diameters roughly around 1 μm [332]. These particles, rather than being used for surface-seeding, were endocytosed by cells to demonstrate their potential as drug-carriers [332]. The use of microfluidic flow focusing to produce silk microcarriers seems rare but not unprecedented: Luetchford *et al.* were able to synthesise microcarriers composed of silk fibroin and gelatin (blended to various ratios) via microfluidic flow focusing which showed positive cytocompatibility [89].

Initial attempts to produce silk fibroin microparticles by microfluidic flow focusing used vegetable oil as the continuous phase, and the particles collected into methanol solution (chapter 2, section 2.2.3.2). The disperse phase was aqueous silk fibroin solution. The solutions were pumped through bespoke 3D printed apparatus as illustrated in chapter 2: figure 2.07. The results of this experiment are shown in figure 5.47 and 5.50-D

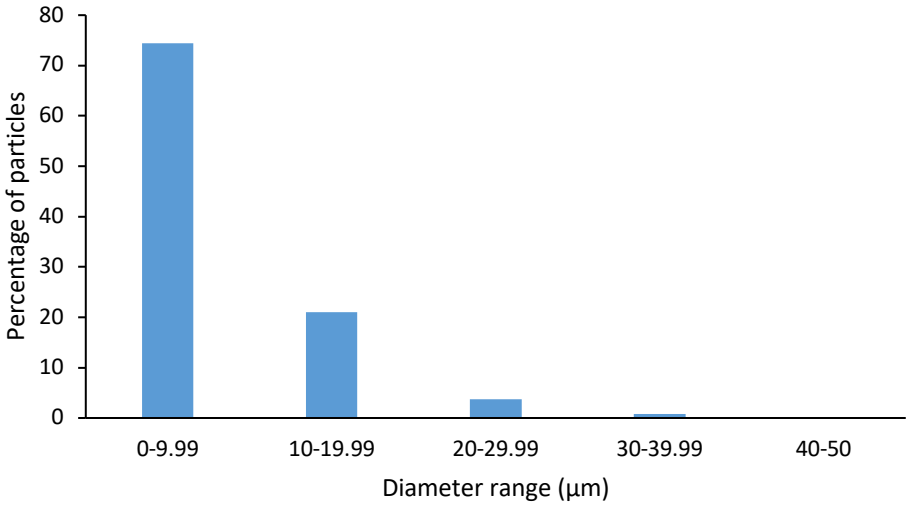

Figure 5.47: Size range of silk fibroin microparticles produced by microfluidic flow focusing, using vegetable oil as the continuous phase and methanol as the coagulation bath. $Q_o = Q_i \times 20$. Q_i represents a disperse phase flow rate of 0.015 ml / min. Data represent individual observations. Median particle diameter was 7.65 ± 3.99 µm.

Particles in this initial experiment were far too small to accommodate surface-seeded cells, with no particles showing a diameter in excess of 50 µm. The experiment was retried with a new continuous phase (chapter 2, section 2.2.3.2), which in this case consisted of oleic acid, methanol, and span 80 (at ratios of 73 : 25 : 2 (respectively). The particles in this instance were collected in a solution composed of methanol and continuous phase at a ratio of 50 : 50. The results of this experiment are given in figures 5.49 – 5.50.

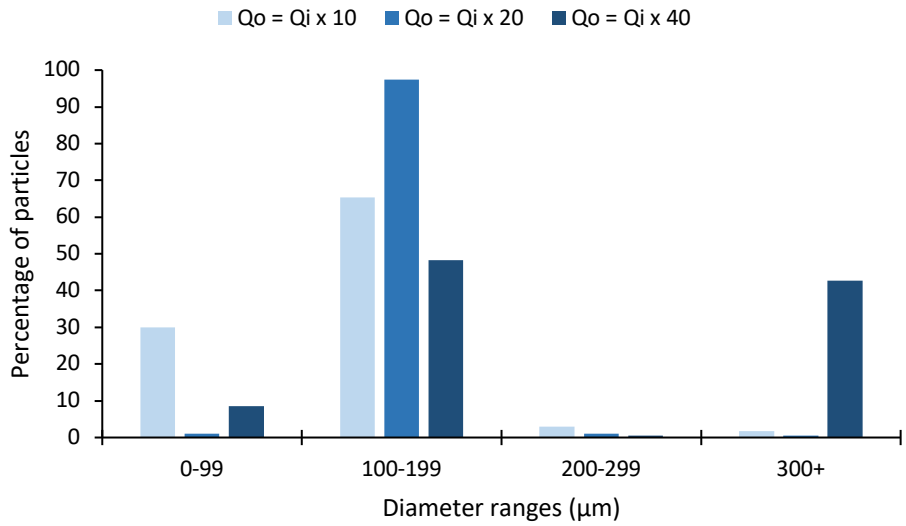

Figure 5.48: Size distribution of silk fibroin microparticles produced by microfluidic flow focusing, using oleic acid : methanol : span 80 as the continuous phase and methanol : continuous phase as the coagulation bath. Q_i represents a disperse phase flow rate of 0.015 ml / min. Data represent individual observations.

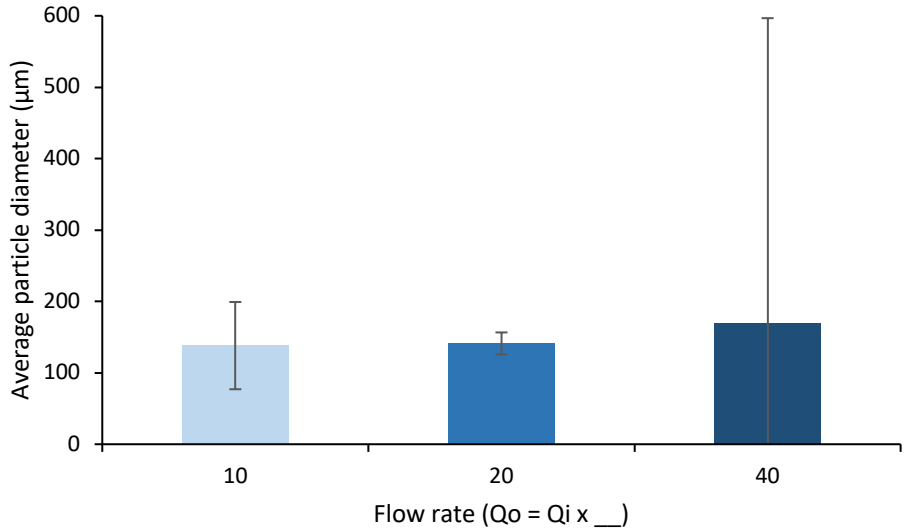

Figure 5.49: Mean particle diameter of silk fibroin microparticles produced by microfluidic flow focusing using oleic acid : methanol : span 80 as the continuous phase and methanol : continuous phase as the coagulation bath. Q_i represents a disperse phase flow rate of 0.015 ml / min. Data represent median ± interquartile range.

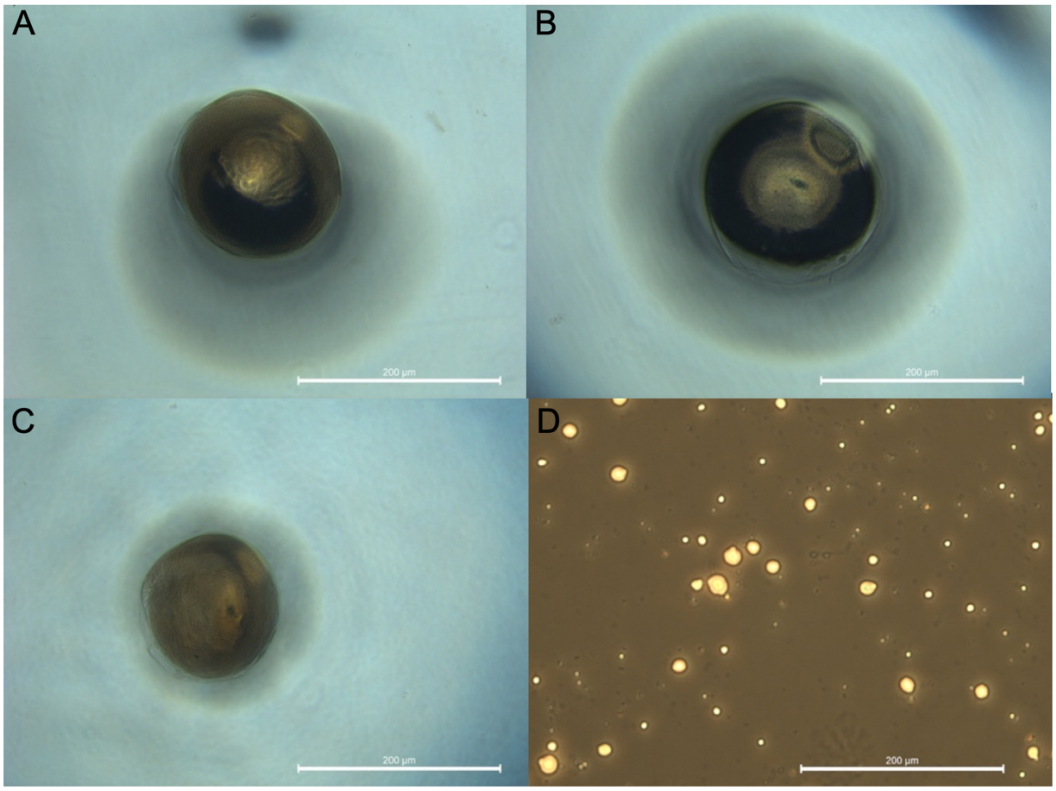

Figure 5.50 Representative images of silk fibroin microparticles produced by microfluidic flow focusing. A – C represent microparticles formed under conditions as stated for particles of figure 5.49 and 5.50: (A: $Q_o = Q_i$ x 10, B: $Q_o = Q_i$ x 20, C: $Q_o = Q_i$ x 40). D represents microparticles formed under conditions as stated for particles of figure 5.48. Q_i was maintained at 0.015 ml / min. Scale bars represent 200 µm.

All images (figure 5.50) were captured under white light microscopy, particles for A-C were removed from solution and photographed individually whilst those for D, due to their much smaller size, were photographed in solution. As a result, the background appears substantially darker in D than in A-C. Use of a different continuous phase has clearly had an impact on the resultant particles. With a flow rate of $Q_o = Q_i$ x 20 where Q_i represents a disperse phase flow rate of 0.015 ml / min, the switch from vegetable oil + span 80 to oleic acid + methanol + span 80 as the outer phase triggered an increase in mean diameter of the particles from 9.21 µm (figure 5.47) to 144 µm (figure 5.49).

The mean diameters of silk fibroin / gelatin microparticles produced by Luetchford *et al.* with the lowest gelatin content, showed a negative correlation with continuous phase flow rate; the mean diameter decreased as the flow rate of the continuous phase increased relative to the disperse phase [89]. Oddly, the microparticles generated here did not appear to follow this trend. There seemed to be a slight increase in mean particle diameter as the continuous phase flow rate increased from 10x that of the disperse phase to 20x, but a drastic increase

from 20x to 40x (figure 5.49). Figure 5.50 shows that this increase in mean diameter is owed to an increase in microparticles of above 300 μm in diameter. This may warrant further experimental repeats in order to ascertain whether the lack of a negative correlation between continuous phase flow rate and resultant particle diameter is an anomalous result. As discussed in section 5.1.3, microparticles with an approximate diameter range of 125 – 300 μm have been shown to be compatible with myogenic cells. This would suggest that microfluidic flow focusing procedure (using oleic acid, methanol, and span 80 as the continuous phase) successfully produces silk fibroin microparticles of sufficient size as to accommodate surface-seeded myogenic cells.

Given that silk fibroin microparticles were produced with sufficient diameters as to accommodate surface-seeded cells, a clear next step for these scaffolds is to analyse their compatibility with myogenic cells. As stated in section 3.3.3, silk fibroin from various species of insect may be worth investigating. If silk fibroin microparticles were produced in the same way using silk fibroin originating from various species of insect, a comparative analysis of cytocompatibility and surface characterisation (such as measurement of porosity) may also prove to be worthwhile avenues of investigation.

5.3.5: Refinement and further exploration of electrospun fibre crosslinking

As discussed, treatment of electrospun zein fibres using EDC/NHS appeared to impair the fibres' ability to bind cells. This was unfortunate, as this treatment could be carried out in a much shorter timeframe than treatment via citric-acid. A brief analysis of the ability of zein films treated with various amounts of EDC/NHS crosslinker to support cell growth was carried out, however a more thorough exploration of this relationship may be called for, using a narrower and more precise range of crosslinker amounts, and analysing proliferation over a longer period of time (as well as differentiation). This should also be done for fibre stability (denoted by fibre diameter over time). It may be possible to clearly define a range of EDC/NHS crosslinker amount wherein the critical stability of fibres in aqueous environments is achieved, but without significant loss of cytocompatibility.

There may be other crosslinking techniques applicable to electrospun zein scaffolds which may prove more effective than those analysed herein. Deng *et al.* for example, employed crosslinking via glucose to stabilise their electrospun blends of zein / gelatin [333]. This technique relied on the Malliard reaction [333], wherein reducing sugars react with amino acids [334]. Selling *et al.* utilised glyoxal as the crosslinking agent for their electrospun zein

fibres [335], glyoxal is known to be an intermediate product in the Malliard reaction [336]. If proven to be time-efficient, crosslinking techniques relying on naturally occurring and non-toxic crosslinking agents such as sugars would be preferable to expensive, toxic crosslinking agents such as EDC and NHS.

5.3.6: Structural properties of fibres

5.3.6.1: Fibre diameter

Fibre diameter is noted to be an influential factor on the behaviour of cells [137]. Yang *et al.* noted that as the diameter of their zein / gelatin nanofibers was increased, the ability of human periodontal ligament stem cells to adhere and proliferate thereon was enhanced [137]. Hsia *et al.* also report a significant effect of electrospun fibre diameter on the behaviour of cells, they noted that cells cultured on nanofibers proliferated more quickly than those on microfibres within the first week of culture, but by the end of the second week microfibres held a more dense cell population than nanofibers [337]. Of course, the conditions of the electrospinning process can be manipulated in order to produce fibres of various mean diameters. Tan *et al.* note that the voltage applied to the spinneret, the needle gauge, the distance from the spinneret to the collector (which would influence the degree of stretching and whipping of the fibre), and the flow rate to be factors which impact the diameter of electrospun fibres [338]. They, as well as Mit-uppatham *et al.* noted that the properties of the polymer solution, such as viscosity and conductivity, can also influence the diameter of electrospun fibres [338, 339], these factors may be adjustable by varying the solvent in which the zein is dissolved. It may be an enlightening avenue of investigation to produce electrospun zein fibres with a range of mean diameters by varying these conditions, and analysing the effect on cell behaviour.

5.3.6.2: Fibre alignment

In order to induce alignment of myotubes cultured on the electrospun fibre matrices, it is necessary to produce aligned electrospun fibres. An interesting, and commonly cited, approach to generating aligned electrospun fibres is the use of a high-speed rotating mandrel as the collector. Ghasemi-Mobarakeh *et al.* used a disk rotating at 1000 rpm to collect aligned nanofibers electrospun from blends of PCL / gelatin [340]. Choi *et al.* rotated a stainless steel plate at various speeds in order to control the orientation of their PCL / collagen nanofibers [9]. Subramanian *et al.* rotated a tubular mandrel at speeds varying

from 1000 rpm to 2500 rpm to control alignment of their PLGA nanofibers [341]. The aforementioned of study of Aviss *et al.* whose PLGA nanofibers showed compatibility with C2C12 myoblasts, also used a rotating mandrel as their collector plate, and noted that an increase in rotation speed from 300 rpm to 1500 rpm resulted in production of aligned nanofibers [49]. This rotating mandrel approach to generating aligned electrospun fibres may hold the potential to intertwine with bioreactor design in a model of cultured meat production.

5.3.7 Dynamic cell-seeding at high densities

The adherence of cells to the electrospun fibre matrices appeared to impart additional stability, with some areas of the fibre matrix appearing to have suffered no structural changes even after more than a week of cell culture (figure 5.43). If cells were seeded onto these scaffolds with high initial densities, with a uniform distribution, this effect could potentially be maximised. As stated, the study of Wendt *et al.* noted that oscillating perfusion of cell suspension through a porous scaffold resulted in uniform distributions of cells seeded thereon [25]. It may be beneficial to analyse the effect of dynamic seeding, in a manner similar to that of Wendt *et al.* [25], on cell adhesion and distribution. This could also be done in order to ascertain whether or not cell adhesion to the fibres imparts stability to the matrix by crosslinking, similar to the mechanism described by Lee *et al.* [212]. Furthermore, Wendt *et al.* cite a study in which high densities of seeded cells enhanced the differentiation of cardiac cells [25, 342]. The aforementioned experimental design could also be employed with the aim of studying the effect of high seeding-densities on skeletal muscle myoblast behaviour.

5.3.8: Bioreactor design

Allowing the electrospun zein fibres to remain in contact with the surface of the collector appears to be a simple and effective means by which to prevent their degradation in aqueous solutions. An ideal bioreactor design may, therefore, incorporate the collector into its design. With this in mind, a particularly attractive design for the collector is the wire-drum mandrel as designed and employed by Katta *et al.* [343]. In their model, a series of copper wires are stretched between two discs to form a cylinder 30 cm in length, which is placed horizontally beneath the spinneret and rotated as electrospinning takes place (figure 5.51).

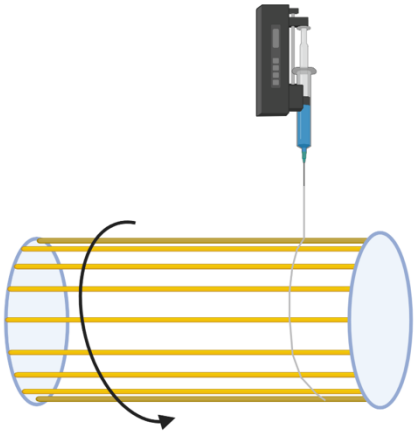

Figure 5.51: Schematic of the rotating wire-drum mandrel used by Katta *et al.* [343] to produce aligned electrospun fibres. Created with biorender.com.

An immediate advantage of their technique is the production of highly aligned fibres with an extremely slow rotation speed (reported as 1 rpm [343]), compared to previously mentioned studies where rotation speeds in excess of 1000 rpm were required in order to generate aligned fibres [49, 341]. A drawback to their technique was a loss of fibre alignment as the thickness of the mat increased, though the reason for this phenomenon was not ascertained [343]. Katta *et al.* theorised that the insulative nature of the polymer being electrospun (nylon) may be the causal factor [343]. This may indicate that production of thick mats is possible under the appropriate conditions.

It is speculated here that zein fibres could be electrospun onto a wire-drum mandrel similar to that of Katta *et al.*. This mandrel could then be, along with the aligned nanofibers, transferred to a bioreactor. The structure of intermittent copper wires (as opposed to a fully solid rotating drum) may allow for a direct-perfusion system for delivery of culture medium (wherein culture medium flows through pores in the scaffold), and perhaps even cell-seeding within the bioreactor itself (eliminating the need to seed the cells separately). As discussed in chapter 1, such direct-perfusion approaches to cell seeding are noted to facilitate high levels of cell adherence, even when compared with other dynamic seeding systems such as stirred flasks [25]. The copper wiring would also allow for electrical stimulation of adhered myogenic cells to produce contractile mechanical stimuli. This spaced-wire design may also be adaptable so as to allow for exertion of longitudinal stress forces. If some expandable vessel were placed at the centre of the cylinder, it could

theoretically be inflated in order to stretch the surrounding copper wires apart, thusly stretching the fibre matrix and adhered cells (figure 5.52).

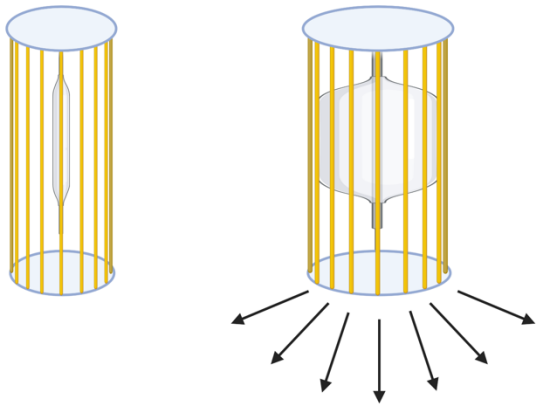

Figure 5.52: Theoretical schematic of the wire-drum mandrel with an inflatable vessel at the centre in order to exert longitudinal stress stimuli on cultures cells. Created with biorender.com.

Alternately, it may be possible to design the wire-drum in such a way that, after fibres have been produced, a section of connecting material between two of the wires can be ‘uncoupled’, and the cylinder unrolled into a sheet. If the copper wires were connected by a material with some degree of elasticity, it could be stretched along a single axis, as illustrated in figure 5.53, rather than by increasing the diameter of the cylindrical model (figure 5.52). This would also simplify the direct-perfusion system of cell-seeding and nutrient delivery.

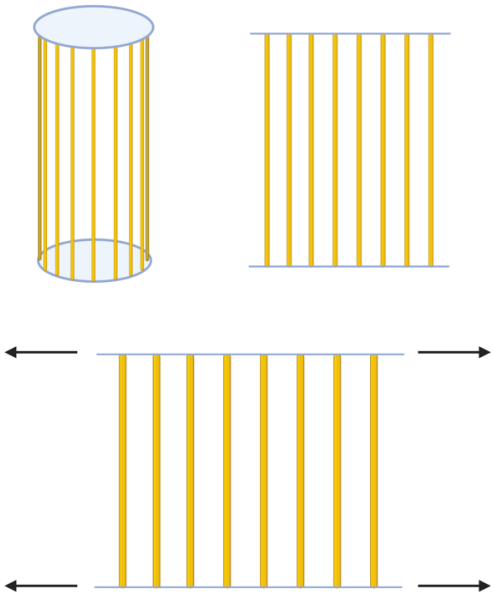

Figure 5.53: Theoretical model in which the wire-drum mandrel is ‘unrolled’, and tensile forces applied. Created with biorender.com.

After cells have been cultured on electrospun zein nanofibres into muscle tissue, the sheets of tissue could be removed from the copper wires and layered atop one another. These may be further treated with transglutaminase in order to bind them together into a continuous block of meat; this transglutaminase-mediated binding of meat is in fact a technique used in the food industry, wherein it is referred to as “meat glue” [344]. This concept is illustrated in figure 5.54. If muscle-tissue were produced in this way using autologous progenitor cells from a patient, it could theoretically be applied in the form of grafts to repair damaged muscle tissue *in vivo*. Indeed, zein scaffolds have been utilised *in vivo*; Tu *et al.* were able to produce porous zein scaffolds onto which they seeded rabbit-derived mesenchymal stem cells [138]. When these constructs were implanted into the thigh muscle-pouches of mice, and bone formation was noted after 12 weeks [138]. Therefore, this design of bioscaffold may hold potential for regenerative medicine applications. This concept is illustrated in figure 5.55.

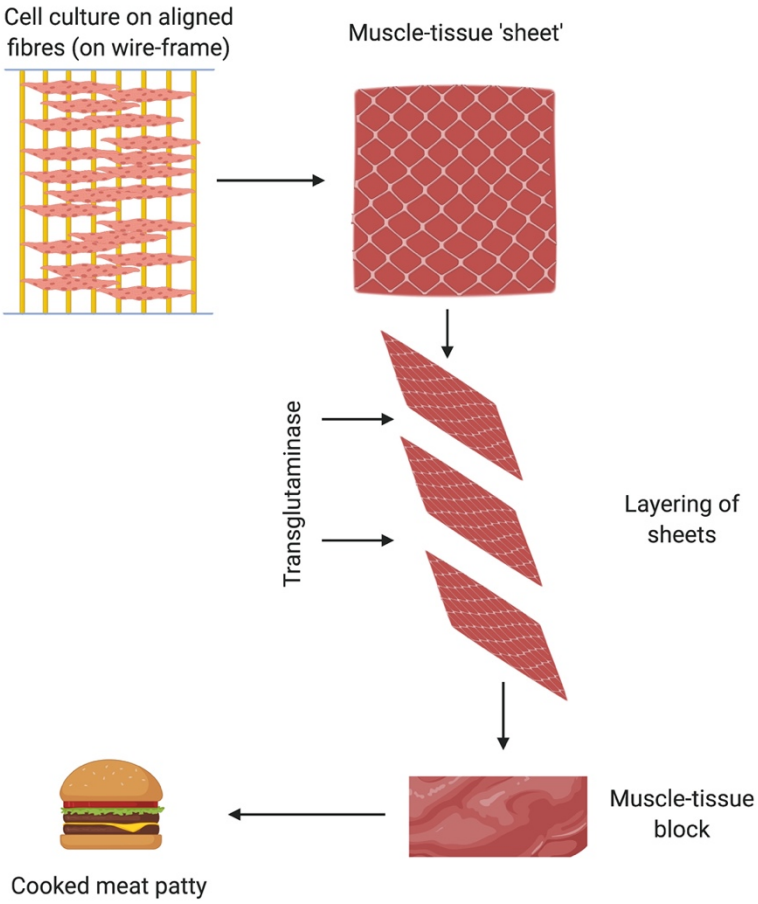

Figure 5.54: Concept of cultured meat produced using aligned electrospun zein fibres on wire-frame substrates. Created with Biorender.com.

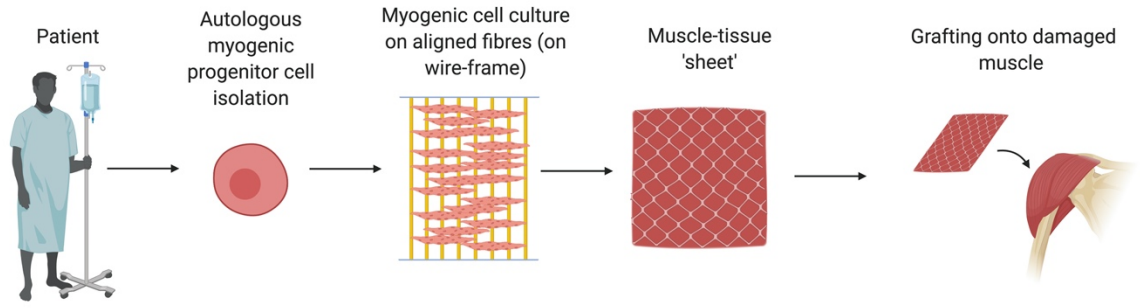

Figure 5.55: Concept of autologous muscle-tissue production using aligned electrospun zein fibres on wire-frame substrates for regenerative medicine applications. Created with Biorender.com.

5.4 Concluding remarks

The use of vegetable oil (plus a surfactant) as the continuous phase in microfluidic flow focusing failed to generate microparticles of sufficient size for surface-seeded cells. Further

exploration of continuous phase may provide a means to increase the size of these microparticles. Emulsification precipitation also failed to generate zein particles of sufficient size.

Wet-spinning techniques failed to generate zein fibre membranes. This was likely due to inadequate diffusion of the polymer solvent into the surrounding water, which acted as a non-solvent for the zein. Exclusive use of solvents which are miscible in water (such as aqueous ethanol) may improve results.

Electrospinning consistently produced matrices of zein nanofibers. These electrospun fibres, however, were noted to be unstable in water, and collapsed into films when immersed in aqueous solutions. This is likely due to the plasticising effect of water on the fibres. Crosslinking via chemical treatment showed promise in terms of providing a means by which to stabilise these fibres. Treatment with EDC/NHS, as well as with citric acid (with subsequent heat treatment) resulted in fibre mats which did not appear to shrink (when analysed at the macroscopic level), and whose fibres maintained their fibrous shape even after a week immersed in water. These techniques were not without their drawbacks, however. EDC/NHS treatment appeared to impair the ability of the zein to support myogenic cells, and citric-acid treatment was not time-efficient, requiring multiple days to carry out. It was noted that fibres did not appear to destabilise in water when affixed to a rigid substrate (in this case, glass cover slides), and this may be due to physical anchorage preventing the fibre mat from shrinking. These stabilised zein fibres were shown to be able to support proliferation and, crucially, differentiation of C2C12 myoblasts, and so electrospun zein fibres show significant promise as potential bioscaffold on which muscle-tissue can be grown.

Silk fibroin microparticles of sufficient size to accommodate surface-seeded cells were produced, however as shown in chapter 4, zein appears to show more inherent cytocompatibility, and so would appear to be the preferential choice for a scaffold.

Whilst the wet-spinning approach to producing zein fibres may be developed by further exploration of polymer solvents (and resultant scaffolds applicable to hollow-fibre membrane reactors), electrospinning appears to be the most effective method by which to produce a zein scaffold compatible with bioreactors.

Electrospun zein nanofibres can be easily stabilised by allowing them to remain adsorbed to a rigid substrate, and can effectively support the proliferation of myoblasts as well as their

fusion into differentiated myotubes. This was a highly positive result, as a bioscaffold was successfully produced from an edible, renewable, plant-based biomaterial which could support growth and differentiation of myogenic cells. Furthermore, the method by which this scaffold was produced was simple and largely automated after the initial setup. The scaffold required only adsorption to a substrate material in order to overcome instability in aqueous environments, with no need for chemical modification. Electrospun zein fibres appear to be a highly promising candidate for an ideal bioscaffold for cultured meat applications, and its strengths in terms of scalability may also open avenues for regenerative medicine applications.

Chapter 6 – Summary, further work, and final conclusions

6.1 Summary

6.1.1 Carrageenan hydrogels

Carrageenan hydrogels were produced, in fibrous and particulate forms, by extruding 2% (w/v) carrageenan solution into 5% (w/v) crosslinker bath. The carrageenan gels were unable to support myoblastic cell growth in this form, as they degraded over time. Carrageenan concentration and crosslinker concentration were varied, and the mass of the gels was recorded over time in PBS solution (at 37˚C) in order to ascertain what effect this had on the stability of the gels. Increasing the concentration of the carrageenan solution resulted in longer degradation times of scaffolds, and this positive correlation was more clearly defined in the case of beads than fibres. This increase in carrageenan concentration also resulted in an exponential increase in swelling of beads, though no particular correlation was noted for fibres. This is likely due to differences in amounts of exposed surface area between beads and fibres which, mass for mass, would be higher in the case of beads.

Increasing the concentration of the KCl crosslinker solution resulted in what may have been a slight increase in the degradation time of fibrous hydrogels, but had no particular effect on the degradation time of beads. Crosslinker concentration did not appear to correlate with degree of swelling for either beads or fibres.

An additional step was taken in the formation of carrageenan hydrogels, that being lyophilisation. Carrageenan solutions were placed into 24-well plates and allowed to cool at room temperature, with subsequent freezing at -80˚C overnight and lyophilisation. The crosslinker solution was then applied as before. Carrageenan hydrogels formed in this way showed a significant improvement in stability over beads and fibres. It was theorised that this was due to the polymer chains being drawn more closely together as the water was sublimed, resulting in more efficient crosslinking.

Carrageenan hydrogels were then maintained in culture medium in order to compare their degradation to those maintained in PBS. Hydrogels maintained in DMEM showed improved stability compared to those maintained in PBS. Attempts were made to induce crosslinking by way of cell adhesion, which has been noted to be a legitimate means of crosslinking hydrogels [212]. However, when these gels were exposed to working resazurin sodium salt

solution, they showed significantly hastened degradation than even those maintained in PBS. It was theorised that the presence of high concentrations of sodium ions in these solutions was what contributed to hydrogel degradation, displacing the potassium ions which form the crosslinks between carrageenan polymer chains, resulting in weaker gels. This would suggest that one of the many components of culture media serves to impart a degree of resistance to this ionic displacement, perhaps by way of surface-adsorption of serum proteins. This would also suggest that the organic component of resazurin sodium salt has a particularly destabilising effect on carrageenan hydrogels.

Surface-coating of carrageenan hydrogels was shown to be the most effective method, of those assayed, by which the gels could be stabilised. Surface-coating with *Bombyx mori* silk fibroin appeared to lengthen degradation times of the hydrogels compared to uncoated controls. In the case of beads, coating with silk fibroin did not lead to any increase in degree of swelling. Chitosan demonstrated the ability to impart a high degree of stability to carrageenan hydrogels when used as a surface-coating. Gels coated with chitosan retained their gelatinous form even after 3 weeks in culture conditions (whereas uncoated control samples reliquified after less than 2 weeks.

The silk fibroin and chitosan materials were formed into films and tested independently for their ability to support myogenic cell culture. Silk fibroin was demonstrated to be the superior biomaterial in this regard, being able to support the proliferation of C2C12 myoblasts, as well as their differentiation into myotubes. Stock chitosan did not show compatibility with C2C12 myoblasts, with no evidence of proliferation occurring on films thereof. However, when deacetylated further by way of reacting with NaOH under nitrogen atmosphere at 90˚C, there was evidence of proliferation. Thus the degree of deacetylation of chitosan appears correlated with cytocompatibility.

Despite the demonstrated cytocompatibility of silk fibroin, coated hydrogels still failed to support a satisfactory degree of cell growth, as did those coated with chitosan. Further processing of the hydrogels may have yielded more positive results, however given the aim of producing a bioscaffold for myogenic cell culture in a simple, time and cost effective manner, from a highly renewable plant-based material, carrageenan hydrogels were determined to be unsuitable.

6.1.2 Cytocompatibility of zein

The compatibility of zein with C2C12 myoblasts was analysed on flat films before commitment was made to production of more complex scaffold designs. Zein was shown to support myoblastic proliferation to a degree not significantly different to that on TCP controls, which was a positive result. The degree of cell spreading on zein was also comparable to that on TCP, though cell spreading on zein was noted to be significantly (but not drastically) reduced at the 24-hour timepoint. This was theorised to be a result of the mechanisms by which cells adhere to zein. In the absence of RGD motifs or similar integrin-binding structures, zein appears to bind cells by way of its many glutamine residues. Though the possibility of serum-protein adsorption to zein, which would play a role in its ability to bind cells, cannot be discounted. Zein was also shown to be capable of facilitating myoblastic differentiation, as myotubes were confirmed to have been formed. Fusion index of myotubes formed on zein appeared slightly lower than that on TCP controls, and in contrast, myotube length on zein appeared to be slightly increased compared to that on TCP controls. The precise mechanism by which the myoblastic membranes fuse during myotube formation is not known, but is theorised to involve phosphatidylserine (a component of the cell membrane), as this has been shown to enhance the degree of myoblastic fusion [39]. Furthermore, phosphatidylcholine, which is also a component of the cell membrane, has been shown to facilitate production of myotubes with greater length but lessened fusion index [39]. Zein has been noted to be capable of complexing with phosphatidylcholine liposomes, which may suggest a similar mechanism between zein and myoblastic cell membranes, which produced this same effect of longer myotubes with lessened fusion indices.

6.1.3 Production of fibrous and particulate zein scaffolds

Various methods of producing bioreactor-compatible scaffolds from zein were explored. Microparticles produced using microfluidic flow focusing and emulsification precipitation were too small to be used as microcarriers. Attempts to produce wet-spun fibre membranes of zein also failed, as the streams of zein solution did not precipitate into solid fibres. This was theorised to be a result of inadequate miscibility between the polymer solvent and the non-solvent phase. Further exploration of polymer solvent choices may have served to improved results. However, electrospinning was demonstrated to be a simple means by which nanofibrous zein matrices could be reliably produced. These fibre matrices showed instability in aqueous environments, however, and would collapse into sheets after some time in the presence of water. Two methods of chemical treatment were shown to impart

stability to the electrospun fibres. Carbodiimide treatment of fibres prevented them from losing their fibrous morphology after a week in water. However, when zein films were treated in this way in order to analyse the impact on cytocompatibility, it was demonstrated that such carbodiimide treatment impaired the zein's ability to support cell growth. Variance of the degree of crosslinking showed that there may be room for optimisation with regard to this procedure, wherein a balance between fibre stability and cytocompatibility may be achieved. Crosslinking via aging zein solutions with citric acid, with subsequent heat treatment after the production of fibres, also successfully stabilised the fibres. This method of crosslinking was not shown to impact the cytocompatibility of the zein. However, this approach lengthened the time taken to produce the scaffolds, from a matter of hours to a matter of days.

Fibres which remained adsorbed to a rigid collector substrate were shown to be stable in water. This approach did not increase the time taken to produce the scaffolds at all, and did not impact the cytocompatibility of the zein; the fibre matrices were shown to support myoblastic proliferation to a degree comparable to that on films, and cells cultured on the fibres were able to differentiate into myotubes. This demonstrates that zein, an edible, renewable, plant-based biomaterial can be easily formed into fibrous scaffolds via electrospinning, and that these scaffolds can support myoblastic cell functions to a degree comparable to TCP controls, and which compare well to gold-standard, ECM-based scaffolds in literature.

6.2 Further work

6.2.1 Immediate next steps

One immediate avenue for further research is the generation of aligned fibres. The use of aligned electrodes as collectors was unsuccessful as a means by which to do so. Rotating collectors may prove to be more successful in this regard. The second is analysis of dynamic seeding conditions onto zein fibre matrices. This would provide the opportunity to analyse whether cell adhesion to the fibres provides additional stability, which would further increase the scaffolds already considerable potential for cultured meat applications, and if so, to maximise this effect by ensuring a uniform distribution of seeded cells. Mechanical properties of the electrospun matrices must also be ascertained, as the fibre mats may exhibit lessened stiffness in comparison to the excessively stiff films. Further steps may need to be taken to lessen scaffold stiffness, such as loading the fibre matrices with zein microparticles as previously discussed. Seeding at high densities may

also serve to optimise fibre stability, and may even enhance myoblastic cell functions, and so this is also a worthwhile course of investigation in the near future.

6.2.2 Long-term goals

After research goals outlined in section 6.2.1 were achieved, the next stage would be to analyse the scaffold's ability to support growth of primary myogenic cells. That is, satellite cells harvested from muscle biopsies and stimulated to renter a proliferative phase. Such cells would, of course, eventually be used in a functional system of cultured meat production, and so their ability to interact with the scaffold must be clearly demonstrated.

The ultimate end-goal of the scaffold's development would be its adaptation for use in bioreactors. As discussed in chapter 5, the use of a rotating wire-drum mandrel as described by Katta *et al.* shows promise for application to this scaffold, in theory [343]. A wire-drum mandrel should be constructed and tested for its ability to collect electrospun nanofibers with a high degree of alignment. Subsequently, the design should be analysed for its ability to carry mechanical stimuli to the cultured cells, both tensile stress stimuli and electrical stimuli inducing contraction.

Zein should also, ideally, be analysed for its ability to support cell growth in a serum-free environment.

6.2.3 Wider implications

Though the carrageenan hydrogels did not provide a scaffold on which myogenic cells could be cultured, there may be potential applications for cell immobilisation. Hydrogels of hydrocolloid polymers have been noted for their ability to maintain the viability of encapsulated, immobilised cells, even at temperatures which would normally lead to cell-death [238]. Given that stabilised carrageenan hydrogels were produced via surface-coating, they may have potential applications in this regard.

Electrospun zein fibres have been analysed for their potential as drug carriers, by Alhusein *et al.* for example [280, 293]. In these studies, it was necessary to blend the zein with PCL in order to overcome the aforementioned instability in aqueous environments. Though the carbodiimide treatment procedures used in this work decreased the fibres' ability to bind myogenic cells, it may be possible to use such treatment to produce stabilised, pure-zein fibres with potential applications as drug carriers without the need for cross-material blending.

6.3 Final conclusions

Zein is an edible, renewable, plant-based biomaterial which has demonstrated the ability to support growth, spreading, and differentiation of myogenic cells. The process of electrospinning is simple and efficient, and reliably produces matrices of zein nanofibers. Allowing these nanofibers to remain anchored to a substrate imparts much-needed stability in aqueous environments, and fibres produced in this way are shown to support myogenic cell culture without the need for chemical modification of any kind. The theoretical use of a rotating, wire-frame mandrel as a collector to produce aligned fibres may hold potential for applications to bioreactor designs, facilitating perfusion-based cell-seeding systems and affording the ability to apply mechanical stimuli to cultured cells. A potential weakness of zein scaffolds is the high stiffness of films, as this would impair the ability of myotubes to develop striations, which would enhance their contractile abilities and protein content. Though the mechanical properties of electrospun fibre mats must be investigated. Methods of reducing stiffness can potentially be applied if needed, such as interspersing the porous nanofibre matrix with zein microparticles as previously discussed. Therefore, this weakness need not significantly damage zein's potential as a biomaterial. This work attempted to ascertain whether a purely plant-based scaffold could be constructed which could support myogenic cell growth to a degree comparable to gold-standard materials, and electrospun zein nanofibres show outstanding potential as a bioscaffold on which myogenic cells may be cultured into muscle-tissue for cultured meat purposes, with potential implications for regenerative medicine, and their further development is certainly called for.

References

1. Tuomisto, HL., de Mattos, MJT. 2011. Environmental Impacts of Cultured Meat Production. *Environmental science & technology*. **45**(14): p. 6117-6123.
2. Datar, I., and Betti, M. 2010. Possibilities for an in vitro meat production system. *Innovative Food Science and Emerging Technologies*. **11**(1): p. 13-22.
3. Post, MJ. 2012. Cultured meat from stem cells: Challenges and prospects. *Meat science*. **92**(3): p. 297-301.
4. Vacanti, JP., Lagner, R. 1993. Tissue engineering. *Science*. **260**(5110): p. 920-926.
5. Kirouac, DC. Zandstra, PW. 2008. The Systematic Production of Cells for Cell Therapies. *Cell Stem Cell*. **3**(4): p. 369-381.
6. O'Brien, FJ. 2011. Biomaterials & scaffolds for tissue engineering. *Materials Today*. **14**(3): p. 88-95.
7. Dzobo, K., Thomford, NE., Senthebane, DA., Shipanga, H., Rowe, A., Dandara, C., Pillay, M., Motaung, KSCM. 2018. Advances in Regenerative Medicine and Tissue Engineering: Innovation and Transformation of Medicine. *Stem Cells International*.
8. Trachtenberg, J., Kasper, K., Mikos, A. 2014. Polymer Scaffold Fabrication. In Lanza ed. *Principles of Tissue Engineering*. Elsevier Science.
9. Choi, JS., Lee, JS., Christ, GJ., Atala, A., Yoo, JJ. 2008. The influence of electrospun aligned poly(ε-caprolactone)/collagen nanofiber meshes on the formation of self-aligned skeletal muscle myotubes. Biomaterials. **29**(19): p. 2899-2906.
10. Wung, N., Acott, SM., Tosh, D., Ellis, MJ. 2014. Hollow fibre membrane bioreactors for tissue engineering applications. Biotechnology Letters. **36**(12): p. 2357-2366.
11. Alberts, B. 2008. *Molecular biology of the cell*. 5th ed. New York ; Abingdon. Garland Science.
12. Stevens, MM. George, J. 2005. Exploring and engineering the cell surface interface. *Science*. **310**(5751): p. 1135-1138.
13. Li, D., Y. Xia. 2004. Electrospinning of Nanofibers: Reinventing the Wheel?. *Advanced Materials*. **16**(14): p. 1151-1170.
14. Kariduraganavar, MY., AA. Kittur., Kamble, RR. 2014. Polymer Synthesis and Processing. In Kumbar, Laurencin, Deng (eds). *Natural and Synthetic Biomedical Polymers*. Burlington, Massachusetts ; San Diego, California : Elsevier.
15. Ellis, MJ., Chaudhuri, JB. 2007. Poly(lactic-co-glycolic acid) hollow fibre membranes for use as a tissue engineering scaffold. *Biotechnology and Bioengineering*. **96**(1): p. 177-187.
16. Verbruggen, S., Luining, D., Essen, AV., Post, MJ. 2018. Bovine myoblast cell production in a microcarriers-based system. *Cytotechnology*. **70**(2): p. 503-512.
17. Rivest, C., Morrison, DWG., Ni, B., Rubin, J., Yadav, Vikramaditya., Mahdavi, A., Karp, JM., Khademhosseini. 2007. Microscale hydrogels for medicine and biology: synthesis, characteristics and applications. *Journal of Mechanics of Materials and Structures*. **2**(6): p. 1103-1119.
18. Nisisako, T., Torii, T., Higuchi, T. 2002. Droplet formation in a microchannel network. *Lab on a Chip*. **2**(1): p. 24-26.
19. Allan, SJ., De Bank, PA., Ellis, MJ. 2019. Bioprocess Design Considerations for Cultured Meat Production With a Focus on the Expansion Bioreactor. *Frontiers in Sustainable Food Systems*. **3(44)**.
20. Martin, I., Wendt, D., Heberer, M. 2004. The role of bioreactors in tissue engineering. *Trends in Biotechnology*. **22**(2): p. 80-86.
21. Ellis, M. Jarman-Smith, M. Chaudhuri, J. 2005. Bioreactor systems for tissue engineering: A four-dimensional challenge. in Chaudhuri, Al-Rubea (eds).

Bioreactors for Tissue Engineering : Principles, Design and Operation. Springer: Dordrecht.
22. Lanza, RP. Langner, R. Chick, WL. 1997. Principles of tissue engineering*. Nature*. **389**(6650): p. 453-453.
23. Bhumiratana, S., Bernhard, J., Cimetta, E., Vunjak-Novakovic, G. 2014. Principles of Bioreactor Design for Tissue Engineering. In Lanza (ed). *Principles of Tissue Engineering.* Elsevier Science.
24. Vunjak-Novakovic, G., Freed, LE., Biron, RJ., Lagner, R. 1996. Effects of mixing on the composition and morphology of tissue-engineered cartilage*. AIChE Journal*. **42**(3): p. 850-860.
25. Wendt, D., Marsano, A., Jakob, M., Heberer, M., Martin, I. 2003. Oscillating perfusion of cell suspensions through three- dimensional scaffolds enhances cell seeding efficiency and uniformity*. Biotechnology and Bioengineering*. **84**(2): p. 205-214.
26. Goodwin, T., Jessup, JM., Wolf, D. 1992. Morphologic differentiation of colon carcinoma cell lines HT-29 and HT-29KM in rotating-wall vessels. *In Vitro Cellular & Developmental Biology - Animal*. **28**(1): p. 47-60.
27. Storm, MP., Sorrell, I., Rebecca, S., Regan, S., Luetchford, KA., Sathish, J., Webb, S., Ellis, MJ. 2016. Hollow Fiber Bioreactors for In Vivo-like Mammalian Tissue Culture*. Journal of Visualized Experiment.* (111).
28. Ondrey, G. 2010. Microbubble generator enhances performance of airlift bioreactor. *Chemical engineering.* p. 13.
29. Pörtner, R., Barradas, OBJP. 2007. Cultivation of Mammalian Cells in Fixed-Bed Bioreactors. In Pörtner (ed). *Animal Cell Biotechnology: Methods and Protocols.* Humana Press: Totowa, NJ.
30. Nikravesh, N., Cox, SC., Ellis, MJ., Grover, LM. 2017. Encapsulation and Fluidization Maintains the Viability and Glucose Sensitivity of Beta-Cells*. Acs Biomaterials Science & Engineering*. **3**(8): p. 1750-1757.
31. Frontera, WR., Ochala, J. 2014. Skeletal Muscle: A Brief Review of Structure and Function*. Calcified tissue international*. **96**(3): p. 183-195.
32. Sanchez, B., Li, J., Rutkove, SB. 2014. Differentiation of the intracellular structure of slow- versus fast-twitch muscle fibers through evaluation of the dielectric properties of tissue*. Physics in medicine & biology*. **59**(10): p. 2369-2380.
33. Yiangou, L., Grandy, RA., Osnato, A., Ortmann, D., Sinha, S., Vallier, L. 2019. Cell cycle regulators control mesoderm specification in human pluripotent stem cells. *The Journal of biological chemistry*. **294**(47): p. 17903.
34. Mazères, G., Leloup, L., Daury, L., Cottin, P., Brustis, J. 2006. Myoblast attachment and spreading are regulated by different patterns by ubiquitous calpains*. Cell Motility and the Cytoskeleton*. **63**(4): p. 193-207.
35. Knudsen, KA., Myers, L., McElwee, SA. 1990. A role for the Ca 2+-dependent adhesion molecule, N-cadherin, in myoblast interaction during myogenesis*. Experimental Cell Research*. **188**(2): p. 175-184.
36. Przewoźniak, M., Czaplicka, I., Czerwinska, M., Markowska-Zagrajek, A., Moraczewski, J., Streminska, W., Janczyk-Ilack, K., Ciemerych, MA., Brzoska, E. 2013. Adhesion Proteins - An Impact on Skeletal Myoblast Differentiation*. PLoS ONE*. **8**(5).
37. Pizzey, J., Jones, GE., Walsh, FS. 1988. Requirements for the Ca2+-independent component in the initial intercellular adhesion of C2 myoblasts. *The journal of cell biology*. **107**(6): p. 2307-2317.
38. Kim, JH., Jin, P., Duan, R., Chen, EH. 2015. Mechanisms of myoblast fusion during muscle development*. Current Opinion in Genetics & Development*. **32**: p. 162-170.
39. Jeong, J., Conboy, IM. 2011. Phosphatidylserine directly and positively regulates fusion of myoblasts into myotubes*. Biochemical and Biophysical Research Communications*. **414**(1): p. 9-13.

40. Danoviz, M.E., Yablonka-Reuveni, Z. 2012. Skeletal Muscle Satellite Cells: Background and Methods for Isolation and Analysis in a Primary Culture system. In DiMario (ed). *Myogenesis Methods and Protocols*. Humana press: Totowa, NJ. p. 21 -52.
41. Mauro, A. 1961. Satellite cell of skeletal muscle fibres. *The journal of cell biology*. **9**(2): p. 493-495.
42. Laguens, R. 1963. Satellite cells of skeletal muscle fibers in human progressive muscular dystrophy*. Virchows archiv fur pathologische anatomie und physiologie und fur klinische medizin.* **336**(6).
43. Kaur, G., Dufour, JM. 2012. Cell lines: Valuable tools or useless artifacts. *Spermatogenesis*. **2**(1): p. 1-5.
44. Stacey, G. 2005. Primary Cell Cultures and Immortal Cell Lines. PLoS One. **10**(6): p. 180-184.
45. Pan, C., Kumar, C., Bohl, S., Klingmueller, U., Mann, M. 2009. Comparative Proteomic Phenotyping of Cell Lines and Primary Cells to Assess Preservation of Cell Type-specific Functions*. Molecular & cellular proteomics*. **8**(3): p. 443-450.
46. Alge, CS., Hauck, SM., Priglinger, SG., Kampik, A., Ueffing, M. 2006. Differential Protein Profiling of Primary versus Immortalized Human RPE Cells Identifies Expression Patterns Associated with Cytoskeletal Remodeling and Cell Survival*. Journal of Proteome Research*. **5**(4): p. 862-878.
47. Petreaca, M., Martins-Green, M. 2014. The Dynamics of Cell-ECM Interactions with Implications for Tissue Engineering. In Lanza (ed). *Principles of Tissue Engineering*. Elsevier Science.
48. Griffith, L., 2002. Emerging design principles in Biomaterials and scaffolds for tissue engineering*. Reparative Medicine: Growing Tissues And Organs*. **961**: p. 83-95.
49. Aviss, KJ., Gough, JE., Downes, S. 2010. Aligned electrospun polymer fibres for skeletal muscle regeneration. European Cells & Materials. **19**: p. 193-204.
50. Chaturvedi, V., Dye, DE., Kinnear, BF., Van Kuppevelt, TH. Grounds, MD. Coombe, DR., Engler, AJ. 2015. Interactions between Skeletal Muscle Myoblasts and their Extracellular Matrix Revealed by a Serum Free Culture System. *PLoS ONE*. **10**(6).
51. Von Der Mark, K., Park, J. 2013. Engineering biocompatible implant surfaces*. Progress in Materials Science*. **58**(3): p. 327-381.
52. Wilschut, KJ., Haagsman, HP., Roelen, BAJ. 2010. Extracellular matrix components direct porcine muscle stem cell behavior*. Experimental Cell Research*. **316**(3): p. 341-352.
53. Echave, MC., Burgo, LS., Pedraz, JL., Orive, G. 2017. Gelatin as Biomaterial for Tissue Engineering*. Current pharmaceutical design*. **23**(24): p. 3567-3584.
54. Hughes, CS., Postovit, LM., Lajoie, GA. 2010. Matrigel: A complex protein mixture required for optimal growth of cell culture*. Proteomics*. **10**(9): p. 1886-1890.
55. Bardouille, C., Lehmann, J., Heimann, P., Jockusch, H. 2001. Growth and differentiation of permanent and secondary mouse myogenic cell lines on microcarriers*. Applied Microbiology and Biotechnology*. **55**(5): p. 556-562.
56. Wang, Y., Kim, HJ., Vunjak-Novakovic, G., Kaplan, DL. 2006. Stem cell-based tissue engineering with silk biomaterials*. Biomaterials*. **27**(36): p. 6064-6082.
57. Leal-Egaña, A., Scheibel, T. 2012. Interactions of cells with silk surfaces. *Journal of Materials Chemistry*. **22**(29): p. 14330-14336.
58. Mita, K., Ichimura, S., James, T. 1994. Highly repetitive structure and its organization of the silk fibroin gene*. Journal of Molecular Evolution*. **38**(6): p. 583-592.
59. Chaturvedi, V., Naskar, D., Kinnear, BF., Grenik, E., Dye, D., Grounds, MD., Kundu, SC., Coombe, DR. 2017. Silk fibroin scaffolds with muscle-like elasticity support in vitro differentiation of human skeletal muscle cells*. Journal of Tissue Engineering and Regenerative Medicine*. **11**(11): p. 3178-3192.

60. Yadav, M., Goswami, P., Paritosh, K., Kumar, M., Pareek, N., Vivekanand, V. 2019. Seafood waste: a source for preparation of commercially employable chitin/chitosan materials. *Bioresources and Bioprocessing*. **6**(1): p. 1-20.
61. Hussain, R., Murshid, Iman., Maji, TK. 2013. Determination of Degree of Deacetylation of Chitosan and Their effect on the Release Behavior of Essential Oil from Chitosan and Chitosan-Gelatin Complex Microcapsules. *International Journal of Advanced Engineering Applications: Department of Chemical Sciences*. **2**(4): p. 4-12.
62. Yuan, Y., Chesnutt, BM., Haggard, WO., Bumgardner, JD. 2011. Deacetylation of Chitosan: Material Characterization and in vitro Evaluation via Albumin Adsorption and Pre-Osteoblastic Cell Cultures. *Materials*. **4**(8): p. 1399-1416.
63. Freier, T., Koh, HS., Kazazian, K., Shoichet, MS. 2005. Controlling cell adhesion and degradation of chitosan films by N-acetylation. *Biomaterials*. **26**(29): p. 5872-5878.
64. Benesch, J., Tengvall, P. 2002. Blood protein adsorption onto chitosan. *Biomaterials*. **23**(12): p. 2561-2568.
65. Parisi, L., Toffoli, A., Bianchi, MG., Bergonzi, C., Bianchera, A., Bettini, R., Elviri, L., Macaluso, GM. 2019. Functional Fibronectin Adsorption on Aptamer-Doped Chitosan Modulates Cell Morphology by Integrin-Mediated Pathway. *Materials*. **12**(5): p. 812.
66. Hajiabbas, M., Mashayekhan, S., Nazaripouya, A., Naji, M., Hunkeler, D., Rajabi, ZS., Sharifiaghdas, F. 2015. Chitosan-gelatin sheets as scaffolds for muscle tissue engineering. *Artificial Cells, Nanomedicine, and Biotechnology*. **43**(2): p. 124-132.
67. Tonda-Turo, C., Ruini, F., Ramella, M., Boccafoschi, F., Gentile, P., Gioffredi, E., Falvo, DLG., Ciardelli, G. 2017. Non-covalently crosslinked chitosan nanofibrous mats prepared by electrospinning as substrates for soft tissue regeneration. *Carbohydrate polymers*. **162**: p. 82-92.
68. Lee, KY., Mooney, DJ. 2012. Alginate: Properties and biomedical applications. *Progress in Polymer Science*. **37**(1): p. 106-126.
69. Larsen, B., Haug, A. 1971. Biosynthesis of alginate. 1. Composition and structure of alginate produced by Azotobacter vinelandii (Lipman). *Carbohydrate research*. **17**(2): p. 287.
70. Rowley, JA., Madlambayan, G., Mooney, DJ. 1999. Alginate hydrogels as synthetic extracellular matrix materials. *Biomaterials*. **20**(1): p. 45-53.
71. Genes, NG., Rowley, JA., Mooney, DJ., Bonassar, LJ. 2004. Effect of substrate mechanics on chondrocyte adhesion to modified alginate surfaces. *Archives of Biochemistry and Biophysics*. **422**(2): p. 161-167.
72. Tsur-Gang, O., Ruvinov, E., Landa, N., Holbova, R., Feinberg, MS., Leor, J., Cohen, S. 2009. The effects of peptide-based modification of alginate on left ventricular remodeling and function after myocardial infarction. *Biomaterials*. **30**(2): p. 189-195.
73. Bidarra, SJ., Barrias, CC., Barbosa, MA., Soares, R., granja, PL. 2010. Immobilization of human mesenchymal stem cells within RGD-grafted alginate microspheres and assessment of their angiogenic potential. *Biomacromolecules*. **11**(8): p. 1956.
74. George, M., Abraham, TE. 2006. Polyionic hydrocolloids for the intestinal delivery of protein drugs: Alginate and chitosan — a review. J*ournal of Controlled Release*. **114**(1): p. 1-14.
75. Braccini, I., Perez, S. 2001. Molecular basis of Ca2+-induced gelation in alginates and pectins: the egg-box model revisited. *Biomacromolecules*. **2**(4): p. 1089-1096.
76. Swioklo, S., Connon, CJ. 2016. Keeping cells in their place: the future of stem cell encapsulation. *Expert Opinion on Biological Therapy*. **16**(10): p. 1181-1183.
77. Wright, B., De Bank, PA., Luetchford, K., Acosta, FR., Connon, CJ. 2014. Oxidised alginate hydrogels as niche environments for corneal epithelial cells. *Journal of Biomedical Materials Research, Part A*. **102**(10): p. 3393-3400 .

78. Siegel, SJ., Makadia, HK. 2011. Poly Lactic-co-Glycolic Acid (PLGA) as Biodegradable Controlled Drug Delivery Carrier. *Polymers*. **3**(3): p. 1377-1397.
79. Pubchem Database, N.C.B.I., 2020. *Caprolactone, CID=10401*. Available from: https://pubchem.ncbi.nlm.nih.gov/compound/Caprolactone. [cited 2020 26/02];.
80. Labet, M., Thielemans, W. 2009. Synthesis of polycaprolactone: a review. *Chemical Society Reviews*. **38**(12): p. 3484-3504.
81. Zhang, Y., Lei, Y., Chang, J., Li, L., He, B., Gu, Z. 2012. Guidance of myoblast migration on aligned electrospun PLGA nanofibrous meshes. *Materials Letters*. **68**: p. 218-221.
82. Sirivisoot, S., Harrison, BS. 2011. Skeletal myotube formation enhanced by electrospun polyurethane carbon nanotube scaffolds. *International Journal of Nanomedicine*. **6**: p. 2483-2497.
83. Riboldi, SA., Sampaolesi, M., Neuenschwander, P., Cossu, G., Mantero, S. 2005. Electrospun degradable polyesterurethane membranes: potential scaffolds for skeletal muscle tissue engineering. *Biomaterials*. **26**(22): p. 4606-4615.
84. Meneghello, G., Parker, DJ., Ainsworth, BJ., Perera, S., Chadhuri, J., Ellis, MJ., De Bank, PA. 2009. Fabrication and characterization of poly(lactic-co-glycolic acid)/polyvinyl alcohol blended hollow fibre membranes for tissue engineering applications. *Journal of Membrane Science*. **344**(1): p. 55-61.
85. Molnar, G., Nancy, AS., Gonda, SR., Hartzell, CR. 1997. Skeletal muscle satellite cells cultured in simulated microgravity. *In Vitro Cellular & Developmental Biology - Animal*. **33**(5): p. 386-391.
86. Kankala, RK., Zhao, J., Liu, Chen-Guang., Song, XJ., Yang, DY., Zhu, K., Wang, SB., Zhang, YS., Chen, AZ. 2019. Highly Porous Microcarriers for Minimally Invasive In Situ Skeletal Muscle Cell Delivery. *Small*. **15**(25).
87. Torgan, C., Burge, SS., Collinsworth, AM., Truskey, GA., Kraus, WE. 2000. Differentiation of mammalian skeletal muscle cells cultured on microcarrier beads in a rotating cell culture system. *Medical and Biological Engineering and Computing*. **38**(5): p. 583-590.
88. Liu, Y., Huang, Q., Wang, J., Fu, F., Ren, J., Zhao, Y. 2017. Microfluidic generation of egg-derived protein microcarriers for 3D cell culture and drug delivery. *Science bulletin*. **62**(18): p. 1283-1290.
89. Luetchford, K., Chaudhuri, J., De Bank, PA. 2020. Silk fibroin/gelatin microcarriers as scaffolds for bone tissue engineering. *Materials Science & Engineering C*. 106: p. 110116.
90. Wong, R., Ashton, M., Dodou, K. 2015. Effect of Crosslinking Agent Concentration on the Properties of Unmedicated Hydrogels. *Pharmaceutics*. **7**(3): p. 305-319.
91. Geckil, H., Xu, F., Zhang, X., Moon, S. 2010. Engineering hydrogels as extracellular matrix mimics. *Nanomedicine*. **5**(3): p. 469-484.
92. Peppas, NA., Hilt, JZ., Khademhosseini, A., Langer, R. 2006. Hydrogels in Biology and Medicine: From Molecular Principles to Bionanotechnology. *Advanced Materials*. **18**(11): p. 1345-1360.
93. Gouveia, RM., Jones, RR., Hamley, IW., Connon, CJ. 2014. The bioactivity of composite Fmoc-RGDS-collagen gels. *Biomaterials Science*. **2**(9): p. 1222-1229.
94. Mi, S., Khutoryanskiy, VV., Jones, RR., Zhu, X., Hamley, IW., Connon, CJ. 2011. Photochemical cross-linking of plastically compressed collagen gel produces an optimal scaffold for corneal tissue engineering. *Journal of biomedical materials research. Part A*. **99**(1): p. 1.
95. Azab, AK., Orkin, B., Doviner, V., Nissan, A., Klein, M., Srebnik, M., Rubinstein, A. 2006. Crosslinked chitosan implants as potential degradable devices for brachytherapy: In vitro and in vivo analysis. *Journal of Controlled Release*. **111**(3): p. 281-289.
96. Kim, HJ., Kim, UJ., Kim, HS., Li, C., Wada, M., Leisk, GG., Kaplan, DL. 2008. Bone tissue engineering with premineralized silk scaffolds. *Bone*. **42**(6): p. 1226-1234.

97. Mooney, DJ., Rowley, JA., Mooney, DJ. 2002. Alginate type and RGD density control myoblast phenotype. *Journal of biomedical materials research*. **60**(2): p. 217-223.
98. Leitinger, B., 2011. Transmembrane Collagen Receptors. A*nnual Review of Cell and Developmental Biology*. **27**: p. 265-290.
99. Ruoslahti, E. 1996. RGD and other recognition sequences for integrins. *Annual review of cell and developmental biology*. **12**: p. 697.
100. Wells, RG. 2008. The role of matrix stiffness in regulating cell behavior. *Hepatology*. **47**(4): p. 1394-1400.
101. Foster, JW., Jones, RR., Bippes, CA., Gouveia, RM., Connon, CJ. 2014. Differential nuclear expression of Yap in basal epithelial cells across the cornea and substrates of differing stiffness. *Experimental Eye Research*. **127**: p. 37-41.
102. Ricardo, MG., Vajda, F., Wibowo, JA., Figueiredo, F., Connon, CJ. YAP, ΔNp63, and β-Catenin Signaling Pathways Are Involved in the Modulation of Corneal Epithelial Stem Cell Phenotype Induced by Substrate Stiffness. *Cells*. **8**(4): p. 347.
103. Engler, AJ., Griffin, MA., Sen, S., Carsten, GB., Lee, SH., Discher, DE. 2004. Myotubes differentiate optimally on substrates with tissue-like stiffness. *The journal of cell biology*. **166**(6): p. 877-887.
104. Altman, GH., Lu, HH., Horan, RL., Colabro, T., Ryder, D., Kaplan, DL., Stark, P., Martin, I., Richmond, JC., Vunjak-Novakovic, G. 2002. Advanced Bioreactor with Controlled Application of Multi-Dimensional Strain For Tissue Engineering. *Journal of biomechanical engineering*. **124**(6): p. 742-749.
105. Berger, HJ., Prasad, SK., Davidoff, AJ., Pimental, D., Ellingsen, O., Marsh, JD., Smith, TW., Kelly, RA. 1994. Continual electric field stimulation preserves contractile function of adult ventricular myocytes in primary culture. *American Journal of Physiology-Heart and Circulatory Physiology*. **266**(1): p. H341-H349.
106. Radisic, M., Park, H., Shing, H., Consi, T., Schoen, FJ., Langer, R., Freed, LE., Vunjak-Novakovic, G. 2004. Functional Assembly of Engineered Myocardium by Electrical Stimulation of Cardiac Myocytes Cultured on Scaffolds. *Proceedings of the National Academy of Sciences of the United States of America*. **101**(52): p. 18129-18134.
107. Edelman, PD., MacFarland, DC., Mironov, VA., Matheny, JG. Commentary: In Vitro -Cultured Meat Production. *Tissue engineering*. **11**(5-6): p. 659-662.
108. Van Mensvoort, K., Grievink, HJ. 2014. *The in vitro Meat Cookbook*. 1 ed. Amsterdam, Netherlands: Bis Publishers.
109. Datar, I. and D. Luining. 2015. *Mark Post's Cultured Beef*. Available from: https://www.new-harvest.org/mark_post_cultured_beef. [cited 2020 26/02].
110. Dumanski, J. 1994. Progress towards an international Framework for Evaluating Sustainable Land Management (FESLM). *15th World Congress of Soil Science, Vol 6A, Transactions*. p. 373-378.
111. McGrath, M. 2020. *UK faces 'significant' shortage of farmland by 2030*. Available from: https://www.bbc.co.uk/news/science-environment-28003435]. [Cited 2020 26/02].
112. Goering, S., 1998. Babies and Beasts: The Argument from Marginal Cases. *Ethics*, 1998. **109**(1): p. 226.
113. Maastricht University. 2020. *Save the Date - 6th International Scientific Conference on Cultured Meat*. Available from: https://www.culturedmeatconference.com/. [cited 2020 26/02];.
114. Tuomisto, H., Ellis, MJ., Haastrup, P. 2014. Environmental impacts of cultured meat: alternative production scenarios. *Proceedings of the 9th International Conference on Life Cycle Assessment in the Agri-Food Sector*.
115. Kolkmann, AM., Post, MJ., Rutjens, MAM., Van Essen, AL., Moutsatsou, P. 2020. Serum-free media for the growth of primary bovine myoblasts. *Cytotechnology*. **72**(1): p. 111-120.

116. Brienne, JP., Denoyelle, C., Baussart, H., Daudin, JD. 2001. Assessment of meat fat content using dual energy X-ray absorption. *Meat Science*. **57**(3): p. 235-244.
117. Motoyama, M., Sasaki, K., Watanabe, A. 2016. Wagyu and the factors contributing to its beef quality: A Japanese industry overview. *Meat Science*. **120**: p. 10-18.
118. Beloor, J., Kang, HK., Moon, YS. 2010. Serum Lipids Can Convert Bovine Myogenic Satellite Cells to Adipocytes. *Asian-Australasian Journal of Animal Sciences*. **23**(11): p. 1519-1526.
119. Schubert, FM., Noah, AC., Bedi, A., Gumucio, JP., Mendias, C. 2019. Reduced Myogenic and Increased Adipogenic Differentiation Capacity of Rotator Cuff Muscle Stem Cells. *The Journal of Bone and Joint Surgery*. **101**(3): p. 228-238.
120. Impossible™. 2020. *Heme + The Science behind Impossible™*. Available from: https://impossiblefoods.com/heme/. [cited 2020 01/03];].
121. Simsa, R., Yuen, J., Stout, A., Rubio, N., Fogelstrand, P., Kaplan, DL. 2019. Extracellular Heme Proteins Influence Bovine Myosatellite Cell Proliferation and the Color of Cell-Based Meat. *Foods*. **8**(10): p. 521.
122. Shit, SC., Shah, PM. 2014. Edible Polymers: Challenges and Opportunities. *Journal of Polymers*. **2014**: p. 1-13.
123. Meyer, M. 2019. Processing of collagen based biomaterials and the resulting materials properties. *Biomedical engineering online*. **18**(1): p. 24-74.
124. Merck KGaA. 2020. *Polycaprolactone*. Available from: https://www.sigmaaldrich.com/catalog/product/aldrich/440752?lang=en&region=GB. [cited 2020 05/09]
125. Merck KGaA. 2020. *Gelatin from bovine skin Type B*. Available from: https://www.sigmaaldrich.com/catalog/product/sigma/g9391?lang=en&region=GB. [cited 2020 05/09].
126. Merck KGaA. 2020. *Alpha-Cellulose powder*. Available from: https://www.sigmaaldrich.com/catalog/product/sigma/c8002?lang=en&region=GB&cm_sp=Insite-_-caContent_prodMerch_gruCrossEntropy-_-prodMerch10-1. [cited 2020 05/09]
127. Charest, JL., García, AJ., King, WP. 2007. Myoblast alignment and differentiation on cell culture substrates with microscale topography and model chemistries. *Biomaterials*. **28**(13): p. 2202-2210.
128. Stephens, N., Ellis, MJ. 2020. Cellular agriculture in the UK: a review. *Wellcome open research*. **5**: p. 12.
129. Mihaila, SM., Popa, EG., Reis, RL., Marques, AP., Gomes, ME. 2014. Fabrication of endothelial cell-laden carrageenan microfibers for microvascularized bone tissue engineering applications. *Biomacromolecules*. **15**(8): p. 2849.
130. Fernández-Romero, JA., Ciby, JA., Aixa, R., Larisa, K., Ninochka, JP., Radhika, M., Othell, B., Seidor, S., Ford, BE., Gil, PI., Peters, J., Katz, D., Robbiani, M., Zydowksy, TM. 2012. Zinc acetate/carrageenan gels exhibit potent activity in vivo against high-dose herpes simplex virus 2 vaginal and rectal challenge. *Antimicrobial agents and chemotherapy*. **56**(1): p. 358.
131. Shukla, D., Agelidis, AM. 2015. Cell entry mechanisms of HSV: what we have learned in recent years. *Future Virology*. **10**(10): p. 1145-1154.
132. Zhang, Y., Lei, Y., Cui, M., Yang, B., Li, J., Hong, S., Ya, F. 2015. Physically crosslinked poly(vinyl alcohol)carrageenan composite hydrogels: pore structure stability and cell adhesive ability. *RSC Advances*. **5**(95): p. 78180-78191.
133. Pourjavadi, A., Doroudian, M., Ahadpour, A., Azari, S. 2019. Injectable chitosan/κ-carrageenan hydrogel designed with au nanoparticles: A conductive scaffold for tissue engineering demands. *International Journal of Biological Macromolecules*. **126**: p. 310-317.
134. Mihaila, SM., Gaharwar, AK., Reis, RL., Marques, AP., Manuela, EG., Khademhosseini, A. 2013. Photocrosslinkable Kappa -Carrageenan Hydrogels for Tissue Engineering Applications. *Advanced Healthcare Materials*. **2**(6): p. 895-907.

135. Shukla, R., Cheryan, M. 2001. Zein: the industrial protein from corn. *Industrial Crops and Products*. **13**(3): p. 171-192.
136. Geraghty, D., Peifer, MA., Rubenstein, I., Messing, J. 1981. The primary structure of a plant storage protein: zein. *Nucleic acids research*. **9**(19): p. 5163.
137. Yang, F., Miao, Y., Wang, Y., Zhang, L., Lin, X. 2017. Electrospun Zein/Gelatin Scaffold-Enhanced Cell Attachment and Growth of Human Periodontal Ligament Stem Cells. *Materials*. **10**(10): p. 1168.
138. Tu, J., Wang, H., Li, H., Dai, K., Wang, J., Zhang, X. 2009. The in vivo bone formation by mesenchymal stem cells in zein scaffolds. *Biomaterials.* **30**(26): p. 4369-4376.
139. Jing, L., Wang, X., Liu, H., Lu, Y., Bian, J., Sun, J., Huang, D. 2018. Zein Increases the Cytoaffinity and Biodegradability of Scaffolds 3D-Printed with Zein and Poly(ϵ-caprolactone) Composite Ink. *ACS Applied Materials and Interfaces*. **10**(22): p. 18551-18559.
140. Lian, H., Liu, X., Meng, Z. 2019. Enhanced mechanical and osteogenic differentiation performance of hydroxyapatite/zein composite for bone tissue engineering. *Journal of Materials Science*. **54**(1): p. 719-729.
141. Li, D., Wang, Y., Xia, Y. 2003. Electrospinning of Polymeric and Ceramic Nanofibers as Uniaxially Aligned Arrays. *Nano Letters*. **3**(8): p. 1167-1171.
142. Drury, JL., Mooney, DJ. 2003. Hydrogels for tissue engineering: scaffold design variables and applications. *Biomaterials.* **24**(24): p. 4337-4351.
143. Chen, X. 2013. Chondrogenic differentiation of umbilical cord-derived mesenchymal stem cells in type I collagen-hydrogel for cartilage engineering. *Injury*. **44**(4): p. 540-550.
144. Nguyen, A., Narayan, RJ., Jaipan, P. 2017. Gelatin-based hydrogels for biomedical applications. *MRS Communications*. **7**(3): p. 416-426.
145. Vlachos, PP., Rylander, MN., Antoine, EE. 2014. Review of Collagen I Hydrogels for Bioengineered Tissue Microenvironments: Characterization of Mechanics, Structure, and Transport. *Tissue engineering*. **20**(6): p. 683-696.
146. Andersen, T., Strand, BL., Formo, K., Alsberg, E., Christensen, BE. 2012. Alginates as biomaterials in tissue engineering. *Carbohydratate chemistry*. **37**: p. 227-258.
147. Leroux, MA., Guilak, F., Setton, LA. 1999. Compressive and shear properties of alginate gel: Effects of sodium ions and alginate concentration. *Journal of Biomedical Materials Research*. **47**(1): p. 46-53.
148. Kong, HJ., Wong, E., Mooney, DJ. 2003. Independent control of rigidity and toughness of polymeric hydrogels. *Macromolecules*. **36**(12): p. 4582-4588.
149. Zhao, X., Huebsch, N., Mooney, DJ., Suo, Z. 2010. Stress-relaxation behavior in gels with ionic and covalent crosslinks. *Journal of applied physics*. **107**(6): p. 063509.
150. Rhein-Knudsen, N., Ale, M., Meyer, A. 2015. Seaweed Hydrocolloid Production: An Update on Enzyme Assisted Extraction and Modification Technologies. *Marine Drugs*. **13**(6): p. 3340-3359.
151. Syed KH., Gulrez, SA., Al-Assaf, S., Phillips, GO. 2010. Hydrogels: Methods of Preparation, Characterisation and Applications. In Carpi (ed). *Progress in Molecular and Environmental Bioengineering - From Analysis and Modeling to Technology Applications*. InTech.
152. Viebke, C., Piculell, L., Nilsson, S. 1994. On the Mechanism of Gelation of Helix-Forming Biopolymers. *Macromolecules*. **27**(15): p. 4160-4166.
153. Popa, EG., Gomes, ME., Reis, RL. 2011. Cell delivery systems using alginate--carrageenan hydrogel beads and fibers for regenerative medicine applications. *Biomacromolecules*. **12**(11): p. 3952.
154. Patil, S., Singh, N. 2019. Silk fibroin-alginate based beads for human mesenchymal stem cell differentiation in 3D. *Biomaterials Science*. **7**(11): p. 4687-4697.
155. Pérez-Madrigal, MM., Torras, J., Casanovas, J., Haring, M., Aleman, C., Diaz, DD. 2017. Paradigm Shift for Preparing Versatile M-Free Gels from Unmodified Sodium Alginate. *Biomacromolecules*. **18**(9): p. 2967.

156. Zhang, QZ., Konno, M., Saito, S. 1993. Sol-Gel Transition of Alginate Solution by Addition of Calcium-Ions - Alginate Concentration-Dependence of Gel Point. *Journal de Physique II*. **3**(1): p. 1-7.
157. Kuo, CK., Ma, PX. 2008. Maintaining dimensions and mechanical properties of ionically crosslinked alginate hydrogel scaffolds in vitro. *Journal of Biomedical Materials Research Part A*. **84**(4): p. 899-907.
158. Okay, O. 2009. General Properties of Hydrogels. In Urban (ed). *Hydrogel Sensors and Actuators*. Vol. 6. Berlin, Heidelberg: Springer.
159. Jang, J., Seol, YJ., Kim, HJ., Kundu, J., Kim, SW., Cho, DW. 2014. Effects of alginate hydrogel cross-linking density on mechanical and biological behaviors for tissue engineering. *Journal of the Mechanical Behavior of Biomedical Materials*. **37**: p. 69-77.
160. Mohammed, A., Ahmad, MB., Ibrahim, NA., Zainuddin, N. 2018. Effect of crosslinking concentration on properties of 3-(trimethoxysilyl) propyl methacrylate/ N -vinyl pyrrolidone gels. *Chemistry Central Journal*. **12**(1): p. 1-9.
161. Braudo, EE. 1992. Mechanism of galactan gelation. *Food Hydrocolloids*. **6**(1): p. 25-43.
162. Al-Jaibaji, O., Swioklo, S., Gibels, K., Vaes, B., Figuerido, FC., Connon,CJ., Ljubimov, AV. 2018. Alginate encapsulated multipotent adult progenitor cells promote corneal stromal cell activation via release of soluble factors. *PLoS ONE*. **13**(9).
163. Hatch, A., Hansmann, G., Murthy, SK. 2011. Engineered alginate hydrogels for effective microfluidic capture and release of endothelial progenitor cells from whole blood. *Langmuir : the ACS journal of surfaces and colloids*. **27**(7): p. 4257.
164. Swioklo, S., Constantinescu, A., Connon, CJ. 2016. Alginate-Encapsulation for the Improved Hypothermic Preservation of Human Adipose-Derived Stem Cells. *STEM CELLS Translational Medicine*. **5**(3): p. 339-349.
165. Williams, P., Phillips, P. 2003. GUMS: Properties of Individual Gums - Encyclopedia of Food Sciences and Nutrition. *Academic Press*. p. 2992-3001.
166. Myslabodski, DE., Stancioff, D., Heckert, RA. 1996. Effect of acid hydrolysis on the molecular weight of kappa carrageenan by GPC-LS. *Carbohydrate Polymers*. **31**(1): p. 83-92.
167. Hermansson, A., Eriksson, E., Jordansson, E. 1991. Effects of Potassium, Sodium, and Calcium on the Microstructure and Rheological Behaviour of Kappa-Carrageenan Gels. *Carbohydr. Polym*. **16**(3): p. 297-320.
168. Funami, T., Hiroe, M., Noda, S., Asai, Iwao., Shinya, I., Nishinari, K. Influence of molecular structure imaged with atomic force microscopy on the rheological behavior of carrageenan aqueous systems in the presence or absence of cations. *Food Hydrocolloids*. **21**(4): p. 617-629.
169. Hoon, TG. 1995. Studying Activity Series of Metals. *Journal of Chemical Education*. **72**(1): p. 51.
170. Potter, K., Balcom, BJ., Carpenter, TA., Hall, LD. 1994. The gelation of sodium alginate with calcium ions studied by magnetic resonance imaging (MRI). *Carbohydrate research*. **257**(1): p. 117-126.
171. Elsabee, MZ., Abdou, ES. 2013. Chitosan based edible films and coatings: A review. *Materials Science & Engineering C*. **33**(4): p. 1819-1841.
172. Marelli, B., Brenckle, MA., Kaplan, DL., Omenetto, FG. 2016. Silk Fibroin as Edible Coating for Perishable Food Preservation. *Scientific Reports*. **6**(1).
173. Lee, DW., Lim, C., Israelachvili, JN., Dong, S. 2013. Strong adhesion and cohesion of chitosan in aqueous solutions. *Langmuir : the ACS journal of surfaces and colloids*. **29**(46): p. 14222.
174. Lim, C., Lee, DW., Israelachvili, JN., Jho, Y., Hwang, DS. 2015. Contact time- and pH-dependent adhesion and cohesion of low molecular weight chitosan coated surfaces. *Carbohydrate Polymers*. **117**(C): p. 887-894.

175. Chang, KLB., Tsai, G., Lee, J., Fu, WR. 1997. Heterogeneous N-deacetylation of chitin in alkaline solution. *Carbohydrate Research*. **303**(3): p. 327-332.
176. Foster, LJR., Ho, Sonia., Hook, J., Basuki, M., Marcal, HB. 2015. Chitosan as a Biomaterial: Influence of Degree of Deacetylation on Its Physiochemical, Material and Biological Properties. *PLoS ONE*. **10**(8).
177. Cai, SJ., Li, CW., Weihs, D., Wang, GJ. 2017. Control of cell proliferation by a porous chitosan scaffold with multiple releasing capabilities. *Science and Technology of Advanced Materials*. **18**(1): p. 987-996.
178. Ji, C., Khademhosseini, A., Dehghani, F. 2011. Enhancing cell penetration and proliferation in chitosan hydrogels for tissue engineering applications. *Biomaterials*. **32**(36): p. 9719-9729.
179. Mandal, BB. Kundu, SC. 2009. Cell proliferation and migration in silk fibroin 3D scaffolds. *Biomaterials*. **30**(15): p. 2956-2965.
180. Sakunphanitphan, S., Jeeeraphat, J., Hathatip, S., Bovornlak, O., Hargreaves, KM. 2019. The effect of silk fibroin hydrogel on proliferation of human stem cells from the apical papilla. *Mahidol Dental Journal*. p. 35-40.
181. Carrasco-Torres, G., Valdes-Madrigal, MA., Vasquez-Garzon., Veronica, R., Baltierrez-Hoyos, R., De La Cruz-Burelo, E., Roman-Doval, R., Valencia-Lazcano, AA. 2019. Effect of Silk Fibroin on Cell Viability in Electrospun Scaffolds of Polyethylene Oxide. *Polymers*. **11**(3).
182. Sivashankari, P., Prabaharan, M. 2016. Deacetylation modification techniques of chitin and chitosan. In Jennings, Bumgardner (eds). *Chitosan Based Biomaterials Volume 1: Fundamentals*. Elsevier Science.
183. Harish Prashanth, KV., Kittur, FS., Tharanathan, RN. 2002.Solid state structure of chitosan prepared under different N-deacetylating conditions. *Carbohydrate Polymers*. **50**(1): p. 27-33.
184. Berg, JM., Tymoczko, L., Stryer, L., Gatto, GJ. 2012. *Biochemistry*. 7th ed. Basingstoke: Basingstoke : W.H. Freeman.
185. Hoven, V., Tangpasuthadol, V., Angkitpaiboon, Y., Vallapa, N., Kiatkamjornwong, S. 2007. Surface-charged chitosan: Preparation and protein adsorption. *Carbohydrate Polymers*. **68**(1): p. 44-53.
186. Merck KGaA. 2020. *Chitosan low molecular weight*. Available from: https://www.sigmaaldrich.com/catalog/product/aldrich/448869?lang=en&region=GB. [cited 2020 06/09/20].
187. Kim, MK., Lee, J., Jo, MR., Kim, MK., Kim, HM., Oh, JM., Song, NM., Choi, SJ. 2015. Cytotoxicity, Uptake Behaviors, and Oral Absorption of Food Grade Calcium Carbonate Nanomaterials. *Nanomaterials* (Basel, Switzerland). **5**(4): p. 1938-1954.
188. Tokatlı, K. 2018. Optimization of chitin and chitosan production from shrimp wastes and characterization. *Journal of Food Processing & Preservation*. **42**(2): p. 1-14.
189. Bajaj, M., Winter, J., Gallert, C. 2011. Effect of deproteination and deacetylation conditions on viscosity of chitin and chitosan extracted from Crangon crangon shrimp waste. *Biochemical engineering journal*. **56**(1): p. 51-62.
190. Tapani, E., Taavitsaninen, M., Lindros, T., Vehmas, T., Lehtonen, E. 1996. Toxicity of ethanol in low concentrations - Experimental evaluation in cell culture. *Acta Radiologica*. **37**(6): p. 923-926.
191. VWR international. 2020. *Ethanol absolute ≥99.8%, AnalaR NORMAPUR® ACS, Reag. Ph. Eur. analytical reagent*. Available from: https://uk.vwr.com/store/product/733157/ethanol-absolute-99-8-analar-normapur-acs-reag-ph-eur-analytical-reagent. [cited 2020 06/09/20]
192. Dou, H., Zuo, B. 2015. Effect of sodium carbonate concentrations on the degumming and regeneration process of silk fibroin. *The Journal of The Textile Institute*. **106**(3): p. 311-319.
193. Fernandes, H., Moroni, L., Van Blitterswijk, C., De Boer, J. 2009. Extracellular matrix and tissue engineering applications. *Journal of Materials Chemistry*. **19**(31): p. 5474-5484.

194. Youhwan, K., Ko, H., Kwon, IK., Shin, K. 2016. Extracellular Matrix Revisited: Roles in Tissue Engineering. *International Neurourology Journal*. **20**(Suppl 1): p. S23-29.
195. Jenkins, TL., Little, D. 2019. Synthetic scaffolds for musculoskeletal tissue engineering: cellular responses to fiber parameters. *Regenerative Medicine*. **4**(1): p. 1-14.
196. Yi, S., Fei, D., Gong, L., Gu, X. 2017. Extracellular Matrix Scaffolds for Tissue Engineering and Regenerative Medicine. *Current Stem Cell Research & Therapy*. **12**(3): p. 233-246.
197. Martinez-Mora, C., Mrowiec, A., Garcia-Vizcaino, EM., Alcaraz, A., Cenis, JL., Nicolas, FJAK. 2012. Fibroin and sericin from Bombyx mori silk stimulate cell migration through upregulation and phosphorylation of c-Jun. *Journal Of Tissue Engineering And Regenerative Medicine*. **6**: p. 177-177.
198. Shi, J., Zeng, X., Zhou, M., Chen, Q. 2009. Activation of ERK-FAK Signaling Pathway and Enhancement of Cell Migration Involved in the Early Interaction Between Oral Keratinocytes and Candida albicans. *Mycopathologia*. **167**(1): p. 1-7.
199. Quach, NL., Biressi, S., Reichardt, LF., Keller, C., Rando, TAA. 2009. Focal adhesion kinase signaling regulates the expression of caveolin 3 and β1 integrin, genes essential for normal myoblast fusion. *American Society for Cell Biology*. **20**(14): p. 3422-3435.
200. Grenha, A., Gomes, ME., Rodrigues, M., Santo, VE., Mano, JF., Neves, NM., Reis, RL. 2010. Development of new chitosan/carrageenan nanoparticles for drug delivery applications. *J. Biomed. Mater. Res. Part A*. **92A**(4): p. 1265-1272.
201. Pinheiro, AC., Bourbon, AI., Medeiros, BG., Da Silva, LHM., Da Silva, MCH., Carneiro-da-Cunha, MG., Coimbra, MA., Vicente, AA. 2012. Interactions between kappa-carrageenan and chitosan in nanolayered coatings-Structural and transport properties. *Carbohydr. Polym*. **87**(2): p. 1081-1090.
202. Piyakulawat, P., Praphairaksit, N., Chantarasiri, N., Muangsin, N. 2007. Preparation and evaluation of chitosan/carrageenan beads for controlled release of sodium Diclofenac. *AAPS PharmSciTech*. **8**(4).
203. Gotoh, Y., Tsukada, M., Minoura, N. 1998. Effect of the chemical modification of the arginyl residue in Bombyx mori silk fibroin on the attachment and growth of fibroblast cells. *Journal of biomedical materials research*. **39**(3): p. 351.
204. Drummy, LF., Phillips, DM., Stone, MO., Farmer, BL., Naik, RR. Thermally induced alpha-helix to beta-sheet transition in regenerated silk fibers and films. *Biomacromolecules*. **6**(6): p. 3328-3333.
205. Ruan, QX., Zhou, P. 2008. Sodium ion effect on silk fibroin conformation characterized by solid-state NMR and generalized 2D NMR–NMR correlation. *Journal of Molecular Structure*. **883**(1-3): p. 85-90.
206. Gaotian, S., Hu, X., Guan, G., Wang, LM. 2015. Surface Modification and Characterisation of Silk Fibroin Fabric Produced by the Layer-by-Layer Self-Assembly of Multilayer Alginate/Regenerated Silk Fibroin. *PLoS ONE*. **10**(4): p. e0124811.
207. Merck KGaA. 2020. *Carrageenan suitable for gel preparation*. Available from: https://www.sigmaaldrich.com/catalog/product/sigma/c1013?lang=en&region=GB. [cited 2020 06/09/20]
208. Azevedo, G., Torres, MD., Sousa-Pinto, I., Hilliou, L. 2015. Effect of pre-extraction alkali treatment on the chemical structure and gelling properties of extracted hybrid carrageenan from Chondrus crispus and Ahnfeltiopsis devoniensis. *Food hydrocolloids*. **50**: p. 150-158.
209. Garland, EM., Parr, JM., Williamson, DS., Cohen, SM. 1989. In vitro cytotoxicity of the sodium, potassium and calcium salts of saccharin, sodium ascorbate, sodium citrate and sodium chloride. *Toxicology in vitro*. **3**(3): p. 201-205.
210. Merck KGaA. 2020. Alginic acid sodium salt from brown algae. Available from: https://www.sigmaaldrich.com/catalog/product/sigma/a1112?lang=en&region=GB. [cited 2020 05/09].

211. Sondermeijer, HP., Witkowski, P., Woodland, D., Seki, T., Aangenendt, FJ., Van der Laarse, A., Itescu, S., Hardy, MA. 2016. Optimization of alginate purification using polyvinylidene difluoride membrane filtration: Effects on immunogenicity and biocompatibility of three-dimensional alginate scaffolds. *Journal of biomaterials applications*. **31**(4): p. 510-520.
212. Lee, KY., Kong, HJ., Larson, RG., Mooney, DJ. 2003. Hydrogel Formation via Cell Crosslinking. *Advanced Materials*. **15**(21): p. 1828-1832.
213. Sandvig, I., Karstensen, K., Rokstad, AM., Aachmann, FL., Formo, K., Sandvig, A., Skjak-Braek, G., Strand, BL. 2015. RGD-peptide modified alginate by a chemoenzymatic strategy for tissue engineering applications. *Journal of Biomedical Materials Research Part A*. **103**(3): p. 896-906.
214. Sara, P., Martella, E., De Girolamo, L., Perucca, OC., Pierini, M., Fumagalli, V., Pintacude, DV., Chlapanidas, T., Vigano, M., Farago, S., Torre, ML., Lucarelli, E. 2017. Fabrication of Innovative Silk/Alginate Microcarriers for Mesenchymal Stem Cell Delivery and Tissue Regeneration. *International Journal of Molecular Sciences*. **18**(9): p. 1829.
215. Sosnik, A. 2014. Alginate Particles as Platform for Drug Delivery by the Oral Route: State-of-the-Art. *ISRN pharmaceutics*. **2014**: p. 926157.
216. Severino, P., Da Silva, CF., Andrade, LN., De Lima Oliveira, D., Campos, J., Souto, EB. 2019. Alginate Nanoparticles for Drug Delivery and Targeting. *Current Pharmaceutical Design*. **25**(11): p. 1312-1334.
217. Li, P., Dai, YN., Zhang, JP., Wang, AQ., Wei, Q. 2008. Chitosan-alginate nanoparticles as a novel drug delivery system for nifedipine. *International journal of biomedical science*. **4**(3): p. 221.
218. González-Díaz, EC., Varghese, S. 2016. Hydrogels as Extracellular Matrix Analogs. *Gels*. **2**(3): p. 20.
219. Lam, MT., Sim, S., Zhu, X., Takayama, S. 2006. The effect of continuous wavy micropatterns on silicone substrates on the alignment of skeletal muscle myoblasts and myotubes. *Biomaterials*. **27**(24): p. 4340-4347.
220. Jana, S., Levengood, SKL., Zhang, M. 2016. Anisotropic Materials for Skeletal-Muscle-Tissue Engineering. *Advanced materials (Weinheim)*. **28**(48): p. 10588-10612.
221. Kalač, P. 2013. A review of chemical composition and nutritional value of wild-growing and cultivated mushrooms. *Journal of the science of food and agriculture.* **93**(2): p. 209-218.
222. Erdogan, S., Kaya, M., Akata, I. 2017. Chitin extraction and chitosan production from cell wall of two mushroom species (Lactarius vellereus and Phyllophora ribis). *AIP Conference procedings.*
223. Synowiecki, J., Al-Khateeb, NA. 2003. Production, Properties, and Some New Applications of Chitin and Its Derivatives. *Critical Reviews in Food Science and Nutrition*. **43**(2): p. 145-171.
224. Vetter, J. 2007. Chitin content of cultivated mushrooms Agaricus bisporus, Pleurotus ostreatus and Lentinula edodes. *Food Chemistry*. **102**(1): p. 6-9.
225. Ospina Álvarez, SP., Ramirez Cadavid, DA., Escobar Sierra, DM., Ossa Orozco, CP., Rojas Vahos, DF., Zapata Ocampo, P., Atehortua, LR. 2014. Comparison of Extraction Methods of Chitin from Mushroom Obtained in Submerged Culture. *BioMed Research International*. **2014**: p. 1 - 7.
226. Pochanavanich, P., Suntornsuk, W. 2002. Fungal chitosan production and its characterization. *Letters in applied microbiology*. **35**(1): p. 17.
227. Nakamura, M., Iketani, A., Shioi, Y. 2011. A survey of proteases in edible mushrooms with synthetic peptides as substrates. *Mycoscience*. **52**(4): p. 234-241.
228. Medronho, B., Romano, A., Miguel, MG., Stigsson, L., Lindman, BD. 2012. Rationalizing cellulose (in) solubility: reviewing basic physicochemical aspects and role of hydrophobic interactions. *Cellulose*. **19**(3): p. 581-587.

229. Pubchem Database, N.C.B.I. 2019. *Cellulose, CID=16211032*. Available from: https://pubchem.ncbi.nlm.nih.gov/compound/Cellulose]. [cited 2019 11/12]
230. Pubchem Database, N.C.B.I. 2019. *Chitosan, CID=71853*. Available from: https://pubchem.ncbi.nlm.nih.gov/compound/Chitosan] [cited 2019 11/12]
231. Patra, Chinmoy., Talukdar, S., Novoyatleva, T., Velagala, SR., Muhlfeld, C., Kundu, B., Kundu, SC., Engel, FB. 2012. Silk protein fibroin from Antheraea mylitta for cardiac tissue engineering. *Biomaterials*. **33**(9): p. 2673-2680.
232. Gasperini, L., Mano, JF., Reis, RL. 2014. Natural polymers for the microencapsulation of cells. *Journal of the Royal Society, Interface*. **11**(100): p. 20140817.
233. Popa, EG., Caridade, SG., Mano, JF., Reis, RL., Gomes, ME. 2015. Chondrogenic potential of injectable κ-carrageenan hydrogel with encapsulated adipose stem cells for cartilage tissue-engineering applications. *Journal of Tissue Engineering and Regenerative Medicine*. **9**(5): p. 550-563.
234. Rocha, PM., Santo, VE., Gomes, ME., Reis, RL., Mano, JF. 2011. Encapsulation of adipose-derived stem cells and transforming growth factor-β1 in carrageenan-based hydrogels for cartilage tissue engineering. *Journal of Bioactive and Compatible Polymers*. **26**(5): p. 493-507.
235. Pubchem database, N.C.B.I. 2020. *5-Chloromethylfluorescein diacetate, CID = 1222297*. Available from: https://pubchem.ncbi.nlm.nih.gov/compound/5-Chloromethylfluorescein-diacetate. [cited 2020 11/2]
236. Pubchem database, N.C.B.I. 2020. *CID=23686673, Phenol red sodium salt*. Available from: https://pubchem.ncbi.nlm.nih.gov/compound/Phenol-Red-sodium-salt]. [cited 2020 11/2].
237. Kim, JH., Lee, SB., Kim, SJ., Lee, YM. 2002. Rapid temperature/pH response of porous alginate- g-poly(N-isopropylacrylamide) hydrogels. *Polymer*. **43**(26): p. 7549-7558.
238. Chen, B., Wright, B., Sahoo, R., Connon, CJ. 2012. A novel alternative to cryo-preservation for the short term storage of stem cells for use in cell therapy using alginate encapsulation. *Tissue Engineering Part C: Methods*. 2012: p. 121202192344007.
239. Li, M., Mondrinos, MJ., Chen, X., Gandhi, MR., Ko, FK., Lelkes, PIH. 2006. Co-electrospun poly(lactide- co -glycolide), gelatin, and elastin blends for tissue engineering scaffolds. *Journal of Biomedical Materials Research Part A*. **79A**(4): p. 963-973.
240. Novikova, LN., Mosahebi, A., Wiberg, M., Terenghi, G., Kellerth, J., Novikov, LNH. 2006. Alginate hydrogel and matrigel as potential cell carriers for neurotransplantation. *Journal of Biomedical Materials Research Part A*. **77**(2): p. 242-252.
241. Maria, OM., Maria, O., Liu, Y., Komarova, SV., Tran, SD. 2011. Matrigel improves functional properties of human submandibular salivary gland cell line. *International Journal of Biochemistry and Cell Biology*. **43**(4): p. 622-631.
242. Dong, J., Sun, Q., Wang, JY. 2004. Basic study of corn protein, zein, as a biomaterial in tissue engineering, surface morphology and biocompatibility. *Biomaterials*. **25**(19): p. 4691-4697.
243. Arnesen, S., Mosler, S. Larsen, NB. Gadegaard, N., Purslow, PP., Lawson, M. 2004. The Effects of Collagen Type I Topography on Myoblasts In Vitro. *Connective Tissue Research*. **45**(4-5): p. 238-247.
244. Fisher scientific. 2020. *Zein, purified, ACROS Organics*. 2020 Available from: https://www.fishersci.com/shop/products/zein-acros-organics-3/AC179311000. [cited 2020 28/08/20]
245. Sessa, DJ., Eller, FJ., Palmquist, DE., Lawton, JW. 2003. Improved methods for decolorizing corn zein. *Industrial Crops & Products*. **18**(1): p. 55-65.

246. Merck KGaA. 2020. *Zein from maize*. Available from: https://www.sigmaaldrich.com/catalog/product/sigma/z3625?lang=en&region=GB. [cited 2020 28/08/20].
247. PubChem Database, N.C.B.I. 2019. *Xanthophyll, CID=5368396*. Available from: https://pubchem.ncbi.nlm.nih.gov/compound/5368396]. [cited 2019 10/11].
248. Alija, AJ., Bresgen, N., Sommerburg, O., Siems, W., Eckl, PM. 2004. Cytotoxic and genotoxic effects of beta-carotene breakdown products on primary rat hepatocytes. *Carcinogenesis* (New York). **25**(5): p. 827.
249. Nowak, SJ., Nahirney, PC., Hadjantonakis, AK., Baylies, MK. 2009. Nap1-mediated actin remodeling is essential for mammalian myoblast fusion. *Journal of cell science*. **122**(18): p. 3282.
250. Goh, Q., Dearth, CL., Corbett, JT., Pierre, P., Chadee, DN., Pizza, FX. 2015. Intercellular adhesion molecule-1 expression by skeletal muscle cells augments myogenesis. *Experimental Cell Research*. **331**(2): p. 292-308.
251. Ryan, JA. 2008. Evolution of Cell Culture Surfaces. *BioFiles*. **3**(8): p. 21. Sigma Aldrich. [Online]. Available from: https://www.sigmaaldrich.com/technical-documents/articles/biofiles/evolution-of-cell.html.
252. Schvartz, I., Seger, D., Shaltiel, S. 1999. Vitronectin. *International Journal of Biochemistry & Cell Biology*. **31**(5): p. 539-544.
253. Leahy, DJ., Aukhil, I., Erickson, HP. 1996. 2.0 Å Crystal Structure of a Four-Domain Segment of Human Fibronectin Encompassing the RGD Loop and Synergy Region. *Cell*. **84**(1): p. 155-164.
254. Argos, P., Pedersen, K., Marks, MD., Larkins, BA. 1982. A structural model for maize zein proteins. *The Journal of biological chemistry*. **257**(17): p. 9984.
255. Akimov, SS., Krylov, D., Fleischman, LF., Belkin, AM. 2000. Tissue transglutaminase is an integrin-binding adhesion coreceptor for fibronectin. *The Journal of cell biology*. **148**(4): p. 825.
256. Jones, RA., Nicholas, B., Mian, S., Davies, PJ., Griffin, M. 1997. Reduced expression of tissue transglutaminase in a human endothelial cell line leads to changes in cell spreading, cell adhesion and reduced polymerisation of fibronectin. *Journal of cell science*. **110 (Pt 19)**: p. 2461.
257. Belkin, AM., Tsurupa, G., Zemskov, E., Veklich, Y., Weisel, JW., Medved, L. 2005. Transglutaminase-mediated oligomerization of the fibrin(ogen) alphaC domains promotes integrin-dependent cell adhesion and signaling. *Blood*. **105**(9): p. 3561.
258. Csosz, E., Bagossi, P., Nagy, Z., Dosztanyi, Z., Simon, I., Fesus, L. 2008. Substrate Preference of Transglutaminase 2 Revealed by Logistic Regression Analysis and Intrinsic Disorder Examination. *Journal of Molecular Biology*. **383**(2): p. 390-402.
259. Zhao, X. Guan, JL. 2011. Focal adhesion kinase and its signaling pathways in cell migration and angiogenesis. *Advanced Drug Delivery Reviews*. **63**(8): p. 610-615.
260. Stern-Straeter, J., Bonaterra, GA., Kassner, SS., Zugel, S., Hormann, K., Kinscherf, R., Goessler, UR. 2011. Characterization of human myoblast differentiation for tissue-engineering purposes by quantitative gene expression analysis. *Journal of Tissue Engineering and Regenerative Medicine*. **5**(8): p. e197-e206.
261. Duronio, RJ., Xiong, Y. 2013. Signaling pathways that control cell proliferation. *Cold Spring Harbor perspectives in biology*. **5**(3): p. a008904.
262. Pollak, NM., Hoffman, M., Goldberg, IJ., Drosatos, K. 2018. Krüppel-Like Factors. *JACC: Basic to Translational Science*. **3**(1): p. 132-156.
263. Kogan, MJ., Lopez, O., Cocera, M., Lopez-Iglesias, C., De la Maza, A., Giralt, E. 2004. Exploring the interaction of the surfactant N-terminal domain of γ-Zein with soybean phosphatidylcholine liposomes. *Biopolymers*. **73**(2): p. 258-268.
264. D'Andrea, P., Civita, D., Cok, M., Ulloa, SL., Vita, F., Scaini, D., Casalis, L., Lorenzon, P., Donati, I., Bandiera, A. 2016. Myoblast adhesion, proliferation and differentiation on human elastin-like polypeptide (HELP) hydrogels. *Journal of Applied Biomaterials & Functional Materials*. **15**(1): p. 43-53.

265. Gribova, V., Liu, CY., Nishiguchi, A., Matsusaki, M., Boudou, T., Picart, C., Akashi, MB. 2016. Construction and myogenic differentiation of 3D myoblast tissues fabricated by fibronectin-gelatin nanofilm coating. *Biochemical and Biophysical Research Communications*. **474**(3): p. 515-521.
266. Vaz, R., Martins, GG., Thorsteinsdottir, S., Rodrigues, G. 2012. Fibronectin promotes migration, alignment and fusion in an in vitro myoblast cell model. *Cell and Tissue Research*. **348**(3): p. 569-578.
267. Sotiropoulos, A., Ohanna, M., Kedzia, C., Menon, RK., Kopchick, JJ., Kelly, PA., Pende, M. 2006. Growth Hormone Promotes Skeletal Muscle Cell Fusion Independent of Insulin-Like Growth Factor 1 Up-Regulation. *Proceedings of the National Academy of Sciences of the United States of America*. **103**(19): p. 7315-7320.
268. Pelham, RJ., Wang, YL. 1997. Cell locomotion and focal adhesions are regulated by substrate flexibility. *Proceedings of the National Academy of Sciences of the United States of America*. **94**(25): p. 13661-13665.
269. Fuoco, C., Petrilli, LL., Cannata, S., Gargioli, C. 2016. Matrix scaffolding for stem cell guidance toward skeletal muscle tissue engineering. *Journal of orthopaedic surgery and research*. **11**(1): p. 86.
270. Brozovich, FV., Nicholson, CJ., Degen, CV., Gao, YZ., Aggarwal, M., Morgan, KG., Watts, SW. 2016. Mechanisms of Vascular Smooth Muscle Contraction and the Basis for Pharmacologic Treatment of Smooth Muscle Disorders. *Pharmacological reviews*. **68**(2): p. 476-532.
271. Powell, CA., Smiley, BL., Mills, J., Vandenburgh, HH. 2002. Mechanical stimulation improves tissue-engineered human skeletal muscle. *American Journal of Physiology: Cell Physiology*. **283**(5): p. C1557-C1565.
272. Ghane, N., Mazinani, S., Gharehaghaji, AA. 2018. Comparing the performance of electrospun and cast nanocomposite film of polyamide-6 reinforced with multi-wall carbon nanotubes. *Journal of plastic film & sheeting*. **35**(1): p. 45-64.
273. Jana, S., Leung, M., Chang, J., Zhang, M. 2014. Effect of nano- and micro-scale topological features on alignment of muscle cells and commitment of myogenic differentiation. *Biofabrication*. **6**(3): p. 035012.
274. Voigtländer, B. 2019. *Atomic Force Microscopy*. Second edition. Cham : Springer International Publishing.
275. Zatti, S., Zoso, A., Serena, E., Luni, C., Cimetta, E., Elvassore, N. 2012. Micropatterning Topology on Soft Substrates Affects Myoblast Proliferation and Differentiation. *Langmuir*. **28**(5): p. 2718-2726.
276. Pegg , EC., Matboli, F., Marriott, T., Khan, I., Scotchford, CA. 2014. Topographical and chemical effects of electrochemically assisted deposited hydroxyapatite coatings on osteoblast-like cells. *Journal of Biomaterials Applications*. **28**(6): p. 946-53.
277. Ghasemi-Mobarakeh, L., Prabhakaran, MP., Tian, L., Shamirzaei-Jeshvaghani, E., Dehghani, L., Ramakrishna, S. 2015. Structural properties of scaffolds: Crucial parameters towards stem cells differentiation. *World journal of stem cells*. **7**(4): p. 728-744.
278. Marsano, A., Maidhof, R., Wan, LQ., Wang, Y., Gao, J., tandon, N., Vunjak-Novakovic, G. 2010. Scaffold stiffness affects the contractile function of three-dimensional engineered cardiac constructs. *Biotechnology Progress*. **26**(5): p. 1382-1390.
279. Levy-Mishali, M., Zoldan, J., Levenberg, S. 2009. Effect of Scaffold Stiffness on Myoblast Differentiation. *Tissue engineering. Part A*. **15**(4): p. 935-944.
280. Alhusein, N., Blagbrough, IS., Beeton, ML., Bolhuis, A., De Bank, PA. Electrospun Zein/PCL Fibrous Matrices Release Tetracycline in a Controlled Manner, Killing Staphylococcus aureus Both in Biofilms and Ex Vivo on Pig Skin, and are Compatible with Human Skin Cells. *Pharmaceutical research*. **33**(1): p. 237.

281. Lim, H., Hoag, SW. 2013. Plasticizer Effects on Physical–Mechanical Properties of Solvent Cast Soluplus® Films. *AAPS PharmSciTech*. **14**(3): p. 903-910.
282. Sothornvit, R., Krochta, JM. 2005. Plasticizers in edible films and coatings. In *Innovations in Food Packaging.* Elsevier Ltd. p. 403-433.
283. Lau, ETL., Johnson, SK., Mikkelsen, D., Halley, PJ., Steadman, KJ. 2012. Preparation and in vitro release of zein microparticles loaded with prednisolone for oral delivery. *Journal of Microencapsulation*. **29**(7): p. 706-712.
284. Lau, ETL., Giddings, SJ., Mohammed, SG., Dubois, P., Johnson, SK., Roger, A., Halley, PJ., Steadman, KJ. 2013. Encapsulation of hydrocortisone and mesalazine in zein microparticles. *Pharmaceutics*. **5**(2): p. 277.
285. Jin, M., Davidson, PM., Zivanovic, S., Zhong, Q. 2009. Production of corn zein microparticles with loaded lysozyme directly extracted from hen egg white using spray drying: Extraction studies. *Food Chemistry*. **115**(2): p. 509-514.
286. Farris, E., Brown, DM., Rammer-Tait, AE., Pannier, AK. 2017. Chitosan-zein nano-in-microparticles capable of mediating in vivo transgene expression following oral delivery. *Journal of Controlled Release*. **249**: p. 150-161.
287. Yang, J., Guertin, P., Jia, G., Lv, Z., Yang, Hongyan., Ju, Dianwen. 2019. Large-scale microcarrier culture of HEK293T cells and Vero cells in single-use bioreactors. *AMB Express*. **9**(1): p. 1-14.
288. Malda, J., Frondoza, CG. 2006. Microcarriers in the engineering of cartilage and bone. *Trends in Biotechnology*. **24**(7): p. 299-304.
289. Aytac, Z., Ipek, S., Durgun, E., Tekinay, T., Uyar, T. 2017. Antibacterial electrospun zein nanofibrous web encapsulating thymol/cyclodextrin-inclusion complex for food packaging. *Food Chemistry*. **233**: p. 117-124.
290. Aytac, Z., Ipek, S., Durgun, E., Uyar, T. 2018. Antioxidant electrospun zein nanofibrous web encapsulating quercetin/cyclodextrin inclusion complex. *Journal of Materials Science*. **53**(2): p. 1527-1539.
291. Kayaci, F., Uyar, T. 2012. Electrospun zein nanofibers incorporating cyclodextrins. *Carbohydrate Polymers*. **90**(1): p. 558-568.
292. Jiang, Q., Yang, Y. 2011. Water-Stable Electrospun Zein Fibers for Potential Drug Delivery. *Journal of Biomaterials Science Polymer Edition*. **22**(10): p. 1393-1408.
293. Alhusein, N., Blagbrough, I., De Bank, PA. 2013. Zein/polycaprolactone electrospun matrices for localised controlled delivery of tetracycline. *Drug Delivery and Translational Research*. **3**(6): p. 542-550.
294. Walczak, ZK. 2002. *Processes of fiber formation*. 1st ed. Amsterdam ; New York : Elsevier.
295. Van Ballegooie, C., Man, A., Andreu, I., gates, BD., Yapp, D. 2019. Using a Microfluidics System to Reproducibly Synthesize Protein Nanoparticles: Factors Contributing to Size, Homogeneity, and Stability. *Processes*. **7**(5): p. 290.
296. Feng, Y., Lee, Y., Olenskyj, AG. 2017. Continuous microfluidic production of zein nanoparticles and correlation of particle size with physical parameters determined using CFD simulation. *Journal of food engineering*. **211**: p. 50-59.
297. Feng, Y., Lee, Y. 2019. Microfluidic fabrication of wrinkled protein microcapsules and their nanomechanical properties affected by protein secondary structure. *Journal of Food Engineering*. **246**: p. 102-110.
298. Figoli, A., Cassano, A., Basile, A. 2016. Polymeric Membranes in Biorefinery. In Figoli, Cassano, Basile (eds). *Membrane technologies for biorefining.* Amsterdam, Netherlands. Woodhead publishing.
299. Li, SG., Koops, GH., Mulder, MHV., Van Den Boomgaard, T., Smolders, CA. 1994. Wet spinning of integrally skinned hollow fiber membranes by a modified dual-bath coagulation method using a triple orifice spinneret. *Journal of Membrane Science*. **94**(1): p. 329-340.
300. Yao, J., Wang, Kun., Ren, M., Zhe Liu, J., Wang, Huanting. Phase inversion spinning of ultrafine hollow fiber membranes through a single orifice spinneret. *Journal of Membrane Science*. **421-422**: p. 8-14.

301. Strathmann, H., Kock, K. 1977. The formation mechanism of phase inversion membranes. *Desalination*. **21**(3): p. 241-255.
302. Wishart, DS., Yannick, DF., Marcu, A., Chi Go, A., Liang, K., Vazquez-Frenso, R., Sajed, T., Johnson, D., Li, C., Naama, K., Sayeeda, Z., Lo, E., Assempour, N., Berjanskii, M., Singhal, S., Arndt, D., Liang, Y., Badran, H., Grant, J., Serra-Cayuela, A., Liu, Y., Mandal, R., Neveu, V., Pon, A., Knox, C. Wilson, M., Manach, C., Scalbert, A. 2018. HMDB 4.0: the human metabolome database for 2018. *Nucleic Acids Research*. **46**(D1): p. D608-D617.
303. Park, C., Vo, CLN., Kang, T., Oh, E., Lee, BJ. 2015. New method and characterization of self-assembled gelatin-oleic nanoparticles using a desolvation method via carbodiimide/N-hydroxysuccinimide (EDC/NHS) reaction. *European journal of pharmaceutics and biopharmaceutics*. **89**: p. 365-373.
304. Morgan, A., babu, D., Reiz, B., Whittal, R., Suh, L., Siraki, AG. 2019. Caution for the routine use of phenol red – It is more than just a pH indicator. *Chemico-Biological Interactions*. **310**: p. 108739.
305. El-Nahhal, IM., Issa, M., Livage, J., Zourab, SM., Kodeh, FS., Al Swearky, A. 2015. Entrapment of phenol red (PR) pH indicator into sol–gel matrix in presence of some surfactants. *Journal of Sol-Gel Science and Technology*. **75**(2): p. 313-322.
306. Jiang, QR., Reddy, N., Yang, YQ. 2010. Cytocompatible cross-linking of electrospun zein fibers for the development of water-stable tissue engineering scaffolds. *Acta Biomaterialia*. **6**(10): p. 4042-4051.
307. Tarus, B., Fadel, N., Al-Oufy, A., El-Messiry, M. 2016. Effect of polymer concentration on the morphology and mechanical characteristics of electrospun cellulose acetate and poly (vinyl chloride) nanofiber mats. *Alexandria Engineering Journal*. **55**(3): p. 2975-2984.
308. Zhu, G., Zhao, LY., Deng, XY., Chen, WL. 2017. Effect of Experimental Parameters on Nanofiber Diameter from Electrospinning with Wire Electrodes. *International Conference on Materials Sciences and Nanomaterials*. **230**: p. 12043.
309. Li, T., Wang, C., Li, T., Ma, L., Sun., D., Hou, J., Jiang, Z. 2018. Surface Hydrophobicity and Functional Properties of Citric Acid Cross-Linked Whey Protein Isolate: The Impact of pH and Concentration of Citric Acid. *Molecules*. **23**(9).
310. Reddy, N., Li, Y., Yang, Y. 2009. Alkali-catalyzed low temperature wet crosslinking of plant proteins using carboxylic acids. *Biotechnology Progress*. **25**(1): p. 139-146.
311. Neves-Petersen, MT., Petersen, S., Gnana, PG. 2012. UV Light Effects on Proteins: From Photochemistry to Nanomedicine. In Saha (ed). *Photochemistry - Various Aspects*. InTech. P. 126 - 158.
312. Mali, KK., Dhawale, SC., Dias, RJ., Dhane, N., Ghorpade, V. 2018. Citric Acid Crosslinked Carboxymethyl Cellulose-based Composite Hydrogel Films for Drug Delivery. *Indian Journal of Pharmaceutical Sciences*. **80**(4): p. 657-667.
313. Pierschbacher, MD., Ruoslahti, E. 1987. Influence of stereochemistry of the sequence Arg-Gly-Asp-Xaa on binding specificity in cell adhesion. *The Journal of biological chemistry*. **262**(36): p. 17294.
314. PubChem Database, N.C.B.I. 2019. *Aspartic acid, CID=5960*. Available from: https://pubchem.ncbi.nlm.nih.gov/compound/Aspartic-acid. [cited 2019 Nov 10];
315. PubChem Database, N.C.B.I. 2019. *D-Aspartic acid, CID=83887*. Available from: https://pubchem.ncbi.nlm.nih.gov/compound/D-Aspartic-acid]. [cited 2019 Nov 10]
316. Greenberg, CS., Birckbichler, PJ., Rice, RH. 1991. Transglutaminases: multifunctional cross-linking enzymes that stabilize tissues. *Federation of American Societies for Experimental Biology*. **5**(15): p. 3071.
317. PubChem Database, N.C.B.I. 2019. *beta-carotene, CID=5280489*. Available from: https://pubchem.ncbi.nlm.nih.gov/compound/beta-Carotene. [cited 2019 10/11]
318. Matveev, YI., Grinberg, VY., Tolstoguzov, VB. 2000. The plasticizing effect of water on proteins, polysaccharides and their mixtures. Glassy state of biopolymers, food and seeds. *Food Hydrocolloids*. **14**(5): p. 425-437.

319. Elamparithi, A., Punnoose, AM., Kuruvilla, S. 2016. Electrospun type 1 collagen matrices preserving native ultrastructure using benign binary solvent for cardiac tissue engineering. *Artificial Cells, Nanomedicine, and Biotechnology*. **44**(5): p. 1318-1325.
320. Prabst, K., Engelhardt, H., Ringgeler, S., Hubner, H. 2017. Basic Colorimetric Proliferation Assays: MTT, WST, and Resazurin. In Gilbert, Friedrich (eds). *Cell Viability Assays: Methods and Protocols.* **1601**: p. 813-17.
321. Ladd, MR., Lee, SJ., Stitzel, JD., Atala, A., Yoo, JJ. 2011. Co-electrospun dual scaffolding system with potential for muscle–tendon junction tissue engineering. *Biomaterials*. **32**(6): p. 1549-1559.
322. Choi, HF., Blemker, SS., Sampaolesi, M. 2013. Skeletal Muscle Fascicle Arrangements Can Be Reconstructed Using a Laplacian Vector Field Simulation. *PLoS ONE*. **8**(10).
323. Teo, WE., Ramakrishna, S. 2006. A review on electrospinning design and nanofibre assemblies. *Nanotechnology.* **17**(14): p. R89-R106.
324. Yue, X., Zhang, F., Wu, H., Ming, J., Fan, Z., Zuo, B. 2014. A novel route to prepare dry-spun silk fibers from CaCl2–formic acid solution. *Materials letters*. **128**: p. 175-178.
325. Sun, M., Zhang, Y., Zhao, Y., Shao, H., Hu, X .2012. The structure–property relationships of artificial silk fabricated by dry-spinning process. *Journal of Materials Chemistry*. **22**(35): p. 18372.
326. Lopes, A.R., Sousa, VM., Estevinho, BN., Leite, JP., Moreira, NFF., Gales, L., Rocha, F., Nunes, OC. Production of microparticles of molinate degrading biocatalysts using the spray drying technique. *Chemosphere*. **161**: p. 61-68.
327. Rajkhowa, R., Gil, ES., Kluge, J., Numata, K., Wang, L., Wang, X., Kaplan, DL. 2010. Reinforcing Silk Scaffolds with Silk Particles. *Macromolecular bioscience*. **10**(6): p. 599-611.
328. Purwanti, N., Moerkens, A., Van der Goot, AJ., Boom, R. 2012. Reducing the stiffness of concentrated whey protein isolate (WPI) gels by using WPI microparticles. *Food Hydrocolloids*. **26**(1): p. 240-248.
329. Malumba, P., Vanderghem, C., Deroanne, C., Bera, F., 2008. Influence of drying temperature on the solubility, the purity of isolates and the electrophoretic patterns of corn proteins. *Food Chemistry*. **111**(3): p. 564-572.
330. Singh, RP., Bornhorst, GM. 2013. Kinetics of in Vitro Bread Bolus Digestion with Varying Oral and Gastric Digestion Parameters. *Food biophysics*. **8**(1): p. 50-59.
331. Nisal, A., Sayyad, R., Dhavale, P., Khude, B., Deshpande, R., Mapare, V., Shukla, S., Venugopalan, P. 2018. Silk fibroin micro-particle scaffolds with superior compression modulus and slow bioresorption for effective bone regeneration. *Scientific Reports* **8**(1): p. 7235.
332. Li, X., Zhang, Q., Feng, Y., Yan, S., Qu, J., You, RB. 2016. *Preparation of Antheraea pernyi* Silk Fibroin Microparticles through a Facile Electrospinning Method. *Advances in Materials Science and Engineering*. **2016**.
333. Deng, L., Li, Y., Feng, F., Zhang, Hui. 2019. Study on wettability, mechanical property and biocompatibility of electrospun gelatin/zein nanofibers cross-linked by glucose. *Food Hydrocolloids*. **87**: p. 1-10.
334. Soe, JB., Petersen, LW. 2005. *An enzyme such as hexose (HOX) or glucose (GOX) oxidase, which oxidises the reducing group of a monosaccharide and thereby prevent the Malliard reaction*. Patent US6872412B2.
335. Selling, GW., Woods, KK., Biswas, A. 2012. Electrospun zein fibers using glyoxal as the crosslinking reagent. *Journal of Applied Polymer Science*. **123**(5): p. 2651-2661.
336. Glomb, MA., Monnier, VM. 1995. Mechanism of protein modification by glyoxal and glycolaldehyde, reactive intermediates of the Maillard reaction. *The Journal of biological chemistry*. **270**(17): p. 10017.

337. Hsia, HC., Nair, MR., Mintz, RC., Corbett, SA. 2011. The Fiber Diameter of Synthetic Bioresorbable Extracellular Matrix Influences Human Fibroblast Morphology and Fibronectin Matrix Assembly. *Plastic and Reconstructive Surgery*. **127**(6): p. 2312-2320.
338. Tan, SH., Inai, R., Kotaki, M., Ramakrishna, S. 2005. Systematic parameter study for ultra-fine fiber fabrication via electrospinning process. *Polymer*. **46**(16): p. 6128-6134.
339. Mit-Uppatham, C., Nithitanakul, M., Supaphol, P. 2004. Ultrafine Electrospun Polyamide-6 Fibers: Effect of Solution Conditions on Morphology and Average Fiber Diameter. *Macromolecular Chemistry and Physics*. **205**(17): p. 2327-2338.
340. Ghasemi-Mobarakeh, L., Prabhakaran, M., Morshed, M., Nasr-Esfahani, M., Ramakrishna, S. 2008. Electrospun poly(epsilon-caprolactone)/gelatin nanofibrous scaffolds for nerve tissue engineering. *Biomaterials*. **29**(34): p. 4532.
341. Subramanian, A., Krishnan, UM., Sethuraman, S. 2011. Fabrication of uniaxially aligned 3d electrospun scaffolds for neural regeneration. *Biomedical Materials.* **6**(2): p. 025004.
342. Carrier, R.L., Papadaki, M., Rupnick, M., Schoen, F., Bursac, N., Langer, R., Freed, LE., Vunjak-Novakovic, G. 1999. Cardiac tissue engineering: Cell seeding, cultivation parameters, and tissue construct characterization. *Biotechnology and Bioengineering*. **64**(5): p. 580-589.
343. Katta, P., Alessandro, M., Ramsier, R., Chase, G. 2004. Continuous electrospinning of aligned polymer nanofibers onto a wire drum collector. *Nano Letters*. **4**(11): p. 2215-2218.
344. Howard, C. 2011. *Names You Need To Know: Meat Glue. Yum Or Yuck?* Forbes. Available from: https://www.forbes.com/sites/carolinehoward/2011/05/13/names-you-need-to-know-meat-glue-yuck-or-yum/#52283de45682. [Cited 2020, Feb 17].